DOCTOR OF PHILOSOPHY

SGK3 activity and regulation in PI3K-Akt pathway inhibitor resistance in breast cancer

Tovell, Hannah

Award date:
2020

University of Dundee

SGK3 activity and regulation in PI3K-Akt pathway inhibitor resistance in breast cancer

Hannah Tovell

A thesis submitted for the degree of Doctor of Philosophy

University of Dundee

2020

Contents

Table of Contents

List of Figures

List of Tables

Declarations

I declare that the following thesis is based on the results of investigations conducted by myself, and that this thesis is of my own composition. Work other than my own is clearly indicated in the text by reference to the relevant researchers or to their publications. This dissertation has not in whole, or in part, been previously submitted for a higher degree.

Hannah Tovell

I certify that Hannah Tovell has spent the equivalent of at least nine terms in research work in the Medical Research Council Protein Phosphorylation and Ubiquitylation Unit (MRC-PPU), School of Life Sciences, University of Dundee and that she has fulfilled the conditions of the Ordinance General No. 14 of the University of Dundee and is qualified to submit the accompanying thesis in application for the degree of Doctor of Philosophy.

Dario Alessi

Acknowledgements

Firstly, I would like to thank my supervisor, Dario Alessi. For giving me the opportunity to train in his laboratory and for providing such a great project to work on. My PhD has been so rewarding in terms of experiences, techniques and collaborations. Thank you for your patience and support over the last 4 years.

A huge thank you as well to my collaborators in this project. My PhD was supported by a Studentship with AstraZeneca, and Claire Crafter and Darren Cross were a fantastic support on the project. Claire, thank you especially for overseeing my work in Cambridge and Sladjana Gagricia for all your help supervising in me in the lab. You made my stay very enjoyable. This project also involved a close collaboration with Alessio Ciulli and his team. In particular, Andrea Testa and Chiara Maniaci, this project would not have happened without all your hard work. You were fantastic collaborators, support and friends, and I enjoyed exploring the new world of targeted protein degradation with you! Thank you as well to Houjiang Zhou for the mass spectrometry help.

In addition I would like to mention all members of Dario's lab, past and present, for being so helpful and welcoming throughout my PhD. To the original "Princess Bay" in Bay 4 – Kristina, Nazma, Annika – for being so welcoming and accepting. Nazma was a fantastic lab buddy and taught me many of the techniques I used throughout my PhD. Also to my new Bay mates Thanos, Toby and Asad. You kept the office a fun place to be, even throughout the writing process. Thank you for putting up with my hyper days and my moody days! I also want to particularly mention Thanos, the other half of "Team SGK3" and a wonderful friend! Your kindness, generosity and, of course, your amazing baking will not be forgotten. Elena – I couldn't have done this without you.

I would all like to thank all of the MRC PPU staff and students, who have made the unit a fantastic place to work. To all of my "PhD Buddies", for keeping the last 4 years full of fun and laughter, and for our many adventures outside of the lab. To Allison and Michele, for putting up with my constant requests, for the chats/rants and providing snacks in times of need. To Alison, Emma & Helen, and also Janis & Alison, for all your hard work and support. And finally to Paul Davies, for always keeping me grounded!

Finally, and most importantly, I would like thank my family for all their love and support. Thank you for always believing in me and encouraging me, I would not have reached this point without you.

Abbreviations

ACN	Acetonitrile
AdPROM	Affinity-directed Protein Missile
AGC	Protein Kinase A, Protein Kinase G, Protein Kinase C family
Akt	v-akt murine thymoma viral oncogene homologue 1(PKB)
ATG	Autophagy related gene
ATP	Adenosine Triphosphate
BSA	Bovine serum albumin
Cas9	CRISPR-associated protein 9
CRISPR	Clustered Regularly Interspaced Short Palindromic Repeats
DMSO	dimethyl sulphoxide
FYVE	Fab1, YOTB, Vac1 and EEA1 zinc finger binding domain
GPCR	G-protein coupled receptor
gRNA	guide RNA
GSK3	Glycogen synthase kinase 3
HA	YPYDVPDYA peptide(haemagglutinin)
HEK293	Human Embryonic Kidney 293
IB	Immunoblot
IF	Immunofluorescence
IGF1	insulin-like growth factor 1
IP	Immunoprecipitation
mLST8	mammalian lethal with SEC13 protein8
mTOR	Mammalian/Mechanistic Target of Rapamycin
mTORC1/2	mTOR complex 1/2
NDRG1	N-myc downregulated protein 1
PBS	Phosphate Buffered Saline
PDK1	phosphoinositide dependent protein kinase 1
PH	pleckstrin homology
PI3K	phosphatidylinositol-3 kinase
PIF	PDK1-interacting fragment
PROTAC	Proteolysis Targeting Chimera
PtdIns	Phosphatidylinositol
PX	phox homology
Rictor	Rapamycin-insensitive companion of mTOR
RTK	Receptor Tyrosine Kinase
SDS	Sodium dodecyl sulphate
SDS-PAGE	SDS polyacrylamide gel electrophoresis
SGK	serum and glucocorticoid regulated protein kinase
Sin1	SAPK-interacting protein1
TSC2	tuberous sclerosis complex 2
UVRAG	UV radiation resistance associated gene
VPS	Vacuolar protein sorting
WGA	Wheat Germ Agglutinin

Amino Acid code

Amino acid	Three letter code	One letter code
Alanine	Ala	A
Arginine	Arg	R
Asparagine	Asn	N
Aspartic acid	Asp	D
Cysteine	Cys	C
Glutamine	Gln	Q
Glutamic acid	Glu	E
Glycine	Gly	G
Histidine	His	H
Isoleucine	Ile	I
Leucine	Leu	L
Lysine	Lys	K
Methionine	Met	M
Phenylalanine	Phe	F
Proline	Pro	P
Serine	Ser	S
Threonine	Thr	T
Tryptophan	Trp	W
Tyrosine	Tyr	Y
Valine	Val	V

Thesis Abstract

The PI3K-Akt signalling pathway is central to cell proliferation and growth, and hyperactivating mutations in this pathway are found in a large number of cancers. Downstream of PI3K, Akt is heavily studied, however the highly related SGK family of protein kinases have recently been identified as driving cancer cell growth in certain contexts. In particular, my research interest and the focus of this thesis is the role these kinases, in particular SGK3, has in resistance to Class I PI3K and Akt inhibitors in certain ER+ breast cancers.

The first major aim of my PhD was to develop a method by which the signalling of SGK3 can be specifically modulated in cancer cells. Due to the high homology between the SGK family of protein kinases, chemical inhibition of SGK3 specifically has not been possible. Further, model cancer cell lines have been intractable to genome modification. I therefore, in collaboration with the Ciulli lab, designed and characterised SGK3-PROTAC1, a Proteolysis Targeting Chimera (PROTAC) which targeted SGK3 for specific ubiquitylation by VHL E3 ligase and subsequent proteasomal degradation. I demonstrated by quantitative Mass Spectrometry that SGK3-PROTAC1 mediated degradation was highly specific. Rapid, reversible degradation of SGK3 provided a tool for specifically modulating SGK3 in cancer cells. Further analysis using this compound in ZR-75-1 cells suggested some possible, previously unknown functions of SGK3 in cAMP signalling and mitochondrial metabolism. On degradation of SGK3, I observed a downregulation of the phosphodiesterase PDE4D and upregulation of a host of proteins mediating Oxidative Phosphorylation in mitochondria. These effects were observed only on degradation of the protein and not inhibition of its kinase activity, suggesting putative kinase-independent roles of SGK3. These findings would be extremely exciting to follow up in future work, and demonstrate the power of the PROTAC approach.

Given the potential of the PROTAC approach to probe biological systems, I also collaborated with the Ciulli lab to generate HaloPROTAC-E. This compound utilizes the bacterial dehalogenase activity of HaloTag7 to specifically induce degradation of any endogenously Halo-tagged protein.

I demonstrated that HaloPROTAC-E was able to induce degradation of the entire VPS34 complex to impact on downstream biology. This compound will be a useful tool within the unit and wider field to study proteins with no known ligands or validate target proteins for potential PROTAC development.

The second aim of my PhD was to study how SGK3 is activated in the context of PI3K inhibition. In this thesis, I studied the mTORC2 component mSin1, and provide preliminary data to show that certain regions of this protein may explain the differential regulation of Akt and SGK3. I also performed a preliminary assay to study interactors regulating the activity of Class III PI3K VPS34. Together, these experiments represent important preliminary results in understanding the activation of SGK3 and how it mediates Class I PI3K and Akt inhibitor resistance.

List of Publications

Tovell H, Testa A, Zhou H, Shpiro N, Crafter C, Ciulli A, Alessi DR., 2019 Design and characterization of SGK3-PROTAC1, an isoform specific SGK3 kinase PROTAC degrader. ACS Chem Biol. 2019, https://doi.org/10.1021/acschembio.9b00505

Tovell H, Testa A, Maniaci C, Zhou H, Prescott AR, Ciulli A, Alessi DR., 2019. Rapid and Reversible Knockdown of Endogenously Tagged Endosomal Proteins via an Optimized HaloPROTAC Degrader. ACS Chem Biol. 2019 May 17;14(5): 822-892

Malik N, Macartney T, Hornberger A, Anderson KE, **Tovell H**, Prescott AR, Alessi DR., 2018. Mechanism of activation of SGK3 by growth factors via the Class 1 and Class 3 PI3Ks. Biochem J. 2018 Jan 2;475(1):117-135

1. Introduction

1.1 Post-Translational modifications, and protein phosphorylation, in signal transduction

For survival, it is critical for cells to be able to respond to signals both internally and from their external environment. Sophisticated signalling mechanisms have therefore evolved for cells to recognise and appropriately respond to stimuli. Signalling cascades typically result from the binding of a signalling molecule, for example external growth factors or internal nutrient levels, to a receptor, altering its activity and mediating downstream cellular enzymes. This activation results in a cellular response (Figure 1A). A strong advantage to these signalling cascades is that sensitivity to subtle changes in the cellular environment can be amplified through the cascade.

In order to propagate signals, cellular enzymes will frequently modify their substrates through mechanisms such as proteolytic cleavage or post translational modifications, for example the conjugation of phosphates, carbohydrates or ubiquitin onto substrate proteins (Figure 1.1A). These post-translational modifications can dynamically modulate the activity, localisation and stability of almost all proteins encoded by the human genome. Additionally, many of these cascades are also reversible. For example, as will be discussed further in Chapter 3, polyubiquitylation of a target protein can act as a signal for its proteasomal degradation. Addition of a carbohydrate moiety to a substrate protein can form a transduction signal or a protein interaction motif. Many highly abundant post-translational modifications remain largely understudied, due to the lack of tools or analysis to detect them. A recently published study used new mass spectrometry analytical techniques to increase known sites of proline hydroxylation 10-fold (Devabhaktuni *et al.*, 2019). Another vast class of signal transduction, and the focus of this thesis, is protein phosphorylation.

Protein phosphorylation is the conjugation of a phosphate group to a substrate protein, and is a key component of most signal transduction cascades. This is carried out by protein kinases, which transfer the γ-phosphate of ATP to their protein substrate. Protein phosphorylation

typically occurs on the hydroxyl group of Ser, Thr, or Tyr residues, however other non-canonical phosphorylation sites are less well studied (Hunter, 2012). This modification is reversed by the action of protein phosphatases. Phosphorylation is an ideal mechanism for signal transduction as it is a rapid and reversible process, creating a simple “molecular switch” which does not require the synthesis or degradation of any new proteins. Protein phosphorylation results in the local addition of 2 negative charges, and therefore a considerable local charge change, which often results in conformational change of the substrate protein. This can have a number of downstream effects. The most common effect of enzyme phosphorylation is activation or deactivation of that enzyme, by revealing or occluding an active site. Alternatively, this conformation or charge change can result in altered interaction with downstream substrates and binding partners, creating a change in protein localisation, stability or function (Figure 1.1B) (Cohen, 2002; Hunter, 2012).

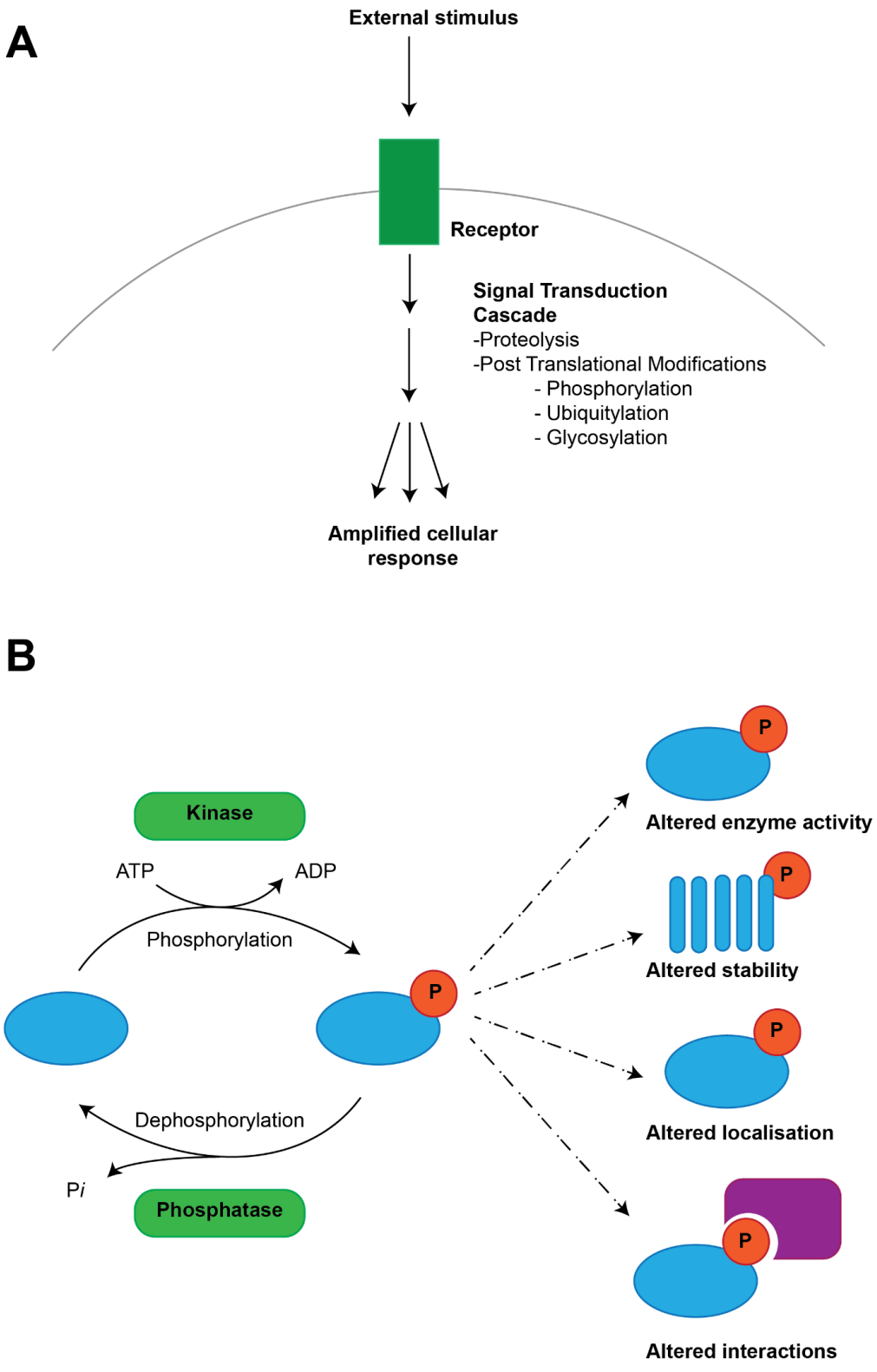

Figure 1.1 Protein phosphorylation is a reversible switch in signal transduction
A. *Signal Transduction cascades involve a series of enzymes and effectors, which allow internal cellular responses to an external or intracellular signal.* ***B****. Protein kinases catalyse the transfer of the γ-phosphate from ATP to their substrate protein, producing ADP. This modification can be reversed by protein phosphatases. Results of protein phosphorylation include activation of an enzyme, or altered interactions, localisation or stability of a target protein.*

'Canonical' protein phosphorylation has been extensively studied as the conjugation of phosphate to the hydroxyl group of serine, threonine or tyrosine. However, increasing evidence suggests that extensive non-canonical phosphorylation also occurs on histidine, arginine, asparagine, lysine, glutamate and cysteine residues. The study of these phosphorylation sites has remained behind that of canonical phosphorylation due to the lack of tools to study them. The bonds formed on phosphorylation of these residues are highly acid- and heat-labile and most traditional methods to detect canonical protein phosphorylation are not suitable (Hardman *et al.*, 2019). However, recent development of tools such as monoclonal antibodies against pHis have allowed for functional relevance of these phosphorylation events to be determined (Besant and Attwood, 2012; Fan *et al.*, 2012; Fuhs *et al.*, 2015; Wieland and Attwood, 2015; Srivastava *et al.*, 2016; Fuhs and Hunter, 2017). For example, it was recently determined that the histidine phosphatase LHPP can act as a tumour suppressor in hepatocellular carcinoma, suggesting that deregulated histidine phosphorylation can be oncogenic (Hindupur et al., 2018). Phosphorylation of histidine residues is of particular interest, as many enzymes have a catalytic histidine in their active site, due to the ability of its sidechain to rapidly transition from a charged to uncharged state. The charge change associated with phosphorylation, therefore, could strongly impact on catalysis. True to the lack of tools available to study non-canonical phosphorylation, little is known about the enzymes which catalyse phosphorylation and dephosphorylation of these sites. However elegant work has identified 2 histidine kinases, NME1 and NME2, and 3 histidine phosphatases, PHPT1, LHPP and PGAM5 (Fuhs and Hunter, 2017).Recently published work presented a modified mass spectrometry method for detection of 'non-canonical' phosphorylation, and estimated that these phosphorylation events are far more frequent than previously believed, and equal one third of total phosphorylation events (Hardman et al., 2019) Such techniques greatly improve our ability to study these phosphorylation events.

1.1.1 Protein kinases, their structure and activation

The human genome encodes 538 known kinases, of which 518 are protein kinases and 20 are lipid kinases. This collection of proteins is commonly referred to as the 'kinome'. Based on sequence similarity and functional annotation, the kinome is subdivided into 10 groups. 478 belong to a single superfamily, the typical eukaryotic protein kinases (ePKs), which evolved to share a common kinase domain fold, described further below. A further 40 'atypical' protein kinases (aPKs) do not share the typical kinase fold, however do carry kinase activity. One example of an atypical protein kinase is mTOR which is described in further detail in section 1.2.5 (G. Manning *et al.*, 2002).

The ePKs diverge into 9 groups, namely AGC (PKA, PKG, PKC family), CAMK (Ca^{2+}/Calmodulin-dependent kinases), CK1 (Casein Kinase 1 family), CMGC (CDK, MAPK, GSK and CLK family), STE (homologues of the yeast *sterile* kinases family), TK (Tyrosine kinase), TLK (Tyrosine kinase-like kinase family), RGC (Receptor Guanylate Cyclase), and 'Other' protein kinases that do not fit a particular group. (G. Manning *et al.*, 2002) (Figure 1.2). Protein kinases within a certain family typically have similar substrate preferences, and often also similar methods of activation and regulation. Highlighted in Figure 1.2 are the closely related SGK and Akt protein kinases, which are the focus of this thesis.

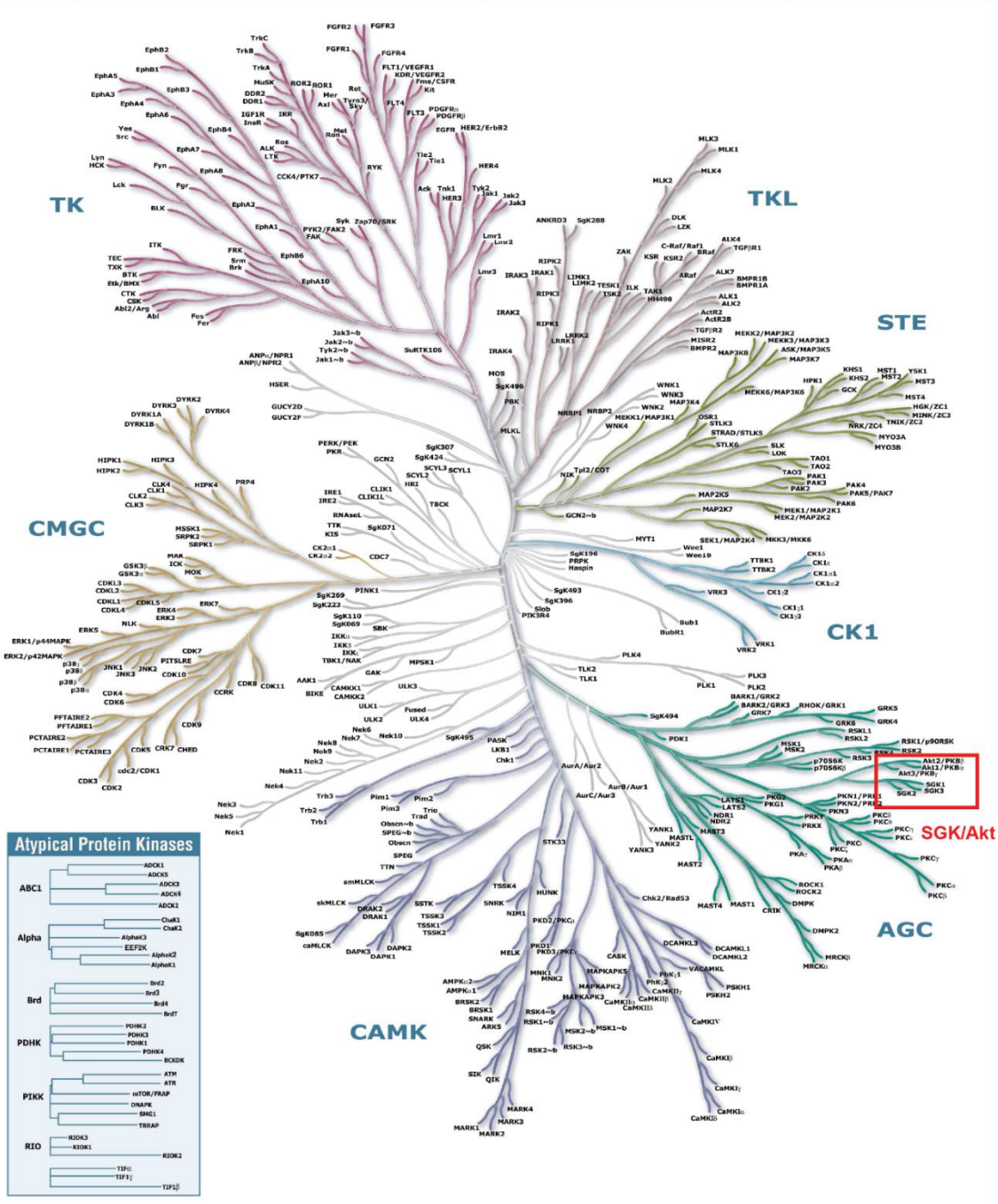

Figure 1.2 Tree of known human protein kinases
Protein kinases have evolved from a conserved kinase fold to form 10 kinase groups. Derived from (G. Manning et al*., 2002)*. Highlighted in red box are the SGK and Akt protein kinases, the focus of this thesis.

Protein kinases share a remarkably conserved catalytic region, termed the kinase domain. This kinase fold of 250-300 residues is highly conserved throughout evolution, however regulatory regions outside of this domain vary widely, particularly between kinase families. Figure 1.3

demonstrates the kinase domain of Akt (also known as Protein Kinase B). Akt is a member of the AGC protein kinase family, and its kinase domain is typical of this family of kinases. The kinase fold consists of 12 subdomains, organised into 2 lobes. The smaller N-lobe is formed of subdomains I-IV and contains a 5-stranded β-sheet and the regulatory αC-helix. The remaining subdomains V-XII form the largely α-helical C lobe. A hinge region links these 2 lobes, and the interface between them forms an important part of the active site. The N lobe is responsible for binding and coordination of the ATP for phosphotransfer, whereas the C lobe coordinates substrate binding and catalysis.

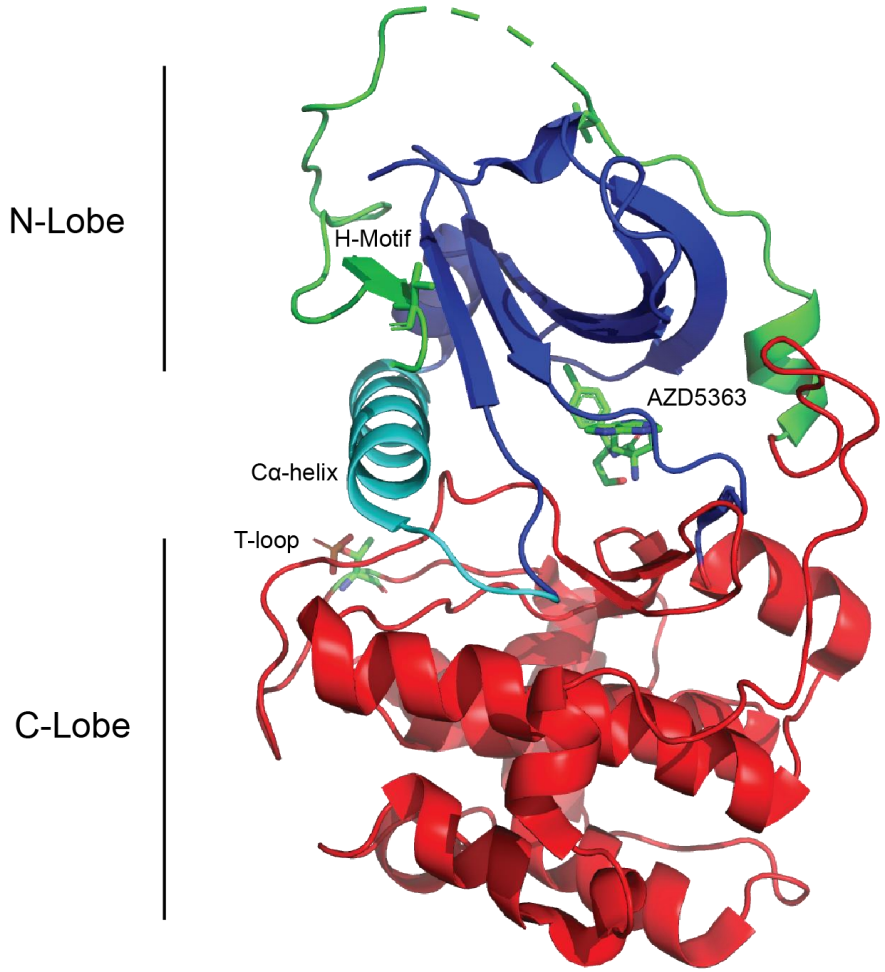

Figure 1.3 Crystal structure of Akt kinase domain from PDB 1GV1
The crystal structure of the Akt kinase domain was solved bound to the ATP competitive inhibitor AZD5363 (Addie *et al.*, 2013). *From PDB 1GV1, this structure shows the key structural features of the AGC kinase domain. The smaller N-lobe (blue) coordinates ATP (in this case, AZD5363) for transfer to substrate by the C-lobe (red). In cyan is demonstrated the Cα-helix, and, in green, the hydrophobic motif residues which interact with the N lobe, to stabilize the domain in an active conformation.*

There are a number of motifs highly conserved in protein kinases that are critical for activation and catalytic activity. Motifs within the N lobe are responsible for ATP binding and coordination. A GxGxxG motif binds the α and β phosphates of ATP, which are not transferred during phosphorylation, meanwhile the VAIK motif binds and positions the ATP. The lysine of this VAIK motif is the catalytic lysine critical for phosphorylation activity. Motifs within the C lobe are responsible for substrate binding and phosphotransfer. The HRDxxxxN motif contributes an Asp as proton acceptor for the catalytic reaction and the Asn coordinates one Mg^{2+} ion, while the DFG motif, which coordinates the second Mg^{2+} ion and its responsible for orientation of the ATP γ-phosphate. In addition, in this region an APE motif forms a salt bridge to subdomain XI for stabilization of the C lobe. In between these two motifs lies the critically important activation region of the T loop.

Surprisingly, 10% of the kinome comprises pseudokinases. These proteins are structurally related to kinases, and have maintained the typical protein kinase fold, however have lost residues critical for catalysis (Kwon *et al.*, 2019). Pseudokinases are well conserved and evolved alongside active kinases, likely evolving from gene duplication, which implies they still have, currently unknown, functional roles in signal transduction. For example, pseudokinases may act through regulating the activity of an active kinase, of through dynamic scaffolding functions (Rajakulendran and Sicheri, 2010; Shaw *et al.*, 2014). For example, pseudokinase FAM20A has no catalytic activity, however is a regulator of its counterpart FAM20C (Cui *et al.*, 2015, 2017). Some predicted pseudokinases bind nucleotides in different binding modes. For example, the SelO pseudokinase was found to bind ATP in an inverted conformation, and instead 'AMPylate' its substrate proteins (Sreelatha *et al.*, 2018). Further the bacterial pseudokinase SidJ was found to use a protein kinase fold to glutamylate the SidE family of E3 ligases and inhibit their activity (Black *et al.*, 2019).

Protein kinases are molecular switch proteins which can rapidly be activated or inactivated through phosphorylation. AGC protein kinases are typically activated by phosphorylation on two important residues, the T-loop (or activation loop) and the C-terminal hydrophobic motif residues. In the case of Akt, these residues are Thr308 and Ser473 respectively. The T loop of Akt is phosphorylated by 3-phosphoinositide dependent protein kinase-1 (PDK1) (Alessi, Deak, *et al.*, 1997; Alessi, James, *et al.*, 1997; Mora *et al.*, 2004). Phosphorylation of this residue allows for the displacement of the Cα-helix and stabilisation of the N- and C-lobes in the active conformation, permitting the proper orientation of the substrate (Hanks and Hunter, 1995; Johnson *et al.*, 1998). In figure 1.3, the T loop of AKT is observed to orientate the Cα-helix in cyan. Another critical activation residue of the AGC protein kinases is the hydrophobic motif residues. In AKT, this is Ser473 as is phosphorylated by mTORC2 (Sarbassov *et al.*, 2005). The hydrophobic motif residues interact with the N lobe of the protein, for further stabilization. In Figure 1.3 this is shown for AKT in green. For AKT, this additional phosphoactivation event maximally activates the kinase towards certain additional substrates (Guertin *et al.*, 2006; Jacinto *et al.*, 2006). For other kinases, such as the Serum and Glucocorticoid regulated protein kinases (SGKs), prior phosphorylation of this residue is critical for subsequent phosphorylation of the T-loop residue by PDK1 (Garcia-Martinez and Alessi, 2008). This mechanism is described in greater detail in section 1.4.1.

1.1.3 Protein phosphorylation in disease

Protein phosphorylation regulates a vast array of cellular processes. It is therefore unsurprising that mutations of the enzymes regulating phosphorylation cascades are linked to a wide spectrum of human diseases. Hereditary conditions linked to mutations of kinases have been extensively reviewed by Lahiry *et al,* and Alessi and Cohen. Inactivating and activating mutations in protein kinases can impact on a wide range of pathologies, including neurological disorders, immune disorders and hypertension, as well as skeletal abnormalities and errors in metabolism

(Lahiry *et al.*, 2010; Cohen and Alessi, 2013). For example, activating mutations in Leucine Rich Repeat Kinase 2 (LRRK2) are a risk factor for familial Parkinson's Disease (PD) (Alessi and Sammler, 2018). Although the mechanism by which LRRK2 mutations lead to PD are not yet known, all known pathogenic mutations result in an increase in kinase activity, therefore LRRK2 inhibitors are being investigated as a possible therapeutic in the clinic. Another example is the WNK1 (with-no-K(Lys)) and WNK4 kinases, which phosphorylate 2 downstream kinases STE20/SPS1-related proline/alanine-rich kinase (SPAK) and oxidative stress-responsive kinase 1 (OSR1) in the regulation of blood pressure, and mutation of these kinases can lead to hypertension (Vitari *et al.*, 2005; Richardson and Alessi, 2008). Activated SPAK/OSR1 phosphorylate and activate ion cotransporters such as the Na^+/Cl^- co-transporter (NCC) to regulate salt homeostasis (Gamba, 2005). Therefore, targeting of these kinases is an attractive target in lowering blood pressure.

The importance of protein phosphorylation in human disease is highlighted by the significant effort that has been devoted for the development of protein kinase inhibitors for the clinic, to treat a range of conditions (Cohen and Alessi, 2013). There are currently 52 kinase inhibitors approved for clinical use by the Food and Drug Administration (FDA), with many more in clinical development (See www.kinase-screen.mrc.ac.uk).

In addition, both hereditary and sporadic mutations of protein and lipid kinases are commonly found in human cancers. A current list of kinases implicated in oncogenesis by somatic or hereditary mutations is summarised in Table 1.1. This dataset is summarised from the COSMIC Cancer Gene Census (CGC), and describes 'Tier 1' genes with substantial evidence as a driver in tumorigenesis (Forbes *et al.*, 2011; Sondka *et al.*, 2018). A primary driver in many cancers is mutation in the PI3K-Akt-mTOR anabolic pathway, discussed in more detail in section 1.2

Table 1.1 Protein and Lipid kinases mutated in cancer.

Protein and Lipid kinases implicated in cancer, with either somatic or germline mutations. Adapted from the COSMIC Cancer Gene Census (CGC), described in (Forbes et al., 2011; Sondka et al., 2018) Only Tier 1 census genes, with extensive evidence demonstrating a functional role in cancer, are listed. OG = oncogene, TSG = Tumour suppressor gene, T = translocation, Mis = missense mutation, N = nonsense mutation, D = deletion, F = frameshift mutation, S = splice site mutation

Gene	Tumour Types (Somatic)	Tumour Types (Germline)	Cancer Syndrome	Role in Cancer	Mut Types
ABL2	AML			OG, fusion	T
ALK	ALCL, NSCLC, neuroblastoma, inflammatory myofibroblastic tumour, Spitzoid tumour	neuroblastoma	familial neuroblastoma	OG, fusion	T, Mis, A
ATR	endometrial, gastric, epithelial ovarian, myeloma	oropharyngeal	familial cutaneous telangiectasia and cancer syndrome	TSG	F; Mis
BTK	CLL, mantle cell lymphoma, WM			OG, TSG	Mis
CDK12	serous ovarian			TSG	Mis, N, F
CDK4		melanoma	familial malignant melanoma	OG	Mis
CDK6	ALL			OG, fusion	T
CDKN1B	breast, small intestine neuroendocrine tumours	pituitary, parathyroid	multiple endocrine neoplasia type IV	TSG	F
CDKN2A	melanoma, multiple other tumour types	melanoma, pancreatic	familial malignant melanoma	TSG	D, Mis, N, F, S
CDKN2C	glioma, MM			TSG	D
ERBB3	colon, gastric, head and neck, bladder, skin			OG	Mis, N
ERBB4	melanoma, gastric, NSCLC			OG, TSG	Mis, N
ETNK1	aCML, CMML, SM-AHD, HES			TSG	Mis
FES	HNSCC, ovarian carcinoma			OG, TSG	Mis, F
FLT3	AML, ALL			OG	Mis, O
FLT4	soft tissue sarcoma			OG	A
IKBKB	SMZL			OG	Mis
ITK	peripheral T-cell lymphoma			fusion	T
JAK1	ALL			OG, TSG	Mis
JAK2	ALL, AML, MPN, CML			OG, fusion	T, Mis, O
JAK3	acute megakaryocytic leukaemia, ETP ALL			OG	Mis
LATS1	skin basal cell carcinoma			TSG	Mis, N
LATS2	malignant mesothelioma			TSG	D, F, N
LCK	T-ALL			OG, fusion	T
MAP2K1	NSCLC, melanoma, colorectal			OG	Mis
MAP2K2	NSCLC, melanoma			OG	Mis
MAP2K4	pancreatic, breast, colorectal			OG, TSG	D, Mis, N
MAP3K1	luminal A breast			OG, TSG	N, F, Mis, O, S
MAP3K13	breast			OG, TSG	F
MAPK1	CLL, ovarian mixed germ cell tumour, cervical carcinoma			OG	Mis
NTRK1	papillary thyroid, Spitzoid tumour			OG, TSG, fusion	T, A
NTRK3	congenital fibrosarcoma, secretory breast			OG, fusion	T
PIK3CA	colorectal, gastric, glioblastoma, breast			OG	Mis
PIK3CB	SCC, NSCLC			OG	Mis
PIK3R1	glioblastoma, ovarian, colorectal			TSG	Mis, F, O
PRKACA	fibrolamellar hepatocellular carcinoma, cortisol secreting adrenal adenoma			OG	T, Mis, N
PRKAR1A	papillary thyroid	myxoma, endocrine, papillary thyroid	Carney complex	OG, TSG, fusion	T, Mis, N, F, S
PTK6	renal, gastric, head and neck, ovarian, others			OG, TSG	Mis, N
SRC	colorectal cancer, endometrial carcinoma			OG	Mis, N
STK11	NSCLC, pancreatic	jejunal hamartoma, ovarian, testicular, pancreatic	Peutz-Jeghers syndrome	TSG	D, Mis, N, F, S
SYK	MDS, peripheral T-cell lymphoma			OG, fusion	T

1.2 PI3K-mTOR pathway hyperactivation in breast cancer

1.2.1 Phosphatidylinositol signalling is mediated by phosphatidylinositol kinases and phosphatases.

As demonstrated in Figure 1.4, Phosphatidylinositol (PtdIns) is a glycerophospholipid, containing a glycerol backbone, two nonpolar fatty acid tails and a phosphate group linked to an inositol polar headgroup. This inositol headgroup is phosphorylated on various sites to produce a range of phosphatidylinositides (PtdInsP). These molecules form a minority of phospholipids on biological membranes, and yet are central in cellular signalling and as anchors for peripheral membrane proteins. Phosphorylation occurs on one of three hydroxyl groups (positions 3, 4, and 5) on the inositol ring, either alone or in combination to generate seven known PtdInsP. These phosphorylation events are performed by phosphatidylinositol kinases (PIKs) and removed by lipid phosphatases (Figure 1.4) (Bishé, Syed and Siddiqui, 2012).

Much of the work in this thesis focusses on the PI3Ks, which phosphorylate the 3-OH on the inositol headgroup of PtdIns on cellular membranes. These phospholipids then act as recruitment signals for effector proteins carrying, for example, PH domains (PtdIns(3,4,5)P_2) or PX and FYVE domains (PtdIns(3)P). As will be discussed in this section, the PI3K signalling pathway is a central pathway by which cells can detect and respond to external signals and regulate functions such as glucose metabolism and cell proliferation. The roles in growth and metabolism regulation implicate hyperactivation of this pathway in a number of human diseases including cancer.

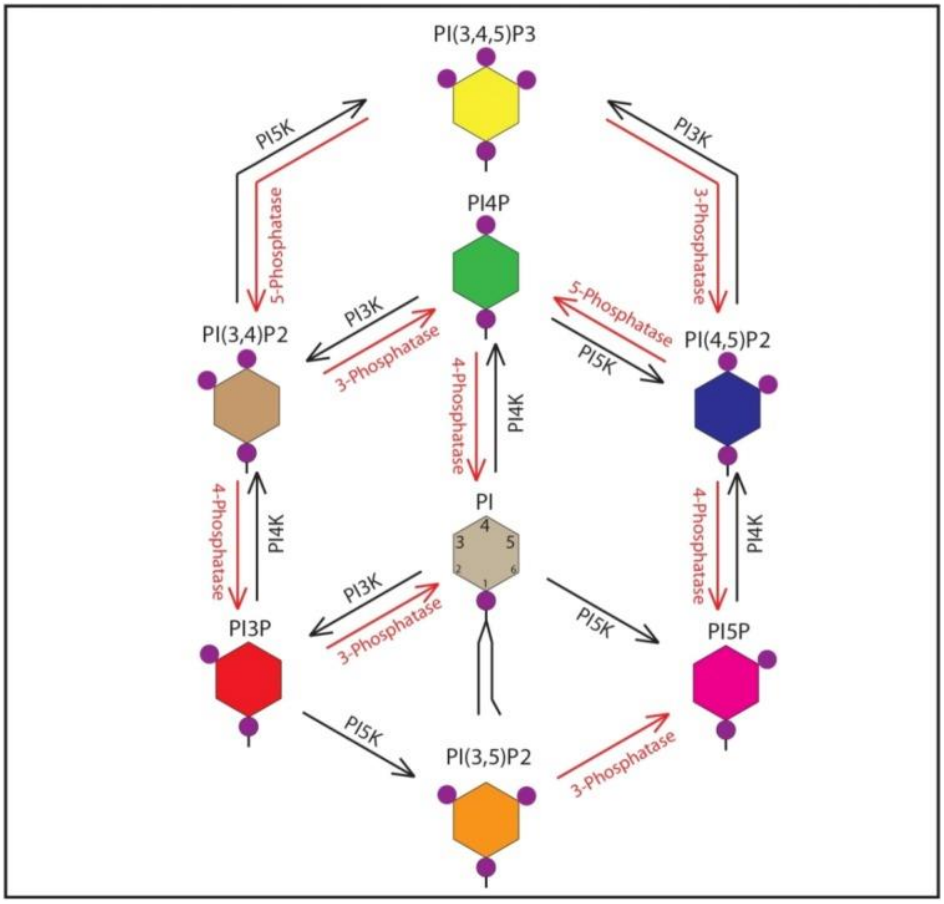

Figure 1.4 7 varieties of PtdInsP formed from phosphatidylinositol.
PtdInsP is modulated by phosphatidylinositol kinases (PIKs), represented in black, and lipid phosphatases, in red. From (Bishé, Syed and Siddiqui, 2012)

PI3Ks are grouped into 3 classes based on their domain organisation, however all contain a structurally related lipid kinase domain. Figure 1.5 describes the classification and domain structure of the PI3K family. The class I PI3Ks are the largest class and most highly studied, using phosphatidylinositol 4,5-bisphosphate (PtdIns(4,5)P_2) as a substrate to generate PtdIns(3,4,5)P_3. The generated PtdIns(3,4,5)P_3 has an important role in activating the PI3K-Akt-mTOR signalling axis, which will be discussed further below. Class II PI3Ks are less well understood, and contain a catalytic core similar to Class I, however contain a C-terminal PX-C2 domain and a variable N-terminal region. The Class III PI3K family consists of just one member, VPS34. VPS34 is present in all eukaryotes and is therefore considered the ancestral PI3K. Overall the domain structure of VPS34 is simpler than of the Class I and Class II PI3K, however instead acts within

heterotetrameric complexes (Vanhaesebroeck *et al.*, 2010; Vanhaesebroeck, Stephens and Hawkins, 2012).

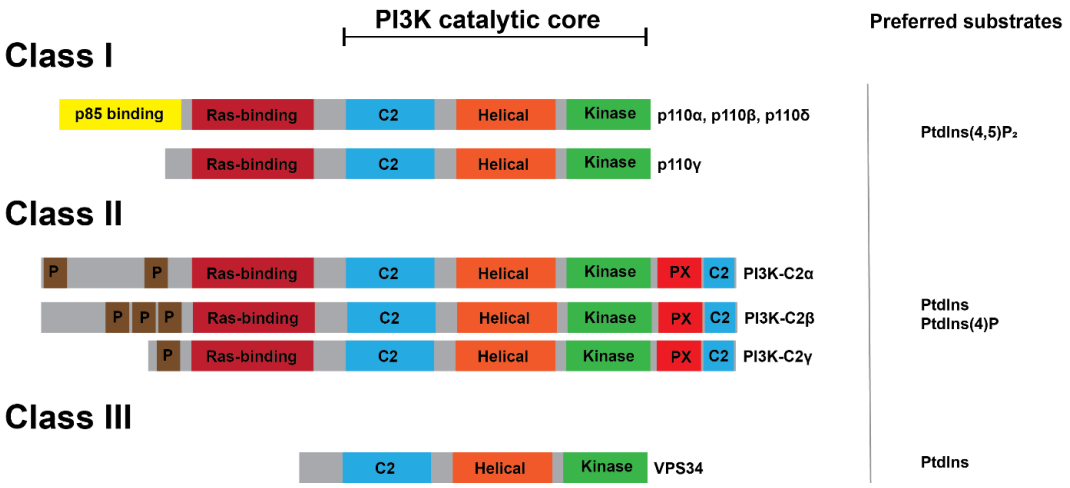

Figure 1.5 The catalytic subunits of the PI3K lipid kinase family.
The kinases are classified into three different classes based on their structural and biochemical features. The common, core catalytic domain consists of a C2 domain, a helical domain, and the catalytic kinase domain. Class I PI3K also contain a Ras-binding domain and a domain for binding to regulatory subunits. Class II PI3K, also known as PI3K-C2, contain an additional C-terminal PX and C2 domain. In addition, variable N-terminal Proline rich domains may mediate protein interactions, localisation and regulation. The sole Class III PI3K member, VPS34, is much simpler and contains just the catalytic core. Activity of VPS34 is regulated by a large complex. P = Proline rich region, PX = Phox Homology Domain. Adapted from (Vanhaesebroeck et al., 2010)

1.2.2 Class I PI3K

PI3K Class I act as heterodimers in cells. These dimers consist of a catalytically active p110 subunit, of which there are α, β, γ and δ variants, and a regulatory subunit. PI3K p110α, β and δ form a dimer with regulatory p85 subunits and are activated by Tyrosine autophosphorylation of Receptor Tyrosine Kinases (RTKs) (Figure 1.6A). There are 5 different regulatory subunits which activate class I PI3K under different stimuli (Vanhaesebroeck, Stephens and Hawkins, 2012). Docking of the p85 SH2 domain to pTyr allows for allosteric activation of the dimer. PI3K p110γ binds to either p101 or p84 regulatory subunits and is activated downstream of G-protein-coupled receptors (GPCR) signalling. p101 links p110γ to Gβγ subunits released from heterotrimeric G proteins downstream of GPCRs (Stephens *et al.*, 1994). Additionally, interaction of p110 with the small G-protein Ras can also contribute to the activation of PI3K (Rodriguez-Viciana *et al.*, 1994).

Class I PI3K form the major axis of canonical PI3K signalling, and the subsequent activation of Akt and mTORC1 in response to growth factor signals recognised by RTKs (Figure 1.6). Dimerization and autophosphorylation of RTKs generates phosphotyrosine for the recruitment of p85 by its SH2 domain (Escobedo *et al.*, 1991; Skolnik *et al.*, 1991). This process recruits PI3K to the plasma membrane and also relieves autoinhibition of p110 by p85 (Yu et al., 1998). The preferred substrate for Class I PI3K is PtdIns(4,5)P_2, which is phosphorylated at the 3-OH position to generate PtdIns(3,4,5)P_3 (Whitman *et al.*, 1988; Stephens and Downes, 1990). This action is reversed by the tumour suppressor, lipid phosphatase PTEN (phosphatases and tension homolog deleted on chromosome 10) (Maehama and Dixon, 1998; Myers *et al.*, 1998; Stambolic *et al.*, 1998) (Figure 1.6A).

Production of PtdIns(3,4,5)P_3, and its immediate product PtdIns(3,4)P_2, results in the recruitment of pleckstrin homology (PH) domain-containing effector proteins. Two critical proteins in the pathway containing a PH domain are 3-phosphoinositide-dependent protein kinase-1 (PDK1) (Alessi, Deak, *et al.*, 1997) and Akt (James *et al.*, 1996). This recruitment allows for the phosphorylation of Akt by PDK1 on its activation loop Thr308 and therefore its activation (Alessi, James, *et al.*, 1997). Activated Akt phosphorylates a number of substrates in the cell effecting biological processes such as cell growth and proliferation (Figure 1.6B).

1.2.3 Class II PI3K

Unlike Class I PI3K, Class II PI3K do not constitutively associate with regulatory subunits. There are 3 members of the PI3K Class II, PI3K-C2α, β or γ, which contain variable N- and C-terminal regions which may regulate their activity. In particular, all PI3K-C2 isoforms contain an additional C-terminal C2 domain (Gulluni *et al.*, 2019). Unlike the Class I and Class III PI3K, Class II PI3K isoforms are active as monomers, with no known obligatory regulatory subunits (MacDougall, Domin and Waterfield, 1995).

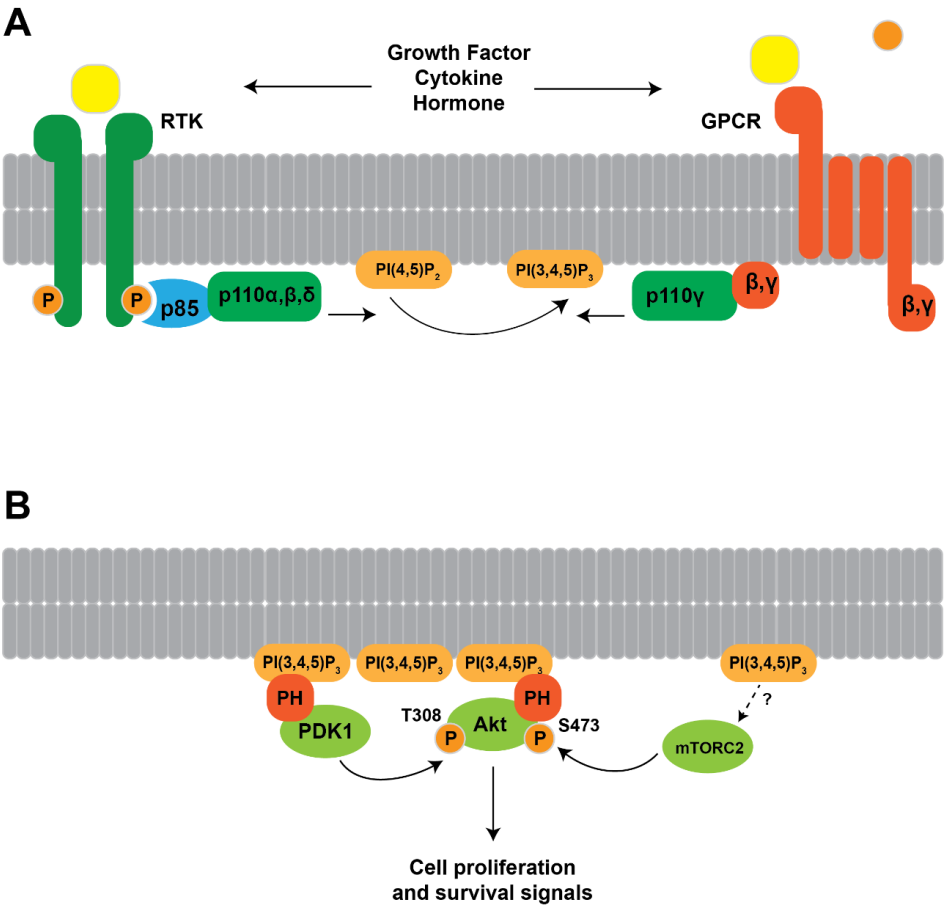

Figure 1.6. Activation and downstream effect of PI3K Class I
A. *Class I PI3K are activated by external stimuli such as growth factors, cytokines or hormones binding to Receptor Tyrosine Kinases (RTK) or G-protein coupled receptors (GPCR). Phosphorylated RTKs bind to regulatory p85, relieving inhibition of p110α,β,δ. p110γ is activated by binding to Gβγ proteins released from GPCRs. p110 preferentially uses PtdIns(4,5)P_2 as a substrate to generate PtdIns(3,4,5)P_3 on the plasma membrane* ***B.*** *PtdIns(3,4,5)P_s rich regions on the plasma membrane recruit Akt and PDK1 by virtue of their PH domains. mTORC2 is also recruited to the membrane by the PtdIns(3,4,5)P_3 signal. Colocalization of Akt with its activating kinases allows for its phosphorylation and activation, stimulating cell growth and survival signals. Modified from* (Vanhaesebroeck *et al.*, 2010; Yang *et al.*, 2019).

Until recently, the PI3K-C2 kinases were largely understudied, however recent findings suggests roles in both cell signalling and vesicle trafficking (Gulluni *et al.*, 2019). The Class II Isoforms each have the enzymatic capability to produce both PI(3)P and PI(3,4)P_2 in vivo, depending on their cellular context. Each isoform carries distinct and non-overlapping cellular roles in different tissues and cellular compartments (Margaria *et al.*, 2019).

PI3KC2α on early endosomal membranes will produce PtdIns(3)P from readily available PtdIns containing membranes, and mediates vesicle trafficking (Yoshioka *et al.*, 2012; Franco *et al.*, 2014). However, this isoform can also produce PtdIns(3,4)P_2 from PtdIns(4)P-rich areas of the plasma membrane to regulate clathrin-mediated endocytosis (Posor *et al.*, 2013).

PI3KC2β, however, primarily synthesises PtdIns(3)P both *in vitro* and *in vivo* (Maffucci and Falasca, 2014). Enzymatic activity of PI3KC2β has been linked to cell migration and formation of actin-rich lamellipodia (Domin *et al.*, 2005). PI3KC2β has also been linked to insulin sensitivity and regulation of mTORC1 (Alliouachene *et al.*, 2015; Marat *et al.*, 2017). PI3KC2α and PI3KC2β both have essential roles in clathrin-mediated pinocytosis, however PI3K-C2β was required for actin filament formation at the clathrin-coated structures (Aung *et al.*, 2019). PI3KC2γ can produce both PtdIns(3)P and PtdIns(3,4)P_2 *in vitro*, however in vivo primarily produces a pool of PtdIns(3,4)P_2 on endosomal membranes in response to insulin (Braccini *et al.*, 2015).

1.2.4 Class III PI3K

Class III PI3K, VPS34, generates PtdIns(3)P from PtdIns and is found in two distinct complexes within cells. The catalytically active VPS34 subunit forms a constitutive heterodimer with VPS15. VPS15 is myristoylated at Gly2, acting as a member anchor. This dimer forms 2 major complexes in cells, with different biological roles (Figure 1.7). In VPS34 Complex I, VPS34/VPS15 form a heterotetramer with Beclin1 and ATG14L. This complex is primarily on Rab7-containing membranes and involved in the activation and regulation of autophagy, and response to nutrient starvation (Kihara *et al.*, 2001; Itakura *et al.*, 2008; Matsunaga *et al.*, 2009). Complex II is formed with UVRAG in place of ATG14. This complex is found on Rab5- and Rab9-containing endosomal membranes and is critical for endocytic sorting, lysosome recycling and LC3-mediated phagocytosis (Liang *et al.*, 2008; Thoresen *et al.*, 2010; Martinez *et al.*, 2015; Munson *et al.*, 2015).

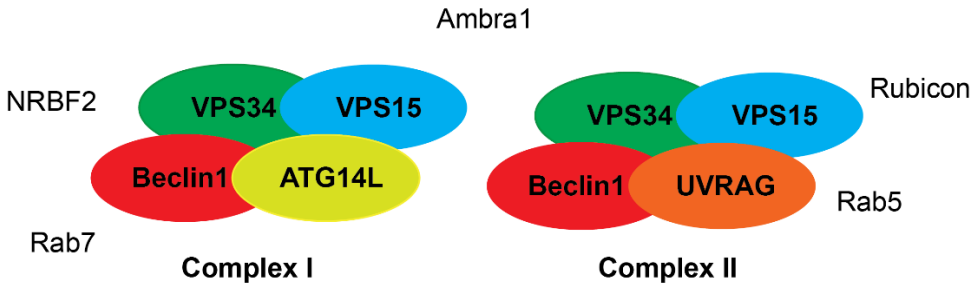

Figure 1.7 Complexes formed by Class III PI3K VPS34.
VPS34, VPS15 and Beclin1 form a heterotetramer with either ATG14L or UVRAG to form complex I or complex II respectively. More transient, accessory interactors include Rubicon and Rab5 interacting with Complex II, and NRBF2 and Rab7 interacting with Complex I. AmbraI has been observed to form very transient interactions with both complexes.

Differing complexes and localisation allows for the independent regulation of many distinct pathways controlled by PtdIns(3)P in the cell. For example, in the context of amino acid starvation, complex I is activated to regulate autophagy while other complexes are inhibited. This is due to the recruitment of ATG14L by ULK1, which phosphorylates Beclin1 for activation of the complex (Russell *et al.*, 2013). Differing activity of the complexes can also be regulated by curvature of the target membrane, therefore differentiating between different intracellular organelles. While, *in vitro*, both complexes I and II displayed similar activity on high curvature membranes, complex I had no measurable activity in flat membranes (Rostislavleva *et al.*, 2015).

Structural information on VPS34 complex

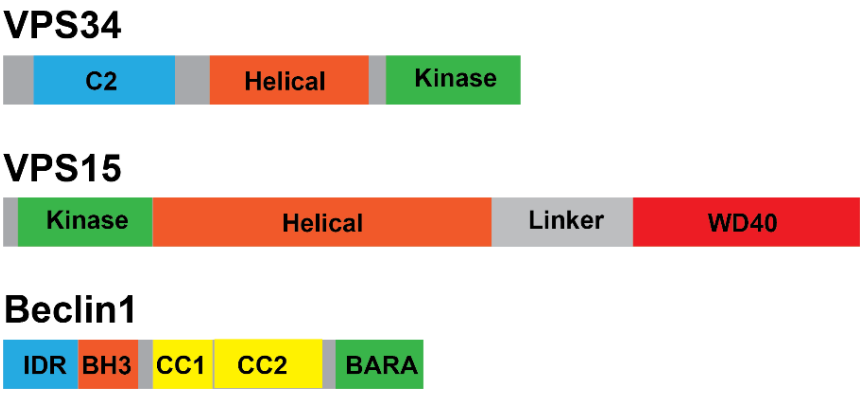

Figure 1.8 Domain structure of the core VPS34 complex members.
VPS34 interacts and dimerises with the WD40 domain of VPS15 via its N-terminal C2 domain. Binding to substrate membranes is via the kinase domain of VPS34 and the BARA domain of Beclin1. The core complex will associate with either ATG14L in Complex I or UVRAG in Complex II

Comprehensive structural studies of the VPS34 complexes has revealed additional information on the mechanisms of VPS34 activation. Both complexes form a “Y” shape on the target membrane. VPS34/VPS15 form as an obligate dimer and form a catalytic arm of the “Y” (Baskaran *et al.*, 2014; Rostislavleva *et al.*, 2015; M. Ma *et al.*, 2017). Beclin1 with ATG14 or UVRAG form a second, regulatory arm of the “Y”. These 2 arms bind to target membranes via the BARA domain of Beclin1 and the kinase domain of VPS34. Myristoylation of VPS15 at Gly2 also acts as a membrane anchor (Herman, Stack and Emr, 1991). *In vitro* studies of the human protein have also observed a high mobility of the VPS34 kinase domain relative to the rest of the complex (M. Ma *et al.*, 2017; Stjepanovic *et al.*, 2017).

VPS34 has a similar domain structure to the other PI3Ks, with an N-terminal C2 domain, Helical domain and a C-terminal Kinase domain (Figure 1.8). However, this domain structure is very simple in comparison to the Class I and Class II PI3K and the polypeptide does not contain other regulatory elements, as regulation is mediated by its complex members. The C2 domain is critical for interaction with the WD40 domain of VPS15 (Rostislavleva *et al.*, 2015). Also, residues of this domain can be phosphorylated by CDK1, CDK5 and AMPK which causes a reduction in VPS34 activity, possibly due to weakened complex stability (Furuya *et al.*, 2010; Kim *et al.*, 2013). Additionally, cleavage of this domain by caspase 8 causes decreased affinity for Beclin1, and reduced activity, demonstrating how critical this region is for VPS34 activity (Jiang *et al.*, 2017).

VPS15 is composed of an N-terminal pseudokinase domain, followed by a Helical domain, linker region and C-terminal WD40 domain critical for binding to VPS34 (Figure 1.8). Despite having no known kinase activity, the pseudokinase domain of VPS15 has been demonstrated to be critical for complex formation and VPS34 activation (Nemazanyy *et al.*, 2013). Somatic mutations in the pseudokinase domain have also been detected in cancer (Herman, Stack and Emr, 1991; Shull *et al.*, 2012). Beclin1 is extensively decorated with posttranslational modifications, which mediate its localization, binding partners and stability. For example, as described above, phosphorylation of Beclin1 by ULK1 and AMPK increases the activity of the autophagic complex I (Kim *et al.*, 2013;

Russell *et al.*, 2013; Egan *et al.*, 2015). Generally, autophagy-promoting modifications are largely found in the N-terminus and BH3 domain. Conversely, autophagy-inhibiting modifications are commonly found in its CC domains and membrane-binding BARA domain (Zalckvar *et al.*, 2009; Shi and Kehrl, 2010; Maejima *et al.*, 2013).

ATG14L completes VPS34 complex I, and contains 3 coiled coil domains, a C-terminal domain and a Barkor/Atg14L autophagosome targeting sequence (BATS) domain. At the N-terminus of ATG14L, two heavily conserved CXXC motifs are critical for localisation of ATG14 to the ER (Matsunaga *et al.*, 2010). Additionally, an N-terminal extension, present only in metazoans, contains a phosphorylation site at S27. Phosphorylation of this site by Ulk1 is triggered by amino acid starvation or inhibition of mTORC1 and activates VPS34 complex I activity, however it is currently unclear how this activation occurs (Park *et al.*, 2016). UVRAG is the subunit found exclusively in complex II. UVRAG-contained complexes are found to localise to Rab5- and Rab9-positive endosomes, and UVRAG is not found with autophagic complexes. Instead, the function of UVRAG-containing complexes is in endocytic trafficking and potentially autophagosome maturation (Knaevelsrud *et al.*, 2010; Takats *et al.*, 2014). Importantly, Rab5-positive endosomes have only UVRAG-containing complexes, not ATG14.

In addition to these stable complex members, there are several accessory subunits which bind to the complex more transiently. NRBF2 binds specifically to complex I, and boosts activity of the complex (Ohashi *et al.*, 2016; Young *et al.*, 2016). Phosphorylation of NRBF2 by mTORC1 decreases binding to complex I and reduces VPS34 activity (X. Ma *et al.*, 2017). Rubicon, alternatively, binds specifically to complex II and regulates its activity, however it has been reported to both increase and decrease activity of the complex and its role is not entirely clear (Matsunaga *et al.*, 2009; Matsunaga, Noda and Yoshimori, 2009; Zhong *et al.*, 2009; Martinez *et al.*, 2015). Additionally, AMBRA1 (activating molecule in Beclin-1-regulated autophagy) is an adaptor molecule which weakly associates with both complexes (Antonioli *et al.*, 2014). It is a largely disordered protein acts as a hub coordinating several processes to promote autophagy

and regulate mTOR signalling. It has been demonstrated to interact with Beclin1 and increase VPS34 complex activity (Cianfanelli *et al.*, 2015).

Posttranslational modifications regulating VPS34 activity

Binding of regulatory subunits to VPS34 is critical for mediating its subcellular activity. However, a range of post translational modifications also vastly regulate its activity. As described above, Beclin1 is heavily decorated with modifications which alter its localisation and activity of the VPS34. In addition, VPS34 itself can also be regulated by PTMs. For example, VPS34 can be acetylated by p300 at K29, K771 and K781. K771 is situated in the activation loop of VPS34 kinase domain and, importantly, binds to substrate PtdIns. Acetylation at this site by p300 substantially reduces VPS34 activity. Additionally, acetylation at K29 has been observed to reduce Beclin1 interaction and increase Rubicon interactions, potentially activating and deactivating VPS34 under the appropriate conditions. Within the helical domain of VPS34, two highly conserved lysine residues are poly-ubiquitinated by the UBC-13/UEV-1/CHN-1 complex. This polyubiquitylation stabilizes VPS34 and increases autophagosome maturation.

1.2.5 mTOR signalling downstream of PI3K

The mammalian target of rapamycin (mTOR) is a Ser/Thr protein kinase, and central integrator of a wide variety of cellular signals that control cell growth and homeostasis. It is an atypical protein kinase of the PI3K-like Kinase (PIKK) family. mTOR is the mammalian homolog of yeast target of rapamycin (TOR). It is inhibited by the macrolide Rapamycin, discovered due to its anti-proliferative properties (Heitman, Movva and Hall, 1991; Brown *et al.*, 1994; Sabatini *et al.*, 1994; Sabers *et al.*, 1995). mTOR exists in at least two distinct complexes termed mTOR complex 1 (mTORC1) and mTORC2, shown in figure 1.9. Both complexes contain mTOR and accessory proteins termed mammalian lethal with sec-13 protein 8 (mLST8, also known as GβL) (Kim *et al.*, 2003; Jacinto *et al.*, 2006), DEP domain containing mTOR-interacting protein (Deptor) (Peterson *et al.*, 2009) and Tti1/Tel2 complex (Kaizuka *et al.*, 2010). mTORC1 is completed by regulatory-associated protein of mammalian target of rapamycin (Raptor) (Hara *et al.*, 2002; Kim *et al.*,

2002), and proline-rich Akt substrate 40 kDa (PRAS40) (Sancak *et al.*, 2007; Thedieck *et al.*, 2007; Vander Haar *et al.*, 2007; Wang *et al.*, 2007). mTORC2 uniquely contains Rapamycin-insensitive companion of mTOR (Rictor) (Jacinto *et al.*, 2004; Sarbassov *et al.*, 2004), mammalian stress-activated map kinase-interacting protein 1 (mSin1) (Frias *et al.*, 2006; Jacinto *et al.*, 2006) and protein observed with Rictor 1 and 2 (Protor1/2) (Pearce *et al.*, 2007; Thedieck *et al.*, 2007; Woo *et al.*, 2007).

Activity of these 2 distinct complexes can be delineated with Rapamycin. mTORC1 is acutely sensitive to rapamycin whereas mTORC2 is only affected by chronic rapamycin treatment (Sarbassov *et al.*, 2004, 2006; Phung *et al.*, 2006). Cryo-EM advances have allowed the structure of both complexes to be solved, providing insights into their differential activity and regulation (Aylett *et al.*, 2015; X. Chen *et al.*, 2018).

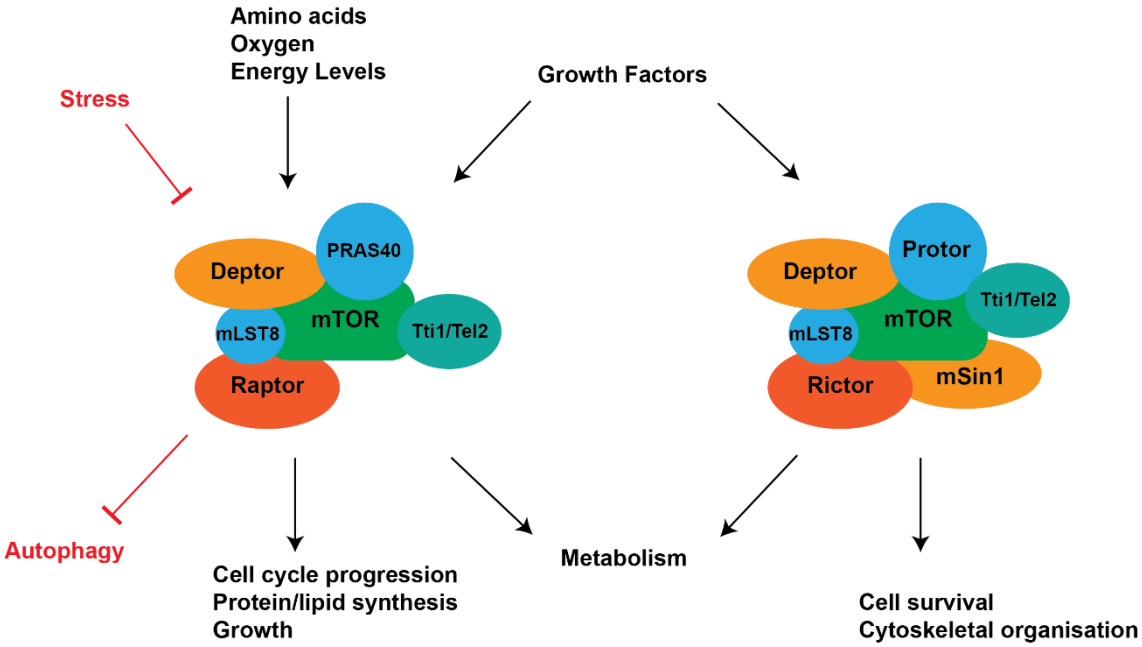

Figure 1.9 mTOR forms two complexes in cells
mTORC1 is formed of mTOR, Raptor and mLST8, with PRAS40 and Deptor. mTORC2 is formed of mTOR, Rictor and mLST8, with Deptor and Protor. These two complexes are activated by different cellular signals and perform different functional roles. Adapted from (Saxton and Sabatini, 2017)

mTORC1

mTORC1 is the better characterised complex of mTOR and coordinates a vast array of upstream signals relating to cell growth and metabolism. mTORC1 has been demonstrated to be regulated by a) growth factor signalling, b) cellular stress, c) cellular energy status, d) oxygen, and e) amino acids. Downstream of these signals, mTORC1 regulates cell growth and proliferation by promoting anabolic processes and by inhibiting the catabolic process of autophagy (Figure 1.9) (Saxton and Sabatini, 2017).

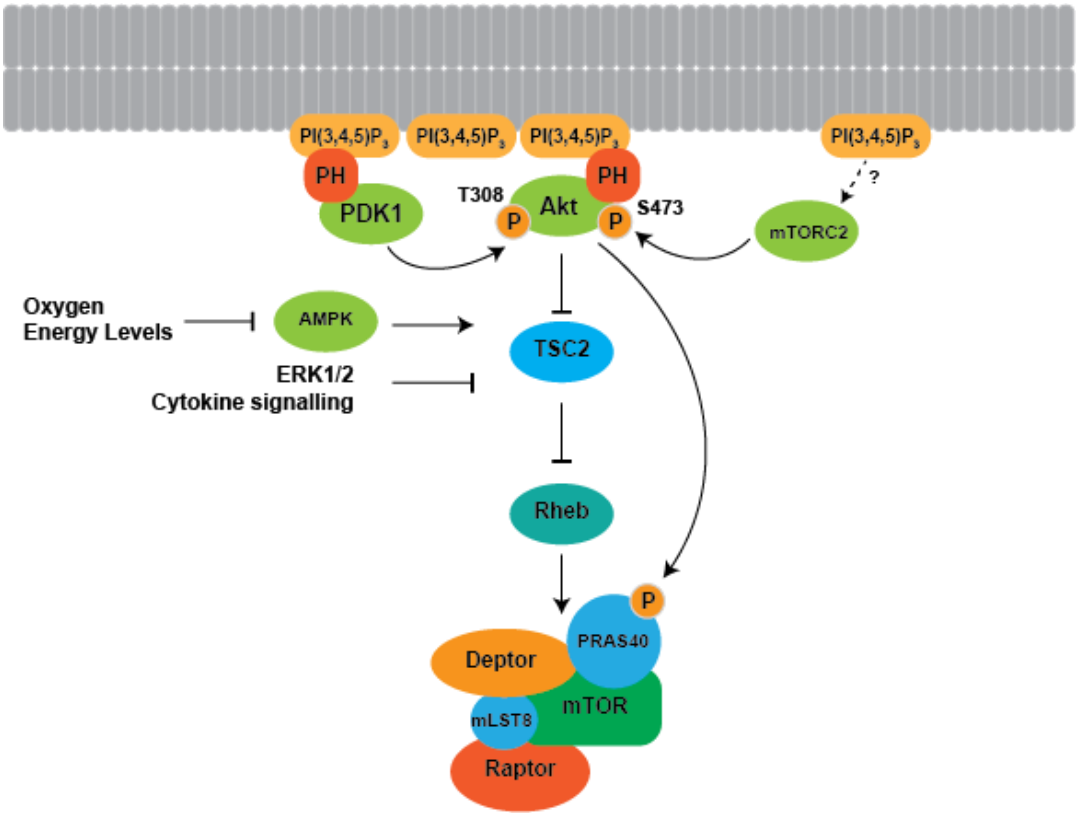

Figure 1.10 Activation of mTORC1 in response to growth factors and cellular energy through TSC2.
On activation of the PI3K signalling pathway, Akt is activated by phosphorylation by PDK1 and mTORC2. Active Akt phosphorylates TSC2, relieving its inhibition on Rheb. Activation of Rheb allows the activation of mTORC1 signalling. Akt also phosphorylates PRAS40, releasing the inhibitory factor from the mTORC1 complex. Other signals of cellular energy mediate mTORC1 activation through TSC2, via AMPK or MAPK and cytokine signalling.

A key signal for mTORC1 activation is in response to Growth Factors, and cellular energy levels, mediated through tuberous sclerosis 2 (TSC2). Within the PI3K-Akt-mTOR signalling axis, Akt mediates the activation of mTORC1 via phosphorylation of TSC2 and PRAS40. Akt phosphorylates TSC2 at Ser939 and Thr1462. This results in the dissociation of the TSC1/2

heterodimer from the GTPase Ras homolog enriched in brain (Rheb) (B. D. Manning *et al.*, 2002; Inoki *et al.*, 2002). In its GTP-bound state, Rheb will directly bind to and activate mTORC1. TSC1/2 complex acts as a GTPase-activating protein (GAP) for Rheb, therefore its dissociation allows accumulation of Rheb-GTP to activate mTORC1 (Inoki *et al.*, 2003; Tee *et al.*, 2003). The TSC1/2 is also phosphorylated at alternative sites and inactivated by other effector kinases of growth factor signalling pathways, such as the extracellular-signal-regulated kinases 1/2 (ERK1/2) and cytokines (Ma *et al.*, 2005; Lee *et al.*, 2007; Laplante and Sabatini, 2012). Akt also phosphorylates PRAS40 at Thr246, triggering its dissociation from mTORC1, relieving its inhibition of the complex (Sancak *et al.*, 2007; Thedieck *et al.*, 2007; Vander Haar *et al.*, 2007; Wang *et al.*, 2007) (Figure 1.10).

However, it is important that mTORC1-mediated anabolism only occurs under conditions of sufficient cellular energy and substrates for macromolecular synthesis. Glucose deprivation and hypoxia activate the AMP-regulated protein kinase AMPK, which will phosphorylate and activate TSC2 (Brugarolas *et al.*, 2004; Kalender *et al.*, 2010; Efeyan *et al.*, 2013), leading to inhibition of mTORC1 activity. Further, exquisite mechanisms have evolved by which mTORC1 senses cellular amino acid levels, and activation of mTORC1 by Rheb-GTP only occurs in the presence of amino acids (Figure 1.10).

This has been shown to be mediated by the Rag GTPases, vacuolar v-ATPase and Ragulator (E. Kim *et al.*, 2008; Sancak *et al.*, 2008, 2010; Zoncu *et al.*, 2011; Bar-Peled *et al.*, 2012). Accumulation of amino acids in the lysosomal lumen promotes the loading of the RagA/B heterodimer with GTP, allowing its interaction with the mTORC1 subunit Raptor, and translocation of mTORC1 from the cytosol to the lysosomal surface (Laplante and Sabatini, 2012; Jewell, Russell and Guan, 2013). On the lysosomal surface, the RagA/B dimer docks onto Ragulator, and mTORC1 can interact with Rheb-GTP, located throughout the endomembrane system. This checkpoint mechanism ensures that mTORC1 will only be activated if amino acids

are available, irrespective of other positive signals. Interaction of the v-ATPase with Ragulator is also believed to be important for mTORC1 activation on lysosomal membranes (Zoncu *et al.*, 2011).

More recent advances have also determined how Rag-mediated activation of mTORC1 senses cytosolic amino acid levels, through the GATOR1/GATOR2 complexes. The GATOR1 complex acts as a GTPase-activating protein (GAP) for RagA/B, and therefore inhibits mTORC1 activation on the lysosomal membrane. GATOR2, on the other hand, is a positive regulator of mTORC1 signalling, as it interacts with and inhibits GATOR1 (Bar-Peled *et al.*, 2013; Wolfson *et al.*, 2017). The activity of GATOR2 is then regulated by cytosolic amino acid sensors, which bind and inhibit GATOR2 in the absence of amino acids. Sestrin2 is a cytosolic leucine sensor, which binds GATOR2 in the absence of leucine, and releases it upon leucine binding (Chantranupong *et al.*, 2014; Parmigiani *et al.*, 2014; Saxton, Knockenhauer, *et al.*, 2016; Wolfson *et al.*, 2016). CASTOR similarly binds and inhibits GATOR2, dissociating upon binding of cytosolic arginine (Chantranupong *et al.*, 2016; Saxton, Chantranupong, *et al.*, 2016).

mTORC2

mTORC2 is insensitive to nutrients, however is also regulated by growth factors via relatively poorly understood mechanisms mediated by PI3K. mTORC2 has also been shown to associate with ribosomes following PI3K activation and the activation of mTORC2 is suggested to be dependent on ribosomes, but not protein synthesis (Zinzalla *et al.*, 2011)

PI3K-dependent activation of mTORC2 may be mediated by PtdIns(3,4,5)P_3 itself. Increased PtdIns(3,4,5)P_3 levels correlate with increased mTORC2 activity and recent studies suggest a direct activation of mTORC2 by PtdIns(3,4,5)P_3 (Gan *et al.*, 2011; Liu *et al.*, 2015). Liu *et* al., recently proposed that PtdIns(3,4,5)P_3 is activating mTORC2 via the PH domain of mSin1. Their proposed model suggested an autoinhibition of mTOR by the PH domain of mSin1, which was relieved on PH binding to PtdIns(3,4,5)P_3 (Liu *et al.*, 2015).

The best-characterised substrates of mTORC2 are the AGC protein kinases, phosphorylating their hydrophobic motif residues leading to their activation. Akt activity against certain substrates appears to be modulated by mTORC2 activity, whereas hydrophobic motif phosphorylation of SGK is critical for its activation (Guertin *et al.*, 2006; Jacinto *et al.*, 2006; Garcia-Martinez and Alessi, 2008). Through phosphorylation of its substrates, mTORC2 has roles in controlling cell survival and proliferation, as well as cytoskeletal organisation (Laplante and Sabatini, 2012).

1.2.6 Hyperactivation of the PI3K pathway in breast cancer

Due to its role in mediating many processes in cell growth and metabolism, aberrant activation of the PI3K pathway is frequently observed in breast cancer. It is estimated that 70% of all breast cancer cases harbour hyperactivated PI3K signalling (Miller *et al.*, 2011). This hyperactivation of the pathway can be achieved in a number of ways. Frequently observed alterations include, but are not limited to, amplification of RTKs, loss of PTEN or INPP4B (inositol polyphosphate-4-phosphatase) function, activating mutations of p110 catalytic subunit of PI3K, inactivating mutations of p85 regulatory subunit of PI3K or activating mutations of Akt or Ras. Mutations of the pathway in breast cancer was extensively reviewed by McKenna *et al*., and is summarised in table 1.2 below.

The most frequent pathway mutations, and the most important in the context of therapy, are PI3K and PTEN. The PI3KCA gene, encoding the p110α catalytic subunit, is the most frequently mutated PI3K pathway component in breast cancer (Zardavas, Fumagalli and Loi, 2012). 80% of these mutations occur in 1 of three hotspot regions, described by Samuels *et al*., which modulate PI3K regulation and activity (Samuels *et al.*, 2004). One hotspot is the E545K mutation in exon 9, located in the helical domain, which interferes with inhibitory binding of the p85 subunit. Mutations around H1047 in the kinase catalytic domain increase interaction of the kinase with the lipid membrane (Ikenoue *et al.*, 2005; Kang, Bader and Vogt, 2005; Vogt *et al.*, 2007; Jiang

et al., 2018). These mutations act by different mechanisms and therefore can combine for a synergistic effect on PI3K pathway activation (Zhao and Vogt, 2008). Additionally, important activating mutations also occur in the C2 domain (Croessmann *et al.*, 2018). Gene mutations in PTEN are relatively uncommon, and loss of function of PTEN frequently occurs through loss of heterozygosity at the 10q23 locus. This occurs in 30-40% breast cancer tumours, and results in constitutive activation of Akt (Li *et al.*, 1997; Liaw *et al.*, 1997; Wang *et al.*, 2014; C.-Y. Chen *et al.*, 2018). These alterations also occur in 80% of Cowden's syndrome patients, a condition which predisposes to breast cancer (Liaw *et al.*, 1997).

Table 1.2 Mutations within the PI3K pathway associated with breast cancer, stratified by subtype. *Modified from (McKenna, McGarrigle and Pidgeon, 2018). HR+ = hormone-receptor positive. HER2+ = human epidermal growth factor receptor 2 positive, TNBC = triple negative breast cancer. Data extracted from a = (Miller, 2011), b = (Kriegsmann et al., 2014), c = (Gonzalez-Angulo and Blumenschein, 2013), d = (Ellis and Perou, 2013), e = (Stern et al., 2015), f = Cancer Genome Atlas Network (CGAN, 2012), g = (Chin et al., 2014)*

Gene	Alteration	Effect on signalling pathway	HR+ (%)	HER2+ (%)	TNBC, (%)	Refs.
Receptors						
EGFR	Amplification	Activation of EGFR signalling	0.8	0.8	0.8-0.9	a, b
ERBB2	Amplification/Overexpression	Activation of ErbB2 signalling	10	100	0-3.8	a, b
FGFR1	Amplification/Activating mutation	Activation of FGFR signalling	8.6-11.6	5.4	5.6	a
IGF1R	Activating mutation/Amplification	Activation of IGF-1R signalling	41-48	18-64	42	a
PI3K						
PIK3CA	Activating mutation/Amplification	Activation of PI3K signalling	28-47	23-42	8-25.9	a, c, b
PIK3CB	Amplification	Unknown	5	5	5	a
PIK3R1	Inactivating mutation (p85α, p55α, p50α)	Increased p110a, catalytic activity	0.4-2	2-5	0-2	a, c, d
PIK3R3	Activating mutation (p55γ)	Activation of PI3K signalling	0-0.8	0	0	c
Lipid phosphatases						
PTEN	Loss of heterozygosity	Activation of PI3K signalling	4-44	5.4-22	4.8-67	a, b, e, f
INPP4B	Under-expression	Loss of AKT signalling regulation	10-33	30-54	30-53	a, c
Akt						
AKT1	Activating mutation	Activation of AKT signalling	2-4	0-2	0-0.9	a, c, b
AKT2	Amplification	Activation of AKT signalling	0-2.8	0-2.8	0-2.8	a, c
AKT3	Activating mutation/ Amplification	Activation of AKT signalling	0.4-0.8	0	1-28	c, g
Other regulators						
KRAS	Activating mutation	Hyperactivation of PI3K and MEK	4-6	4-6	0.9-6	a, b
LKB1	Under-expression	Loss of AKT signalling regulation	4.3-8.6	-	-	a
PDK1	Amplification/Overexpression	Activation of AKT signalling	22	22	38	a
RPS6K1	Amplification	Unknown	3.8-12.5	3.8-12.5	3.8-12.5	a

1.2.7 PI3K Inhibitors to treat cancer

Due to the hyperactivation of PI3K-signalling being frequently observed in breast cancer, a wide range of inhibitors have been developed targeting this pathway with the aim of therapeutically targeting cancer. These inhibitors commonly target either PI3K, Akt or mTOR. In addition, PI3K-mTOR dual inhibitors have been developed, as well as isoform specific PI3K inhibitors. Current inhibitors in clinical trials are summarised in Figure 1.11. P110α inhibitor BYL719 from Novartis has recently been approved by the FDA for treatment of advanced ER+ PI3KCA mutant breast cancer under the brand name Piqray. The drug has been approved in combination with Fulvestrant, after their SOLAR-1 study demonstrated the combination almost doubled progression-free survival (PFS) compared to Fulvestrant alone, extending PFS to 11 months compared to 5.7, and more than doubled the overall response rate to 38% from 16% (André *et al.*, 2019). Targeting p110α specifically reduced off target toxicity associated with pan inhibitors which also target the p110β/δ isoforms (Baselga *et al.*, 2018).

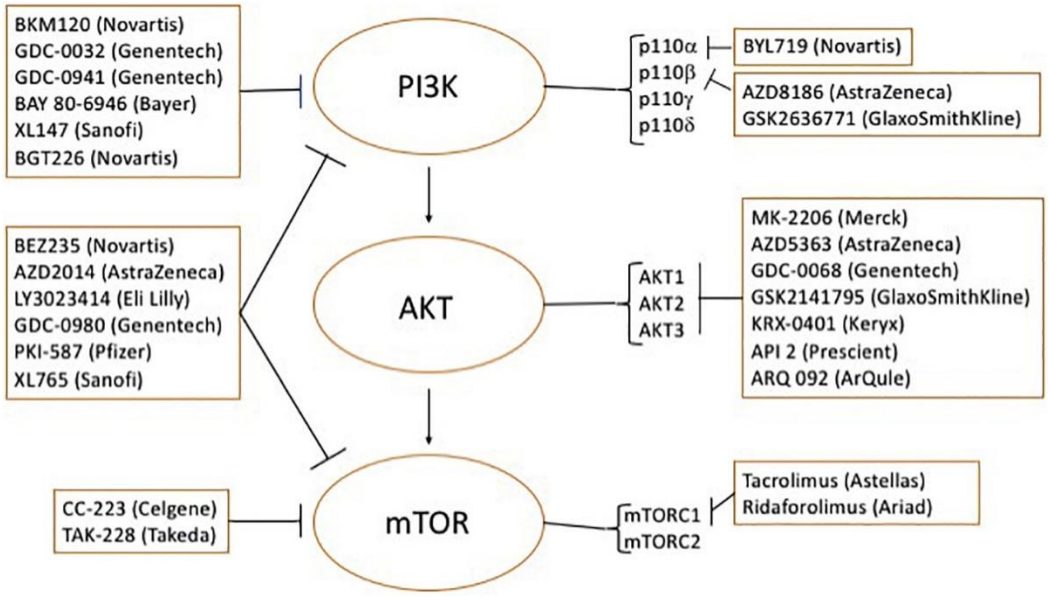

Figure 1.11 Inhibitors of the PI3K-Akt-mTOR pathway in clinical trials against Breast Cancer.
From (McKenna, McGarrigle and Pidgeon, 2018).

1.3 Akt protein kinases

The Akt isoforms are members of the AGC family of Ser/Thr protein kinases. As discussed above, Akt is critical in the activation of mTORC1 by phosphorylation of PRAS40 and TSC2. As well as mTORC1 activation, Akt phosphorylates a wide array of substrates involved in regulating metabolism, and cell survival and proliferation (Manning and Cantley, 2007).

1.3.1 Activation of Akt

Akt is activated downstream of PtdIns(3,4,5)P_3 production by Class I PI3K on the plasma membrane. Akt is recruited to PtdIns(3,4,5)P_3 rich membranes by virtue of its N-terminal PH domain, where it is phosphorylated on its activation loop residue Thr308 by PDK1, and its hydrophobic motif residue Ser473 by mTORC2 (James *et al.*, 1996; Alessi, Deak, *et al.*, 1997; Alessi, James, *et al.*, 1997; Sarbassov *et al.*, 2005). Many AGC protein kinases, such as the SGK family, require prior phosphorylation on their hydrophobic motif residue for subsequent phosphorylation of the activation loop by PDK1. This occurs via a PDK1-interacting fragment (PIF)-dependent mechanism by which a conformational change allows the protein to dock to the PIF-pocket of PDK1, leading to its activation loop phosphorylation. Akt, however, can be phosphorylated by PDK1 by a PIF-independent mechanism, through co-recruitment to PtdIns(3,4,5)P_3 rich plasma membranes.

Akt is also autoinhibited in the cytosol, through allosteric inhibition by its PH domain in the absence of PI(3,4,5)P_3. On engagement with PtdIns(3,4,5)P_3 on the membrane, this autoinhibition is relieved. The autoinhibited form of Akt in the cytosol is also held more susceptible to phosphatase mediated inactivation (Ebner, Lučić, *et al.*, 2017; Lučic *et al.*, 2018).

The precise mechanism of Akt activation in response to membrane binding and hydrophobic motif phosphorylation is still unclear, with 2 recent papers proposed differing mechanisms by which Akt is fully activated. Lučic *et al* proposed a model whereby PtdIns(3,4,5)P_3 binding of the PH domain is critical for Akt activation, as in the inactive state the PH domain occludes substrate

binding in the active site, also maintaining Akt in a conformation more open to cytosolic phosphatases. They also propose that phosphorylation of Akt on its activation sites does not override occlusion of the active site by the PH domain in the absence of membrane binding (Lučic *et al.*, 2018). Alternatively, Chu *et al* used protein semisynthesis to study purified Akt phosphorylated on its hydrophobic motif. They demonstrated motif phosphorylation relieves auto-inhibition of the PH domain on the kinase domain by interaction with a hydrophobic patch on the PH-kinase linker (Chu *et al.*, 2018).

1.3.2 Downstream substrates of Akt

Once activated, Akt phosphorylates a wide array of substrates, which through different mechanisms drive cellular metabolism, as well as proliferation and survival. It is currently under debate whether Akt must remain at the membrane to phosphorylate its substrates, or once activated it can phosphorylate substrates elsewhere in the cell (Ebner, Lučić, *et al.*, 2017; Chu *et al.*, 2018; Lučic *et al.*, 2018). Akt has a very well characterised RXRXXpS/T substrate motif, which it shares with the SGK family of protein kinases, discussed further in section 1.4 (Pearson and Kemp, 1991; Alessi *et al.*, 1996). More recent data has demonstrated that Akt prefers large hydrophobic residues at its +1 site, whereas the SGK kinases can tolerate a wider range of residues at this site (Murray *et al.*, 2005; Malik *et al.*, 2019). The first identified substrate of Akt was the protein kinase Glycogen Synthase Kinase 3 (GSK3) (Cross *et al.*, 1995), which when phosphorylated is inhibited, allowing cell cycle progression. Since then, a variety of substrates have been identified, by which Akt mediates cell growth and metabolism, cell proliferation, and cell survival (Manning and Cantley, 2007). These are summarised in Figure 1.12 and discussed in more detail below.

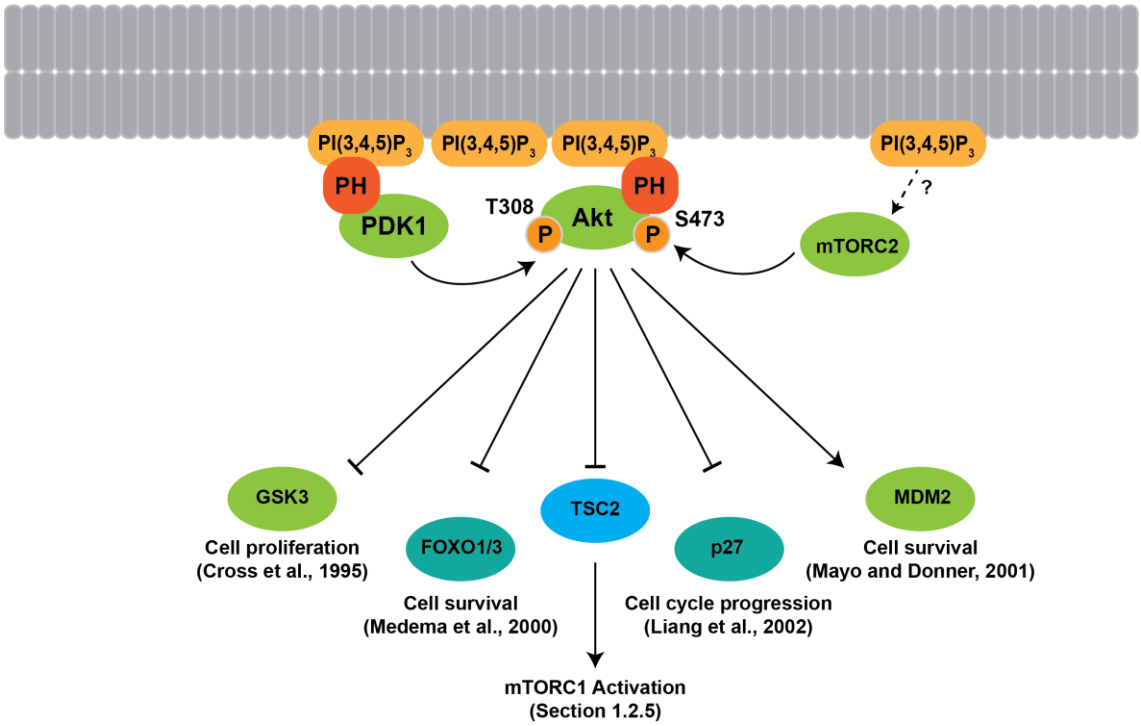

Figure 1.12 Schematic of Akt activation downstream PtdIns(3,4,5)P$_3$, and examples of its downstream substrates in cell growth and survival.

Cell growth and metabolism

The most well characterised role of Akt is in its activation of mTORC1, and subsequent driving of protein and lipid synthesis and other anabolic processes. It was described in section 1.2.4 how Akt activates this process through phosphoinactivation of PRAS40 and TSC2. Once activated, mTORC1 is a promotor of translation initiation and ribosome biogenesis. mTORC1 is therefore critical in enhancing protein and lipid synthesis to mediate cellular growth and metabolism through phosphorylation of its substrates.

Akt is a major regulator in glucose metabolism, through regulation of plasma membrane transporters. A primary glucose transporter in cells is GLUT1 and is regulated largely through its expression levels. Activation of mTORC1 can promote expression of GLUT1 through Hif1α-dependent transcription of the GLUT1 gene and cap-dependent translation of its mRNA (Zelzer *et al.*, 1998; Taha *et al.*, 1999). In addition, activation of Akt has been associated with increased translocation of glucose transporter GLUT4 to the plasma membrane, and therefore increased

glucose uptake (Kohn *et al.*, 1996). It has been proposed that this translocation is mediated by direct phosphorylation by Akt of the Rab GTPase-activating protein AS160 (Sano *et al.*, 2003; Eguez *et al.*, 2005), and alanine mutation of target sites blocked insulin-stimulated GLUT4 translocation (Sano *et al.*, 2003). Akt is also proposed to regulate expression of other nutrient transporters in an mTORC1-dependent manner (Edinger and Thompson, 2002).

Cell proliferation

A number of Akt substrates regulate the process of cell proliferation and cell division, and phosphorylation by Akt can promote these processes. Phosphorylation of GSK3 by Akt inhibits its activity, leading to the stabilization of proteins that play key roles in G_1-S transition (Cross *et al.*, 1995). Phosphorylation of cyclin D and cyclin E, as well as transcription factors c-jun and c-myc, targets them for degradation and inhibits the cell cycle (Diehl *et al.*, 1998; Welcker *et al.*, 2003; Yeh *et al.*, 2004; Wei *et al.*, 2005). Therefore, inhibition of this pathway by Akt-mediated phosphorylation of GSK3 promotes cell proliferation. Activation of mTORC1 by Akt also promotes activation of eIF4E, promoting cap-dependent translation of cell cycle promoters such as cyclin D1 and c-Myc (Mamane *et al.*, 2004).

Additionally, Akt phosphorylates p27, the Cyclin-dependent kinase inhibitor, at T157, creating a 14-3-3 binding site and blocking nuclear localisation (Liang *et al.*, 2002; Shin *et al.*, 2002; Viglietto *et al.*, 2002; Sekimoto, Fukumoto and Yoneda, 2004). This impedes its inhibitory effects and promotes progression through the cell cycle. Akt can also inhibit expression of p27 through FOXO inhibition (Medema *et al.*, 2000), discussed in further detail below. Similarly, Akt has been found to phosphorylate cyclin-dependent kinase inhibitor p21, again leading to its cytosolic localisation (Zhou, Liao, Xia, Spohn, *et al.*, 2001).

Cell survival

Finally, phosphorylation of substrates by Akt blocks the function or expression of many pro-apoptotic proteins, and as a result Akt actively promotes cell survival. Akt regulates the expression and activity of many Bcl2-homology domain 3 (BH3)-only proteins. For example, Akt

will directly phosphorylate FOXO transcription factors, leading to their binding to 14-3-3 proteins, and nuclear export and degradation (Tran *et al.*, 2003). This therefore results in reduced expression of FOXO target genes such as the proapoptotic cytokine FasL (Brunet *et al.*, 1999) and BH3-only protein BIM, which stimulates cell death upon cytokine withdrawal (Dijkers *et al.*, 2002). Akt also phosphorylates and inhibits BAD, a pro-apoptotic Bcl-2 family member. Phosphorylation of BAD at S136 again creates a binding site for 14-3-3 proteins, and triggers the release of BAD from its target proteins (Datta *et al.*, 1997, 2000; del Peso *et al.*, 1997). Finally, Akt will directly phosphorylate MDM2, an E3 ligase which mediates degradation of p53. Phosphorylated MDM2 translocates to the nucleus and there negatively regulates p53 function (Mayo and Donner, 2001; Zhou, Liao, Xia, Zou, *et al.*, 2001) resulting in the downregulation of proapoptotic p53 targets such as Puma and Noxa (Villunger *et al.*, 2003).

Akt mutation and cancer

Given the role Akt plays in a vast array of pro-survival pathways, it is unsurprising that activating mutations in Akt or its upstream regulators are frequently found in a numerous cancers. For example, a Glu17Lys mutation within the PH domain of Akt1 causes constitutive Akt1 plasma membrane association and activation (Carpten *et al.*, 2007), and the analogous mutation has also been reported in Akt2 and Akt3 (Davies *et al.*, 2008; Stephens *et al.*, 2012). Glu17Lys has been identified as a hotspot mutation in a wide range of cancer types (Bleeker *et al.*, 2008; Do *et al.*, 2008; M. S. Kim *et al.*, 2008; Cohen *et al.*, 2010; Chang *et al.*, 2016; Rudolph *et al.*, 2016)**.** Studies by Parikh *et al*. suggested the majority of activating Akt mutations disrupt autoinhibitory PH-kinase domain interactions (Parikh *et al.*, 2012). For example, L52R mutation is predicted to severely weaken PH domain interactions with V270, V271, Y326 and R328 of the kinase domain. Additionally, Q79K mutant PH domain exhibited weaker interaction with the kinase domain (Kan *et al.*, 2010; Parikh *et al.*, 2012; Yi *et al.*, 2012; Yi and Lauring, 2015). Ebner *et al also* observed that a somatic cancer mutation (D323A) drives Akt hyperactivation by relieving autoinhibition, leading to phosphorylated, active Akt in the cytosol (Ebner, Lučić, *et al.*, 2017).

1.4 SGK Protein kinases and Akt-independent oncogenic signalling

The serum- and glucocorticoid-regulated kinase (SGK) family of protein kinases are AGC protein kinases carrying very high homology to Akt. Their kinase domains share 45-55% identity and they share an overlapping RxRxxS/T substrate recognition motif (Webster *et al.*, 1993; Alessi *et al.*, 1996; Murray *et al.*, 2005). They are therefore able to phosphorylate a shared pool of substrate proteins and likely perform overlapping functions. Although their kinase and regulatory domains are highly similar, the SGKs differ from Akt as they lack the N-terminal PH domain which mediates Akt localisation and activation. Therefore, SGK1/2 are localised and activated cytosolically. SGK3 is unique within the SGK family and known protein kinases, as it contains an N-terminal PX domain, which alternatively localises it to PtdIns(3)P produced on early endosomal membranes for its activation (Figure 1.13).

Although the SGK family are highly conserved at the sequence level, they display differences in tissue distribution and expression. SGK1 was the first discovered member of the Serum- and Glucocorticoid-regulated kinase family. It was initially identified as a gene regulated by glucocorticoids and serum, due to a glucocorticoid response element in its gene promoter (Webster *et al.*, 1993). In contrast, SGK2 and SGK3 expression in not induced in response to serum or glucocorticoids, but were named by sequence similarity to SGK1 (Kobayashi *et al.*, 1999). Both SGK1 and SGK3 are ubiquitously expressed in heart, brain, liver, lung, kidney, placenta, skeletal muscle and pancreas but SGK2 showed more restricted expression in liver, kidney, pancreas and brain (Kobayashi *et al.*, 1999).

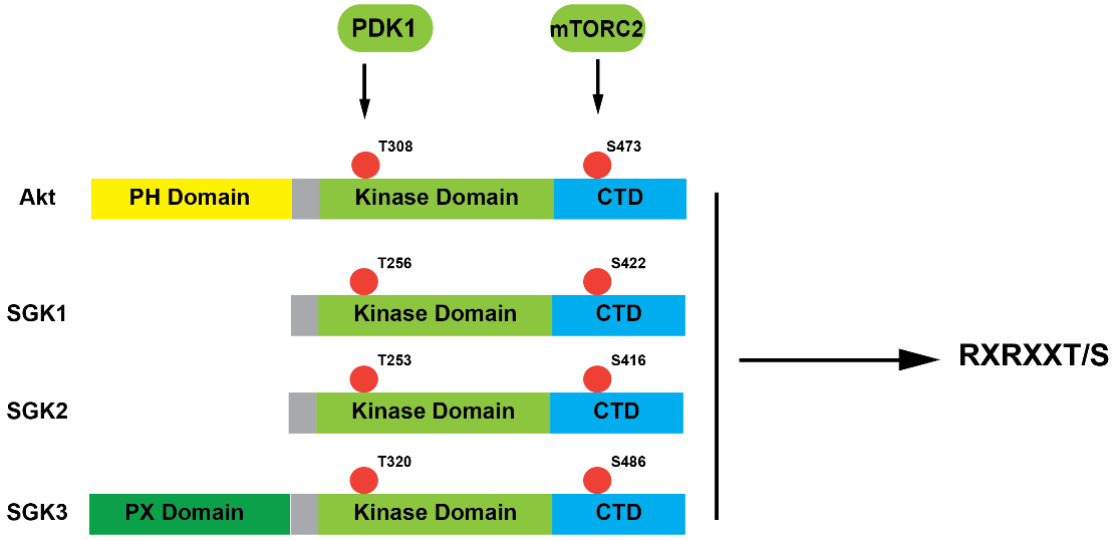

Figure 1.13 Domain structure of the SGK family of protein kinases.
SGK protein kinases are very similar in domain structure to Akt. They contain an AGC family kinase domain and C-terminal regulatory domain (CTD). SGK protein kinases are phosphorylated, like Akt, on their T loop by PDK1 and H-motif by mTORC2 for their activation. SGK3 also contains an N-terminal PX Domain. The SGK protein kinases, like Akt, phosphorylate substrates within an RxRxxpS/T recognition motif.

1.4.1 Regulation of the SGK Protein kinases

The activation and regulation of Akt was discussed in section 1.3.1. As with Akt and many other AGC protein kinases, the SGK family of protein kinases are similarly activated by PI3K signalling, mediated by phosphorylation on their T Loop by PDK1 and Hydrophobic motif by mTORC2. However, as these kinases lack a PH domain, they are not recruited to PDK1 on the plasma membrane as Akt. Therefore, activation of the SGK family of kinases is reliant on a PIF-dependent mechanism, whereby phosphorylation first occurs by mTORC2 on the hydrophobic motif (Garcia-Martinez and Alessi, 2008), which induces a conformational change in this hydrophobic region, promoting interaction with the PDK1 interacting fragment (PIF) pocket of PDK1. This enables PDK1 to dock, allowing phosphorylation of the activation loop residue (Biondi *et al.*, 2001; Collins *et al.*, 2003).

The protein kinase SGK3 is unique among the SGK3 isoforms, as it has an N-terminal PX-domain. Similarly to the recruitment of Akt to PtdIns(3,4,5)P_3 rich membranes, the PX-domain of SGK3 anchors it to PtdIns(3)P rich membranes for its subsequent phosphorylation and activation by PDK1 and mTORC2 (Bago *et al*., 2014, 2016). Mutation of PtdIns(3)P-binding residues of the PX

domain of SGK3 completely ablated localisation to PtdIns(3)P-containing structures, and also its activity (Bago *et al.*, 2016). By shRNA knockdown of the mTORC2 subunit Rictor, Bago *et al.* demonstrated that SGK3 activation and hydrophobic motif phosphorylation is mTORC2 dependent (Bago *et al.*, 2016). Recent research has revealed that SGK3 can be activated through PtdIns(3)P production by the Class III PI3K VPS34, but also by Class I PI3K, via the lipid phosphatases SHIP2 and INPP4B (Bago *et al.*, 2016; Malik *et al.*, 2018). Comparison of the activation mechanisms of the Akt and SGK isoforms is shown in Figure 1.14.

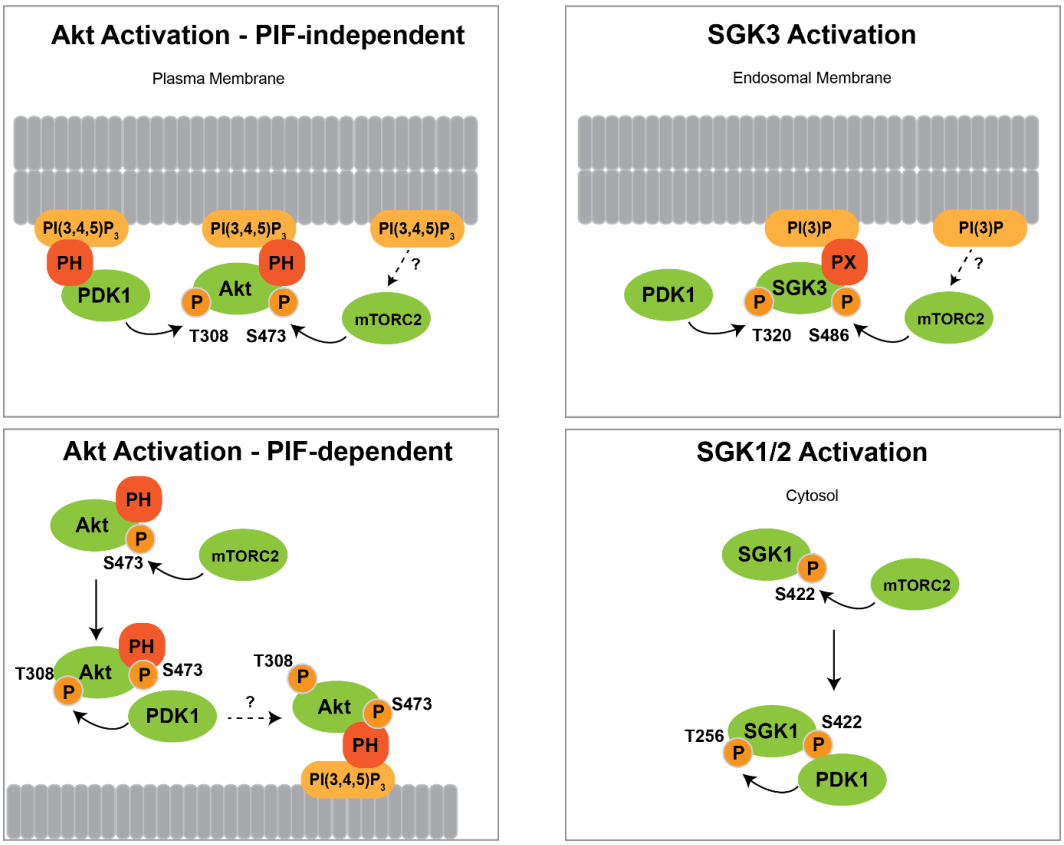

Figure 1.14 Activation mechanisms of Akt, SGK1/2 and SGK3.
Akt can be activated in a PIF-independent mechanism, by colocalization to the plasma membrane with PDK1, or a PIF-dependent mechanism by prior phosphorylation by mTORC2. It is currently contested whether PH-binding to PtdIns(3,4,5)P₃ is required for Akt activation. SGK3 is activated by recruitment to PtdIns(3)P on endosomal membranes by phosphorylation by mTORC2 in a PIF-dependent manner, then PDK1. SGK1/2 are activated by a PIF-dependent mechanism.

SGK1 is also regulated by rapid protein turnover, with a half-life of only 30 minutes. This a mediated by an N-terminal degron motif in SGK1 which targets the protein for proteasomal

degradation (Brickley *et al.*, 2002; Bogusz *et al.*, 2006). This protein-level regulation appears to be in part mediated by SGK1 through feedback regulation. Phosphorylation of Neural Precursor Cell-Expressed Developmentally-Downregulated Protein 4-2 (Nedd4-2) by SGK1 increases Nedd4-2-mediated ubiquitylation of SGK1 (Zhou and Snyder, 2005).

1.4.2 Physiological roles of the SGK Protein Kinases

SGK1

As discussed above, SGK1 was first identified as a gene upregulated in response to serum and glucocorticoids (Webster *et al.*, 1993; Webster, Goya and Firestone, 1993). SGK1 has also been demonstrated to be transcriptionally induced by the mineralocorticoid aldosterone (Chen *et al.*, 1999; Naray-Fejes-Toth *et al.*, 1999) and a range of other factors such as transforming growth factor beta (TGF-β), cytokines, and external stress (Lang *et al.*, 2006; Lang, Artunc and Vallon, 2009).

SGK1 has been linked to multiple cellular and physiological processes including regulation of solute transport, control of blood pressure, memory consolidation and cell survival (Lang *et al.*, 2006). SGK1 gene variants have been associated with elevated blood pressure (Busjahn *et al.*, 2002; Rao *et al.*, 2013), increased incidence of ischaemic stroke and type II diabetes (Schwab *et al.*, 2008; Dahlberg *et al.*, 2011) and increased body mass index (Dieter *et al.*, 2004), and SGK1 is thought to be a driver in the pathophysiology of these conditions. SGK1 has been reported to regulate the activity of a vast number of channels and transporters including sodium, potassium, calcium and chloride channels and amino acid and glucose transporters (Lang *et al.*, 2006; Lang and Voelkl, 2013).

SGK1 is highly expressed in the kidney, and the best mechanistically characterised role of SGK1 is in regulation of the epithelial sodium channel (ENaC), through which SGK1 contributes to the control of renal tubular Na+ reabsorption. Co-expression of SGK1 with ENaC in Xenopus oocytes was found to increase ENaC mediated currents, through increased levels of ENaC at the plasma

membrane (Chen *et al.*, 1999; Naray-Fejes-Toth *et al.*, 1999; Alvarez de la Rosa *et al.*, 2003). Additionally, phosphorylation of Nedd4-2 by SGK1 was found to upregulate levels of ENaC at the plasma membrane. Downregulation of Nedd4-2 activity by SGK1-mediated phosphorylation reduces binding to ENaC and stimulates Nedd4-2 binding to 14-3-3 chaperone proteins, leading to increased levels of ENaC at the cell surface (Debonneville *et al.*, 2001; Snyder, Olson and Thomas, 2002; Bhalla *et al.*, 2005; Ichimura *et al.*, 2005). SGK1 has additionally been suggested to regulate ENaC via WNK4 (Ring *et al.*, 2007) and transcriptionally (Boyd and Naray-Fejes-Toth, 2005; Zhang *et al.*, 2007).

As expected from these findings, SGK1 knockout mice exhibit an impaired ability to regulate urinary Na^+ and water excretion when placed on a low sodium diet (Wulff *et al.*, 2002; Fejes-Toth *et al.*, 2008; Faresse *et al.*, 2012). $SGK1^{-/-}$ mouse kidneys also failed to eliminate acute K^+ load (Huang *et al.*, 2004), and mice were resistant to increases in blood pressure, either induced by dexamethasone or by high salt intake in combination with a high fat diet (Huang, Boini, Friedrich, *et al.*, 2006; Huang, Boini, Osswald, *et al.*, 2006; Boini *et al.*, 2008). However, a surprising result from these knockout mice was that expression of ENaC channels was only modestly reduced, with a greater deficiency in Na^+Cl^- cotransporter (NCC) (Fejes-Toth *et al.*, 2008; Vallon *et al.*, 2009; Faresse *et al.*, 2012). These findings suggest that the primary target of SGK1 may actually be NCC, with mechanisms proposed via Wnk4 (Rozansky *et al.*, 2009) and Nedd4-2 (Arroyo *et al.*, 2011).

SGK1, as well as SGK3, may impact cellular metabolism, as expression in Xenopus oocytes, was shown to stimulate the activity of the Na+-glucose cotransporter SGLT1, which serves to absorb intestinal glucose (Dieter *et al.*, 2004). Consequently, SGK1 knockout mice exhibited reduced glucocorticoid-induced intestinal glucose uptake (Grahammer *et al.*, 2006)

SGK2

Of all the SGK isoforms, SGK2 is the least studied. SGK2 is not transcriptionally induced by glucocorticoids or serum in cells (Kobayashi *et al.*, 1999), and its physiological roles are not yet clear. A handful of studies have implicated SGK2 signalling in regulation of human organic anion transporters 1 and 4 (hOAT1/4) via phosphorylation of Nedd4-2 (Wang *et al.*, 2016; Xu *et al.*, 2016; Wang, Zhang and You, 2019). 2 recent papers have suggested a role for SGK2 in bladder and renal cell carcinoma proliferation (Liu *et al.*, 2017, 2019; J.-B. Chen *et al.*, 2018).

SGK3

SGK3 was first identified as a novel isoform of SGK1 (Kobayashi *et al.*, 1999). It was identified as a mediator of interleukin 3 (IL3)-dependent survival in haematopoietic cells (Liu, Yang and Songyang, 2000). SGK3 can be recruited via its PX domain to PtdIns(3)P at the early endosomal membrane generated by VPS34 (Virbasius *et al.*, 2001; Bago *et al.*, 2014, 2016). As SGK3 is commonly observed on Rab5-positive endosomes, its activation is likely mediated by complex II of VPS34. Additionally, the accessory subunit Rubicon has been associated with growth factor recognition and solely interacts with VPS34 complex II. Unlike SGK1, SGK3 expression is not induced by serum and glucocorticoids and is constitutively expressed (Kobayashi *et al.*, 1999). However, its gene promoter contains oestrogen binding regions and its transcription can be induced by oestrogen (Wang *et al.*, 2011). Additionally, elevated levels of SGK3 have also be observed in ER positive breast cancer cells (Xu *et al.*, 2012).

Like SGK1, SGK3 has been observed to phosphorylate and regulate the activity of the E3 Ligase Need4-2 (Dieter *et al.*, 2004; Lamothe and Zhang, 2013). A role has also been proposed for SGK3 in regulation of vesicular trafficking and receptor sorting at the endosome, through regulation of E3 ligase atrophin-1 interacting protein 4 (AIP4) (Slagsvold *et al.*, 2006).

An additional substrate of SGK1 and SGK3, shared with Akt, is N-myc downstream-regulated gene 1 (NDRG1) and 2 (Murray *et al.*, 2004). However, the functional significance of this

phosphorylation event remains unknown. Phosphorylation at this site is extensively used as a measure of SGK activity in this thesis. Recent data from our lab has identified SGK3-specific endosomal substrates (Malik *et al.*, 2019). It was determined that the identity of the +1 site in the substrate motif was critical in specificity between Akt and SGK3 substrates and may provide a bioinformatic tool for identifying further SGK3-specific substrates.

SGK3 knockout mice display impaired postnatal hair growth due to a hair bulb keratinocyte proliferation defect (McCormick *et al.*, 2004; Alonso *et al.*, 2005). $SGK3^{-/-}$ mice also display a mild growth defect, normal renal salt handling, subtly decreased locomotion, defective mast cell function, increased gastric acid secretion and decreased intestinal glucose transport (McCormick *et al.*, 2004; Sandu *et al.*, 2005; Zemtsova *et al.*, 2010; Pasham *et al.*, 2011).

Combination with SGK1 or Akt deletion models reveals redundancies and unique roles for the kinases in this pathway. For example, depletion of SGK3 further worsens the glucose handling phenotype of Akt2 knockout mice (Yao *et al.*, 2011). $SGK1^{-/-}SGK3^{-/-}$ double knockout mice share the hair growth defect of the SGK3 knockouts and the renal salt retention defect of SGK1 knockouts without showing any novel more severe phenotypes (Grahammer *et al.*, 2006). This suggests these kinases are playing independent physiological roles.

1.4.3 SGK family of kinases in cancer, and Akt and PI3K inhibitor resistance.

As discussed, the high degree of homology between the Akt and SGK protein kinases results in an overlapping substrate-specificity motif and therefore shared substrates between these kinases. These kinases were therefore proposed as possible candidates for mediating Akt independent signalling, considering their regulation by PI3Ks and the similarity in substrate specificity with Akt (Bruhn *et al.*, 2010, 2013)

As Akt, SGK1 has been proposed to phosphorylate and inhibit the pro-apoptotic FoxO transcription factors (Brunet *et al.*, 2001). SGK1 has also been linked to dexamethasone and Glucocorticoid Receptor activation associated breast cancer cell survival (Mikosz *et al.*, 2001;

Wu *et al.*, 2004), and a role for SGK1 in cell invasion and migration has also been reported (Eylenstein *et al.*, 2011; Schmidt, Gu, *et al.*, 2012; Schmidt, Kraemer, *et al.*, 2012). In multiple myeloma SGK1 was identified as a transcriptional target of cytokines that promote proliferation (Fagerli *et al.*, 2011). It has recently been observed, in a panel of breast cancer cell lines carrying PI3K pathway mutations, that high expression of SGK1 confers resistance to Akt inhibitors (Sommer *et al.*, 2013). It was also recently shown that a set of colorectal cancer tissues exhibited high expression of SGK1 in comparison to neighbouring healthy tissue. In addition, targeting of SGK1 by shRNA or kinase inhibition reduced colorectal cancer cell proliferation and migration, and induced apoptosis (Liang *et al.*, 2017). A recent study of diffuse large B cell lymphomas found shRNA knockdown of SGK1 sensitised these cells to Akt inhibition (Lu *et al.*, 2019). $SGK1^{-/-}$ mice were observed to develop significantly fewer chemically induced colonic tumours than their wildtype littermates, and this was determined to be at least partially due to stabilization of FOXO3a and BIM (Nasir *et al.*, 2009). Additionally, crossing these mice with an adenomatous polyposis coli (APC)-deficient background resulted in reduced spontaneous tumorigenesis, and reduced β-catenin abundance was detected by western blot and confocal microscopy (Wang *et al.*, 2010)

It has recently been shown that SGK3 can also be implicated in resistance to inhibition of the PI3K-Akt signalling pathway. Bago *et al*., published that, in certain breast cancer cell lines, SGK3 can be induced to provide acquired resistance after prolonged treatment with PI3K or Akt inhibitors. SGK3 is transcriptionally upregulated and activated independently of Class I PI3K to phosphorylate substrates in the place of Akt. This leads to Akt-independent activation of pathways such as mTORC1-driven proliferation (Figure 1.15). The focus of this thesis will be on this role of SGK3 in resistance to Class I PI3K and Akt inhibitors. In xenograft models of BT474 cells treated with Akt inhibitors alone or in combination with an inhibitor of SGK (14H), it was determined that the combination treatment caused a much better growth arrest and even recession of the tumour (Bago *et al.*, 2016). In a more recent study, SGK3 was also proposed to

mediate liver cancer stem cell expansion after prolonged inhibition of PI3K Class I, through activation of the GSK-3β/β-catenin signalling (Liu *et al.*, 2018).

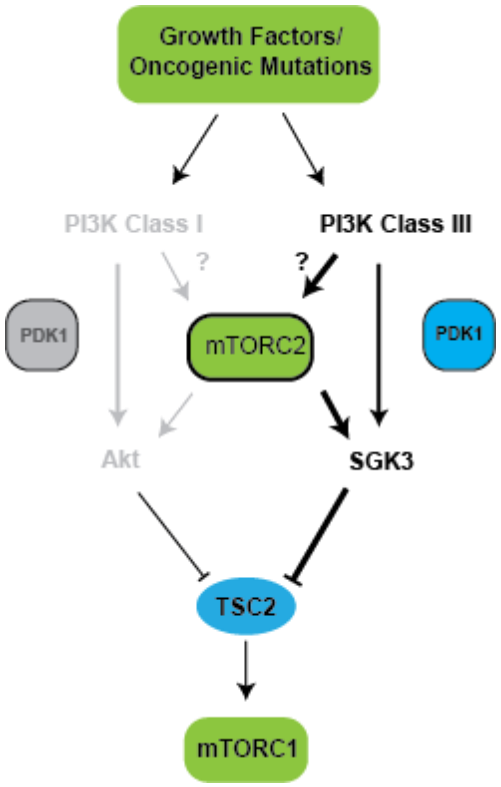

Figure 1.15 Akt-independent activation of mTORC1 via SGK3.
When Class I PI3K or Akt are inhibited, SGK3 can be activated via Class III PI3K VPS34. In the absence of Akt activity, SGK3 can phosphorylate TSC2 leading to the activation of mTORC1.

SGK3 has also been proposed as a driver of cancer cell proliferation itself. SGK3 was originally identified as a mediator of interleukin 3 (IL3)-dependent survival in hematopoietic cells, and again was suggested to inhibit FOXO-mediated transcription and to inhibit pro-apoptotic Bcl-2 family members in a manner similar to Akt (Liu, Yang and Songyang, 2000). A study by Vasudevan noted that growth of breast cancer cells carrying the PIK3CA E545K mutation was promoted through activation of SGK3, with relatively low Akt phosphorylation (Vasudevan *et al.*, 2009). A recent study also used SGK3 KO mice to determine that SGK3 was critical for hepatocarcinoma development downstream of PI3KCA E545K mutation (Cao *et al.*, 2019).

1.5 Thesis Aims

My PhD project aimed to further explore the role that SGK3 plays in resistance to PI3K/Akt inhibition. In order to investigate the regulation and downstream signaling of SGK isoforms, work on the project has been based on 2 key aims.

1. The Development of tools to induce degradation of SGK3 in sensitive cancer cell lines
    a. An SGK-specific PROTAC derived from Sanofi inhibitor compounds (Chapter 3)
    b. Mass-Spectrometry analysis of the impact of PROTAC-mediated degradation in cancer cells (Chapter 4)
    c. A Generalizable HaloPROTAC approach (Chapter 5)
2. Determining the mechanism by which SGK3 can be activated in the context of PI3K inhibition
    a. How is mTORC2 activated against SGK3 under Class I PI3K inhibition? In particular, is this mediated by mSin1? (Chapter 6)
    b. How is the Class III PI3K, VPS34, activated on stimulation with growth factors? (Chapter 6)

2. Materials and Methods

2.1 Materials

2.1.1 Commercial Reagents

Reagents used in this report are categorised into 5 main parts for: bacterial transformation, tissue culture, cell lysis, Immunoblotting (IB), Immunoprecipitation (IP) & Kinase assay, and gDNA extraction and subcloning (Table 2.1).

Table 2.1 Commercial Reagents

Reagent	**Company**	**Origin**
Bacterial transformation		
Ampicillin	Sigma-Aldrich	Poole, UK
Plasmid Maxiprep kit	Qiagen Ltd	Crawley, UK
Plasmid Midiprep kit	Qiagen Ltd	Crawley, UK
Tissue culture		
Blasiticidin	InVivoGen	San Diego, USA
Dimethyl sulfoxide (DMSO)	Sigma-Aldrich	Poole, UK
Doxycycline	Sigma-Aldrich	Poole, UK
Dulbecco's modified eagle medium	Invitrogen	Paisley, UK
Foetal bovine serum (FBS)	Labtech	Brambleside, UK
Hygromycin	InVivoGen	San Diego, USA
L-glutamine	Invitrogen	Paisley, UK
Pen/Strep	Invitrogen	Paisley, UK
Phosphate buffered saline (PBS)	Invitrogen	Paisley, UK
Polyethyleneimine (PEI)	Polyscience	Warrington, PA
Puromycin	Sigma-Aldrich	Poole, UK
Trypsin/EDTA	Invitrogen	Paisley, UK
Zeocin	Invivogen	San Diego, USA
IGF-1 (carrier free)	New England Biolabs	Ipswich, MA
Lysis of cells		

Benzamidine	Sigma-Aldrich	Poole, UK
Dithiothreitol (DTT)	Formedium	Norfolk, UK
EDTA	Sigma-Aldrich	Poole, UK
EGTA	Sigma-Aldrich	Poole, UK
Protease inhibitor cocktail	Roche	Lewes, UK
Sodium b-glycerophosphate	Sigma-Aldrich	Poole, UK
Sodium fluoride	Sigma-Aldrich	Poole, UK
Sodium orthovanadate	Sigma-Aldrich	Poole, UK
Sucrose	VWR International	Radnor, USA
Triton-X-100	Sigma-Aldrich	Poole, UK
Sodium dodecyl sulphate (SDS)	Sigma-Aldrich	Poole, UK
IB, IP & Kinase Assay		
3MM paper	Whatman	Maidstone, UK
40% (w/v) 29:1 Acrylamide	Flowgen Bioscience	Nottingham, UK
Ammonium persulphate (APS)	Sigma-Aldrich	Poole, UK
Bovine serum albumin (BSA)	Sigma-Aldrich	Poole, UK
Coomassie protein assay kits	Thermo Scientific	Essex, UK
Dimethyl pimelimidate (DMP)	Sigma-Aldrich	Poole, UK
Enhanced chemiluminescence (ECL)	GE Healthcare	Piscataway, NJ
Glycine	Sigma-Aldrich	Poole, UK
Immobilon PVDF membrane (0.45µm)	Sigma-Aldrich	Poole, UK
Isopropanol	Sigma-Aldrich	Poole, UK
Methanol	Sigma-Aldrich	Poole, UK
N,*N*,*N*',*N*'-Tetramethylethane-1,2- diamine	Sigma-Aldrich	Poole, UK

NuPAGE LDS sample buffer	Invitrogen	Paisley, UK
NuPAGE MOPS running buffer	Invitrogen	Paisley, UK
NuPAGE Novex SDS Bis-Tris gels	Invitrogen	Paisley, UK
Photographic developer (LX24)	Kodak	Liverpool, UK
Photographic fixer (FX40)	Kodak	Liverpool, UK
Ponceau S	Sigma-Aldrich	Poole, UK
Precision Plus Protein unstained standards	BioRad	Herts, UK
Skimmed milk (Marvel)	Premier Beverages	Stafford, UK
Sodium tetraborate	Sigma-Aldrich	Poole, UK
Sucrose	BDH	Lutterworth, UK
Tris(hydoxymethyl)methylamine (Tris)	BDH	Lutterworth, UK
Super sensitive X-ray films	GE Healthcare	Buckinghamshire, UK
Tween-20	Sigma-Aldrich	Poole, UK
X-ray films	Konica Corporation	Japan
[γ32P]-labelled ATP	GE Healthcare	Buckinghamshire, UK
P81 paper	GE Healthcare	Poole, UK
Acetone	Sigma Aldrich	Poole, UK
Orthophosphoric Acid	Sigma Aldrich	
Magnesium Acetate	Sigma Aldrich	Crawley, UK
gDNA extraction and subcloning		
DNeasy Blood and Tissue Kit	Qiagen	Essex, UK
dNTP Mix	Thermo Scientific	Ipswich, MA
Taq Polymerase	New England Biolabs	Paisley, UK
Custom Primers	Invitrogen	Essex, UK
GeneRuler 100bp Plus DNA Ladder	Thermo Scientific	Ipswich, MA

Strataclone PCR cloning kit	Agilent	Santa Clara, CA
X-Gal	Formedium	Norfolk, UK

2.1.2 In-house Reagents

Calcium competent E. coli DH5α cells and Crosstide Peptide were kindly provided by MRC PPU Reagents and Services. Luria Bertani (LB) broth and agar plates were kindly supplied by the Media Kitchen of the University of Dundee. PROTAC compounds were produced by the Ciulli Lab (BCDD, University of Dundee) and dissolved in DMSO to a 10mM solution. In-house antibodies were provided by MRC PPU Reagents and Services are described in section 2.1.5

2.1.3 DNA constructs

Cloning and mutagenesis of cDNA constructs was performed by Dr R Toth, Mrs M Wightman, Mr T. Macartney and Ms S Weidlich (Table 2.2). All DNA constructs were verified by DNA sequencing performed by Sequencing Service of the University of Dundee using DYEnamic ET terminator chemistry (GE Healthcare, Little Chalfont, UK) on automated DNA sequencers (Applied Biosystems, Foster City, CA). All constructs encoded the human version of the gene.

Table 2.2 cDNA constructs

Expressed	**Plasmid Vector**	**Type**	**DU#**
Chapter 3			
SGK3	pcDNA5 FRT/TO	Mammalian	42866
SGK3 K191A	pcDNA5 FRT/TO	Mammalian	44432
SGK3 T320A	pcDNA5 FRT/TO	Mammalian	62503
SGK3 S486A	pcDNA5 FRT/TO	Mammalian	62504
SGK3 Q125-end	pcDNA5 FRT/TO	Mammalian	62559
SGK3 R50A/R90A	pcDNA5 FRT/TO	Mammalian	44990
HA-SGK1	pcDNA5 FRT/TO	Mammalian	44437
HA-SGK1 K129A	pcDNA5 FRT/TO	Mammalian	44426
Chapter 4			
shSGK3 #1	pLKO puro	Viral	62718

shSGK3 #2	pLKO puro	Viral	62768
shRNA scramble	pLKO puro	Viral	62719
Gag/Pol-Rev	pCMV	Mammalian	Addgene
VSVG	pCMV	Mammalian	Addgene
SGK3 shRNA#1 resistant	pcDNA5 FRT/TO	Mammalian	44539
SGK3 K191A shRNA#1 resistant	pcDNA5 FRT/TO	Mammalian	44540
SGK3 shRNA#2 resistant	pcDNA5 FRT/TO	Mammalian	44496
SGK3 K191A shRNA#2 resistant	pcDNA5 FRT/TO	Mammalian	44538
Chapter 5			
SGK3 Cter Gly5 Halo IRES GFP KI Donor	pMK-RQ	Mammalian	52689
SGK3 Cter KI antisense guide + Cas9 D10A	pX335	Mammalian	52662
SGK3 Cter KI sense guide	pBabeD	Mammalian	52684
VPS34 Nter Halo KI Donor	pMK-RQ	Mammalian	57077
VPS34 Nter KI antisense guide + Cas9 D10A	pX335	Mammalian	52082
VPS34 Nter KI sense guide	pBabeD	Mammalian	52071
SGK3	pcDNA5 FRT/TO	Mammalian	42866
SGK3-Flag	pcDNA5 FRT/TO	Mammalian	42884
SGK3-GFP	pcDNA5 FRT/TO	Mammalian	42883
SGK3-Gly5-Halo	pcDNA5 FRT/TO	Mammalian	50748
SGK3-Gly5-HaloD106A	pcDNA5 FRT/TO	Mammalian	50763
SGK3-Gly10-Halo	pcDNA5 FRT/TO	Mammalian	26756
SGK3-Gly15-Halo	pcDNA5 FRT/TO	Mammalian	26769
SGK3-Gly20-Halo	pcDNA5 FRT/TO	Mammalian	26812
SGK3-Gly5-ATG-Halo	pcDNA5 FRT/TO	Mammalian	54586
SGK3-Lys5-Halo	pcDNA5 FRT/TO	Mammalian	50749
SGK3-Lys5-HaloD106A	pcDNA5 FRT/TO	Mammalian	50764
SGK3-Gly5-HaloMUT1 *	pcDNA5 FRT/TO	Mammalian	26553
SGK3-Gly5-HaloMUT2 *	pcDNA5 FRT/TO	Mammalian	26566
SGK3-Gly5-HaloMUT3 *	pcDNA5 FRT/TO	Mammalian	26575
SGK3-Lys5-HaloMUT1 *	pcDNA5 FRT/TO	Mammalian	26527
SGK3-Lys5-HaloMUT2 *	pcDNA5 FRT/TO	Mammalian	26541
SGK3-Lys5-HaloMUT3 *	pcDNA5 FRT/TO	Mammalian	26559

*MUT1 = R21K, R86K, R204K, R254K, R288K MUT2 = MUT1 + R30K, R146K, H230K MUT3 = MUT2 + R199K			
Chapter 6			
mSin1 KO antisense guide + Cas9 D10A	pX335	Mammalian	52297
mSIN1 KO sense guide	pBabeD	Mammalian	52278
mSIN1 Cter GFP KI Donor	pMK-RQ	Mammalian	57431
mSIN1 Cter KI antisense guide A + Cas9 D10A	pX335	Mammalian	57354
mSIN1 Cter KI sense guide A	pBabeD	Mammalian	57348
mSIN1 Cter KI antisense guide B + Cas9 D10A	pX335	Mammalian	57353
mSIN1 Cter KI sense guide B	pBabeD	Mammalian	57349
Rictor NTer GFP KI Donor	pMK-RQ	Mammalian	57430
Rictor Nter KI antisense guide A + Cas9 D10A	pX335	Mammalian	57356
Rictor Nter KI sense guide A	pBabeD	Mammalian	57350
Rictor Nter KI antisense guide B + Cas9 D10A	pX335	Mammalian	57355
Rictor Nter KI sense guide B	pBabeD	Mammalian	57351
HA-mSin1 TV1	pcDNA5 FRT/TO	Mammalian	26852
HA-mSin1 TV2	pcDNA5 FRT/TO	Mammalian	26882
HA-mSin1 TV3	pcDNA5 FRT/TO	Mammalian	26952
HA-mSin1 TV4	pcDNA5 FRT/TO	Mammalian	26853
HA-mSin1 TV5	pcDNA5 FRT/TO	Mammalian	26886
HA-mSin1 TV1 R393C K428A K464A	pcDNA5 FRT/TO	Mammalian	26854
HA-mSin1 TV1 M1-Q375	pcDNA5 FRT/TO	Mammalian	26862
HA-mSin1 TV1 M1-S356	pcDNA5 FRT/TO	Mammalian	27342
HA-mSin1 TV1 R312L	pcDNA5 FRT/TO	Mammalian	26992
HA-mSin1 TV1 R312A	pcDNA5 FRT/TO	Mammalian	26991
HA-mSin1 TV1 K307D	pcDNA5 FRT/TO	Mammalian	26993
HA-mSin1 TV1 R312L R393C K428A K464A	pcDNA5 FRT/TO	Mammalian	27329
HA-mSin1 TV1 T86A	pcDNA5 FRT/TO	Mammalian	27795
HA-mSin1 TV1 T86E	pcDNA5 FRT/TO	Mammalian	27789

HA-mSin1 TV1 T86A T398A	pcDNA5 FRT/TO	Mammalian	27814
HA-mSin1 TV1 T86E T398E	pcDNA5 FRT/TO	Mammalian	27788
HA-mSin1 TV1 Q68H	pcDNA5 FRT/TO	Mammalian	27538
HA-mSin1 TV2 R393C K428A K464A	pcDNA5 FRT/TO	Mammalian	59340
HA-mSin1 TV2 M1-Q375	pcDNA5 FRT/TO	Mammalian	59186
HA-mSin1 TV2 T86A	pcDNA5 FRT/TO	Mammalian	59104
HA-mSin1 TV2 T86E	pcDNA5 FRT/TO	Mammalian	59103
HA-mSin1 TV2 T86A T398A	pcDNA5 FRT/TO	Mammalian	59282
HA-mSin1 TV2 T86E T398E	pcDNA5 FRT/TO	Mammalian	59132
GST-SGK3 D304A	pEBG	Mammalian	2257
GST-SGK1 60-end K127A	pEBG	Mammalian	143
GST-PKB A K179A	pEBG	Mammalian	6191
Flag-TurboID-aGFP6M	pBabeD	Mammalian	29702
Gag/Pol	pCMV	Mammalian	Addgene
VSV/G	pCMV	Mammalian	Addgene

2.1.4 Buffers and solutions

Mammalian cell lysis buffer: 25 mM Tris (pH 7.5), 1 mM EDTA, 1 mM EGTA, 0.27 M sucrose, 50 mM NaF, 5 mM sodium pyrophosphate, 1mM sodium orthovanadate, 10 mM sodium βglycerophosphate, 1 mM benzamidine, 1mM DTT, one mini Complete protease inhibitor cocktail tablet per 10 ml of lysis buffer and 1% Triton X-100

Glutamate Lysis Buffer: 25mM HEPES (pH 7.4), 2.5mM Mg Acetate, 5mM EGTA (pH 8), 150mM K-Glutamate, 25mM KCl

Tris-Glycine running buffer: 25 mM Tris-HCl (pH 8.3), 192 mM glycine, 0.1% (w/v) SDS

Tris-Glycine transfer buffer: 48 mM Tris-HCl (pH 8.3), 39 mM glycine, 20% (v/v) methanol

TBST buffer: 50 mM Tris-HCl (pH 7.5), 0.15 M NaCl and 0.1% (v/v) Tween-20

Buffer A: 30mM Tris-HCl (pH 7.5), 0.1M EGTA

RIPA Buffer: 50mM Tris-HCl (pH 8), 150mM NaCl, 1mM EDTA, 0.1% SDS, 1% sodium deoxycholate, 1% NP-40, 50mM NaF, 5mM sodium pyrophosphate, one mini Complete protease inhibitor cocktail tablet per 10 ml of lysis buffer.

2.1.5 Antibodies

In-house antibodies (Table 2.3) were raised in sheep and affinity purified with respective antigens by the DSTT and were used at 1 µg/mL in 5% (w/v) skimmed milk in 0.1% TBST. Phospho-specific antibodies were supplemented with 10 µg/ml of the relevant non-phospho peptide to increase specificity and decrease background. Commercial antibodies (Table 2.4) were diluted 1:1000 in 5% (w/v) BSA in 0.1% TBST.

Table 2.3 In-house antibodies produced by MRC PPU Reagents and Services

Antibody	**Immunogen**	**Sheep #**	**Bleed #**
PKB-alpha	Human 466-480	S695B	3rd
NDRG1	Human Full Length	S771D	3rd
PRAS40	Human 238-256	S115B	1st
pPRAS40 (Thr246)	Human 240-251	S114B	2nd
SGK3	SGK3 PX Domain (Human 1-130)	S848D	6th
VPS15	Human 433-667	R1737	2nd
VPS34	Human Full Length	S672B	3rd
Beclin1	Human Full Length	S900B	2nd
UVRAG	Human Full Length	S232D	3rd
P70S6K1	Human 25-44	S417B	2nd
mSin1	Human Full Length	S008C	3rd
mTOR	Human 2-20	S683B	1st
Rictor	Human 6-20	S654B	3rd

Table 2.4 Commercial antibodies.

Antibody	**Catalogue Number**	**Company**	**Species**
pAkt (Thr308)	4046	CST	Rabbit

pAkt (Ser473)	9271	CST	Rabbit
pAkt (Thr450)	9267	CST	Rabbit
pSGK3 (Thr320)	5642	CST	Rabbit
pSGK1 (Ser422)	Sc-16745	Santa Cruz	Rabbit
SGK	S5188	Sigma	Rabbit
pNDRG1 (Thr346)	5482	CST	Rabbit
GAPDH (6C5)	Sc-32233	Santa Cruz	Mouse
HaloTag7 mAb	G9211	Promega	Mouse
HaloTag7 pAb	G9281	Promega	Rabbit
pTSC2 S929	3615	CST	Rabbit
pTSC2 T1462	3617	CST	Rabbit
TSC2	3612	CST	Rabbit
pPRAS40	2997	CST	Rabbit
pS6 S240/244	2215	CST	Rabbit
S6 Total	2317	CST	Mouse
pp70S6K1 T389	9205	CST	Rabbit
p70S6K1	9202	CST	Rabbit
pFOXO3a (Ser253)	9466	CST	Rabbit
p4EBP1 S65	9451	CST	Rabbit
4EBP1	9452	CST	Rabbit
PDE4D	Ab171750	Abcam	Rabbit
RPL14	ab181200	Abcam	Rabbit
TRAF3IP2	NB100-56740SS	Novus	Rabbit
ZNF512B	A303-236A-T	Bethyl	Rabbit
RSAD1	ab104051	Abcam	Rabbit
GHITM	16296-1-AP	Proteintech	Rabbit
COX6C	ab150422	Abcam	Rabbit
COXIV	4844	CST	Rabbit
ATPb	ab15730	Abcam	Rabbit
MT-CO1	ab14705	Abcam	Rabbit
MT-ND6	ab81212	Abcam	Rabbit

mSin1	12860	CST	Rabbit
pmSin1 T86	14716	CST	Rabbit
Rictor	3806	CST	Rabbit
ATG14	PD026	MBL	Rabbit

2.1.6 Inhibitors and compounds

PROTAC compounds were synthesised by Andrea Testa and Chiara Maniaci in Alessio Ciulli's lab. Large amounts of Sanofi 290-R and 308-R were synthesised by Natalia Shpiro for production of the SGK3-PROTAC compounds. Natalia Shpiro also synthesised the inhibitors available in house at MRC PPU Reagents and services.

Table 2.5 Inhibitors

Inhibitor	**Target**	**Source**	**Ref**
AZD5363	Akt	AstraZeneca	(Davies *et al.*, 2012)
14H	SGK	In House	(Halland *et al.*, 2015)
GDC0941	Class I PI3K	In house	(Folkes *et al.*, 2008)
VPS34IN1	VPS34	In house	(Bago *et al.*, 2014)
MLN4924	Nedd8 E3	In house	(Brownell *et al.*, 2010)
VH298	pVHL	Ciulli lab	(Frost *et al.*, 2016)
MG132	Proteasome	Calbiochem	(Lee and Goldberg, 1998)
MK2206	Akt	SelleckChem	(Hirai *et al.*, 2010)
Bafilomycin A	Vacuolar H+-ATPase	Enzo Life Sciences	(Ohkuma *et al.*, 1993)

2.1.7 Cell lines

ZR-75-1, CAMA-1, CAMA-R, BT-474 and JIMT-1 cell lines were provided by AstraZeneca. All other cell lines were supplied by the MRC Protein Phosphorylation and Ubiquitylation Unit.

2.2 Methods

2.2.1. Amplification of cDNA constructs.

cDNA constructs used in this study were produced by MRC PPU Reagents and Services as described in section 2.1.3. Amplification of the constructs for use in experiments was performed in DH5α cells.

2.2.1.1 Transformation of competent E. coli DH5α cells

1 µl DNA was added to 50 µl of competent E. coli DH5α cells and incubated on ice for 20 min followed by a heat shock for 45 seconds at 42°C. The cells were placed back on ice for 5 min and then streaked onto LB agar plates containing ampicillin or kanamycin for selection and incubated overnight at 37°C.

2.2.1.2 Purification of plasmids from E. coli and measurement of DNA concentration

Transformed E. coli DH5α cells were cultured in 250 mL LB containing 200 µg/mL ampicillin or kanamycin. After an incubation time of about 16 h at 37°C, shaking at 180rpm, the samples were pelleted by centrifugation at 6000 x g. Plasmid purification was performed by Maxiprep kit according to the manufacturer's instructions. Finally, DNA concentrations were measured using NanoDrop based on DNA absorption at 260 nm. Absorbance at 230 nm and 280 nm was also measured as a measure of purity.

2.2.2 gDNA Sequencing

gDNA was extracted from HEK293 cells using DNeasy Blood and Tissue Kit according to manufacturer's instructions for Blood. Polymerase Chain Reaction (PCR) was performed in a 25µl reaction, containing 2 ul Buffer, 0.8µM primers, 200µM dNTPs, 1 µl DNA and 1 µl Taq Polymerase. The reaction was performed on the following thermal cycle, using primers described in Table 2.6: 96 °C for 3, 35 cycles of [95 °C for 30'', Tm for 30'', 72 °C for 30''], then 72 °C for 10'' before storage at 4 °C. 5µl PCR product was analysed on a 2% Agarose gel in TAE buffer to detect the correct sized product. 3µl PCR product was subcloned using the StrataClone PCR cloning kit

according to manufacturer's instructions. DNA Sequencing was performed using the M13 Forward Primer by DNA Sequencing and Services (www.dnaseq.co.uk) using Applied Biosystems Big-Dye v 3.1 chemistry on an Applied Biosystems model 3730 automated capillary DNA sequencer.

Table 2.6 PCR primer sequences

Target	Forward Primer (5' -> 3')	Reverse Primer (5' => 3')
SGK3-Halo KI Junction	GTGAATGCCAGTGTATTGGAGG	GAGGAGGTCGGGTTACCGT
SGK3 Exon 17	GCTGGACCAGATGATATCAG	GAGGCACTAGTTATACATATTTG
Halo-VPS34 KI Junction	CCTAACTGCAAGGCTGTGGA	CCTCTATCACCTCCCGTGCT
VPS34 Exon 1	AGCTCAAGCTCAAATGATAGCG	CATCTGCCTGTGTCTACCTCTC
mSin1 Exon 5	TCCATGGTCACAGTAGGTCT	GCTGATTCTCTGAGATGCACA

2.2.3 Cell culture methods

Cells were maintained in an incubator at 37°C and 5% CO2. The passaging of cells was performed by washing the cells with PBS followed by incubation with Trypsin/EDTA. Detached cells were resuspended in cell culture medium and split at 1:2 – 1:8 ratios. HEK293, HEK293FT, HEK293T and U2OS cells were grown in Dulbecco's Modified Eagle Medium (DMEM) in the presence of 10% (v/v) FBS, 2 mM L-glutamine, 100 U/mL penicillin and 0.1 mg/mL streptomycin in DMEM. Stable HEK293 TREx cell lines were grown in selection media containing 100 µg/ml Hygromycin and 15 µg/ml Blasticidin. Virally transfected stable cell lines were grown in media containing 2 µg/ml Puromycin until plating for experiments. ZR-75-1, CAMA-1, BT-474 and JIMT-1 were grown in RPMI-1640 media without phenol red and supplemented as above with the exclusion of penicillin and streptomycin.

2.2.3.1 Freezing and Thawing Cells

Detached cells were centrifuged at 300 x g for 5 min and resuspended in FBS with 10% DMSO. 1 mL aliquots were stored in cryovials at -80 ˚C. Cells were thawed in a 37 ˚C water bath, resuspended in growth medium and allowed to adhere overnight prior to medium change.

2.2.3.2 Transfection of cells using polyethyleneimine (PEI)

For transfection of cells grown in 10cm dishes, 5µg DNA was mixed with 20µl 1mg/ml PEI and 1mL serum-free DMEM and left for 20-30 min at room temperature before being added to cells. For transient transfection, cells were harvested 24 hr post transfection. For generation of HEK293 TREx stable cell lines, media was changed 24 hr post transfection, and media containing Hygromycin and Blasticidin added 48 hr post transfection.

2.2.3.3 Transfection of cells using retroviral and lentiviral constructs.

i. Transfection with pBABE constructs for stable overexpression

Stable expression of the FLAG-TurboID-aGFP6M plasmid was performed using a pBABE retroviral expression vector. To generate retroviral particles, HEK293T cells grown on 10 cm dishes were transfected with 6 µg pBABE construct, 3.8 µg pCMV Gag-Pol and 2.2 µg pCMV VSVG, with 36 µl Lipofectamine 2000 in Optimem. Virus-containing medium was collected 48 and 72 h post-transfection and filtered with a 0.45 µM filter. Cells were transfected at a 5:1 ratio in full media, with 8 µg/ml polybrene. Media was changed after 24 h, and after 48 h selection for transfected cells was performed with media supplemented with 2 µg/ml puromycin.

ii. RNA interference by small hairpin RNAs (shRNA)

shRNA knockdown of SGK3 was performed using pLKO shRNA lentiviral constructs previously optimised in the lab for SGK3 knockdown in a range of cell lines. shRNA sequences are shown in table 2.4 below. To generate lentiviral particles, HEK293T cells grown on 10cm dishes were transfected with 3 µg pLKO plasmid and 3 µg each of the lentiviral packaging plasmids from Addgene with 36 µl PEI. Virus-containing medium was collected 48 and 72 h post-transfection

and filtered with a 0.45 µM filter. Cells were transfected at a 5:1 ratio in full media, with 8 µg/ml polybrene. Media was changed after 24 h, and after 48 h selection for transfected cells was performed with media supplemented with 2 µg/ml puromycin.

Table 2.7 shRNA sequences

shRNA	Sequence insert
shSGK3#1	CCGGGCAGGACTAAACGAATTCATTCTCGAGATAAGAGAAACCAACGAATGCTTTTT
shSGK3 #2	CCGGGCATTCGTTGGTTTCTCTTATCTCGAGATAAGAGAAACCAACGAATGCTTTTT
shRNA scramble	CCGGCCTAAGGTTAAGTCGCCCTCGCTCGAGATAAGAGAAACCAACGAATGCTTTTT

2.2.3.4 Treatment of cells with Growth Factors, Inhibitors or PROTACs

PROTAC compounds and inhibitors were added to cell culture medium at the time and concentration described in text, to a DMSO concentration of 0.1%. In IGF1 stimulation experiments, cells were deprived of serum for 16hr to induce basal conditions prior to stimulation with 50 ng/mL IGF1 for 15 min. 100 µg/mL stock of IGF1 was prepared in 20mM citrate pH 3. In the case of prolonged inhibitor treatments of cancer cell lines, RPMI medium and compounds were replenished every 3 days.

2.2.3.5 Cell lysis

Cells were washed with PBS and lysed on ice using 1 mL of cell lysis buffer per 15 cm dish. Lysates were clarified by centrifugation at 14,000 x g for 15 min at 4 ˚C.

2.2.3.6 Quantification of protein concentration with Bradford assay

The protein concentration of lysates was measured using the Bradford assay in a 96 well plate. 5 µl of a 1:10 diluted sample was added in duplicate to 200 µl of Bradford reagent (Coomassie Brilliant Blue). The standard curve was measured by plotting absorbance at 595 nm against BSA standards of different concentrations.

2.2.4 Western Blotting

2.2.4.1 Resolution of protein samples via SDS-PAGE and transfer to nitrocellulose membranes

To separate proteins according to their electrophoretic mobility, polyacrylamide gel electrophoresis (PAGE) was used. Home-made isogradient or commercial 4-12% Bis-Tris gels were used to resolve different proteins. Samples were made in 1x LDS buffer with 5% β-mercaptoethanol and heated at 70 ˚C for 15 min. 2-30 µg of lysate or 10% of immunoprecipitates were loaded per lane alongside protein standards. In-house gels consist of a resolving gel (375 mM Tris-HCl (pH 8.6), 0.1% SDS and 8/10/12 % acrylamide) and a stacking gel (125 mM Tris HCl pH 6.8, 0.1% SDS, 4% acrylamide). TEMED and APS were used to initiate polymerisation. The electrophoresis was initiated at 80 V until the dye front entered the resolving gel and was then increased to 160-180 V until the dye front reached the end of the resolving gel. Pre-cast gels were run at 160 V for 1 h.

For protein transfer, gels were sandwiched between nylon sponges, Whatman 3MM filter papers and nitrocellulose soaked in transfer buffer. The transfer cell was submerged in transfer buffer and transfer was carried out at 80 V for 80 min.

2.2.4.2 Immunoblotting (IB)

After transfer, membranes were blocked with 5% (w/v) skimmed milk in TBST for 1 h at room temperature. Next, membranes were incubated with primary antibodies diluted in either 5% (w/v) milk or BSA in TBST at 4 ˚C overnight. Membranes were washed four times with TBST at room temperature followed by the incubation with IR-680 or IR-800 dyes, diluted 1:10,000 in TBS/T, for 1 hour at room temperature. The membranes were then washed four times with TBS/T, and fluorescent signal captured with an Odyssey Infrared Imaging System and Quantified in Image Studio.

Where indicated, signals were visualised using Horseradish Peroxidase (HRP)-conjugated enzymes and ECL Chemiluminescent substrate and exposed to X-ray films.

2.2.5 Immunoprecipitation

2.2.5.1 Covalent coupling of antibodies

Protein G-beads were washed in PBS four times followed by coating with 1 µg of antibody per 1 µl of resin for 1 h at 4 ˚C. Beads were then washed 4 times with PBS to remove unbound antibody, followed by 4 washes with 100 mM sodium tetraborate (pH 9.3). Beads were incubated with 20 mM DMP in 100 mM sodium tetraborate twice for 30 min at room temperature followed by four washes with 50 mM glycine (pH 2.5) to remove any non-covalently coupled antibody. To neutralise the pH, two washes were performed with 200 mM Tris-HCl (pH 8). Finally, beads were incubated in 200 mM Tris-HCl (pH 8) at 4 ˚C overnight, before storage in PBS at 4˚C.

2.2.5.1 Immunoprecipitation (IP) of proteins

Covalently coupled antibody was mixed with 0.5-3 mg of lysate, at a ratio of 1µg antibody to 1mg lysate, for 2.5 h at 4 ˚C on a rotating wheel. Beads were then washed once with lysis buffer containing 500mM NaCl and once with lysis buffer containing 150 mM NaCl, followed by 2 washes with Buffer A. The immunoprecipitates were eluted by resuspending the beads in 2x NuPAGE LDS sample buffer, boiled at 70 ˚C for 15 min followed by filtering through 0.22 µM Spin-X columns.

2.2.6 Kinase assays employing a peptide substrate

In vitro kinase activities were measured using Cerenkov counting of incorporation of radioactive 32P from [γ32P]-labelled ATP into a peptide substrate. The following conditions were used: 10 mM Magnesium Acetate, 0.1 mM [γ32P]-ATP, 30 µM Crosstide Peptide (GRPRTSSFAEG) in Buffer A to a final volume of 40 µl. Control reactions contained a pre-immune IgG precipitate. Reactions were incubated at 30˚C for 30 min, shaking at 1100rpm, and terminated by adding 10µl 0.1M EDTA.

40 µl of the reaction mixture was then spotted onto P81 phosphocellulose paper, which specifically binds phosphorylated peptides, and papers washed 3x5 min in 75 mM

orthophosphoric acid to remove any radioactivity not associated with the phosphorylated peptide. Papers were then incubated in acetone for 3 min and air-dried. Cerenkov counting was performed on a scintillation counter for 1 minute per sample and counts normalised to 1ul of the kinase assay reaction mix. One unit of protein kinase activity is defined as the amount of enzyme that catalyses the incorporation of 1 nmol phosphate into the substrate in 1 min.

Protein kinase profiling

Protein kinase profiling against Dundee panel of 140 protein kinases was undertaken at the International Centre for Protein Kinase Profiling. The result for each kinase was presented as a mean kinase activity of the reaction taken in triplicate relative to a control sample treated with DMSO. Assay conditions and abbreviations are available at http://www.kinase-screen.mrc.ac.uk.

IC_{50} determination was performed with MRC PPU International Centre for Protein Kinase Profiling, according the protocol previously described (Hastie, McLauchlan and Cohen, 2006; Bain *et al.*, 2007)

2.2.7 mTORC2 kinase assays

Cells were lysed in CHAPS lysis buffer. Lysates were incubated with 15 µL HA-conjugated sepharose beads at 4 °C for 1 h. Immunoprecipitates were washed six times with CHAPS lysis buffer and twice with HEPES kinase assay buffer. Assays were carried out in a final volume of 25 µL HEPES kinase assay buffer containing 1µg of substrate (GST-Akt1, GST-ΔN-SGK1, or GST-SGK3) and kinase reactions were initiated upon addition of 0.1 mM ATP and 10 mM Magnesium acetate. Reactions were carried out for 30 min at 30°C and terminated by SDS sample buffer. Samples were heated to 70°C for 5 min, passed through a Spin-X column and subjected to immunoblot analysis.

2.2.8 Generation of knock-in cells via CRISPR/Cas9

A detailed description of the CRISPR/Cas9 mechanism is described in Chapter 5. A modified Cas9 nickase system was used for the generation of N–terminal HaloTag7–VPS34, and C–terminal

SGK3–HaloTag7 knock–in mutation, as well as knockout of msin1. Optimal sgRNA pairs were identified [as close as possible to point of HaloTag7 insertion, with a low combined off–targeting score; (VPS34–sgRNA1: GCTACATCTATAGTTGTGACC (DU52071); sgRNA2: GCCCCATCGCACCGTCTGCAA (DU52082); SGK3–sgRNA1: GAGCAAAATAAGTCTATAGA (DU52684)); sgRNA2: GAAAAATAAGTCTTCTGAAGG (DU52662), mSin1-sgRNA1: GCCCGATCAGGTCCTGCACCC; sgRNA2: GTGCTGGCAGTATACAAGCGA] using the Sanger Institute CRISPR web tool (http://www.sanger.ac.uk/htgt/wge/find_crisprs). Complementary oligos with BbsI compatible overhangs were designed for each, annealed and the dsDNA guide inserts ligated into BbsI–digested target vectors; the antisense guides (sgRNA2) were cloned onto the spCas9 D10A–expressing pX335 vector (Addgene plasmid no. 42335) and the sense guides (sgRNA1) into the puromycin–selectable pBABED P U6 plasmid (Dundee–modified version of the original Cell Biolabs pBABE plasmid). Donor constructs (VPS34–DU57077 and SGK3–DU52689) consisting of HaloTag7 or HaloTag7–IRES2–GFP flanked by ~500 bp homology arms were synthesized by GeneArt (Life Technologies); each donor was engineered to contain sufficient silent mutations to prevent recognition and cleavage by Cas9 nuclease.

1 µg each of the sense, antisense and donor plasmid were transfected into cells of 70% confluency using 20µl 1mg/ml PEI. Media was changed 24hr post transfection and puromycin selection (2µg/ml) initiated 48 hr post transfection. Untransfected cells served as negative control since these were not puromycin resistant. After another 48 h, media was changed to normal growth media for recovery. Due to the low efficiency of knockin, the transfection process was performed twice. After 2 rounds of transfection cells were split into two dishes. One half was lysed and used for the immunoblot (IB) screen of the cell pool to assess KI efficiency. The other half of the cells was prepared for single cell sorting by centrifugation at 300 x g for 3 min at room-temperature and resuspending in 1 mL DMEM containing 1% FBS. After single cell sorting into 96 well plates, each plate was centrifuged at 350 x g for 3 min at room-temperature and incubated at 37°C and 5% CO2. After 2-3 weeks, visible clones were transferred into 24-well

plates and expanded until enough cells were obtained to screen by for IB. Possible positive clones were identified by western blot before validation by gDNA sequencing, as described in section 2.2.3

2.2.9 Immunofluorescence

Immunofluorescent imaging was used in this study to determine the correct localisation of proteins of interest, and to measure production of PtdIns(3)P on endosomal membranes. 22x22 cm coverslips were sterilised in ethanol before placing in a well of 6 well plates and allowing to dry. When working with HEK293 cells or using the Freeze-Thaw method of cell permeabilization, cover slips were coated with Poly-L-Lysine to improve adherence of cells to coverslips in later washing steps. Cells were plated on coated coverslips and allowed to adhere overnight, before cell treatments were performed as indicated.

2.2.9.1 Formaldehyde fixation of cells

The goal of fixation is to maintain cells in their current state and to preserve the cells over an extended period. Chemical cross-linkers such as formaldehyde crosslink proteins via their free amino groups and cellular morphology is generally well conserved in this way. Following cell treatments, media was removed, and coverslips immediately incubated with 4% paraformaldehyde for 10 minutes at room temperature to fix the cells. After fixation, coverslips were quenched by 3x 5’ washes with 0.2% BSA in PBS.

2.2.9.2 Permeabilization

i. 1% Nonidet P40 method

Permeabilization of cells were performed by incubating coverslips for 10’ in 1% Nonidet P40 in PBS. This permeabilization enables intracellular structures to become more

accessible to antibodies, which otherwise would not be able to pass the lipid membranes of the cell.

ii. Freeze-Thaw method

Following cell treatments as described in figure legends, and prior to fixation with paraformaldehyde, cells were placed on ice and washed twice with ice-cold PBS. Cells were then washed twice with glutamate lysis buffer before snap freezing in liquid nitrogen. Coverslips were quickly thawed and washed twice more with glutamate buffer, prior to fixation with 4% PFA for 30 minutes at room temperature. After fixation, cover slips were quenched by two washes and 10' incubation with DMEM + 10 mM HEPES, pH 7.4.

2.2.9.3 Immunostaining

Following permeabilization, cover slips were washed 2 x 5' with 0.2% BSA in PBS, then incubated in blocking buffer (1% BSA in PBS) for 15' at room temperature. As with immunoblotting, this blocking minimises non-specific binding of primary antibodies to off-target antigens within the cell. After blocking samples were incubated with a dilution of the primary antibody ranging from 1:500 – 1:1000 for 1 hour at room temperature to specifically target the intracellular protein structure of interest. Following three 10 minute washes with 0.2% BSA to remove unbound antibody, coverslips were incubated with secondary antibodies conjugated to AlexaFluor-488 or AlexaFluor-594 fluorescent dyes (Life Technologies), diluted 1:500 in 0.2% BSA in PBS for 1 hour at room temperature. At the stage of adding fluorescent antibodies samples were protected from light to prevent photobleaching. Surplus antibody was again removed by three further washes for 10 min in 0.2% BSA. Subsequently coverslips were briefly washed with ddH2O to remove PBS salt crystals prior to mounting onto coverslips with ProLong gold® antifade mountant with DAPI (Life Technologies). DAPI stains the nuclei and can assist in orientation of cells. Coverslips were left in the dark at RT overnight to fully dry before imaging.

2.2.9.4 PtdIns(3)P staining and HaloTag7-staining.

PtdIns(3)P was localised by use of recombinant 2xFYVE domain probes, kindly gifted by Ian Ganley. In brief, probes were produced by expression of a tandem 2xFYVE domain of the endocytic Hrs protein (DU45781), which specifically binds PtdIns(3)P. Proteins were cloned, expressed and purified by MRC PPU Reagents and Services. This probe was then conjugated to AlexaFluor 488 (A30006 – Life Technologies) or Alexa-Fluor-594 (A30008 – Life Technologies) according to the manufacturer's protocol. The probes were stored at 1mg/ml in 50 % (v/v) Glycerol at -80 °C.

For detection of PtdIns(3)P inside cells, coverslips were permeabilised by the freeze-thaw method before paraformaldehyde fixation. The freeze-thaw method is necessary for use of these probes to remove cytosolic proteins while preserving membrane-bound proteins to give a clean signal. After blocking, coverslips were incubated with the 2xFYVE probe for 1 hour at room temperature, alongside any endosomal counterstains. After secondary staining, if required, coverslips were briefly washed in ddH20 to remove any PBS crystals and mounted on microscope slides with ProLong gold® antifade mountant with DAPI (Life Technologies). Slides were imaged under the microscope to examine localisation and the probe intensity quantified to determine intracellular PI(3)P levels.

Localisation of HaloTag7 was identified using the HaloTag7-TMR Ligand from Promega, according to the manufacturer's instructions. This ligand contains the 594-fluorescent TMR-dye conjugated to a chloroalkane moiety, which will specifically and covalently bind to HaloTag7. In brief, 5 µM HaloTag7-TMR ligand was added to live cells for 15 minutes, and washout performed for 30 minutes, before fixation and counterstaining for endosomal markers.

2.2.9.5 Imaging and Quantitation

All images were collected on an LSM710 laser scanning confocal microscope (Carl Zeiss) using the x63 Plan - Apochromat objective (NA 1.4), using a pinhole chosen to provide a uniform 0.8um optical section thickness in all the fluorescence channels. For quantitation of PtdIns(3)P production, images from the microscope were imported into Volocity image processing software (Perkin-Elmer) and batch processed using the same custom written programmes for all the images in an experimental group. The graphs show the sum of signal intensity per cell in arbitrary units.

2.2.10 Measurement of cell growth and viability

2.2.10.1 Quantification of cell growth by Incucyte S3 Assay.

To measure the rate of growth of cancer cell lines, cells were seeded into 96-well plates and allowed to adhere overnight. The next morning, cells were treated in triplicate with the compounds indicated and placed in an Essen Incucyte S3, incubated at 37 ˚C. 4 images per well were taken every 4 hours, and cell confluency estimated from these images for the length of time indicated.

2.2.10.2 Quantification of cell number by Sytox Green Assay

Sytox Green is a nucleic acid stain which gives a >500-fold fluorescent enhancement when binding to nucleic acid. However, the stain is also impermeable to live cells. Therefore, dead cells can be measured by brief incubation of a cell population with Sytox Green and excitation of the dye by a 488 nm laser, with an emission peak of 523 nm. After measuring dead cells, adding the mild detergent saponin to a cell population overnight will permeabilise the cells allowing a total cell count. Live cell number can then be calculated by subtracting dead cell count from the total cell count.

This approach can be used to measure sensitivity of a cell population to compound treatment. After seeding 2 plates in parallel and allowing cells to adhere overnight, one plate was taken at ‘Day 0’ and total cell number calculated. The second plate was treated as indicated for 5-7 days,

and remaining surviving cells measured by Sytox Green Assay. Subtracting 'Day 0' counts from the final cell count provides a proxy of cell growth and survival in the presence of the tested compound. The multi-well plate format allows a large number of compounds to be tested over a range of concentrations in parallel. Plates were read using the Acumen laser scanning plate reader, using the 488nm argon-ion laser to excite the dye.

2.2.10.3 Estimation of cell viability by MTS assay.

MTS assay was performed using the CellTiter 96® AQueous One Solution Cell Proliferation Assay kit from Promega. This kit provides a colorimetric method to measure cell viability, as it contains the tetrazolium compound MTS [3-(4,5-dimethylthiazol-2-yl)-5-(3-carboxymethoxyphenyl)-2-(4-sulfophenyl)-2H-tetrazolium, inner salt] which reacts with the electron coupling reagent PES (phenazine ethosulfate) to form a formazan product in live, proliferating cells. This can be measured in a multi-well assay, measuring production of formazan by absorbance at 490 nM. While this assay is in fact a measure of metabolism, it is often used at a proxy for cell viability and proliferation. The production of formazan product, as measured by absorbance at 490nm, is directly proportional to the number of living cells in culture.

For this assay, cells were seeded in 96-well plates and allowed to adhere overnight. The next morning, cells were treated with compounds as indicated in the figure. DMSO treatment was used as a positive control and 0.1% Triton was used as a 100% death negative control. After 48 h treatment, cell viability was measured by addition of MTS reagent for 4 h, and measurement on an optical plate reader at 490 nm. Absorbance was normalised to DMSO control to determine any impact of the compound on cell viability.

2.2.11 Mass Spectrometry Methods

2.2.11.1 Global Proteome Analysis

Cell lysis and sample preparation

Cell pellets were lysed with 2 ml of lysis buffer (8 M Urea, 50 mM Ammonium bicarbonate containing protease inhibitor and phosphatase inhibitor). Samples were incubated on ice for 15 min then sonicated for 5 min (30 sec on/off) in ice-cold water bath. After sonication, benzonase® endonuclease (Merck Millipore) was added 1:100 to degrade DNA and RNA. Lysates clarified by centrifugation at 12,000 rpm, 15 min at 4 °C, and supernatants were transferred into new Eppendorf tubes. Protein concentration was measured with BCA assay (Pierce™ BCA Protein Assay Kit, Thermo). Each sample was reduced with 5 mM DTT at 45 °C for 30 min, before alkylation for 30 min at RT with 10 mM iodoacetamide. Alkylation was quenched by the addition of 5 mM DTT.

Samples were digested by Lys-C (1:200 w/w) for 4 h at 30 °c. Samples were diluted with 50 mM ammonium bicarbonate to 1.5 M Urea concentration. Samples were then digested with trypsin (Pierce trypsin, Thermo) at an enzyme to protein ratio of 1:50 (w/w) at room temperature with gentle shaking overnight. The digest was stopped by the addition of 1% TFA (v/v), centrifuged at 10,000 g for 10 min at room temperature. The supernatants were desalted on 200 mg SepPak C18 cartridge (Waters), and dried by vacuum centrifugation using Speedvac (Thermo).

TMT labelling and Basic C18 reverse phase (bRP) chromatography fractionation

200 µg peptides was re-suspended in 100 µL 100 mM TEAB buffer. The TMT labelling reagents were equilibrated to room temperature and 41 µL anhydrous acetonitrile was added to each reagent channel and softly vortexed for 10 min. Peptides were transferred to the corresponding TMT channels and incubated for 1 h at room temperature. The reaction was quenched with 8 µL of 5% hydroxylamine. To ensure complete labelling, 1 µg of labelled samples from each channel were analysed by LC-MS/MS prior to mix. After evaluation, the complete TMT labelled 9 samples were then combined, acidified and dried. Sep-Pak desalting was then performed, and the elution was dried to completeness.

Pooled peptides were separated by basic reverse phase (bRP) chromatography fractionation. With Ultimate 3000 high-pressure liquid chromatography (HPLC) system (Dionex) operating at 569 µL/min with two buffers: buffer A (10 mM ammonium formate, pH 10) and buffer B (80% ACN, 10 mM ammonium formate, pH 10). Peptides were resuspended in 200 µL of buffer A (10 mM ammonium formate, pH10) and separated on a C18 reverse phase column. A total of 90 fractions (1 min per fraction) were collected before further concatenation into 30 final fractions. Each fraction was then dried and desalted over a C18 StageTip prior to analysis by mass spectrometry.

LC-MS/MS and Data Analysis

LC-MS/MS was performed by Dr Houjiang Zhou at the MRC PPU. Liquid Chromatography (LC) separations were performed with a Thermo Dionex Ultimate 3000 RSLC Nano liquid chromatography instrument. Approximately 1 µg of concatenated peptides (Peptides quantitation by Nanodrop) from bRP chromatography were dissolved in 0.1% formic acid and then loaded on C18 trap column with 3 % ACN/0.1%TFA at a flow rate of 5 µL/min. Eluted peptides were analysed on an Orbitrap Fusion Lumos (Thermo Fisher Scientific, San Jose, CA) mass spectrometer.

All the acquired LC-MS/MS data were analysed using Proteome Discoverer software v.2.2 (Thermo Fisher Scientific) with Mascot search engine. Data were searched against a complete UniProt Human (Reviewed 20,143 entry downloaded at Nov 2018). Reporter ions were quantified from MS3 scans. Protein ratios were calculated from medians of summed sample abundances of replicate groups. Standard deviation was calculated from three biological replicate values. The standard deviation of three biological replicates lower than 25% were used for further analyses. To determine the significant differences between different treatments, ANOVA model is used for statistical significance analysis.

2.2.11.2 Global Phosphoproteome Analysis

Phosphopeptide enrichment

Cell lysates were prepared and desalted as described for total proteomics above. The desalted peptides were resuspended in 1 ml of 2 M lactic acid/50% acetonitrile (ACN) and centrifuged at 15,000 x g for 20 min. Supernatants were transferred to an Eppendorf tube containing 18 mg of titanium dioxide (TiO2) beads (GL sciences, Japan) and vortexed for 1 h at room temperature. The TiO2 beads were washed three times (10 min per wash) with 2 M lactic acid/50% ACN following by three washs with 0.1%TFA/50% ACN. Phosphopeptides were eluted twice with 150 µl of 50 mM ammonia solution (NH4OH) (pH ~10). The combined eluent were dried using vacuum centrifugation and then desalted using a C18 StageTip (3M Empore™). TMT labelling was performed as described for total proteomics.

LC-MS/MS and Data Analysis

LC-MS/MS was performed by Dr Houjiang Zhou at the MRC PPU. The desalted TMT labelled phoshopeptides were dissolved in 0.1% formic acid and then loaded on C18 trap column with 3 % ACN/0.1%TFA at a flow rate of 5 µl/min. Eluted peptides were analysed on an Orbitrap Lumos Tribrid platform with instrument control software version 3.0.

Maxquant was used for processing the collected MS Raw data. The raw data were searched against Uniprot human database (70,947 entries, downloaded on March 10, 2017) using Mascot. The phosphopeptides were quantified using the intensity of TMT reporter ions. Data were further analysed with Perseus software and figures were made using PRISM software.

2.2.11.1 Analysis of biotinylated proteins by TurboID and streptavidin pulldown.

Cell culture and proteomic sample preparation

After stimulation, cells were washed 5 times with ice cold PBS to remove exogenous biotin and lysed in RIPA buffer. Lysates were clarified by centrifugation and quantified using Pierce 660 nM Protein Assay Reagent. Streptavidin pulldown was performed on 500ug-1mg lysate overnight

with 20ul Streptavidin-conjugated sepharose beads. Streptavidin-IP was washed 3x each in RIPA buffer, 500 mM Tris-HCl and Urea Buffer. To prepare proteins for digest, the samples were reduced with 1 mM DTT for 30 minutes, alkylated in the dark with 10 mM iodoacetamide for 30minutes, and quenched with 10 mM DTT for 10 minutes. Samples were first digested with 200ng Trypsin per sample, at 32°C with gentle shaking for 16 h. The digest was stopped by the addition of TFA to a final concentration 1% TFA (v/v), centrifuged at 10,000 g for 10 min at room temperature. The supernatant was desalted on SCX membrane and desalted peptides airdried by vacuum centrifugation using a SpeedVac (Thermo Scientific)

TMT labelling

Each sample was re-suspended in 20 µL of 100 mM TEAB buffer. The TMT labelling reagents were equilibrated to room temperature and 7 ul TMT reagent added with 3 ul anhydrous acetonitrile. Labelling reactions were incubated for 1 h at room temperature with gentle shaking. The reaction was quenched with 0.1% v/v hydroxylamine. To ensure complete labelling, 10% labelled samples from each channel were analysed by LC-MS/MS prior to mix. After evaluation, the complete TMT labelled 9 samples were then combined, acidified and dried. Samples were desalted and fractionated on C18 membrane prior to analysis by mass spectrometry.

LC-MS/MS and Data Analysis

LC-MS/MS was run by MRC PPU Proteomics Facility (Robert Gourley). Peptides were analysed on Orbitrap Fusion Lumos (Thermo Fisher Scientific, San Jose, CA) mass spectrometer. All the acquired LC-MS data were analysed using MaxQuant software v.1.6.6.0. Volcano plots were produced in Perseus 1.6.2.3.

2.12. Statistical Analysis

With the exception of Mass Spectrometry Analysis, described above, all figures are representative of at least n=2 replicate experiments. Statistical analysis was performed in GraphPad Prism v8, and described in figure legends.

3. SGK3-PROTAC1 induces degradation of SGK3 in cancer cell lines

3.1 PROTACs – Proteolysis Targeting Chimeras for targeted protein degradation

Proteolysis Targeting Chimeras (PROTACs) have recently gained momentum as a new therapeutic axis in targeting erroneous signalling axes. These compounds act by 'hijacking' the ubiquitin-proteasome system, allowing target proteins to be ubiquitylated and targeted for degradation by the cells' own degradation machinery. As will be discussed further in section 3.2.1, this approach has numerous benefits over chemical inhibition. I therefore chose as a major aim of my thesis to develop a PROTAC compound targeted against SGK3, designed to degrade the protein from cancer cell lines and modulate PI3K inhibitor resistance.

3.1.1 Ubiquitin-Proteasome mechanism of protein degradation

Like protein phosphorylation, protein ubiquitylation is an evolutionarily conserved posttranslational modification critical to numerous cell signalling processes. It requires the transfer of a 76 amino acid protein Ubiquitin to, typically, lysine residues on substrate proteins. Ubiquitin can be conjugated to substrates in a variety of topologies resulting in different cellular responses. Substrate proteins can be monoubiquitylated, polymonoubiquitylated, or decorated with polyubiquitin chains. Further specificity of the pathway is mediated by different polyubiquitin chain types being formed, from different lysines of ubiquitin. Chains can be formed from K6, K11, K27, K29, K33, K48, and K63, in addition to the N terminal Methionine M1. These chain types signal for different cellular responses, for example, K63 and linear ubiquitin chains can have both scaffolding and signalling roles, regulating many biological processes, including inflammation (Newton *et al.*, 2008; Walczak, Iwai and Dikic, 2012). K48 and K11 chains on substrate proteins specifically target the ubiquitylated protein for degradation via the proteasome (Jin *et al.*, 2008; Newton *et al.*, 2008; Wickliffe *et al.*, 2011). It is this proteasomal degradation which is targeted by the PROTAC mechanism.

3.1.2 E3 Ubiquitin Ligases

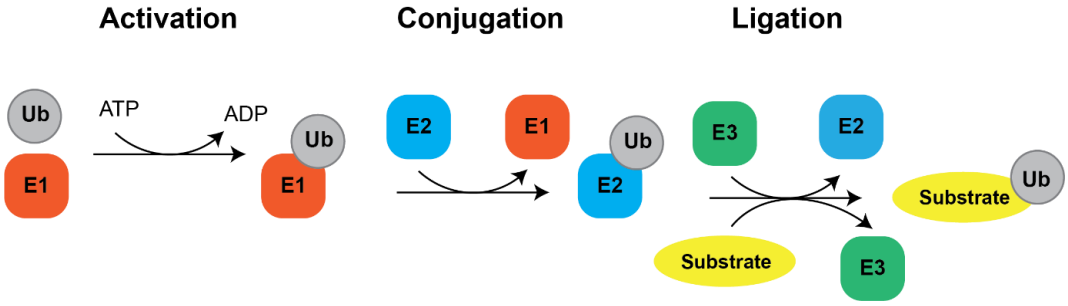

Figure 3.1 Mechanism of substrate ubiquitylation.
Ubiquitin is activating by formation of a thioester bond onto an E1 enzyme, in an ATP dependent manner. Ubiquitin is conjugated onto the E2 conjugating enzyme. E3 ligases catalyse the transfer of ubiquitin from the E2 to the substrate protein

Ubiquitylation is mediated by three families of enzymes. E1 activating enzymes catalyse the formation of an E1-Ub thioester in an ATP-dependent manner (Schulman and Harper, 2009). E2 conjugating enzymes are then 'charged' with the ubiquitin, generating a E2-Ub thioester (Komander, 2009). E3 ubiquitin ligases catalyse the final step of the substrate ubiquitylation cascade. These enzymes interact with both the E2-Ub conjugate and a target protein to catalyse the transfer of Ubiquitin to the substrate. While there are just 2 E1s, UBE1 and UBE1L2, and over 40 E2s, complexity and specificity in the pathway is mediated by the E3. There are >600 E3 ligases, grouped into 3 families, based on their structure and mechanism of ubiquitin transfer (Li *et al.*, 2008). These are the Really Interesting New Gene (RING)-E3 ligases, the HECT-E3 ligases and RING-between-RING (RBR)-E3 ligases. One subset of the RING E3 ligases is the Cullin-RING (CRL) E3 ligases. These enzymes are large E3 ligase complexes, built on a Cullin scaffold. This scaffold then binds adaptor proteins to substrate receptors, and the E3 ligase protein itself. Through this scaffold mechanism, substrate proteins are recruited into proximity of the E3, where transfer of Ubiquitin from the E2 can be catalysed.

An example of such an E3 is the $CUL2^{VHL}$ E3 ligase. Built from a Cullin2 scaffold, the pVHL substrate adaptor protein is joined to the complex by Elongin1/Elongin2. pVHL recognises its substrate, Hif1α, via a hydroxyproline residue on Hif1α. Under normoxic conditions, Hif1α is hydroxylated on this proline by Proline hydroxylase (PHD) enzymes, and is rapidly recognised

and ubiquitylated by VHL, and targeted for degradation (Figure 3.2). Under conditions of hypoxia, PHD enzymes are inhibited, and Hif1α is stabilized, accumulates and triggers the transcription of hypoxia related genes. Also bound to Cullin2 is the RBX1 E3 ligase, and recruitment of Hif1α to the complex by VHL allows ubiquitin transfer to the substrate from an associated E2. Similar mechanisms of ubiquitin transfer are utilised by $CUL4^{CRBN}$ and $CUL1^{SKP2}$.

3.2 PROTAC mechanism - Proximity-based ubiquitylation

The mechanism of action of CRL E3 ubiquitin ligases, identifying substrate proteins for ubiquitylation via an adaptor protein, has recently been exploited for targeted degradation of alternative proteins. As ubiquitylation of substrate proteins by CRL E3 ligases is proximity driven through the substrate receptor, with no specific ubiquitylation motifs, this mechanism can be hijacked to target protein degradation to desired target proteins. By recruiting the target protein of interest to the target E3 ligase, this protein can be ubiquitylated in the place of the endogenous substrate.

One example of this is Proteolysis Targeting Chimeras (PROTACs). PROTACs are chimeric molecules, consisting of an E3 ligase-binding headgroup joined to a protein-targeting headgroup joined by a short linker sequence (Pettersson and Crews, 2019). For example, in order to target VHL E3 Ligase, the ligand VH032 designed as a Hif-1α mimic and a high affinity binder of VHL, has been conjugated to a range of known inhibitors to target a vast array of proteins (Zengerle, Chan and Ciulli, 2015; Gadd *et al.*, 2017; Maniaci *et al.*, 2017; Smith *et al.*, 2019). Similarly, $CUL4^{CRBN}$ E3 ligase has been utilised using compounds derived from pomalidomide and a number of other phthalidomide-related inhibitors (Lu *et al.*, 2015; Winter *et al.*, 2015; Lai *et al.*, 2016; Olson *et al.*, 2018).

To date, PROTAC compounds have been developed targeting a range of protein kinases, such as RIPK2 (Bondeson *et al.*, 2015) BCR-ABL(Lai *et al.*, 2016; Shibata *et al.*, 2018), CDK9 (Olson *et al.*, 2018) and PTK2 (Cromm *et al.*, 2018; Popow *et al.*, 2019). As discussed below, targeting protein

kinases for targeted degradation evades numerous issues with conventional kinase inhibition (Ferguson and Gray, 2018).

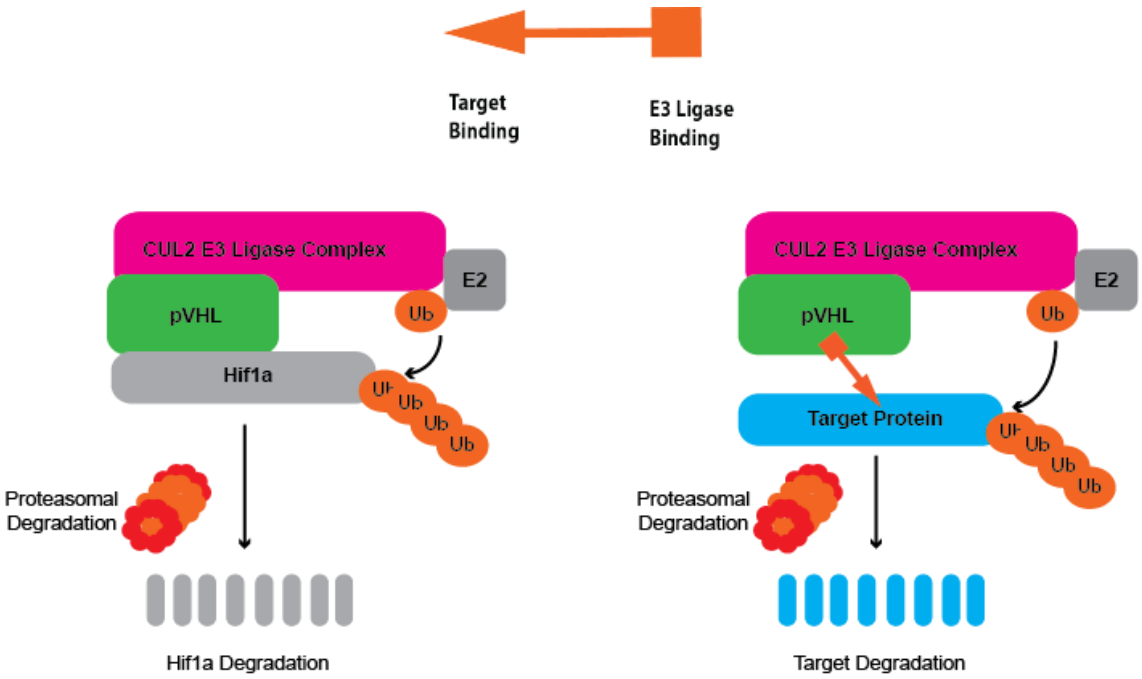

Figure 3.2 Mechanism of action of PROTAC compounds.
A PROTAC consists of an E3 binding motif and target protein binding motif, joined by a short linker. PROTACs act by recruiting a protein of interest to the targeted E3 ligases. The CUL2 VHL E3 Ligase complex typically induces ubiquitylation and degradation of Hif1a under conditions of normoxia. Formation of an E3-PROTAC-target ternary complex results in the polyubiquitylation of the target protein, leading to its proteasomal degradation in cells.

3.2.1 Benefits of targeted degradation over chemical inhibition of protein kinases

The importance of protein phosphorylation to cell signalling and disease means that kinases are commonly the target of therapeutic avenues. Kinase inhibitors have been developed for a wide range of diseases; however, issues arise in resistance and off target effects. Many of these problems with kinase inhibition can be solved by targeted protein degradation. Firstly, chemical inhibition of kinases requires 1:1 occupation of the binding site, and therefore fairly high concentrations of compound are required for a biologically significant, therapeutic effect. This can result in either on-target or off-target toxicity. The catalytic mechanism of action of a PROTAC means that the compound can be applied at sub stoichiometric levels, therefore much

lower amounts are required. This reduces off target effects and is an advantage as both a methodological tool and a potential therapeutic. Additionally, chemical inhibition of a kinase will only remove one function of a protein, its kinase activity. Many kinases also carry additional functions such structural and scaffolding roles, which would not be removed by chemical inhibition. Conversely, targeted degradation of the protein will remove it from the cell completely, therefore removing all its potential roles. Depending on whether these additional functions are beneficial or deleterious, it may be advantageous to remove the entire protein from cells. There is also an additional advantage that these tools allow us to delineate between kinase and non-kinase functions of proteins in disease.

Finally, a common mechanism of resistance to chemical inhibition is for the cell to upregulate a target protein at the transcriptional level, to overcome loss of function. However, this is circumvented by the PROTAC as any newly translated protein can be rapidly degraded (reviewed in (Ferguson and Gray, 2018)).

'Drugging the undruggable'

A large benefit of PROTAC compounds is the ability to target proteins previously considered 'undruggable'. A large portion of the human proteome is implicated in disease, however most cannot be targeted by conventional chemical therapeutic methods. Many identified proteins important in oncogenesis have so far failed to be inhibited by conventional approaches, and therefore deemed 'undruggable' (Huang and Dixit, 2016). In particular, proteins such as Myc, β-catenin and MCL1 have been particularly difficult to target (Nero *et al.*, 2014). Targeted protein degradation opens a whole new realm of potential for interrogating protein function

3.3 Designing a PROTAC compound targeting SGK3 for degradation.

Given the powerful potential of PROTACs as a tool to investigate protein function, and as a new therapeutic modality, one of the leading aims of my thesis was to develop a tool compound for the degradation of SGK3 from relevant model cancer cell lines. HEK293 SGK3 KO cells have been

previously generated using CRISPR/Cas9 technology, and this cell line has been successfully used to expand our knowledge of how SGK3 is activated by growth factor signaling (Malik *et al.*, 2018). However, a caveat to this genome level knockout is that compensatory pathways may replace the role of SGK3 over time, and the effects of the knockout may be diminished. In addition, attempts in the lab to generate a genome level knockout of SGK3 in relevant model breast cancer cell lines, such as the ZR-75-1 and CAMA-1 cell lines have so far been unsuccessful. Use of PROTAC compounds to induce rapid, reversible knockout of SGK3 at the protein level in these cells is a promising solution to these caveats. I therefore aimed, in the first two chapters of my thesis to develop tool compounds to induce degradation of SGK3.

The strategy chosen for this approach involved designing compounds derived from a series of SGK inhibitors recently published by Sanofi (Halland *et al.*, 2015). Because a crystal structure of the SGK3 kinase domain is not yet available, either alone or in complex with an inhibitor, we could not use structure-guided design to build a series of degraders. The Ciulli lab inspected the structure activity relationship (SAR) of the series of SGK inhibitors described in the Sanofi Patent (Halland *et al.*, 2015) (International Patent WO2014140065), to identify potential strategies to elaborate PROTACs.

3.4 Two rounds of compound screening revealed optimal compound SGK3-PROTAC1

A series of inhibitors that have a pyrazolopyrimidine scaffold appeared to tolerate aliphatic and cyclic substituents at the position 4 of the pyrazolopyrimidine core, suggesting that such portion of the molecule could be solvent exposed. Two SGK inhibitors, termed 290 and 308 (Fig 3.3A), were judged particularly amenable for linker conjugation, as the morpholine ring can be selectively N-alkylated by means of reductive amination protocols. (Fig 3.3A). As the inhibitors described in the patent were racemic, we synthesized both the R and S epimers of these compounds and determined by kinase screening that the R forms were marginally more potent

(data available at http://www.kinase-screen.mrc.ac.uk/kinase-inhibitors). The specificity of these compounds was profiled against 140 kinases at 1 μM concentration, revealing that they were relatively selective (Figure 3.3, 3.4 and Appendix Table 1), with S6K1 being a key off target that was most potently inhibited. Further profiling determined that the IC50 of these compounds for SGK1 and SGK3 were between 5 to 40 nM, with S6K1 again being a key off-target with IC50 of 1-10 nM (Table 3.1).

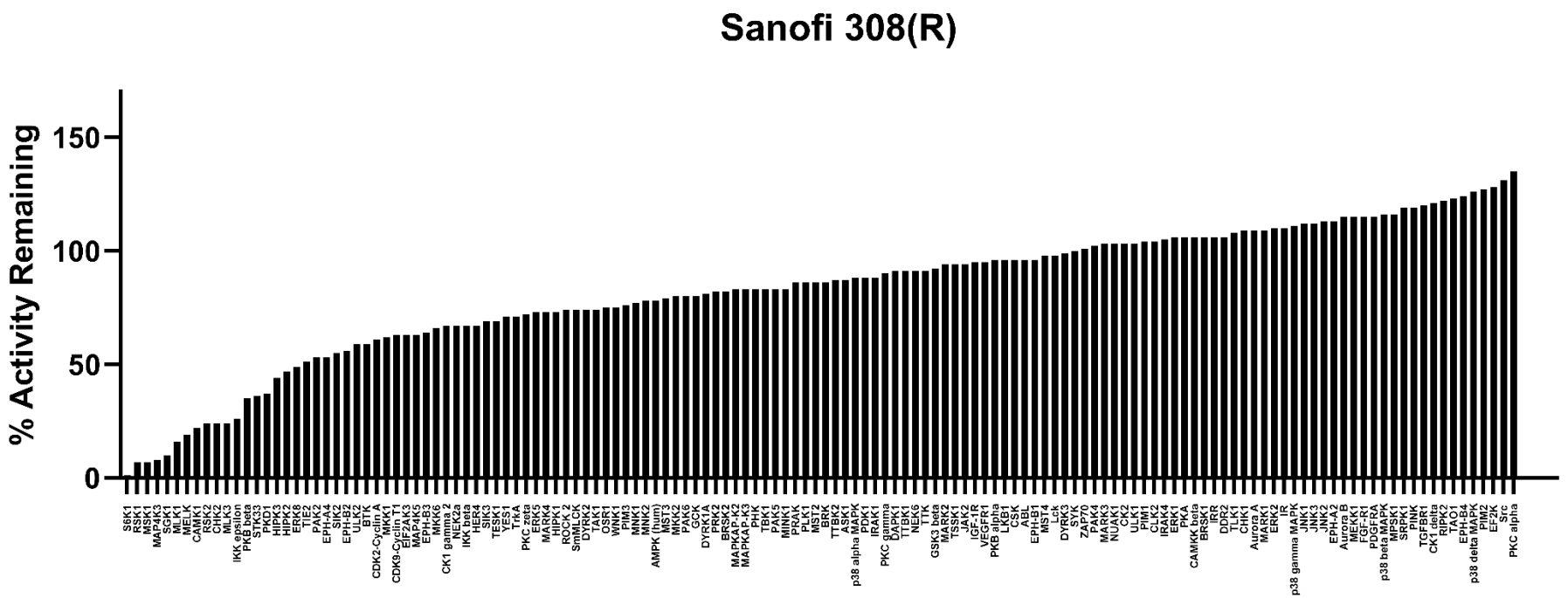

Figure 3.3 In vitro selectively screening of 1 μM Sanofi 308(R).

Kinase selectively profiling was performed by the National Centre for Protein Kinase Profiling (www.kinase-screen.mrc.ac.uk) against 140 protein kinases. Data are presented as mean (n=3) kinase activity remaining in the presence of 1 μM Sanofi 308(R), in comparison to a DMSO control. Raw data is available in Appendix Table 1, and data for the S isoform available online.

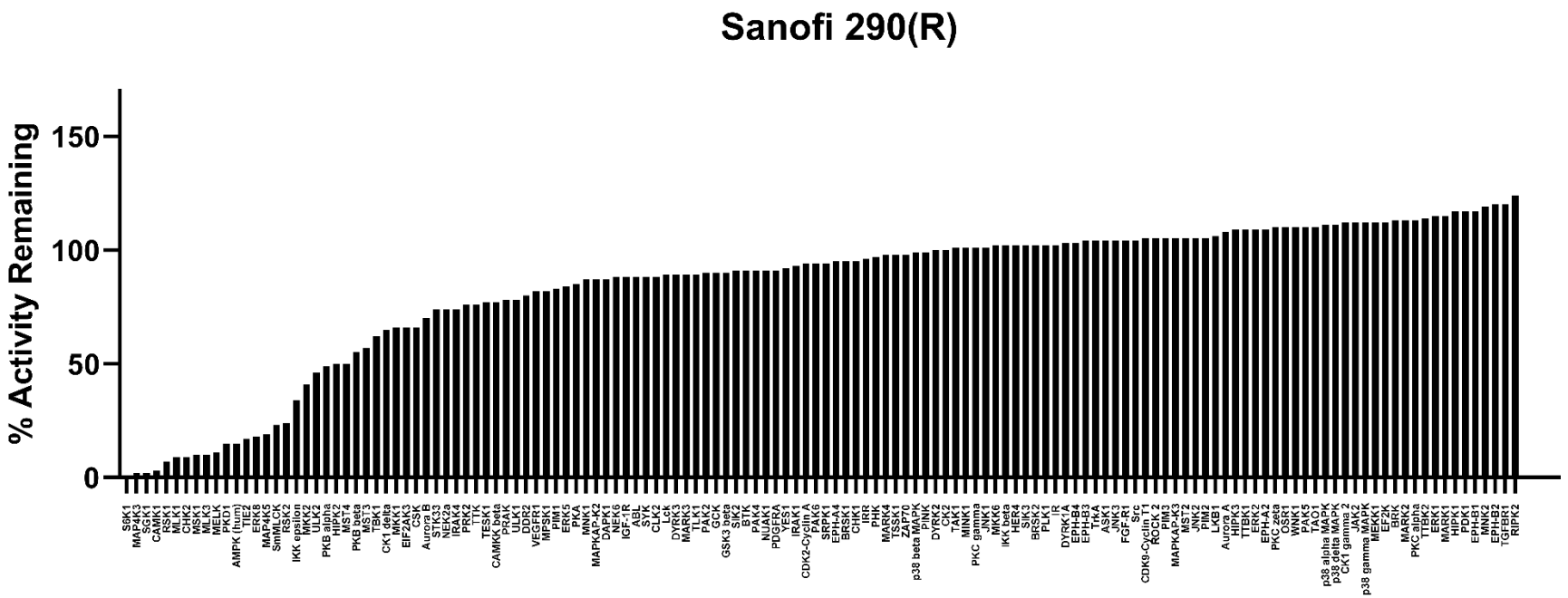

Figure 3.4 In vitro selectively screening of 1 μM Sanofi 290(R).

Kinase selectively profiling was performed by the National Centre for Protein Kinase Profiling (www.kinase-screen.mrc.ac.uk) against 140 protein kinases. Data are presented as mean (n=3) kinase activity remaining in the presence of 1 μM Sanofi 290(R), in comparison to a DMSO control. Raw data is available in Appendix Table 1 and data for the S isoform available online.

Design of 1st Generation compound DAT1

For the first round of compound screening, 4 compounds were developed by the Ciulli lab, with 290-R or 308-R conjugated to either the well characterised VHL ligand VH032 (Galdeano *et al.*, 2014; Frost *et al.*, 2016) or the Cereblon ligand pomalidomide (Lu *et al.*, 2015) (Fig 3.5B). For this first series of compounds, a medium length linker, composed of 3 PEG units, was used (Fig 3.5C).

In order to examine the potency and specificity of the compounds, I administered them to HEK293 cells for 48 hours at concentrations of up to 10 μM and analysed the effect of PROTAC treatment on expression of endogenous SGK isoform or S6K1 expression (Fig 3.3C). Of the four compounds tested only DAT1, composed of 308-R conjugated to VH032, markedly reduced SGK3 expression. Additionally, this reduction in SGK3 occurred without significantly impacting levels of SGK1, SGK2 or S6K1 (Fig 3.5D). DAT1 reduced SGK3 expression by 69% at 1 μM and 77% at 10 μM after 48 h (Fig 3.5D).

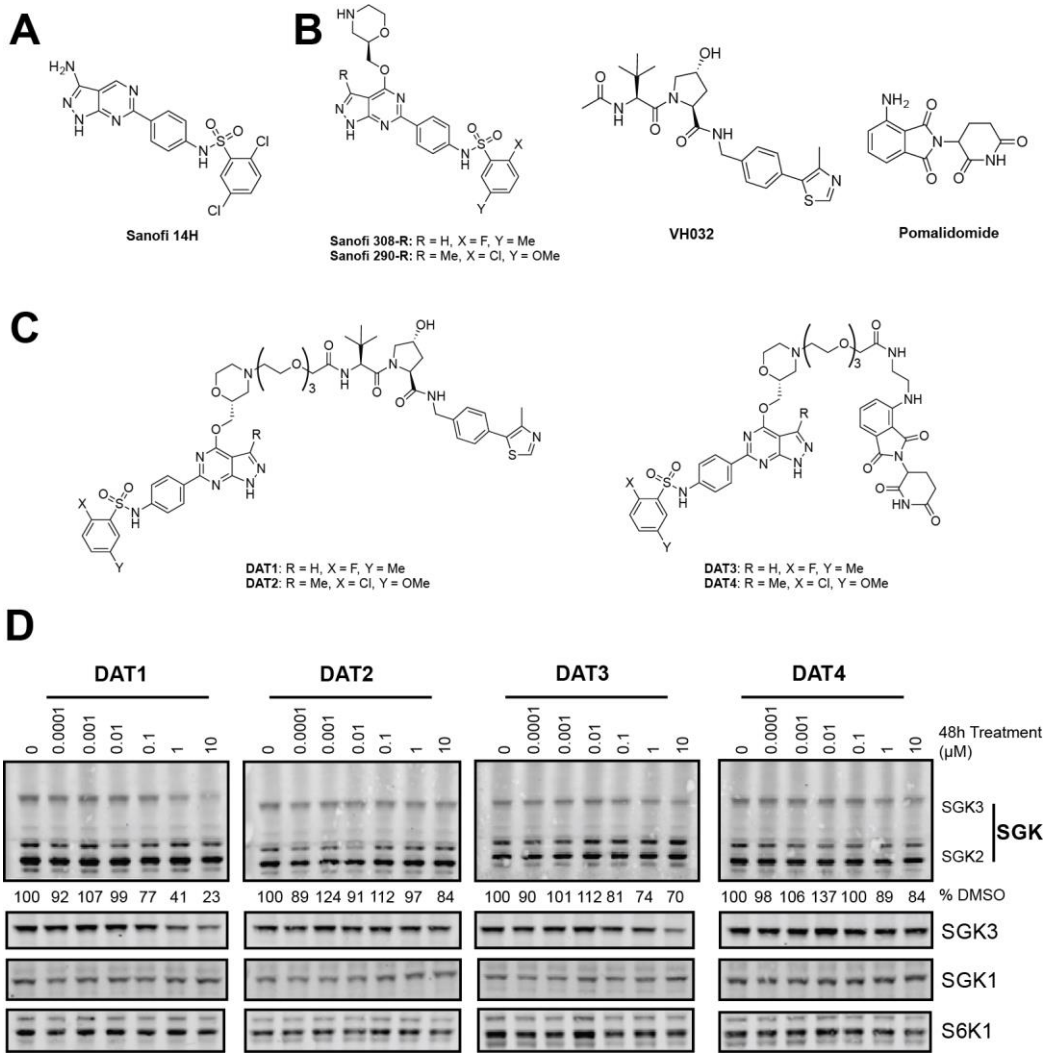

Figure 3.5 Design and cellular activity of first generation SGK3 PROTACs.
A*. Structure of compound 14H, previously published by Sanofi as an inhibitor of SGK3.* ***B****. Starting material for SGK PROTACs. PROTACs were derived from SGK inhibitors 308-R or 290-R linked to either VH032 or Pomalidomide to target the VHL or Cereblon E3 ligases respectively.* ***C****. Structures of first generation SGK PROTACs, generated by the Ciulli lab. SGK and E3 ligase targeting motifs were joined by a 3xPEG linker to produce the PROTACs* ***D****. HEK293 cells were treated for 48 hours with increasing concentrations of each PROTAC compound from 0.1 nM to 10 μM. Cell lysates were subjected to immunoblot analysis with the indicated antibodies, and SGK3 protein levels quantified in Image Studio Lite software (Licor).*

Conjugation of 308-R to E3 ligase ligands for the elaboration of PROTACs markedly decreased the inhibitory activity for SGK isoforms and S6K1 in biochemical kinase assays (5 nM to 440 nM for SGK3 and 1 nM to 160 nM for S6K1) (Table 3.1). We found no correlation between potency of PROTACs for inhibiting SGK3 and ability to induce degradation of SGK3 in cells. For example, DAT2 which does not impact SGK3 protein levels in HEK293 cells, inhibited SGK1 and SGK3 2-4-fold more potently than DAT1.

Table 3.1*. *IC50 values of SGK inhibitors and first generation PROTACs.
The structures of the compounds are shown in Figure 3.5B&C. For degradation efficiency "-" = No Degradation, "+" = >50% Degradation at 10 μM.

	SGK3 IC50 (nM)	SGK1 IC50 (nM)	S6K1 IC50 (nM)	SGK3 Degradation Efficiency
290 (R)	35	19	10	/
308(R)	5	10	1	/
DAT1	440	1600	160	+
DAT2	190	400	180	-
DAT3	640	1000	240	-
DAT4	540	600	190	-

Treatment with 1 μM DAT1 maximally reduced SGK3 expression by 12 hours (Fig 3.6A) and a dose response analysis revealed that 2 μM DAT1 maximally reduced SGK3 expression at an 8 h time point (Fig 3.6B). To validate that this degradation occurred, as expected, via the $CUL2^{VHL}$ E3 Ligase complex and the proteasome, I pre-treated cells with inhibitors of the pathway (Fig 3.7) and measured blockade of DAT1-induced degradation. MLN4924 is an inhibitor of the Neddylation enzyme which conjugates NEDD8 onto the CRL E3 ligases (Brownell *et al.*, 2010). Inhibition of this Neddylation process inactivates the complex. MG132 is an inhibitor of the proteasome and therefore blocks the degradation of ubiquitylated proteins (Lee and Goldberg, 1998). As expected, pre-treatment with MLN4924 (3 μM) or proteasome inhibitor MG132 (50 μM) successfully blocked DAT1-induced degradation of SGK3 (Figure 3.6C). These data demonstrate that DAT1 degradation of SGK3 is both neddylation and proteasome dependent, and therefore acting via the expected mechanism. I therefore selected DAT1 to analyse further and create a range a derivatives to optimize degradation.

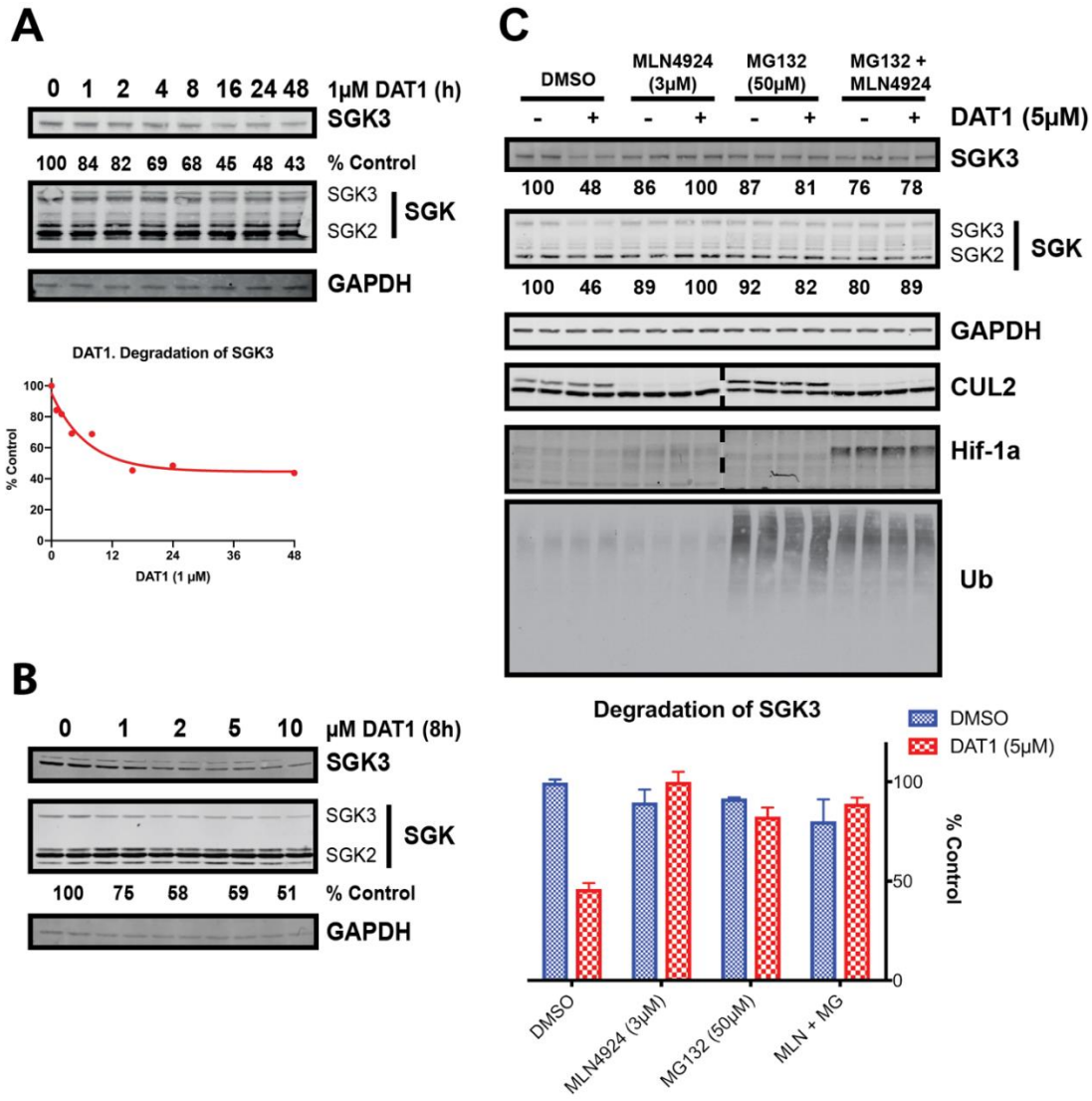

Figure 3.6 Mechanistic characterization of DAT1

A*. HEK293 cells were treated for up to 48h with 1 μM DAT1, and lysates analysed by western blot for SGK3 expression* ***B****. HEK293 cells were treated for 6 h with increasing doses of DAT1, and lysates analysed by western blot.* ***C****. HEK293 cells were pre-treated with the indicated inhibitors before treatment for 6 h with 5 μM DAT1, and lysates analysed by western blot for SGK3 expression.*

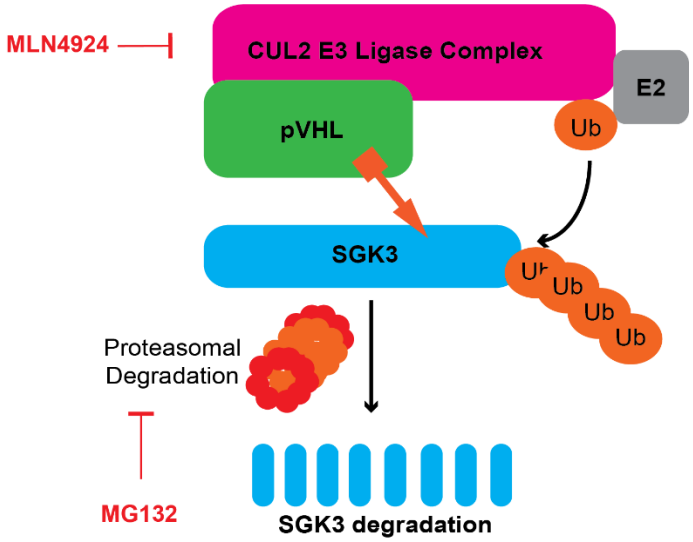

Figure 3.7 Inhibitor treatments for mechanistic validation of SGK PROTACs.
MG132 is an inhibitor of proteasome activity, and blocks degradation of polyubiquitylated proteins. Neddylation inhibitor MLN4924 restricts activity of the CUL2^{VHL} complex, and therefore reduces CUL2^{VHL} E3 activity and blocks ubiquitylation of target proteins.

Design of 2nd Generation compound DAT8 (SGK3-PROTAC1)

The next series of compounds were analogues of DAT1, produced by shortening the linker length from 3 to 2 PEG units (DAT5) or extending the linker length to 4 and 5 PEG units (DAT6-7). (Fig 3.8A). As before, I tested the ability of each of these compounds to decrease SGK3 expression after 48 h treatment in HEK293 cells (Fig 3.8C). From this data I determined that the optimal linker length was 4 PEG units (13 atoms), with DAT6 displaying significant improvements both in terms of potency and amount of reduction of SGK3 observed compared to the original DAT1 (Fig 3.6C). DAT6 induced 55% degradation of SGK3 at 1 µM, and 80% degradation at 10 µM. DAT7 (16 atoms) also induced potent degradation of SGK3. We then changed the composition of the linkers for more lipophilic alkylic moieties of 13 (DAT8) and 16 atoms (DAT9,10). For this set of compounds, we also conjugated the inhibitor 290-R (DAT11,12). This was to determine whether, with an optimized linker, the 290-R derived compounds may show some activity.

DAT8 possessed the best potency for inducing degradation of SGK3, with 65% degradation at 0.1 µM and 75% degradation achieved at 1 µM after treatment for 48 h. This represents a >10-fold increase in potency for DAT8 over DAT6, and is likely a result of increased cell penetrance from a more lipophilic linker region, however this was not further studied. At <1 µM,

degradation was specific for SGK3 with no effect on SGK1/2 or S6K1. At concentrations >1 μM, however, a slight reduction in S6K1 expression can be observed. DAT8 was therefore selected for further use in this thesis and renamed SGK3-PROTAC1 (Fig 3.8D). SGK3-PROTAC1 possesses a linker of 13 atoms, the same as DAT6, however carries 1 less oxygen atom, creating a more lipophilic compound (Fig 3.8A).

At this stage I also decided to generate a control compound for SGK3-PROTAC1 that would bind and inhibit SGK3, but not induce recruitment of the CUL2-VHL E3 ligase complex. We therefore synthesized a version of SGK3-PROTAC1 termed cisSGK3-PROTAC1 that contains a hydroxyl epimer of VH032 moiety that previous work showed ablates binding to VHL (Fig 3.8B) (Bondeson *et al.*, 2015; Zengerle, Chan and Ciulli, 2015; Frost *et al.*, 2016).

In *in vitro* assays, SGK3-PROTAC1 inhibited SGK3 with an IC50 of 300 nM and S6K1 with an IC50 of 1800 nM (Table 3.2). SGK1 was inhibited with an IC50 of 220 nM, however, was not degraded by the compound. The specificity of SGK3-PROTAC1 at 1 μM was assessed in a panel of 140 kinases. This revealed a surprising increase in specificity over the original 308-R compound, with SGK1 and S6K1 the only kinases most potently inhibited by this compound *in vitro* (Figure 3.9 and Appendix Table 1). As expected, cisSGK3-PROTAC1 inhibited our panel of kinases similarly to SGK3-PROTAC1 (Figure 3.10 and Appendix Table 1).

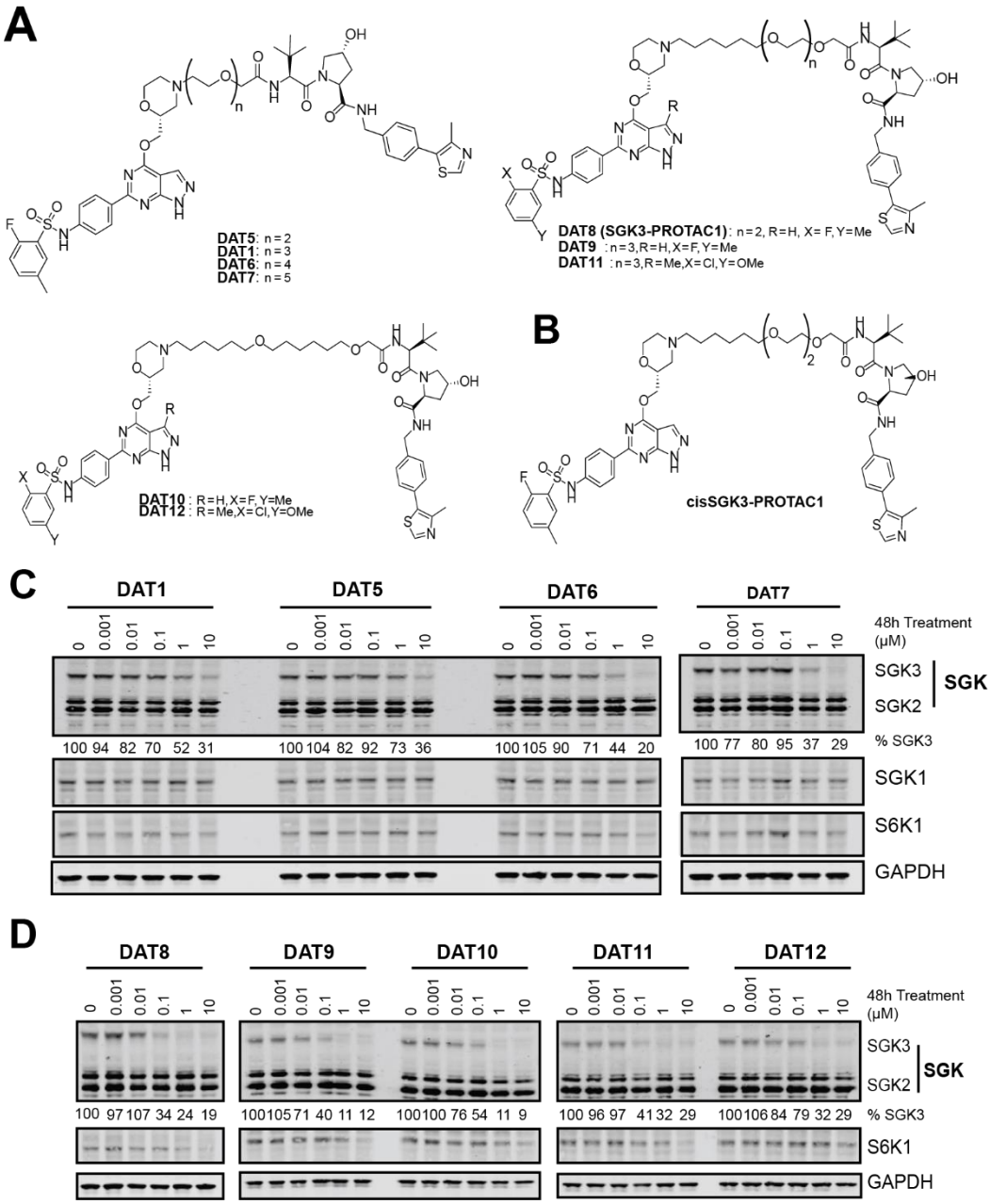

Figure 3.8 Design and cellular evaluation of second and third generation SGK PROTACs.
A. *Chemical structure of compounds DAT5-12, expanding upon DAT1.* ***B.*** *Chemical structure of cisSGK3-PROTAC1* ***C.*** *HEK293 cells were treated for 48 hours with increasing concentrations of each PROTAC compound from 1 nM to 10 μM. Cell lysates were subjected to immunoblot analysis with the indicated antibodies, and SGK3 protein levels quantified in Image Studio Lite software.* ***D****. HEK293 cells were treated for 48 hours with increasing concentrations of each PROTAC compound from 1 nM to 10 μM. Cell lysates were subjected to immunoblot analysis with the indicated antibodies, and SGK3 and S6K1 protein levels quantified in Image Studio Lite software.*

Table 3.2*. IC50 values of second generation of SGK PROTACs.*

The structures of the compounds are shown in Figure 3.6A. "-" = No Degradation, "+" = >50% Degradation at 10 µM. "++" = >50% Degradation at 1 µM. "+++" = >50% Degradation at 0.1 µM. "++++" = >60% Degradation at 0.1 µM.

	SGK3 IC50 (µM)	SGK1 IC50 (µM)	S6K1 IC50 (µM)	SGK3 Degradation efficiency
DAT1	0.44	1.6	0.16	+
DAT5	>10	>10	>10	+
DAT6	>10	>10	>10	++
DAT7	>10	>10	>10	++
DAT8	0.3	0.22	1.8	++++
DAT9	1.79	8.99	4.53	++
DAT10	>10	>10	>10	++
DAT11	0.73	1.34	1.80	+++
DAT12	>10	>10	>10	++

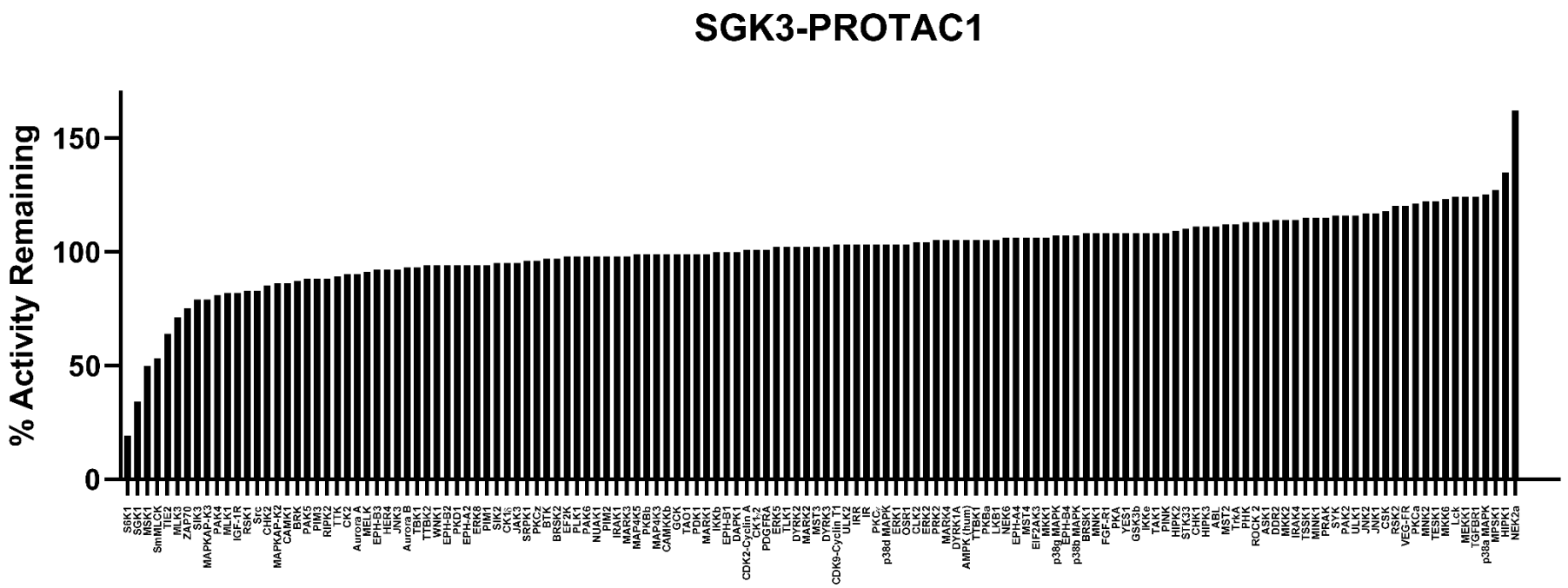

Figure 3.9 In vitro selectively screening of 1 μM SGK3-PROTAC1.

Kinase selectively profiling was performed by the National Centre for Protein Kinase Profiling (www.kinase-screen.mrc.ac.uk) against 140 protein kinases. Data are presented as mean (n=3) kinase activity remaining in the presence of 1 μM SGK3-PROTAC1, in comparison to a DMSO control. Raw data is available in Appendix Table 1.

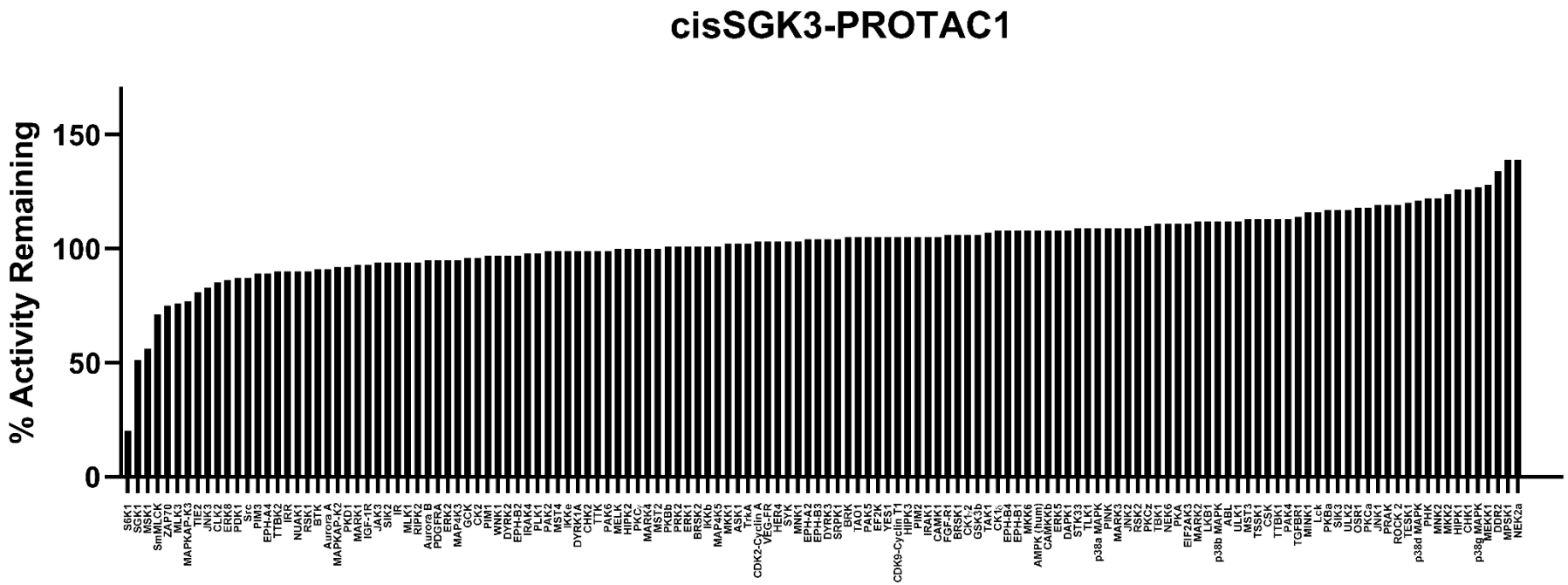

Figure 3.10 In vitro selectively screening of cisSGK3-PROTAC1.
Kinase selectively profiling was performed by the National Centre for Protein Kinase Profiling (www.kinase-screen.mrc.ac.uk) against 140 protein kinases. Data are presented as mean (n=3) kinase activity remaining in the presence of 1 μM cisSGK3-PROTAC1, in comparison to a DMSO control. Raw data is available in Appendix Table 1.

3.5 Cellular characterisation of SGK3-PROTAC1

On the basis of the experiments in section 3.4, I selected SGK3-PROTAC1 for further cellular characterisation, and for use in probing SGK3 biology in an array of cell lines. A cellular degradation assay confirmed that from 0.1 μM SGK3-PROTAC1 markedly reduced SGK3 in HEK293 cells after 8 h treatment, however cisSGK3-PROTAC1 did not induce any loss of SGK3 up to 3 μM. As observed previously, no degradation of S6K1 was observed at concentrations below 1 μM (Figure 3.11A). It was also of interest to study the impact of SGK3 degradation on phosphorylation of its physiological substrate NDRG1 at Thr346 (Sommer *et al.*, 2013). As this site is also phosphorylated by Akt, all conditions were treated with the Akt inhibitor AZD5363 (3 μM) 1 h before lysis. At 0.1-0.3 μM SGK3-PROTAC1, phosphorylation of NDRG1 was markedly reduced. At these concentrations cisSGK3-PROTAC1 had no effect, however at higher concentrations cisSGK3-PROTAC1 lowered NDRG1 phosphorylation (Figure 3.11A). This can be explained by the fact that although this compound does not bind VHL, the 308-R derived SGK-binding head will still bind and inhibit SGK3.

To fully characterize the compound, I performed timecourse analysis of SGK3-PROTAC1 induced degradation of SGK3. In HEK293 cells, 0.3 μM SGK3-PROTAC1 induced 50% degradation of SGK3 within 2 h, and maximal degradation was achieved after 8 h (Fig 3.11B). To demonstrate that SGK3-PROTAC1 induced SGK3 degradation is reversible, HEK293 cells were treated for 24 h with SGK3PROTAC-1, then washed 3 times with DMEM before replacing with fresh DMEM without PROTAC compound. Recovery of SGK3 expression was then tracked by Western Blot. This experiment revealed that increased SGK3 expression began after 1 h, with normal protein levels returning after 10 h (Fig 3.11C). SGK3-PROTAC1 is therefore a potent tool for the rapid and reversible degradation of SGK3 from cells, and manipulation of downstream signaling. As previously observed with DAT1, SGK3-PROTAC1-mediated degradation of SGK3 was also prevented by the neddylation inhibitor MLN4924 as well as the MG132 proteasome inhibitor (Figure 3.11D).

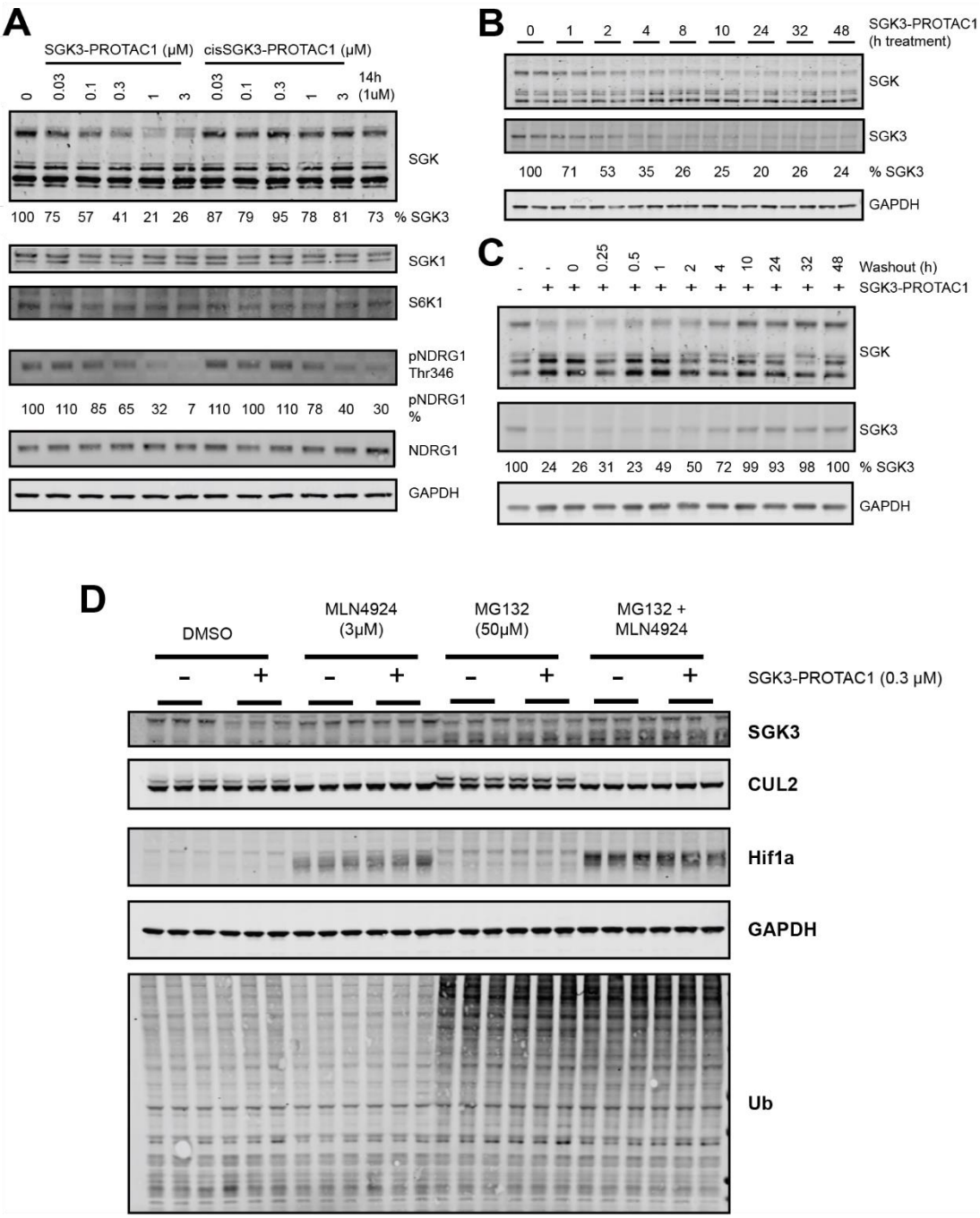

Figure 3.11 Mechanistic characterization of SGK3-PROTAC1.
A. *HEK293 cells were treated for 8h with 0.03-3 μM SGK3-PROTAC1 and cisSGK3-PROTAC1. Cells were also treated 1 h before lysis with 3 μM AZD5363, and protein levels measured by immunoblot.* ***B.*** *HEK293 cells were treated for up to 48 h with SGK3-PROTAC1 (0.3 μM), and lysates analyzed by immunoblot.* ***C.*** *HEK293 cells were treated for 24h with SGK3-PROTAC1, cells washed 3 times with DMEM to wash out compound and recovery of protein analyzed by immunoblot* ***D.*** *HEK293 cells were pretreated with the indicated inhibitors before treatment for 6 h with 0.3 μM SGK3-PROTAC1, and lysates analyzed by western blot for SGK3 expression*

The aim of this project was to develop a tool with which I could study the removal of SGK3 from breast cancer cell lines which rely upon SGK3 for resistance to PI3K-Akt-mTOR pathway

inhibition. I therefore characterized SGK3-PROTAC1 in 2 such cell lines, CAMA-1 and ZR-75-1 (Bago *et al.*, 2016). As in HEK293, in these cells concentrations of >0.1 μM SGK3-PROTAC1 induced degradation of SGK3, but not SGK1 or S6K1 after 8 h. Again, as expected, cisSGK3-PROTAC1 had no impact on SGK3 expression (Fig 3.12A,B). Therefore SGK3-PROTAC1 is expected to be a good tool for interrogation of SGK3 signaling in these cells. It is also interesting to note that in these cancer cell lines, degradation of SGK3 is more potent than in HEK293, possibly due to increased expression or activity of VHL in these cells. A western blot analysis of VHL protein levels revealed higher protein expression in these cancer cell lines than in HEK293 (data not shown).

HEK293, ZR-75-1 and CAMA-1 cells all contain much higher levels of SGK3 than they do SGK1. In order to confirm that SGK3-PROTAC1 mediated degradation is specific for SGK3 and does not induce degradation of endogenous SGK1, I additionally screened these compounds in the JIMT-1 cell line. This cell line has previously been demonstrated to express high levels of SGK1, and cell growth and metabolism is largely driven by SGK1 in these cells (Sommer *et al.*, 2013). Concentrations of up to 3 μM SGK3-PROTAC1 failed to induce degradation of SGK1, whereas SGK3 expression was reduced from 0.1 μM as observed in other cells lines (Fig 3.12C). As previous attempts to generate SGK3-specific inhibitors have so far been unsuccessful, due to high homology of the SGK kinase domains (Gong *et al.*, 2018), it is surprising that SGK3-PROTAC1 degradation is so specific for SGK3. This also places SGK3-PROTAC1 as an important tool in studying SGK3 function and delineating between the roles of SGK3 and SGK1. The specificity of SGK3-PROTAC1 for SGK3 over SGK1 is further explored in section 3.10.

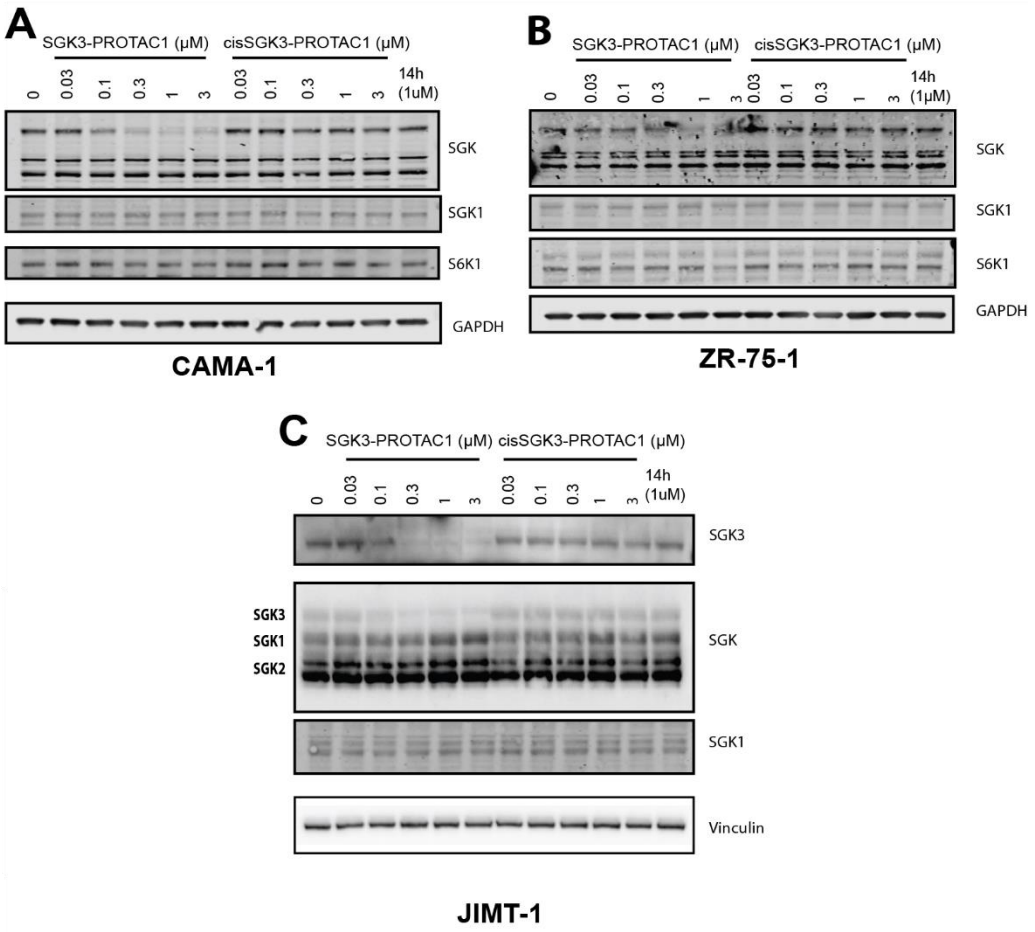

Figure 3.12 Characterization of cellular activities of SGK3-PROTAC1 and cisSGK3-PROTAC1 in cancer cell lines.
CAMA-1 (A), ZR-75-1 (B) and JIMT-1 (C) cells were treated with 0.03-3 μM SGK3-PROTAC1 and cisSGK3-PROTAC1. Lysates were subjected to immunoblot analysis with the indicated antibodies.

3.6 Effect of SGK3-PROTAC1 on SGK3-dependent mTORC1 activation

Previous work has shown that prolonged treatment of breast cancer cell lines such as CAMA-1 and ZR-75-1 cells with PI3K or Akt inhibitors resulted in upregulation of SGK3 leading to the activation of mTORC1 signaling, mediated by SGK3 phosphorylating TSC2 at the same sites as Akt (Bago *et al.*, 2016). Therefore, once I had confirmed that SGK3-PROTAC1 dramatically reduces protein levels of SGK3 in these cell lines, I aimed to investigate the effect that SGK3-PROTAC1 treatment would have on this resistance pathway. In particular, I was interested to determine whether SGK3-PROTAC1 could reverse inhibitor resistance.

In order to investigate the effect of SGK3-PROTAC1 under these conditions, I treated CAMA-1 (Figure 3.13A,C) or ZR-75-1 (Figure 3.13B,D) for 5 days with either a Class IA PI3K inhibitor (GDC0941, 1 μM) (Folkes *et al.*, 2008) or the Akt inhibitor AZD5363 (1 μM) (Davies *et al.*, 2012). These treatments induce increased expression and activity of SGK3, and a rescue of NDRG1 phosphorylation at Thr346 and mTORC1 activity, as measured by S6K1 phosphorylation at Thr389 and S6 protein phosphorylation at Ser240/244 (Bago *et al.*, 2016). To determine the impact of SGK3 degradation on this resistance pathway, I cotreated cells with SGK3-PROTAC1 or cisSGK3PROTAC-1 (0.3 μM), either at the start of treatment, or 8 h before lysis, once resistance had already developed.

SGK3-PROTAC1 substantially reduced SGK3 expression in both the CAMA-1 and ZR-75-1 cells within 8 h, and SGK3 degradation was maintained after 5 days of treatment (media and compound replenished after 72 h). Consistent with SGK3-PROTAC1 blocking mTORC1 activation, we found that these treatments also suppressed mTORC1-mediated phosphorylation of S6K1 at Thr389 resulting in a moderate reduction in S6 protein phosphorylation. In contrast, cisSGK3-PROTAC1 had no significant effect on SGK3 protein level or phosphorylation of TSC2, S6K1 or S6 protein.

In parallel, I also treated these cells with the non-PROTAC SGK inhibitor 14H (1 μM) (Halland *et al.*, 2015). I chose this compound instead of the source inhibitor 308-R, as 14H is more specific in targeting SGK kinases, and therefore was the better control. I observed in these conditions that, in both CAMA-1 and ZR-75-1 cells, SGK3-PROTAC1 inhibited mTORC1 signaling more than the inhibitor, suggesting degradation of SGK3 has a greater effect than mere inhibition of its kinase activity (Fig 3.13).

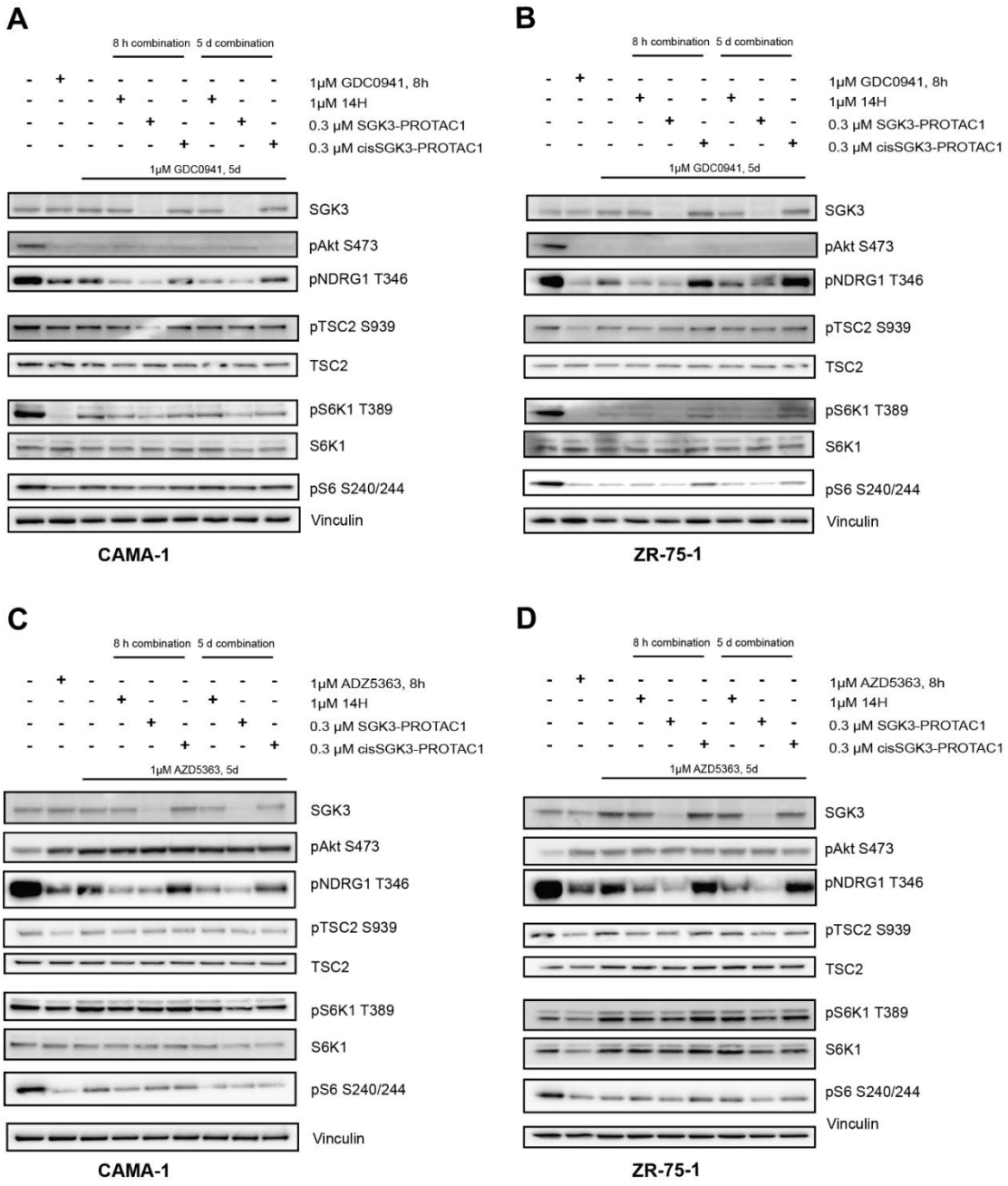

Figure 3.13 SGK3-PROTAC1-mediated degradation of SGK3 inhibits Akt-independent activation of mTORC1 in cancer cell lines treated with Akt or PI3K inhibitors.
CAMA-1 (A, C) or ZR-75-1 (B, D) were treated for 5 days with 1 μM GDC0941 (A, B) or 1 μM AZD5363 (C, D). Cells were treated with the compounds indicated for either 5 days, or 8 h before lysis, cells were treated with the compounds indicated. Cell lysates were subject to immunoblot analysis with the indicated antibodies

3.7 Effect of SGK3-PROTAC1 on cancer cell growth

In section 3.6 I demonstrated that degradation of SGK3 by SGK3-PROTAC1 treatment can inhibit

Akt-independent activation of mTORC1. Therefore, I next chose to investigate whether SGK3-

PROTAC1 impacts on proliferation of cancer cell lines in the context of PI3K-Akt pathway inhibition.

I first sought to determine any effect of SGK3-PROTAC1 or cisSGK3-PROTAC1 treatment on CAMA-1 or ZR-75-1 cells under basal conditions, with no inhibition of PI3K or Akt. Treatment of CAMA-1 or ZR-75-1 cells with SGK3-PROTAC1 alone had no effect on growth (Figure 3.14A,C), consistent with previous work undertaken with high doses of conventional SGK inhibitors (Bago *et al.*, 2016; Castel *et al.*, 2016). This reconfirms that growth of these cells under basal conditions is not mediated by SGK3 and suggests that PROTACs are not exhibiting any off-target toxic or anti-proliferative effect. I also measured sensitivity and toxicity of the compounds by Sytox Green assay. Sytox Green is a fluorescent nucleic acid binding reagent which exhibits >500-fold increased fluorescence on binding nucleic acids, however, is impermeable to live cells. Measuring fluorescence emitted by this reagent with or without cell permeabilization by Saponin provides a quantitative measure of live cell number. This assay can be used to quantify the impact of a compound on cell survival and proliferation. Sytox Green assay determined that these compounds were well tolerated up to 3 μM. In contrast treatment with PI3K inhibitor (GDC0941) or Akt inhibitor (AZD5363) significantly impacted on CAMA-1 and ZR-75-1 cell growth, and reduced the number of surviving cells identified by Sytox Green Assay (Figure 3.14B,D).

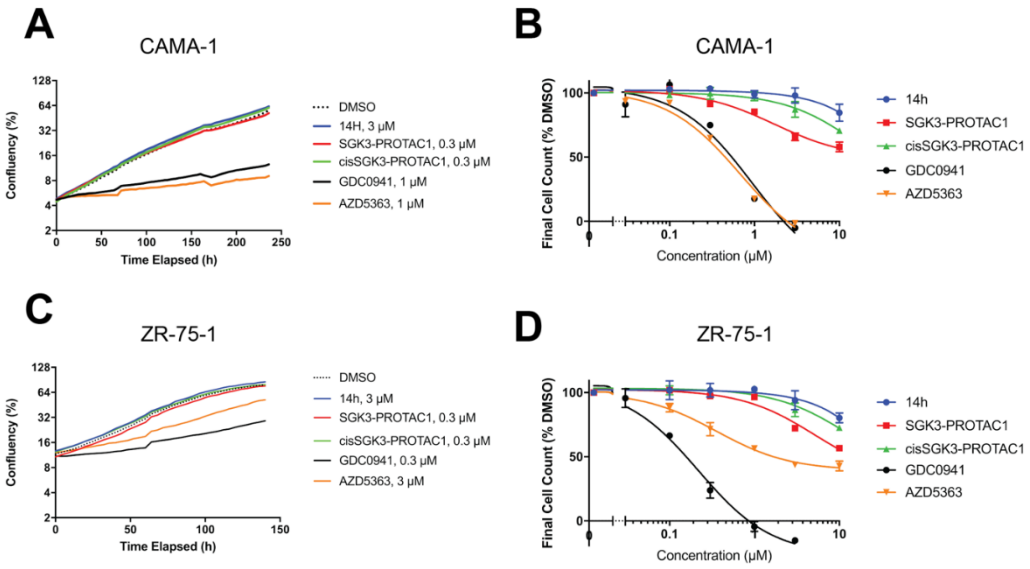

Figure 3.14 SGK3-PROTAC compounds have no effect on cell growth.
CAMA-1 and ZR-75-1 cells were seeded in 96 well plates, allowed to adhere overnight, and treated as indicated in the figure. ***A&C.*** *Confluency of CAMA-1 (**A**) and ZR-75-1 (**C**) cells was measured every 4h on Incucyte S3.* ***B&D.*** *Measurement of cell number by Sytox Green Assay. Surviving cells were measured after 7 day treatment with the indicated concentration of compound. Remaining cells were quantified relative to DMSO treatment. Error bar = SD, n=3.*

I therefore studied the effect that SGK3-PROTAC1 and cisSGK3-PROTAC1 had on the growth of CAMA-1 (Figure 3.14A,C) or ZR-75-1 (Figure 3.14B,D) in the presence of GDC0941 (1 µM) or AZD5363 (1 µM). I studied this effect in long term assays over the course of about 30 days. As previously observed, treatment with GDC0941 or AZD5363 substantially reduced growth of these cells, however a reduced proliferation was recovered after 7 days treatment with the inhibitors (Figure 3.15). Cotreatment with SGK3-PROTAC1 (0.3 µM) further reduced the growth of these cells under conditions that cisSGK3-PROTAC1 had a minimal effect (Figure 3.15). I also studied in parallel the effect of conventional SGK inhibitor 14H (3 µM) on growth of the inhibited cell lines. In the presence of a Class IA PI3K inhibitor 14H further suppressed cell growth, as reported previously (Bago *et al.*, 2016), however this was to a lesser extent than was observed with SGK3-PROTAC1. When 14H was combined with the Akt inhibitor, it suppressed growth to a similar extent as was observed with SGK3-PROTAC1 (Figure 3.15)

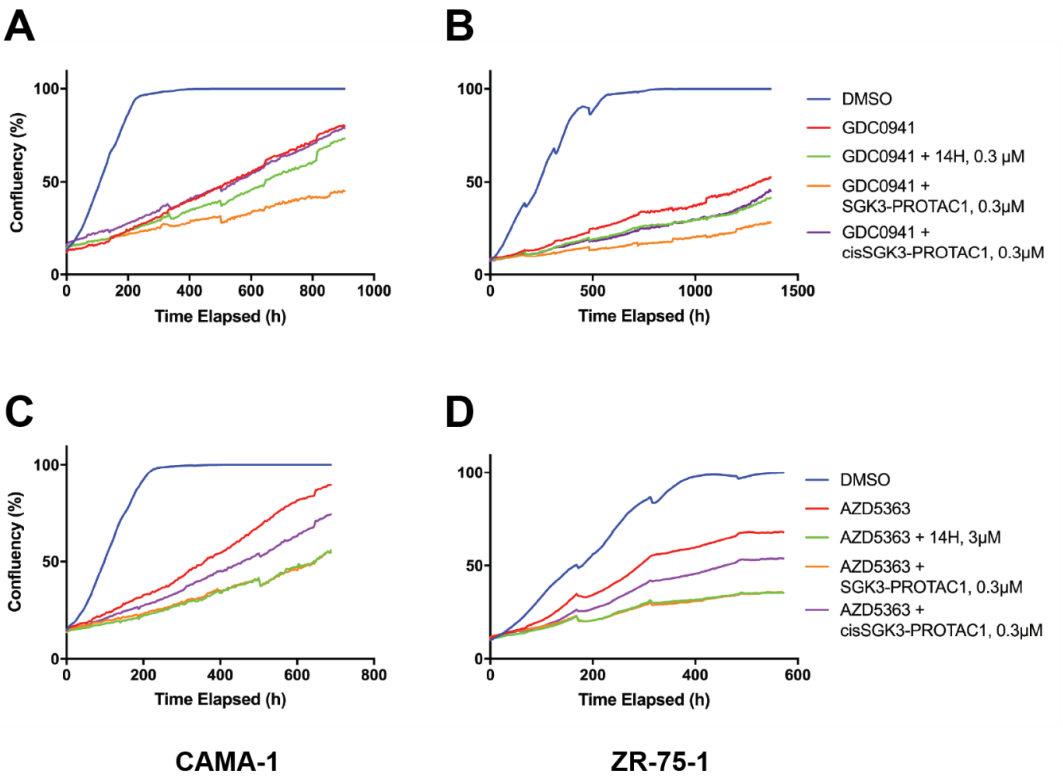

Figure 3.15 SGK3-PROTAC1-mediated degradation of SGK3 further inhibits the growth of cancer cell lines treated with PI3K-Akt pathway inhibitors.
CAMA-1 (A, C) or ZR-75-1 (B, D) were treated with compounds as indicated either as monotherapy or in combination, and confluency measured on the Incucyte S3 every 4 h for up to 4 weeks

I was also interested in the impact of targeting the PI3K-Akt pathway and SGK3 sequentially, with SGK3-PROTAC1, cisSGK3PROTAC1 or 14H added to cells after growth recovery in response to GDC0941 or AZD5363. In these assays, I first treated cells with PI3K or Akt inhibitor, and then sequentially added the SGK3-targetting compound when growth had recovered to 40-50% confluency. In these assays, sequential addition of either the inhibitor or the PROTAC compounds had very little effect on proliferation of the cancer cell lines, with the exception of ZR-75-1 under prolonged treatment with AZD5363 (Figure 3.16). In this condition, an equal effect was seen from the inhibitor or PROTAC. Growth of the cells appeared to stop completely under these conditions, however I did not observe any cell death.

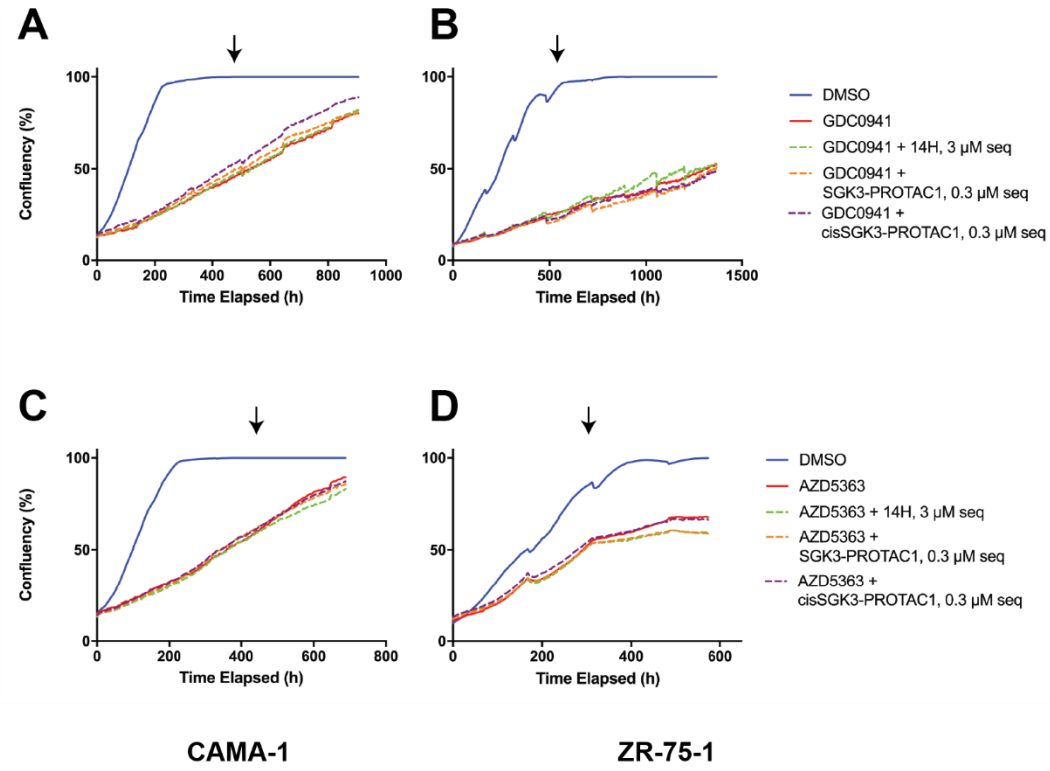

Figure 3.16 SGK3-PROTAC1-mediated degradation of SGK3 further inhibits the growth of cancer cell lines treated with PI3K-Akt pathway inhibitors.
*CAMA-1 (**A, C**) or ZR-75-1 (**B, D**) were treated with compounds as indicated either as monotherapy or in combination, and confluency measured on the Incucyte S3 every 4 h for up to 4 weeks. Sequential treatments (seq) were performed after recovery of cell growth. Arrowheads indicate timepoints of sequential treatment*

3.8 Impact of SGK3-PROTAC1 on a generated, AZD5363-resistant cancer cell line, CAMA-R

In order to study resistance to the Akt inhibitor AZD5363, a CAMA-1 cell line highly resistant to AZD5363 has been generated by AstraZeneca, termed CAMA-R. To generate this cell line, CAMA-1 cells were treated with increasing concentrations of AZD5363 and clonally selected, to produce a cell line which is now resistant to 5 µM AZD5363. This cell line has acquired very high SGK3 levels to mediate resistance to the Akt inhibitor. I was therefore interested to investigate the impact SGK3-PROTAC1 had in this cell line, and whether any of the results differ to the 5 day induction experiments described in sections 3.6 and 3.7.

As in section 3.5, a cellular degradation assay was performed with increasing concentrations of SGK3-PROTAC-1 and cis-SGK3PROTAC1, from 0.03 – 3 µM for 8 h. As was observed in other cell

lines, degradation of SGK3 was observed from 0.1 μM SGK3-PROTAC1, while no degradation was observed with cisSGK3-PROTAC1 treatment up to 3 μM. Studying NDRG1 phosphorylation at Thr346, a significant dephosphorylation of NDRG1 was observed from 0.1 μM, whereas 10-fold more cisSGK3-PROTAC1 was required to impact on NDRG1 phosphorylation. Moreover, SGK3-PROTAC1 at 0.1/0.3 μM had a greater impact on NDRG1 phosphorylation than the non-PROTAC SGK inhibitor 14H (Fig 3.17A).

I next investigated the effect of SGK3-PROTAC1 treatment on cell proliferation and survival of CAMA-R cells. In the context of maintained AZD5363 treatment, SGK3-PROTAC1 had a significant effect on survival and growth of CAMA-R cells, measured by proliferation by Incucyte measurements and also Sytox Green assay (Figure 3.17C,E). When AZD5363 was removed from the cells, SGK3 degradation had no effect (Fig 3.17B,D, “No Drug”). In a similar result to cotreatment of CAMA-1 cells with AZD5363 and SGK3 PROTAC/inhibitor, I observed that 0.1 μM SGK3-PROTAC1 had a similar effect on growth to 3 μM 14H. When treating CAMA-R cells with 0.1 μM 14H I saw no impact on growth. As expected, cisSGK3-PROTAC1 had no effect at this concentration, but had an inhibitory effect at higher concentrations (Fig 3.17C,E).

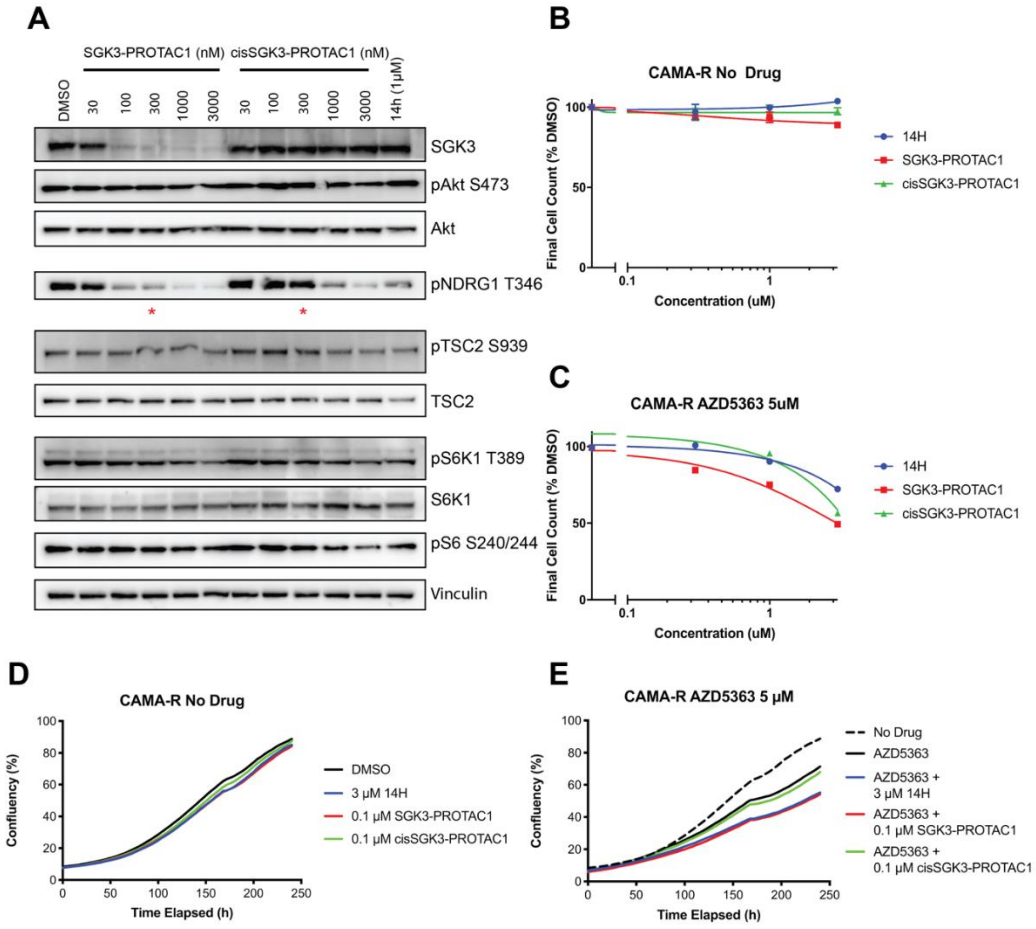

Figure 3.17 The impact on SGK3-PROTAC1 treatment on Akt inhibitor resistant cell line CAMA-R.
A. *CAMA-R cells were grown and seeded in the presence of AZD5363 (5 μM). SGK3-PROTAC1 or cisSGK3-PROTAC1 were added to cells between 0.03-3 μM for 8h then lysed and subject to immune blot. Red asterisk highlights the effect of 0.3 μM compound treatment on substrate phosphorylation, as concentration was used in further experiments.* ***B&C.*** *Sensitivity of CAMA-R cells in the absence* ***(B)*** *or presence* ***(C)*** *of AZD5363 (5 μM) to increasing concentrations of SGK3 inhibitor 14H, SGK3-PROTAC1 or cisSGK3-PROTAC1, as measured by Sytox Green assay after 7 days of treatment.* ***D&E****. Sensitivity of CAMA-R cells in the absence* ***(D)*** *or presence* ***(E)*** *of AZD5363 (5 μM) to SGK3 inhibitor 14H (3 μM), SGK3-PROTAC1 (0.1 μM) or cisSGK3-PROTAC1 (0.1 μM) as measured by Incucyte S3 cell proliferation assay.*

However, when studying mTORC1 activity downstream of SGK3, SGK3-PROTAC1 treatment had little to no effect on downstream phosphorylation of S6K1 and S6 protein (Fig 3.15A). This was surprising as such a strong impact on NDRG1 phosphorylation, and CAMA-R cell growth is significantly impacted by 0.1 μM SGK3-PROTAC1 treatment. I therefore decided to directly compare the pathway in CAMA-R cells against CAMA-1 cells with induced AZD5363 resistance after 5 day treatment with the inhibitor. I observed that SGK3 was upregulated in CAMA-R cells, and there was strong phosphorylation of S6K1 and S6 downstream of mTORC1. However, again I saw no impact of 0.1-0.3 μM SGK3-PROTAC1 treatment on phosphorylation of these sites

(Figure 3.18). Surprisingly, despite activation of mTORC1, I observed very little, if any, phosphorylation of TSC2 at the Ser939 and Thr1462 sites, proposed to be phosphorylated by SGK3 in this resistance model (Figure 3.18). Therefore, although mTORC1 does appear to be reactivated in this cell line, it does not appear to be occurring through the predicted mechanism. TSC2 is phosphorylated on alternative sites by, for example, AMPK and the ERK1/2 kinases, which were not analysed in this experiment but would be important to study in future work. In addition, while SGK3-PROTAC1 treatment does inhibit the growth of CAMA-R cells treated with AZD5363, this does not appear to occur through modulation of the mTORC1 signaling cascade. It is important to consider that the CAMA-R cell line is expanded from 1 resistant clonal line, and therefore resistance may have occurred by a different mechanism. Further experiments would be required to determine the cause of resistance in this case.

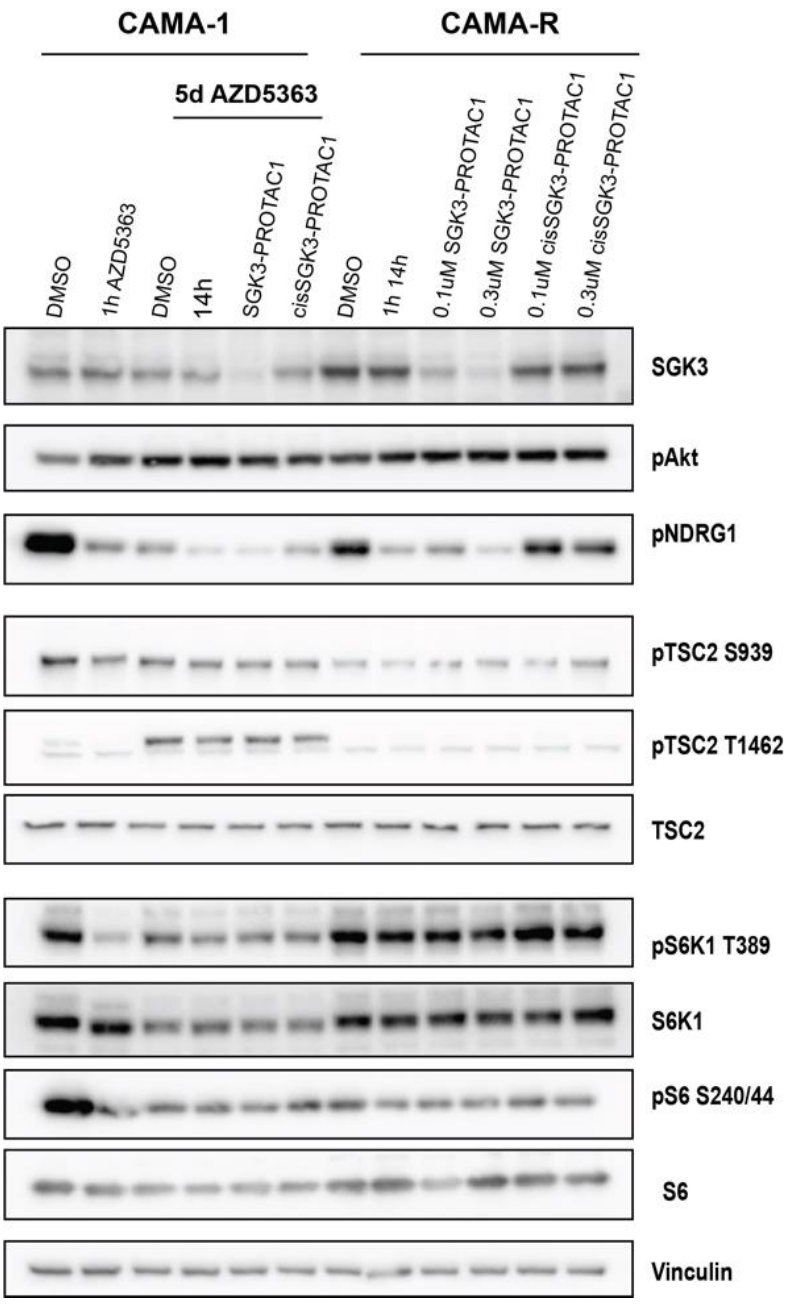

Figure 3.18 mTORC1 is reactivated in CAMA-R cells, but not through TSC2.
CAMA-R cells, grown in 5 µM AZD5363 were treated and analyzed in parallel to parental CAMA-1 cells in the presence of absence of 5d AZD5363 treatment, with SGK3-PROTAC1 or analogue cisSGK3-PROTAC1. Activation of mTORC1 in CAMA-1 induced resistance and CAMA-R constitutive resistance was analyzed by western blot.

3.9 Determining the specificity of SGK3-PROTAC1 in HEK293 cells

An important consideration in the validation of SGK3-PROTAC1 is determining the global specificity of the compound. This is of interest as by western blot degradation of SGK3 was observed to be specific over the other SGK isoforms. Unknown off-target effects may be having an impact on the signaling effects described. Therefore, in collaboration with Dr Houjiang Zhou,

I used a quantitative Tandem-Mass-Tag (TMT)-labelled approach to determine the global proteomic changes occurring after SGK3-PROTAC1 treatment in HEK293 cells. Cell lysis and sample preparation was undertaken after 6 h treatment with SGK3-PROTAC1 (0.3 μM), in comparison to the inactive cisSGK3-PROTAC1 (0.3 μM) or a mock treatment with DMSO. The cis epimer offers a much more appropriate negative control, and also helps identify any global proteomic changes caused by the inhibitory headgroup of SGK3-PROTAC1.

Cells were treated in triplicate for 6 h with either SGK3-PROTAC1 (0.3 μM), cisSGK3-PROTAC1 (0.3 μM) or DMSO, then harvested and lysed in Urea buffer. After trypsin and LysC enzyme digest samples were labelled with TMT reagents, pooled, and fractionated by high pH reverse phase fractionation. Sample analysis was performed in Proteome Discoverer v2.2 using the Mascot search engine. This allowed for the unbiased, relative quantification of 8766 proteins, of which 377 were determined to have protein kinase activity or directly regulate protein kinase activity (pantherdb.org). From this sample set, SGK3-PROTAC1 was revealed to be remarkably selective, with only SGK3 expression being significantly reduced (p value < 10^{-3}) (Figure 3.19, 3.20). This provided higher confidence that the SGK3-PROTAC1 compound was highly selective in cells and that any biological changes should be a result of degradation of SGK3. Due to low expression in these cells, SGK1 and SGK2 were not detected in this analysis and therefore could not be compared. S6K1 and Akt, important possible off-target hits, were unaffected by SGK3-PROTAC1 treatment. This analysis has also been performed in the biologically relevant ZR-75-1 cancer cell line and is discussed in more detail in Chapter 4.

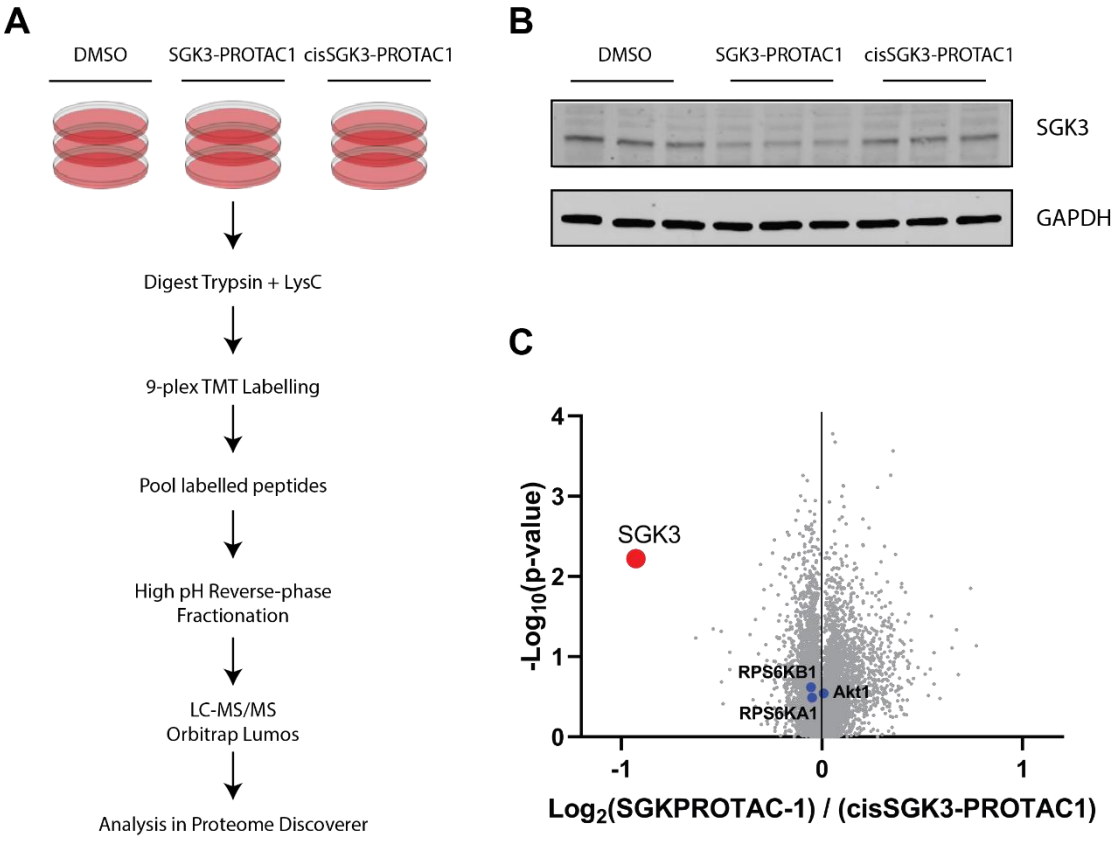

Figure 3.19 TMT Proteomic analysis of HEK293 cells treated with SGK3-PROTAC1.
A. *Workflow for Mass Spec analysis of SGK3-PROTAC1 specificity in HEK293.* ***B.*** *In cell lysates treated with SGK3-PROTAC1 for 8h, SGK3 levels were noticeably reduced. These lysates were used for mass spectrometry analysis of the global proteome.* ***C.*** *Volcano plot demonstrating global proteomic changes upon SGK3-PROTAC1 treatment in HEK23 cells.*

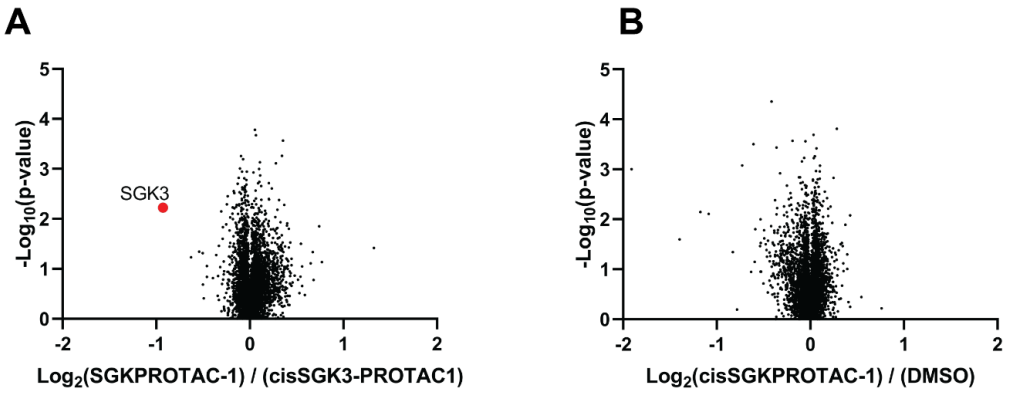

Figure 3.20 TMT Proteomic analysis of HEK293 cells treated with SGK3-PROTAC1 or cisSGK3-PROTAC1
TMT-labelled proteomic analysis of HEK293 cells treated with ***A)*** *SGK3-PROTAC1 compared to cisSGK3-PROTAC1 and* ***B)*** *cisSGK3-PROTAC1 compared to DMSO. Data are represented as a volcano plot of fold-change against p-value.*

3.10 Isoform specificity of SGK3 degradation over SGK1.

Previously published studies have so far been unsuccessful in producing SGK3-specific chemical inhibitors, due to the high structural similarity of the kinase domains of the SGK isoforms, particularly in the ATP binding sites (Figure 3.21) (Gong *et al.*, 2018). It was therefore very interesting that SGK3-PROTAC1 has been revealed as being exquisitely specific for degradation of SGK3 over SGK1. This is particularly surprising given that in *in vitro* kinase assays SGK3-PROTAC1 inhibits these 2 kinases with a very similar IC_{50} (0.3 nM for SGK3, 0.22 nM for SGK1). It was therefore of interest to determine why degradation was specific for SGK3.

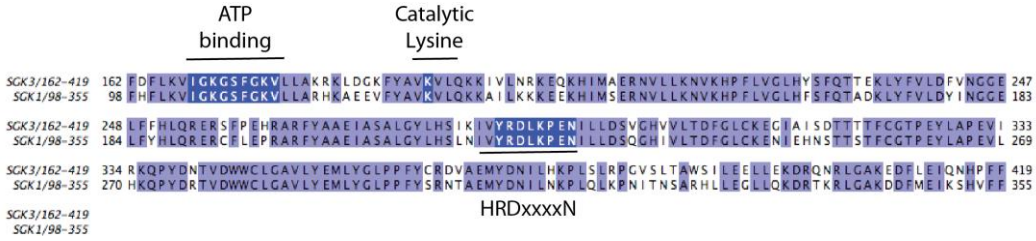

Figure 3.21 Sequence alignment of SGK1 and SGK3 kinase domains.
High sequence similarity is maintained between SGK1 and SGK3. In particular, regions of ATP and substrate binding are highly conserved.

I first chose to study whether any structural features of SGK3 made this protein more amenable to degradation by SGK3-PROTAC1. SGK3 contains an N-terminal PX domain and is localised to endosomes, and in this way, it differs from SGK1. I therefore expressed exogenous SGK3, either wildtype or with deletion or mutation of its PX domain, into SGK3 KO HEK293 cells and measured the ability of SGK3-PROTAC1 to degrade these proteins. I also expressed SGK3 with inactivating mutations in its T-loop (T320A), H-motif (S486A) or kinase domain (K191A) to determine whether activation of SGK3 influenced its susceptibility to degradation (Fig 3.22). I found that, in this overexpression system, SGK3-PROTAC1 induced about 50% degradation of wildtype SGK3. Mutation of the critical residues for SGK3 activity sites had very little effect, increasing SGK3 degradation by an additional 10%. Although deletion of the PX domain had no effect on degradation efficiency, point mutations to inhibit PtdIns(3)P binding (R50A, R90A) and prevent translocation of SGK3 to endosomes increased degradation of SGK3 to ~75%. The kinase domain

mutant of SGK3 was less stable and expressed and much lower levels but appeared to be similarly targeted for degradation by approximately 50% (Fig 3.22).

SGK1 also differs from SGK3 in that SGK1 carries an N-terminal degron motif, which leads to its ubiquitylation by Nedd4-2 and degradation via the proteasome. As this mechanism of SGK1 leads to its rapid turnover and a half-life of ~30 minutes and overlaps with the mechanism of action of the PROTAC, this motif may affect induction of SGK1 degradation by SGK3-PROTAC1. Typically, in our assays SGK1 is expressed with its first 59 amino acids deleted, for more stable expression. As expected, deletion of the residues resulted in a more stable, higher expressed protein, however also sensitised SGK1 to degradation by SGK3-PROTAC1 (Fig 3.22). Therefore, the endogenous turnover mechanism of SGK1 in cells may partially impact on SGK3-PROTAC1 induced degradation. Alternatively, deletion of these residues may have revealed accessible lysine residues for ubiquitylation by $CUL2^{VHL}$.

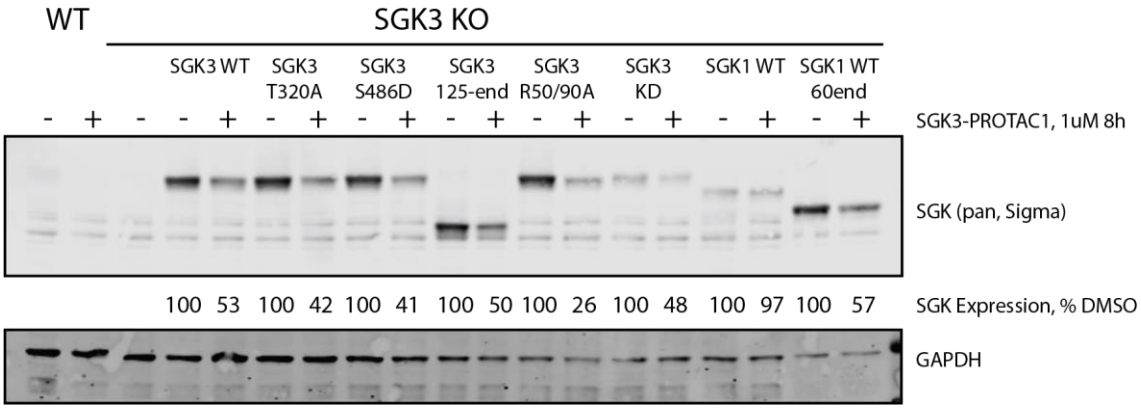

Figure 3.22 Mutations in SGK3 and SGK1 alter their susceptibility to SGK3-PROTAC1 mediated degradation.
A. *SGK3 and SGK1, wildtype and kinase dead, were transiently transfected into SGK3 KO HEK293 cells, and treated for 8 h with SGK3-PROTAC1.* ***B.*** *Mutant forms of SGK3 were transiently transfected into HEK293 cells and treated for 8 h with SGK3-PROTAC1*.

In order to further determine the reasons for SGK3 specificity, I would in future studies perform experiments to assess the ability of SGK1 and SGK3 to form stable ternary complexes with SGK3-PROTAC1 and pVHL. I would examine whether there was a structural element of SGK3 allows the protein to form a more stable complex than SGK1. I would in future studies perform Isothermal Titration Calorimetry (ITC), to determine the thermal effect of compound binding to

SGK1 and SGK3, and therefore identify any differences in the binding affinities of SGK3-PROTAC1 to these proteins. *In vitro* kinase assays are very similar between the two proteins so we would expect similar binding, however subtle binding differences may be revealed by ITC to partially explain this finding.

In addition, treatment with SGK3-PROTAC1 in combination with proteasome inhibitor MG132 may further explain the specificity between these isoforms. For example, co-immunoprecipitation of SGK isoforms with VHL in the presence of SGK3-PROTAC may reveal a stronger complex formed with SGK3 than SGK1. Also, studying ubiquitylation of target isoforms by immunoblot would demonstrate whether an active ternary complex is being formed. In addition, ubiquitylation mapping could be performed on SGK3, to determine where it is being ubiquitylated and whether these regions are conserved in SGK1.

3.11 Discussion

In this chapter, I describe the design and characterisation of the compound SGK3-PROTAC1. This compound is able to induce potent, reversible degradation of SGK3 from a variety of cell lines within 4 h, with a DC_{50} below 100 nM.

Specificity of SGK3-PROTAC1

Quantitative mass spectrometry in HEK293 cells revealed degradation of SGK3 to be highly selective, with SGK3 being the most downregulated protein. It is particularly interesting that SGK3-PROTAC1 was revealed to be remarkably isoform specific for SGK3, with the highly related SGK1/2 isoforms remaining unaffected. This was even observed in cell lines such as JIMT-1 which express high levels of SGK1 and relatively low levels of SGK3. Recent studies attempting to develop isoform specific chemical inhibitors of SGK3 have been unsuccessful, due to the high structural similarity of the SGK1 and SGK3 kinase domains, in particular in the ATP binding site (Gong *et al.*, 2018). SGK3-PROTAC1 is therefore an important tool in modulating SGK3 biology independently of SGK1/2. This ability to generate selective isoform specific inhibitors has

previously been observed in PROTACs derived from the pan-BET inhibitor JQ1 (Zengerle, Chan and Ciulli, 2015; Gadd *et al.*, 2017; Testa *et al.*, 2018) and PROTACs derived from the promiscuous kinase inhibitor Foretinib (Bondeson *et al.*, 2018) or TAE-684 (Huang *et al.*, 2018). It has recently been shown that specificity and potency of PROTACs can be dictated by differential cooperativity and stability of ternary complex formation (Gadd *et al.*, 2017; Hughes and Ciulli, 2017; Roy *et al.*, 2019) as well as geometry/orientation of the recruited E3 ligase (Smith *et al.*, 2019). Future work will investigate the extent to which these molecular recognition features contribute to the exquisite selectivity of SGK3-PROTAC1 for SGK3 induced degradation. Further, the rapid turnover of SGK1 through ubiquitylation and degradation may make it intractable to PROTAC mechanism of action. As the protein is already readily ubiquitylated and degraded, additional PROTAC-mediated ubiquitylation may have minimal effect.

Rana *et al* recently described a CDK6-targeting PROTAC, which had exquisite CDK6 specificity, despite equal inhibition of CDK4 and CDK6 (Rana *et al.*, 2019). While CDK4/6 have overlapping kinase functions, CDK6 is believed to carry a kinase-independent role in transcriptional regulation (Petrocca *et al.*, 2013). Additionally, CDK6 amplification was proposed as a resistance mechanism to CDK4/6 inhibition (Yang *et al.*, 2016). The isoform specificity of the PROTAC yielded an important tool in studying CDK6-mediated regulation of transcription. The authors argued that either a ternary complex could not be formed with CDK4, or rapid deubiquitylation occurred on this protein, however they did not study this finding further.

Benefits of SGK3 degradation over kinase inhibition

In a variety of assays using SGK3-dependent cancer cell lines, SGK3 degradation was demonstrated to have a more potent effect than inhibition of its kinase activity by the conventional 14H inhibitor. This finding provides a further example of the benefit of the PROTAC approach in targeting protein kinase signaling pathways with greater efficacy and selectivity than can be achieved with conventional inhibitors. Other examples include the recent finding

that a BCR-ABL degrader displays more sustained inhibition of Chronic myelogenous leukemia cell growth after removal of compound than can be achieved by a conventional ABL kinase inhibitor (Shibata *et al.*, 2018). I did not explore the restoration of growth after SGK3-PROTAC1 washout in my experiments, however this would be of interest to explore in further work. Han *et al* also recently determined that a potent androgen receptor (AR) degrader ARD-68 was >100 times more potent than an AR antagonist in suppressing gene transcription in two different cell lines (Han *et al.*, 2019)

Further, Crews lab more recently published a PROTAC compound binding allosterically to BCR-ABL which, although potent in decreasing cancer cell growth, was not more effective than the leading active site inhibitor imatinib. However, allosterically targeting kinases for degradation also has the additional benefit of allowing combination treatments of PROTAC with kinase inhibitor. The authors reason that combination of allosteric degraders and kinase inhibitors lower the dose of inhibitor required, and therefore reduce toxicity of ATP mimic compounds (Burslem *et al.*, 2019).

IRAK4 is a Ser/Thr protein kinase downstream of Toll-like Receptor signaling in immune responses. IRAK has been proposed to have kinase-independent roles in IL-1β signaling and cytokine release due to scaffolding functions (Qin *et al.*, 2004), however degradation with PROTAC compounds showed no improvement over kinase inhibition in cytokine production or signal transduction (Nunes *et al.*, 2019)

Other mechanisms by which SGK3-PROTAC1 may inhibit cell growth.

It is of particular interest that, although in the context of PI3K inhibition SGK3 degradation was superior, in the context of Akt inhibition both 14H and SGK3-PROTAC1 had similar effects of cancer cell growth. Future studies should follow up further pathways downstream of PI3K in which SGK3 may have a role, which may explain the difference between the conditions. In addition, when studying the CAMA-R AZD5363 resistant cell line, it was revealed that although

cell growth was inhibited by targeting SGK3, this growth inhibition was not occurring through phosphorylation of TSC2 by SGK3, as observed in previous models. This again suggests additional, as yet undiscovered, pathways in which SGK3 may play a role in PI3K-Akt pathway inhibitor resistance. In CAMA-R cells, mTORC1 activation may be mediated through TSC2 at alternative sites through the ERK pathway or AMPK. Additionally, targeting of SGK3 in PI3K-Akt pathway inhibition appeared to be more effective when treating in combination before resistance occurs. Sequential treatment with 14H or with SGK3-PROTAC1 had minimal effect. This data teaches us that when targeting SGK3 in cancer, SGK3 and PI3K/Akt should be targeted together in combination.

As described in Chapter 1, Akt phosphorylates substrates in mTORC1-dependent roles which regulate cell growth and proliferation, for example in phosphoinactivation of FOXO transcription factors and the p27 and p21 cyclin dependent kinase inhibitors (Zhou, Liao, Xia, Spohn, *et al.*, 2001; Tran *et al.*, 2003; Sekimoto, Fukumoto and Yoneda, 2004). Therefore, degradation of SGK3 in the context of PI3K-Akt inhibition may also regulate these pathways, which have not been fully characterized in this thesis.

Additionally, SGK3 may have a role in alternative pathways as yet undiscovered. Further, these roles may be kinase independent and therefore not revealed by kinase inhibition. In Chapter 4, I further investigate this possibility by global proteomic and phosphoproteomic analysis of SGK3-PROTAC1 treatment in ZR-75-1 cells. This provides evidence for potential newly discovered roles of SGK3, which may mediate the resistant growth phenotype on PI3K-Akt pathway inhibition.

In the BCR-ABL compound described above, degradation was observed to reduce the level of GAB2 phosphorylation downstream of BCR-ABL and upstream of MAPK signaling, however inhibition of its tyrosine kinase activity did not have the same effect. Further analysis revealed this was via a scaffolding mechanism, through autophosphorylation of a docking site at Y177

(Burslem *et al.*, 2019). However, this comparison was performed against the allosteric inactive PROTAC, and not the active site inhibitor.

Conclusion

In this chapter I, in collaboration with the Ciulli lab, optimized and characterized SGK3-PROTAC1 as an important tool in the study of SGK3 signaling in PI3K-Akt pathway inhibition. This compound provides many of the benefits associated with PROTAC-mediated targeting, such as isoform specificity for SGK3 over other family members, and additional potency in inhibitor-resistant growth over conventional kinase inhibition. This compound will be an important addition to our armory of chemical probes to decipher the biological roles of the SGK3 signaling pathway including in mediating resistance to PI3K and Akt inhibitor therapy in cancer. In Chapter 4, I will utilize this compound for quantitative global proteomic and phosphoproteomic analysis of ZR-75-1 cellular response to SGK3 degradation, revealing possible roles for SGK3 in cancer not previously identified by chemical inhibition.

4. Global response to SGK3-PROTAC1 treatment in ZR-75-1 breast cancer cells suggests potential role for SGK3 in cAMP signalling and mitochondrial Oxidative Phosphorylation.

4.1 Introduction

Throughout this study I have been interested in the biology and signalling of SGK3 particularly in the ER+ breast cancer cell lines ZR-75-1 and CAMA-1, which induce SGK3 expression and activity in response to inhibition of the PI3K-Akt-mTOR signalling pathway. In section 3.9, I demonstrated by Tandem Mass Tag (TMT)-labelled quantitative proteomics that SGK3-PROTAC1-mediated degradation was highly specific for SGK3 in HEK293 cells. However, results may differ in a cell-dependent manner and I was interested to determine the specificity and impact of compound-induced SGK3 degradation in a relevant cancer cell line. It was therefore of interest to understand the global effects of SGK3 degradation in the ZR-75-1 cell line.

4.2 Experimental Design - Global Proteomics and Phosphoproteomics in ZR-75-1 cells

In an identical method to that used for HEK293 cells in section 3.9, I treated HEK293 cells for 6 h with SGK3-PROTAC1 (0.3 μM), cisSGK3-PROTAC1 (0.3 μM) or DMSO. In these cell lines I was also interested in phosphoproteomic changes on SGK3-PROTAC1 treatment, in order to potentially identify new substrates or signalling pathways impacted by SGK3 degradation. Therefore, alongside analysis at the proteomic level, I additionally performed TiO_2 enrichment of phosphopeptides from these lysates and performed complementary phosphoproteomic analysis. After treatment with the indicated compounds, cells were harvested, lysed in Urea buffer and digested by LysC and Trypsin digestion. Before mass spectrometry analysis, I confirmed by western blot that SGK3 had been substantially degraded upon SGK3-PROTAC1 treatment, but not cisSGK-PROTAC1. The resulting peptides were split for proteomic or phosphoproteomic analysis, by TMT-labelled quantitative mass spectrometry. After labelling,

proteomic samples were pooled and fractionated by high pH reverse phase fractionation for analysis. For phosphoproteomic analysis, phosphopeptides were enriched before labelling and pooled for quantitative analysis (Figure 4.1).

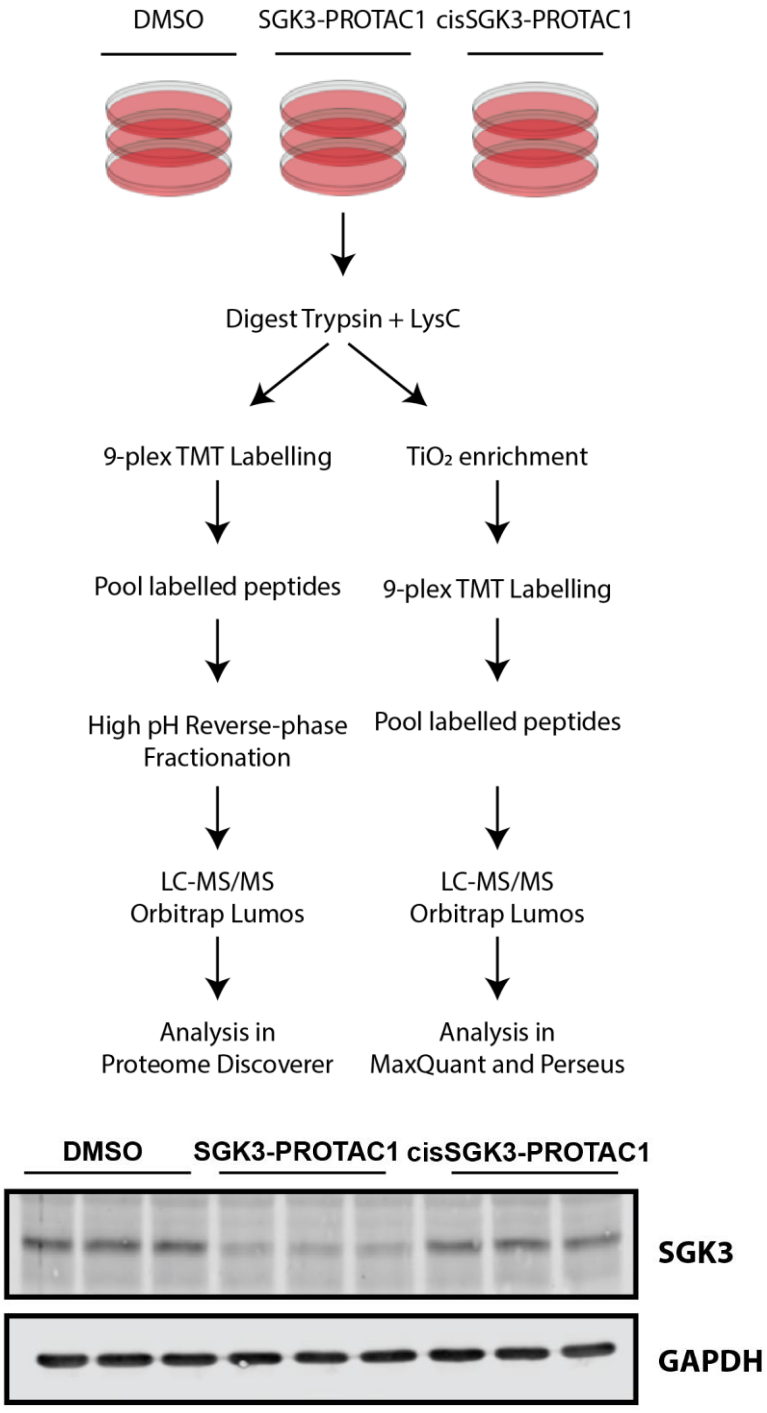

Figure 4.1 Experimental workflow for mass spectrometry analysis of SGK3-PROTAC1 treatment in ZR-75-1 cells.
ZR-75-1 cells were treated for 6 h with DMSO, SGK3-PROTAC1 (0.3 μM) or cisSGK3-PROTAC1 (0.3 μM). Western Blot analysis demonstrated substantial degradation of SGK3 on SGK3-PROTAC1 treatment.

4.3 Global Proteomic Analysis of SGK3-PROTAC1 treatment in ZR-75-1 reveals effects on mitochondrial respiration and cAMP signalling

Global, unbiased analysis in Proteome Discoverer v2.2 identified relative quantification of 8167 proteins. As observed in HEK293 cells, SGK3-PROTAC1 was observed to be highly specific, as SGK3 was identified as the most downregulated protein. A caveat of this analysis is that, as ZR-75-1 cells express relatively low levels of SGK3 under basal conditions, relative quantification of SGK3 was based on one identified unique peptide, so it carries a relatively low p value, but was still determined to be significant (p value = 0.02). Other than SGK3, very few other proteins were identified as significantly downregulated. With the exception of Histone proteins that are likely trace nuclear contaminants, only 4 other proteins, PDE4D, TRAF3IP2, RPL14 and ZNF512B, were also detected as being downregulated in response to treatment, with a >45% reduction in protein levels (Figure 4.2 and Table 4.1). I also detected an unexpected upregulation of a host of mitochondrial proteins, which upon further analysis were revealed to all be components of the electron transport chain. Of 8167 identified proteins, 351 were determined to be significantly upregulated >2fold in response to SGK3-PROTAC1 treatment, in comparison to the inactive analogue cisSGK3-PROTAC1 (Figure 4.2 and Table 4.2, full list in Appendix Table 3). Of these 351 upregulated proteins, 318 were identified by Gene Ontology (GO) analysis to be mitochondrial, specifically components associated with oxidative phosphorylation.

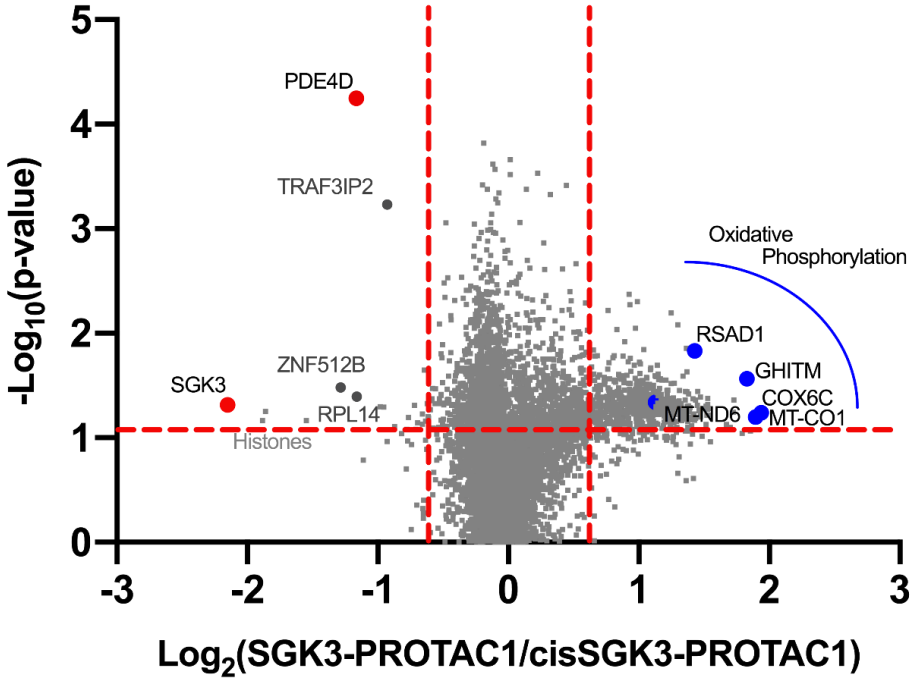

Figure 4.2 Global proteomic analysis of SGK3-PROTAC1 treatment compared to inactive analogue.
ZR-75-1 cells were treated for 6 h with SGK3-PROTAC1 (0.3 μM) or cisSGK3-PROTAC1 (0.3 μM) , and cell lysates subject to quantitative mass spectrometry analysis. Data are presented as a volcano plot

Analysis of SGK3-PROTAC-1/DMSO revealed similar proteomic changes, and as a negative control, cisSGK3-PROTAC1/DMSO has very little global effects (Tables 4.1, 4.2 and Figure 4.3). These controls confirm that these effects are dependent on SGK3-PROTAC1s ability to induce ubiquitylation and subsequent proteasomal degradation.

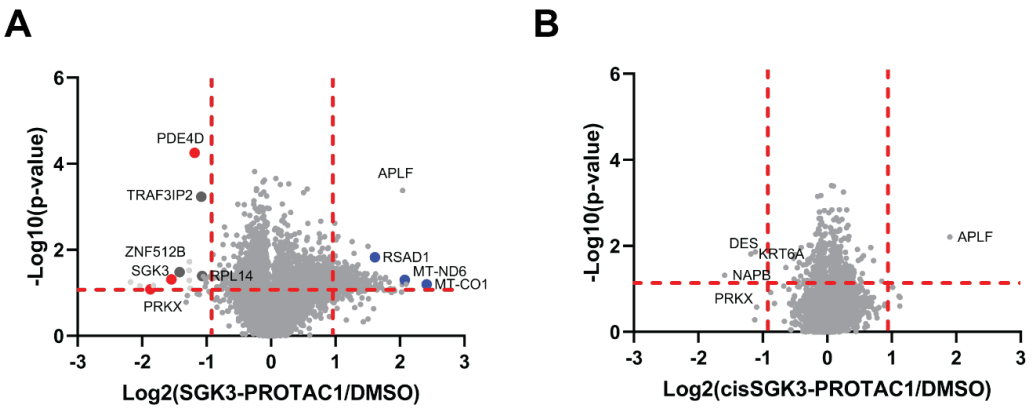

Figure 4.3 Total proteomic changes on treatment with A) SGK3-PROTAC1 or B) cisSGK3-PROTAC1 in ZR-75-1 cells.
ZR-75-1 cells were treated for 6 h with SGK3-PROTAC1 (0.3 μM), cisSGK3-PROTAC1 (0.3 μM) or DMSO, and cell lysates subject to quantitative mass spectrometry analysis. Data are presented as a volcano plot Data are presented as volcano plots.

Table 4.1 List of proteins significantly downregulated on SGK3-PROTAC1 Treatment

After removal of contaminants, identified proteins were filtered for an abundance ratio for SGK3-PROTAC1/cisSGK3-PROTAC1 <0.55 and p value <0.05.

Accession	Gene	Description	Unique Peptides	Coverage	SGK3-PROTAC1/DMSO		SGK3-PROTAC1/cisSGK3-PROTAC1		cisSGK3-PROTAC1/DMSO	
			#	%	Abundance Ratio	p-value	Abundance Ratio	p-value	Abundance Ratio	p-value
Q96BR1	SGK3	Serine/threonine-protein kinase Sgk3	1	2	0.343	0.0486	0.225	0.0259	1.149	0.4726
Q96KM6	ZNF512B	Zinc finger protein 512B	13	17	0.374	0.0329	0.41	0.0206	1.154	0.7151
Q08499	PDE4D	cAMP-specific 3',5'-cyclic phosphodiesterase	5	6	0.44	0.0001	0.446	0.0008	0.988	0.7399
P50914	RPL14	60S ribosomal protein L14	6	27	0.477	0.0404	0.447	0.0040	1.122	0.5306
O43734	TRAF3IP2	Adapter protein CIKS	10	25	0.472	0.0006	0.525	0.0034	0.907	0.1017

Table 4.2 List of top 40 proteins significantly upregulated on SGK3-PROTAC1 Treatment.

After removal of contaminants, identified proteins were filtered for an abundance ratio for SGK3-PROTAC1/cisSGK3-PROTAC1 >2 and p value <0.05. 351 proteins were identified meeting these criteria and the full list is available in Appendix Table 2.

Accession	Gene	Description	Unique Peptides	Coverage	SGK3-PROTAC1/DMSO		SGK3-PROTAC1/cisSGK3-PROTAC1		cisSGK3-PROTAC1/DMSO	
			#	%	Abundance Ratio	p-value	Abundance Ratio	p-value	Abundance Ratio	p-value
P09669	COX6C	Cytochrome c oxidase subunit 6C	3	21	2.25	0.0573	3.83	0.0328	0.99	0.5293
P56134	ATP5J2	ATP synthase subunit f, mitochondrial	2	26	3.51	0.0863	3.62	0.0472	0.80	0.7629
Q9H3K2	GHITM	Growth hormone-inducible transmembrane protein	6	15	2.29	0.0271	3.55	0.0119	0.85	0.2732
Q6UWS5	PET117	Protein PET117 homolog, mitochondrial	2	31	2.74	0.0907	3.46	0.0461	0.92	0.9826
Q00325	SLC25A3	Phosphate carrier protein, mitochondrial	16	41	2.49	0.0437	3.31	0.0140	0.86	0.6578
P08574	CYC1	Cytochrome c1, heme protein, mitochondrial	12	42	2.24	0.0570	3.31	0.0168	0.92	0.7776
Q9NWR8	MCUB	Calcium uniporter regulatory subunit MCUb, mitochondrial	3	9	3.61	0.0800	3.26	0.0389	0.97	0.6884
O75964	ATP5L	ATP synthase subunit g, mitochondrial	5	53	3.03	0.0747	3.19	0.0417	0.84	0.7890
Q6UW78	UQCC3	Ubiquinol-cytochrome-c reductase complex assembly factor 3	3	46	2.25	0.1100	2.93	0.0326	1.22	0.8168
Q6NUK1	SLC25A24	Calcium-binding mitochondrial carrier protein SCaMC-1	26	57	2.05	0.0603	2.89	0.0111	0.94	0.8774
Q9Y2R0	COA3	Cytochrome c oxidase assembly factor 3 homolog, mitochondrial	4	36	2.35	0.0522	2.89	0.0260	0.93	0.8314
P00403	MT-CO2	Cytochrome c oxidase subunit 2	7	31	2.61	0.0536	2.89	0.0216	0.88	0.9554
Q99643	SDHC	Succinate dehydrogenase cytochrome b560 subunit, mitochondrial	1	5	3.39	0.0481	2.89	0.0224	0.91	0.6842
O43674	NDUFB5	NADH dehydrogenase [ubiquinone] 1 beta subcomplex subunit 5, mitochondrial	5	25	2.18	0.0420	2.88	0.0217	0.92	0.6201
P00846	MT-ATP6	ATP synthase subunit a	1	4	3.26	0.0608	2.87	0.0253	0.91	0.6719
O95169	NDUFB8	NADH dehydrogenase [ubiquinone] 1 beta subcomplex subunit 8, mitochondrial	5	36	2.97	0.0499	2.86	0.0405	1.15	0.4244
O60830	TIMM17B	Mitochondrial import inner membrane translocase subunit Tim17-B	5	37	2.84	0.0523	2.81	0.0355	0.95	0.8799
Q9UJS0	SLC25A13	Calcium-binding mitochondrial carrier protein Aralar2	19	46	2.24	0.0543	2.78	0.0147	0.88	0.8598
Q16891	IMMT	MICOS complex subunit MIC60	49	62	2.09	0.0636	2.78	0.0158	0.88	0.8163
Q9Y6M9	NDUFB9	NADH dehydrogenase [ubiquinone] 1 beta subcomplex subunit 9	8	50	2.46	0.0604	2.77	0.0354	1.02	0.8594
P56385	ATP5ME	ATP synthase subunit e, mitochondrial	6	67	2.19	0.0409	2.77	0.0363	0.90	0.4006
P53007	SLC25A1	Tricarboxylate transport protein, mitochondrial	13	45	2.46	0.0568	2.77	0.0281	0.89	0.8677
P05141	SLC25A5	ADP/ATP translocase 2	8	52	2.26	0.0550	2.76	0.0223	0.89	0.7942
Q5RI15	COX20	Cytochrome c oxidase assembly protein COX20, mitochondrial	3	23	2.81	0.0360	2.73	0.0077	1.23	0.9285
O95167	NDUFA3	NADH dehydrogenase [ubiquinone] 1 alpha subcomplex subunit 3	4	50	2.49	0.0489	2.73	0.0249	1.01	0.7860
Q96IX5	USMG5	Up-regulated during skeletal muscle growth protein 5	3	45	2.22	0.0833	2.73	0.0376	0.86	0.6991
Q9H300	PARL	Presenilins-associated rhomboid-like protein, mitochondrial	5	11	2.48	0.0653	2.70	0.0251	0.92	0.9593
O43819	SCO2	Protein SCO2 homolog, mitochondrial	10	43	2.41	0.0437	2.70	0.0224	0.86	0.7113
Q96TA2	YME1L1	ATP-dependent zinc metalloprotease YME1L1	20	26	1.95	0.0677	2.69	0.0180	1.03	0.7877
Q9HA92	RSAD1	Radical S-adenosyl methionine domain-containing protein 1, mitochondrial	5	11	3.05	0.0148	2.69	0.0094	1.06	0.4686
P31930	UQCRC1	Cytochrome b-c1 complex subunit 1, mitochondrial	19	58	2.51	0.0592	2.68	0.0224	0.87	0.9920
A0A0B4J2F	PIGBOS1	Protein PIGBOS1	1	19	1.31	0.2455	2.67	0.0403	0.81	0.6948
Q6PML9	SLC30A9	Zinc transporter 9	9	14	2.01	0.0663	2.67	0.0279	0.98	0.9282
P13073	COX4I1	Cytochrome c oxidase subunit 4 isoform 1, mitochondrial	8	40	2.20	0.0424	2.67	0.0238	0.93	0.7219
Q8N8Q8	COX18	Cytochrome c oxidase assembly protein COX18, mitochondrial	3	8	2.37	0.0920	2.66	0.0115	0.89	0.8118
P22695	UQCRC2	Cytochrome b-c1 complex subunit 2, mitochondrial	18	48	2.73	0.0668	2.65	0.0290	0.79	0.8595
Q6P1K1	SLC48A1	Heme transporter HRG1	1	8	3.28	0.0766	2.65	0.0472	1.13	0.4946
P03905	MT-ND4	NADH-ubiquinone oxidoreductase chain 4	4	8	4.09	0.0640	2.64	0.0241	1.21	0.4522

4.3.1 PDE4D is downregulated in response to SGK3-PROTAC1 treatment

In order to determine the specificity of SGK3-PROTAC1, and whether other proteins were truly downregulated in response to PROTAC treatment, I analysed the expression of PDE4D, TRAF3IP2, RPL14 and ZNF512B by western blot, with commercially validated antibodies after 8h treatment with SGK3-PROTAC1, cisSGK3-PROTAC1 or 14H SGK inhibitor. In this analysis, I detected no observable change in expression of TRAF3IP2, RPL14 or ZNF512B, and these may therefore be false positives from the mass spectrometry procedure. However, PDE4D expression was determined to be downregulated in response to SGK3-PROTAC1, but not cisSGK3-PROTAC1, in ZR-75-1 cells by western blot (Figure 4.4). Importantly, this effect was not observed after inhibition of SGK3 by 14H, and therefore appears to be a degradation-specific effect.

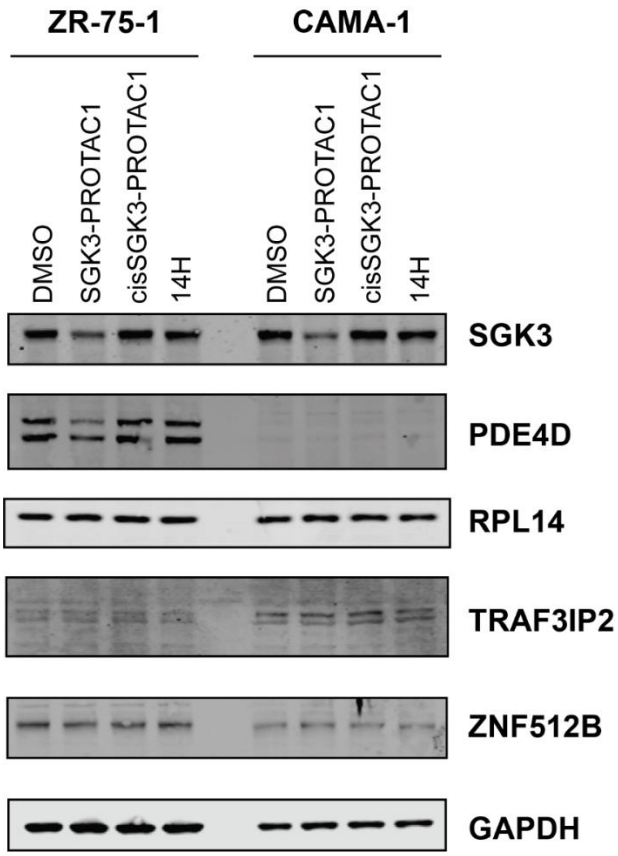

Figure 4.4 PDE4D is reproducibly downregulated on treatment with SGK3-PROTAC1.
ZR-75-1 and CAMA-1 cells were treated for 8 h with SGK3-PROTAC1, cisSGK3-PROTAC1 or 14H. Target proteins were analysed by western blot. Results are representative of n=3 experiments.

PDE4D is a cAMP-specific phosphodiesterase involved in regulation of Protein Kinase A (PKA) activity in response to external and internal stimuli such as cellular calcium levels. Its expression

has also been linked to progression of a range of cancers and resistance to cancer therapy (Lin *et al.*, 2013). Therefore, it would be extremely interesting if PDE4D activity could be mediated by degradation of SGK3, thus providing a secondary mechanism of blocking resistance to cancer therapy.

The PDE4D family of phosphodiesterases consists of at least 9 isoforms generated by alternative splicing of the PDE4D gene. All isoforms share a C-terminal catalytic domain and variable regulatory N terminal domains (Figure 4.5). The isoforms vary on the basis of their UCR1 and UCR2 domains, which are heavily decorated with posttranslational modifications and are believed to regulate activity of the enzyme.

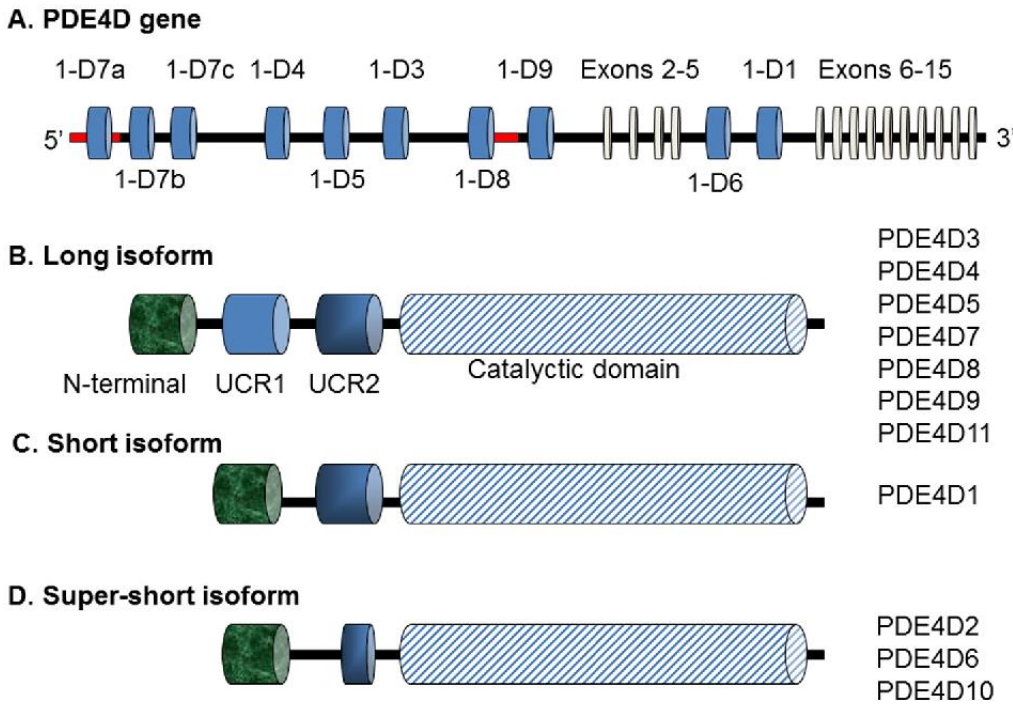

Figure 4.5 Domain structure of PDE4D isoforms.
A. *11 PDE4D isoforms are transcribed by alternative splicing of the PDE4D gene.* ***B-D.*** *Domain structures of the PDE4D isoforms. Long isoforms contain full UCR1 regulatory domains.*

By Western Blot, the isoforms of PDE4D downregulated by SGK3-PROTAC1 treatment correspond to the <80 KDa 'Long isoforms' of PDE4D. In CAMA-1 cells, expression of these isoforms of PDE4D was undetectable by western blot, however the antibody did pick up a lower molecular weight band which may be a short isoform of PDE4D. This isoform was not sensitive

to SGK3-PROTAC1 or 14H treatment. Given that isoforms containing UCR1 are sensitive to SGK3-PROTAC1 treatment, it would be interesting to explore in future work whether there is an interaction between SGK3 and the UCR1 domain of PDE4D. Additionally, the UCR1 domain contains RXRXXS/T Motifs predicted to be phosphorylated by Akt, however treatment with SGK3 kinase inhibitor 14H had no impact on PDE4D levels.

Further analysis in HEK293 cells revealed that PDE4D downregulation in response to SGK3-PROTAC1 treatment is also observed in this cell line (Figure 4.6A). However, the effect is less robust than is observed in ZR-75-1 cells, which may be why the change was not observed in the previous mass spectrometry experiment (Section 3.9). Timecourse analysis of PDE4D expression in these cells showed a slight reduction in PDE4D expression within an hour, with 50% reduction in 4-8 h (Figure 4.6B). An important control is to determine whether this downregulation of PDE4D is occurring on-target through SGK3, or as an off-target effect of the compound. I therefore sought to use genetic approaches targeting SGK3 in order to validate PDE4D as a downstream effector of SGK3.

I continued to study PDE4D levels downstream of SGK3 using an shRNA method to induce significant knockdown of SGK3. Using two different shRNA constructs, targeting the protein coding region (shSGK3#1) and 3'UTR (shSGK3#2), I induced significant downregulation of SGK3, and studied PDE4D expression in the presence of absence of SGK3-PROTAC1 treatment. I detected a reduction in PDE4D expression in response to the shRNA, and remaining PDE4D was less sensitive to SGK3-PROTAC1 treatment (Figure 4.6C). This preliminary data suggests that PDE4D expression, and therefore cAMP and PKA signalling may modulated by SGK3.

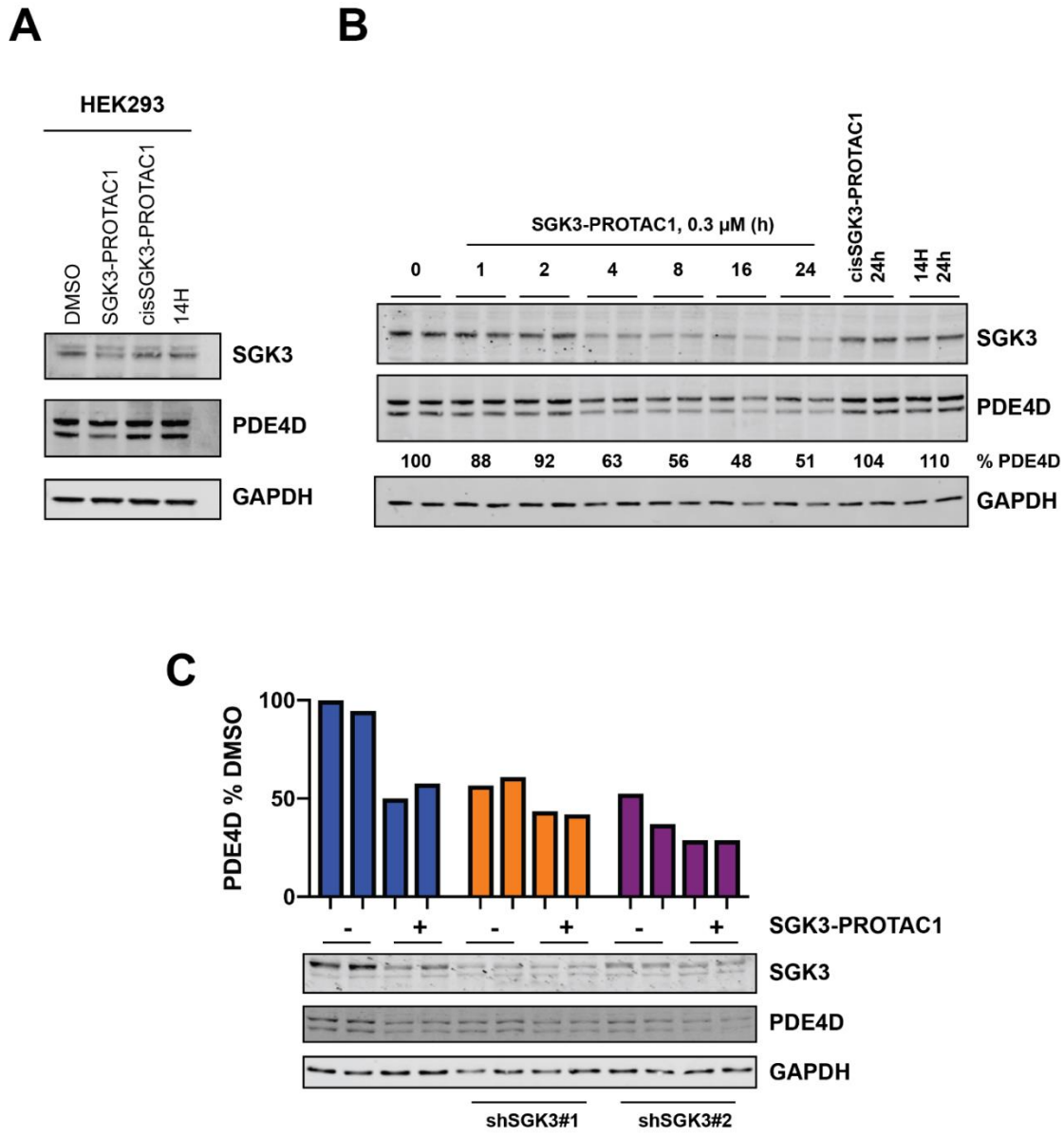

Figure 4.6 PDE4D expression is mediated downstream of SGK3 in HEK293 cells.
A. *SGK3-PROTAC1 treatment reduced PDE4D expression in HEK293 cells, but this was not replicated by cisSGK3-PROTAC1 or 14H treatment.* ***B.*** *Timecourse treatment with 0.3 μM SGK3-PROTAC1 revealed reduced expression of PDE4D after 2 hours.* ***C.*** *SGK3 was knocked down by shRNA treatment, and transfected cells selected for by puromycin treatment. These cells were then treated for 8 h in the presence or absence of SGK3-PROTAC1, and protein levels of SGK3 and PDE4D measured by western blot. Quantification of PDE4D was performed using Image Studio Lite software.*

In order to confirm a mechanism of action through SGK3, I re-expressed in the shSGK3 cell lines either wildtype or kinase inactive (KI) shRNA resistant SGK3. Consistent with a kinase-independent mechanism of action through SGK3, PDE4D expression was rescued by both wildtype and kinase-inactive SGK3 (Figure 4.7). In fact, KI SGK3 rescued to a greater extent than the wildtype. Again, treatment of these cells with the 14H inhibitor or inactive cisSGK3-PROTAC1

analogue had no impact on PDE4D levels, suggesting that PDE4D downregulation is a degradation-specific effect.

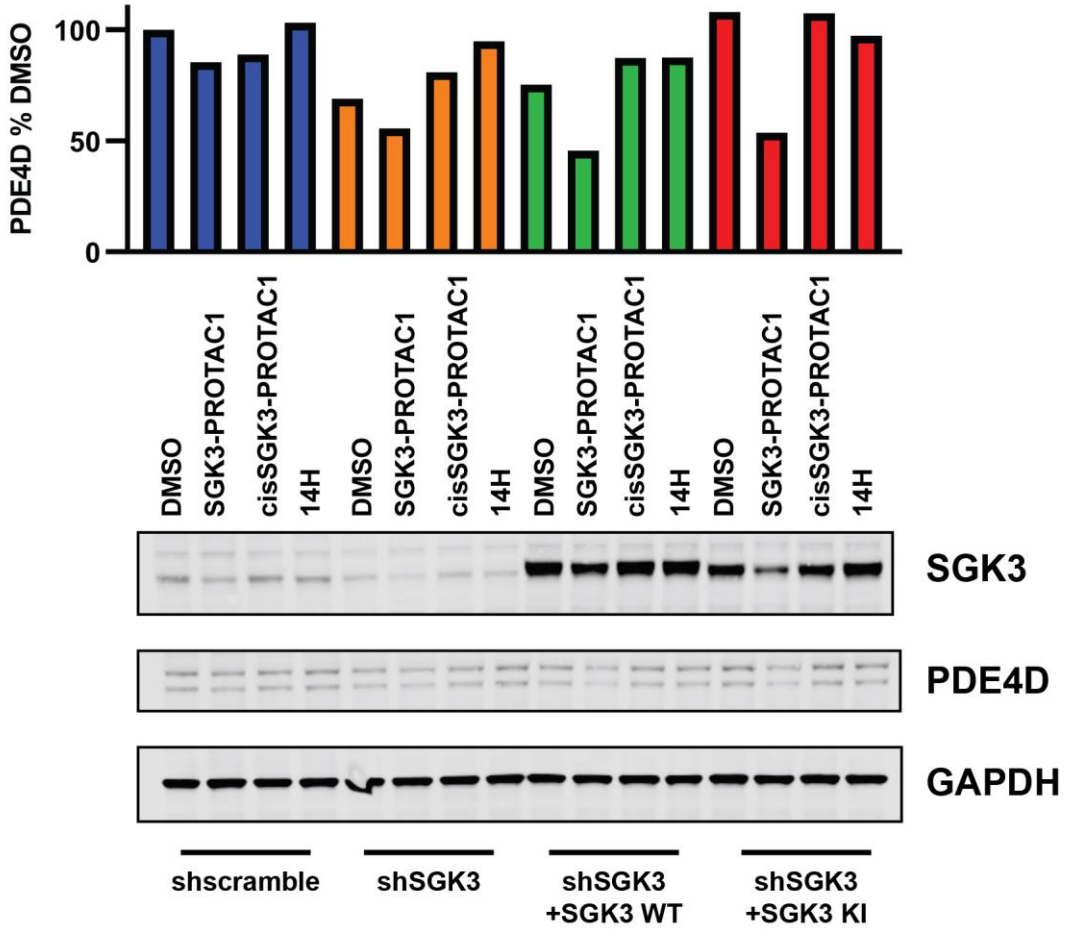

Figure 4.7 Rescue of PDE4D expression by exogenous expression of SGK3 wildtype and kinase inactive. *HEK293 cells were transfected for 24 h with shRNA against SGK3 or a scrambled control. After allowing a further 24 h for recovery, cells were transfected with shRNA resistant SGK3, either wildtype or the kinase inactive mutant. 24 h later, cells were treated for 8 h with SGK3-PROTAC1 (0.3 μM), cisSGK3-PROTAC1 (0.3 μM) or 14H (1 μM). Cells were lysed and subject to immunoblot analysis.*

As additional confirmation that reduction in PDE4D is SGK3-degradation dependent, I treated ZR-75-1 cells with a panel of inhibitors to probe different aspects of the pathway. First, I treated cells with an off-target PROTAC HaloPROTAC-E, described in more detail in chapter 5, and VHL inhibitor VH298 (Frost *et al.*, 2016). These inhibitors showed no effect on PDE4D levels therefore this result is unlikely to be an effect of VHL inhibition or HIF1a stabilization as an effect of PROTAC treatment. I also treated cells with the SGK3 inhibitor 14h, the Class I PI3K inhibitor

GDC0941 or VPS34 inhibitor VSP34-IN1, alone or in combination. These inhibitors were used to block activity of SGK3 and determine that this effect is not due to loss of SGK3 kinase activity, however this may be the result of a scaffolding effect (Figure 4.8A). I also performed timecourse analysis of PDE4D expression in these cells upon SGK3-PROTAC1 treatment and determined that, similar to HEK293 cells, downregulation of PDE4D occurs within an hour of treatment, with expression reduced 50% within 6h.

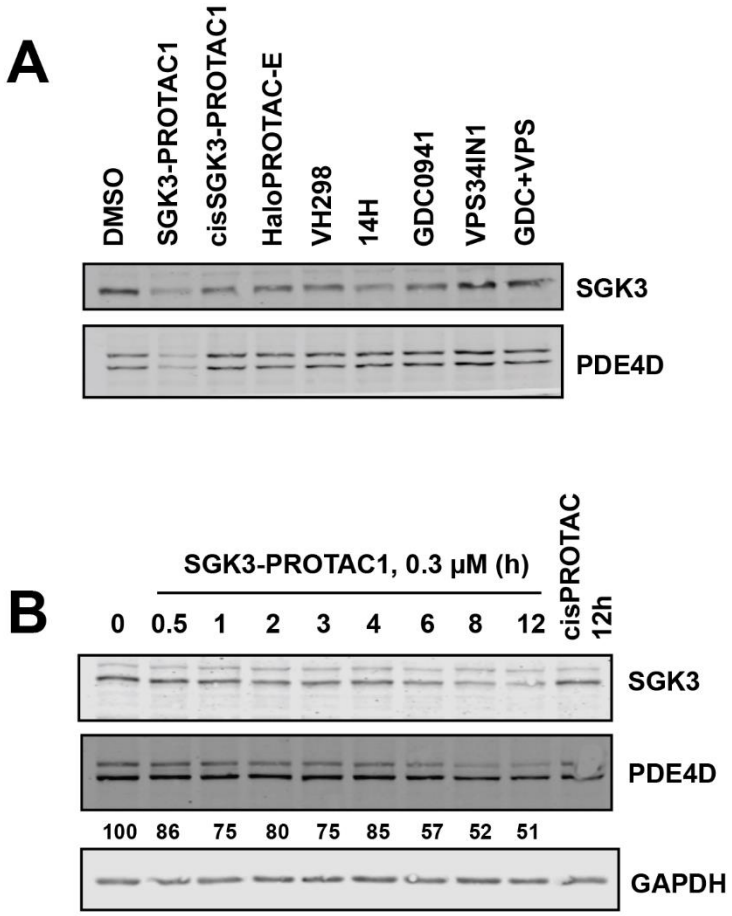

Figure 4.8 Mechanistic validation of PDE4D downregulation in ZR-75-1 cells.
A. *ZR-75-1 cells were treated for 6 h with SGK3-PROTAC1 (0.3 μM), cisSGK3-PROTAC1 (0.3 μM), HaloPROTAC-E (0.3 μM), VH298 (50 μM), 14H (1 μM), GDC0941 (1 μM) or VPS34IN1 (1 μM). Cell lysates were subject to immunoblot analysis with the indicated antibodies, and protein levels quantified in Image Studio software.* ***B.*** *ZR-75-1 cells were treated for up to 12 h with SGK3-PROTAC1 (0.3 μM), or for 12 h with cisSGK3-PROTAC1 (0.3 μM). Cell lysates were subject to immunoblot analysis with the indicated antibodies and protein levels quantified in Image Studio software.*

4.3.2 Mitochondrial proteins involved in the Electron Transport Chain are upregulated on SGK3-PROTAC1 treatment

It was surprising on analysing the proteomic data to identify a global upregulation in mitochondrial proteins involved in oxidative phosphorylation. This effect was not observed in HEK293 cells, and no previous literature to our knowledge has connected SGK3 to mitochondria. Subsequent analysis by western blot revealed that this effect appears to be specific to the SGK3-dependent cancer cell lines, as this result could be reproduced only in the ZR-75-1 and CAMA-1 cells, and not HEK293 cells (Figure 4.9A and B) .Furthermore, analysis of a range of mitochondrial proteins revealed this upregulation is specific to members of the electron transport chain, as a selection of outer mitochondrial membrane (OMM) proteins were unaffected. Additionally, no increased cleaved of OPA-1 was observed on SGK3-PROTAC1 treated, therefore this effect was not due to an effect on mitochondrial membrane polarity (Figure 4.9A).

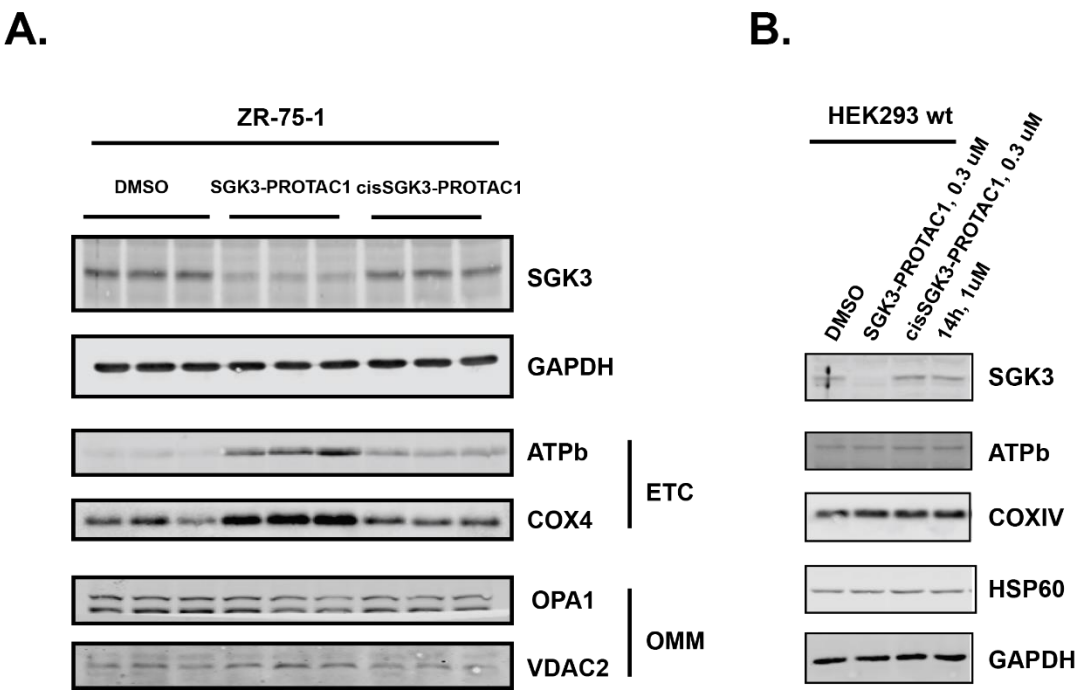

Figure 4.9 SGK3-PROTAC1 treatment induces upregulation of the Electron Transport Chain in ZR-75-1 cells.

A. *ZR-75-1 cells were treated for 6 h with DMSO, SGK3-PROTAC1 (0.3 μM) or cisSGK3-PROTAC1 (0.3 μM). Cells were lysed in urea buffer and subject to immunoblot analysis with the indicated antibodies.* ***B.*** *HEK293 cells were treated for 6 h with DMSO, SGK3-PROTAC1 (0.3 μM) cisSGK3-PROTAC1 (0.3 μM) or SGK3 inhibitor 14H (1 μM). Cells lysates were subject to immunoblot analysis with the indicated antibodies. ETC = proteins of the electron transport chain. OMM = proteins located on the outer mitochondrial membrane, not part of the electron transport chain.*

Oxidative Phosphorylation (OxPhos), is a metabolic pathway in mitochondria which generates ATP by transport of electrons through complexes I, II, III and IV of the electron transport chain (ETC). This process allows protons to be pumped into the intermembrane space by complexes I, III and IV (Figure 4.10). This generates a high proton gradient across the inner mitochondrial membrane, causing protons to flow back to the mitochondrial matrix through complex V, ATP synthase, driving the synthesis of ATP. Interestingly, in my data set I observed upregulation of proteins involved in all 5 complexes, transcribed from both mtDNA and nuclear genes.

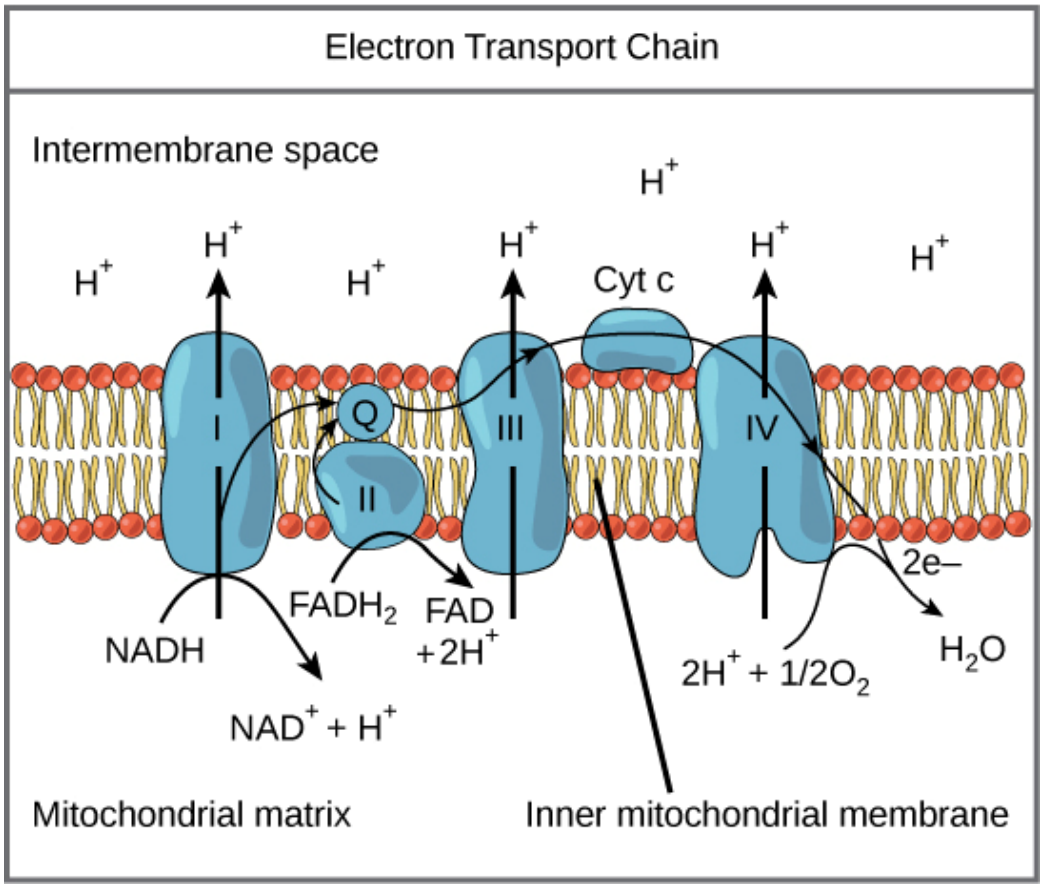

Figure 4.10 Electron Transport Chain process.
Electrons are transferred between ETC complexes I-IV, which also transport protons into the mitochondrial intermembrane space, generating a membrane potential. This membrane potential allows activation of ATP synthase, which produces ATP.

As this mitochondrial effect was observed in response to SGK3-PROTAC1 treatment, but not the inactive cisSGK3-PROTAC1, it was important to verify that this response was occurring through SGK3, and not as an effect of impacting on the VHL pathway. Therefore, in a similar approach to

figure 4.8, I treated CAMA-1 cells for 6 h with a range of compounds to delineate the pathways involved in this upregulation.

SGK3-PROTAC1 and cisSGK3-PROTAC1 treatment confirmed upregulation as a degradation-specific effect of SGK3-PROTAC1 treatment. I also treated cells with the off-target PROTAC (HaloPROTAC-E, 0.3 μM) or the VHL inhibitor VH298 (50 μM), to determine whether mitochondrial upregulation was a PROTAC/VHL-dependent effect in these cells. I also treated cells with the 14H inhibitor (1 μM) to determine whether SGK3 inhibition had the same effect. I additionally treated with Class IA PI3K inhibitor GDC0941 (0.5 μM) or Class III PI3K inhibitor VPS34IN1 (1 μM), alone or in combination, to switch off different components of the pathway.

Western blot for a range of mitochondrial proteins confirmed a robust upregulation of Electron Transport Chain on treatment with SGK3-PROTAC1, but not cisSGK3-PROTAC1. I also did not observe an effect of treating with HaloPROTAC-E or VH298, therefore suggesting this is not an off-target effect through VHL. Finally, while SGK3 inhibition by 14H had very little effect, there was a variable effect observed with inhibition of PI3K Class I or Class III, with upregulation of COX6C, but apparent degradation of MT-CO1 and MT-ND6 (Figure 4.11).

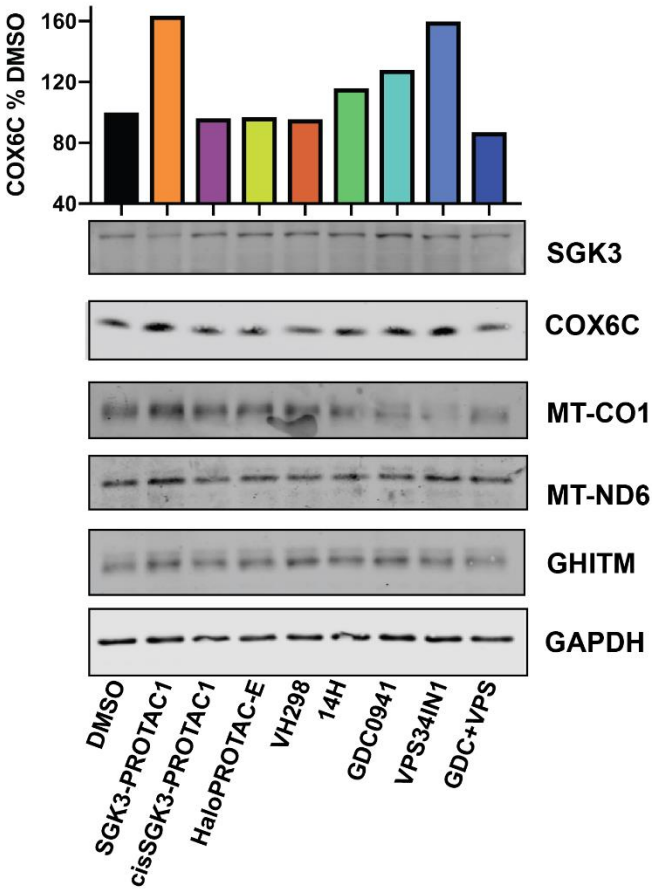

Figure 4.11 Expression of the Electron Transport Chain is upregulated on treatment with SGK3-PROTAC1, but not other VHL-targeting compounds.
CAMA-1 cells were treated for 6 h with SGK3-PROTAC1 (0.3 μM), cisSGK3-PROTAC1 (0.3 μM), HaloPROTAC-E (0.3 μM), VH298 (50 μM), 14H (1 μM), GDC0941 (1 μM) or VPS34IN1 (1 μM). Cell lysates were analyzed by immunoblot with the indicated antibodies, and protein levels quantified in Image Studio software.

In order to further determine response to SGK3-PROTAC1 treatment, I analyzed expression of these proteins in response to SGK3-PROTAC1 (0.3 μM) over a timecourse up to 12 hours. This revealed an immediate response within an hour of treatment of MT-CO1 and GHITM expression, which increased up to the 8 h timepoint. After 12 h, protein expression was maintained but did not increase further. In comparison, 12 h treatment with cisSGK3-PROTAC1 had no effect (Figure 4.12).

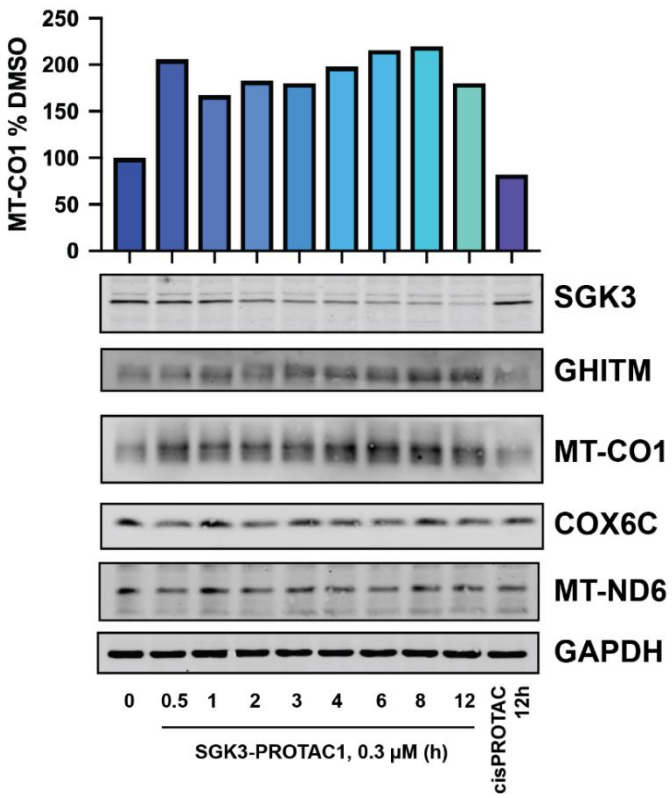

Figure 4.12 Increased expression of ETC components is observed within 30 minutes, and maintained for 12 hours.
CAMA-1 cells were treated for up to 12 h with SGK3-PROTAC1 (0.3 µM), or for 12 h with cisSGK3-PROTAC1 (0.3 µM). Cell lysates were subject to immunoblot analysis with the indicated antibodies and protein levels quantified in Image Studio software.

The functional mechanism and impact of protein upregulation cannot be determined from the western blot data. The increase in protein levels could be due to hyperactivation of mitochondrial respiration, or inhibition of the pathway causing a compensatory increase in protein expression. In future work it would be important to determine what effect PROTAC treatment and ETC upregulation was having on mitochondrial respiration and metabolism. It has currently not been functionally characterized how SGK3 is impacting on mitochondrial proteins. As will be discussed further in section 4.5, SGK3 may be impacting on Nedd4L or another E3 ligase to regulate protein degradation or may act at the mRNA level to influence protein translation.

4.4 Phosphoproteomic analysis in ZR-75-1 cells reveals potential pathways regulated by SGK3.

In parallel to the proteomic analysis described above, I also performed phosphoproteomic analysis of SGK3-PROTAC1 and cisSGK3PROTAC1 (0.3 µM) in ZR-75-1 cells, in comparison to DMSO. Phosphoproteomic analysis was performed to potentially reveal novel substrates phosphorylated specifically by SGK3, and not Akt. After splitting the peptide digest for global proteomic analysis, peptides were enriched for phosphopeptides by TiO_2 enrichment, before TMT labelling and analysis by LC-MS/MS on the Orbitrap Lumos Mass Spectrometer. Identified mass spectra were then analysed in Max Quant (version 1.6.6.0, (Tyanova, Temu and Cox, 2016)) before further analysis in Perseus (Version 1.6.2.3, (Tyanova *et al.*, 2016)).

A previous phosphoproteomic study in HEK293 cells recently discovered Syntaxin7 and Syntaxin12 as specific SGK3 substrates, which are not phosphorylated by Akt (Malik *et al.*, 2019). The study performed 2 phosphoproteomic screens, one comparing HEK293 wildtype cells with an SGK3-KO cell line, and the other comparing phosphorylation of substrates after treatment with the SGK inhibitor 14H. It was interesting to determine whether these substrates were also found in ZR-75-1 cells, or if further substrates could be identified.

The phosphoproteomic analysis identified 29,215 unique phosphosites, of which 18,629 sites were Class I sites, as defined by >0.75 probability. Of these 18,629 sites, 1,152 were significantly downregulated (According to Two tailed Student's T Test, $p<0.05$, FC<=-1.5) in the SGK3-PROTAC1 condition v cisSGK3-PROTAC, while 215 sites were significantly upregulated ($p<0.05$, FC>=1.5). In comparing the SGK3-PROTAC1 and DMSO conditions, 2,806 sites were downregulated, and 147 sites were upregulated in response to the PROTAC. These data are presented as a volcano plot in Figure 4.13 and 4.14 (Full data available in Appendix Table 4).

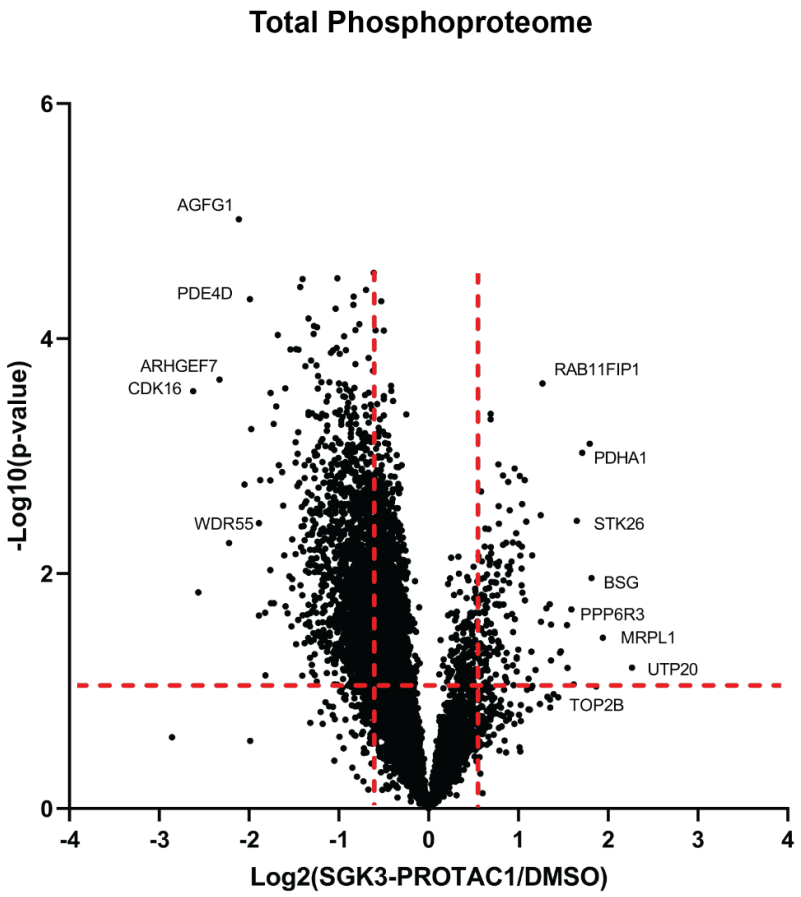

Figure 4.13 Phosphorylation sites modulated upon SGK3-PROTAC1 treatment in comparison to DMSO in ZR-75-1 cells.
ZR-75-1 cells were treated for 6 h with SGK3-PROTAC1 (0.3 μM) or DMSO, and cell lysates subject to quantitative mass spectrometry phosphoproteomic analysis after TiO_2 enrichment for phosphorylated peptides. Data are presented as a volcano plot

Although there was substantial overlap, there were differences between the altered sites in the SGK3-PROTAC1vcisSGK3-PROTAC1 and SGK3-PROTAC1vDMSO conditions. These differences are likely due to the SGK-targeting moiety of the compound still having an inhibitory effect on certain sites (Figure 4.14A). Therefore, an additional control to the study was to compare the negative control cisSGK3-PROTAC1 to DMSO treated samples, which revealed 396 downregulated and 34 upregulated sites (Figure 4.14B). Therefore, the majority of the phosphoproteomic changes identified in response to SGK3-PROTAC1 are mediated through SGK3 degradation.

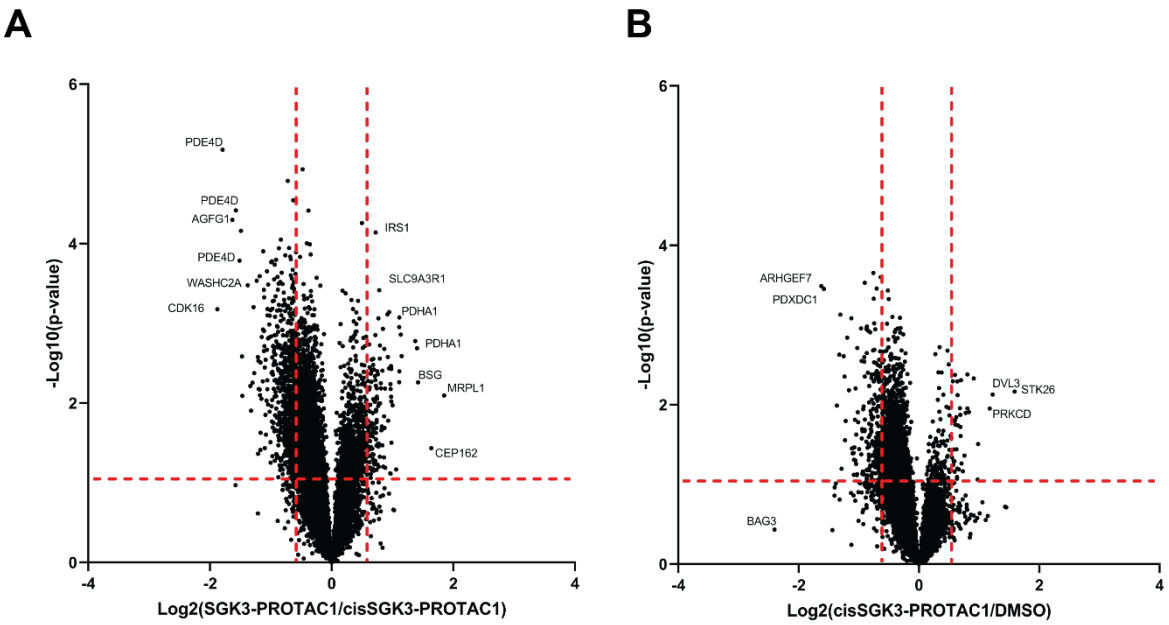

Figure 4.14 Phosphorylation changes in SGK3-PROTAC1/cisSGK3-PROTAC or cisSGK3-PROTAC1/DMSO. *ZR-75-1 cells were treated for 6 h with SGK3-PROTAC1 (0.3 μM) or DMSO, and cell lysates subject to quantitative mass spectrometry phosphoproteomic analysis after TiO_2 enrichment for phosphorylated peptides. Data are presented as a volcano plot.*

I next analysed the phosphoproteomics data for phosphomotif sites enriched in the dataset (Figure 4.15). 86.8% of detected phosphopeptides were phosphorylated on a serine residue, with 12.2% pThr and 1% pTyr. These ratios are typical for phosphoproteomic analysis using these digestion and enrichment methods. I then analysed which phosphomotifs were enriched in the dataset, and whether any of these motifs, for example the RXRXXS/T motif shared by Akt and SGK3, were enriched in the downregulated phosphopeptides after SGK3-PROTAC1 treatment. I found a large enrichment of pSP sites both in the whole dataset and enriched upon SGK3-PROTAC1 treatment. However, while RXRXXS/T sites composed a large proportion of the dataset, very few sites were observed to change upon SGK3-PROTAC1 treatment, discussed further in section 4.4.1.

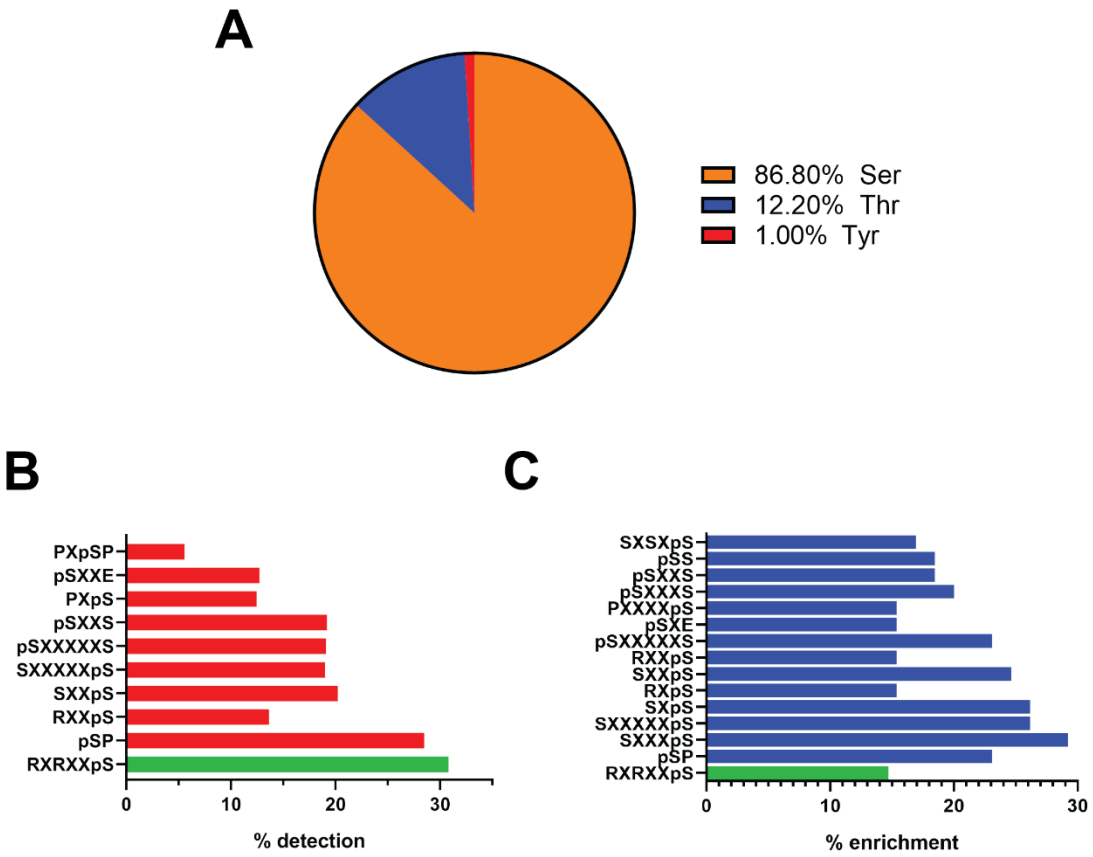

Figure 4.15 Phosphosite analysis in ZR-75-1 phosphoproteomic dataset.
A. *Phosphosite analysis of entire dataset* ***B.*** *Motif analysis of phosphopeptides identified in the whole dataset.* ***C.*** *Motif analysis of phosphopeptides reduced upon SGK3-PROTAC1 treatment compared to cisSGK3-PROTAC1.*

4.4.1 Under basal conditions, much RXRXXS/T motif phosphorylation in ZR-75-1 cells is not controlled by SGK3

Under basal conditions, ZR-75-1 cells express relatively low levels of SGK3. Increased expression and activity is induced on 5 day treatment with PI3K-Akt pathway inhibitors. Instead, growth and signalling are primarily driven through the PI3K pathway via Akt. Therefore, any shared substrates of SGK3 and Akt were not expected to change. However, phosphoproteomic analysis may reveal specific substrates of SGK3 in ZR-75-1 cells.

574 sites in total were identified lying within the RXRXXS/T motif. Of these, on comparison of SGK3-PROTAC1 to cisSGK3-PROTAC1 treatment, just 17 sites were detected to be significantly modulated (FC>1.5, $p<0.05$). 7 sites were upregulated in response to SGK3-PROTAC1 treatment, and 10 showed significant downregulation (Figure 4.16, 4.18).

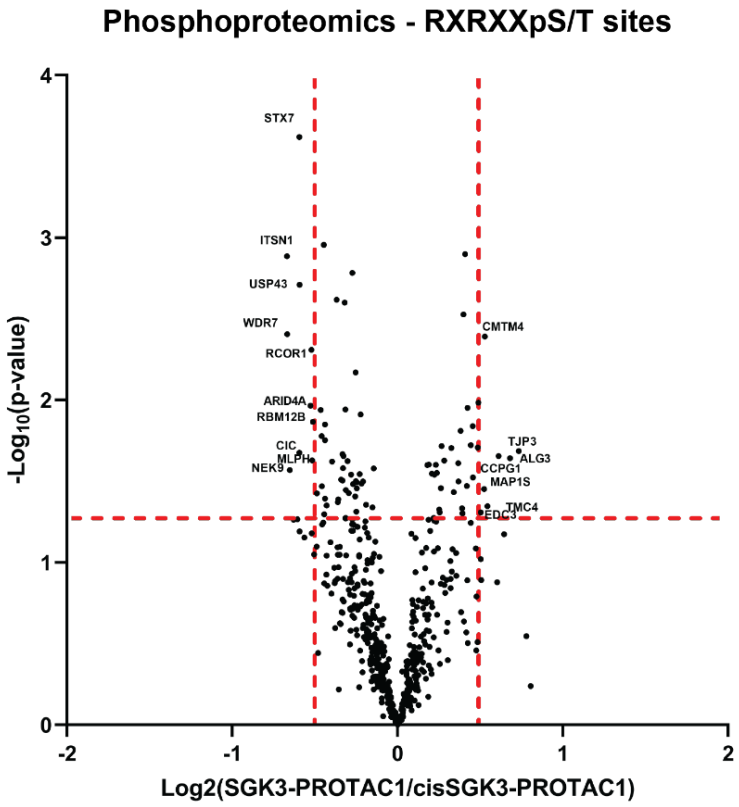

Figure 4.16 RXRXXS/T motif changes upon SGK3-PROTAC1 treatment, compared to cisSGK3PROTAC1. *ZR-75-1 cells were treated for 6 h with SGK3-PROTAC1 (0.3 μM) or cisSGK3-PROTAC1 (0.3μM), and cell lysates subject to quantitative mass spectrometry phosphoproteomic analysis after TiO_2 enrichment for phosphorylated peptides. Data are presented as a volcano plot*

When comparing phosphoproteomic changes between the SGK3-PROTAC1 and DMSO treated conditions, slightly more significant phosphosite changes were identified (Figures 4.17,18). These sites were determined not to be significant when comparing the active and inactive PROTACs, like due to slight inhibitory effects of the inactive compound. Only 6 significantly modulated phosphosites were shared between the 2 analyses (Figure 4.18) Only 2 consensus motif sites were observed to be downregulated in the cisSGK3-PROTAC1 sample in comparison to DMSO treatment. This suggests that cisSGK3-PROTAC is not inhibiting the pathway (Figure 4.18).

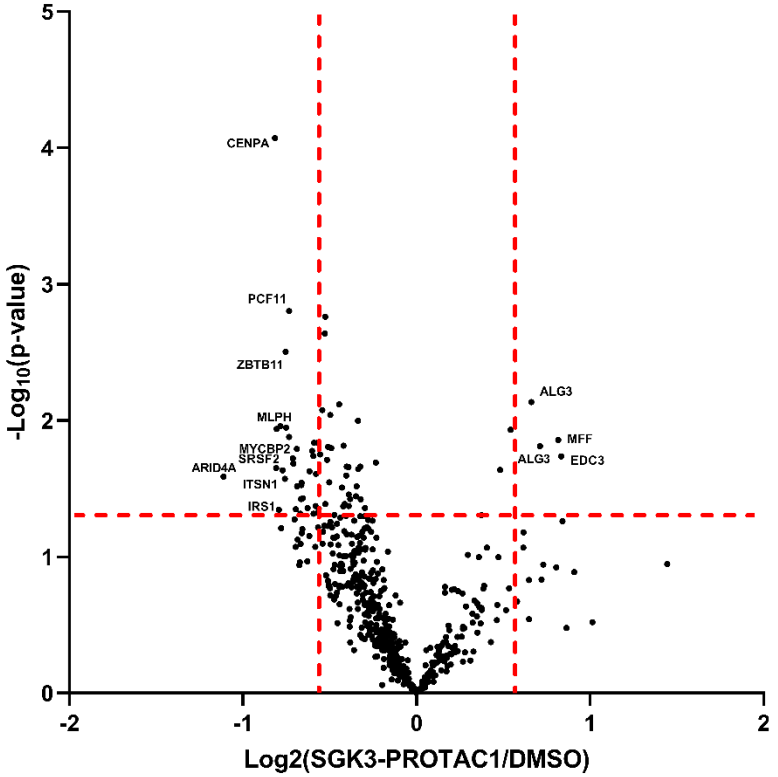

Figure 4.17 RXRXXS/T motif changes upon SGK3-PROTAC1 treatment, compared to DMSO.
ZR-75-1 cells were treated for 6 h with SGK3-PROTAC1 (0.3 μM) or DMSO, and cell lysates subject to quantitative mass spectrometry phosphoproteomic analysis after TiO_2 enrichment for phosphorylated peptides. Data are presented as a volcano plot

Of the significantly modulated sites detected, there were several overlaps with phosphoproteomic analysis of HEK293 cells either carrying an SGK3 KO or with SGK3 inhibited using 14H. These are indicated on the heatmap with a red (SGK3 KO) or green (14H treatment) asterisk (Figure 4.18).

STX7 is a member of the Syntaxin family of SNARE proteins and, along with STX12, was previously identified in our lab to be phosphorylated by SGK3 at S126, both *in vitro* and in cells, confirmed by phostag analysis. Recent data from the lab shows that phosphorylation of STX7 and STX12 at this site impacts on binding to their SNARE complex partners (VAMP4 and STX6 for STX12) and cellular localisation (Malik *et al.*, 2019). Phosphorylation of these sites is specific to SGK3 over Akt, which is reported to favour large, hydrophobic residues after the phosphorylated Ser/Thr. Mutation of the +1 site of Syntaxin12 or Syntaxin7 sensitises the protein for Akt phosphorylation

in vitro (Malik *et al.*, 2019). This represents a possible bioinformatic tool for delineating between SGK3 and Akt substrates.

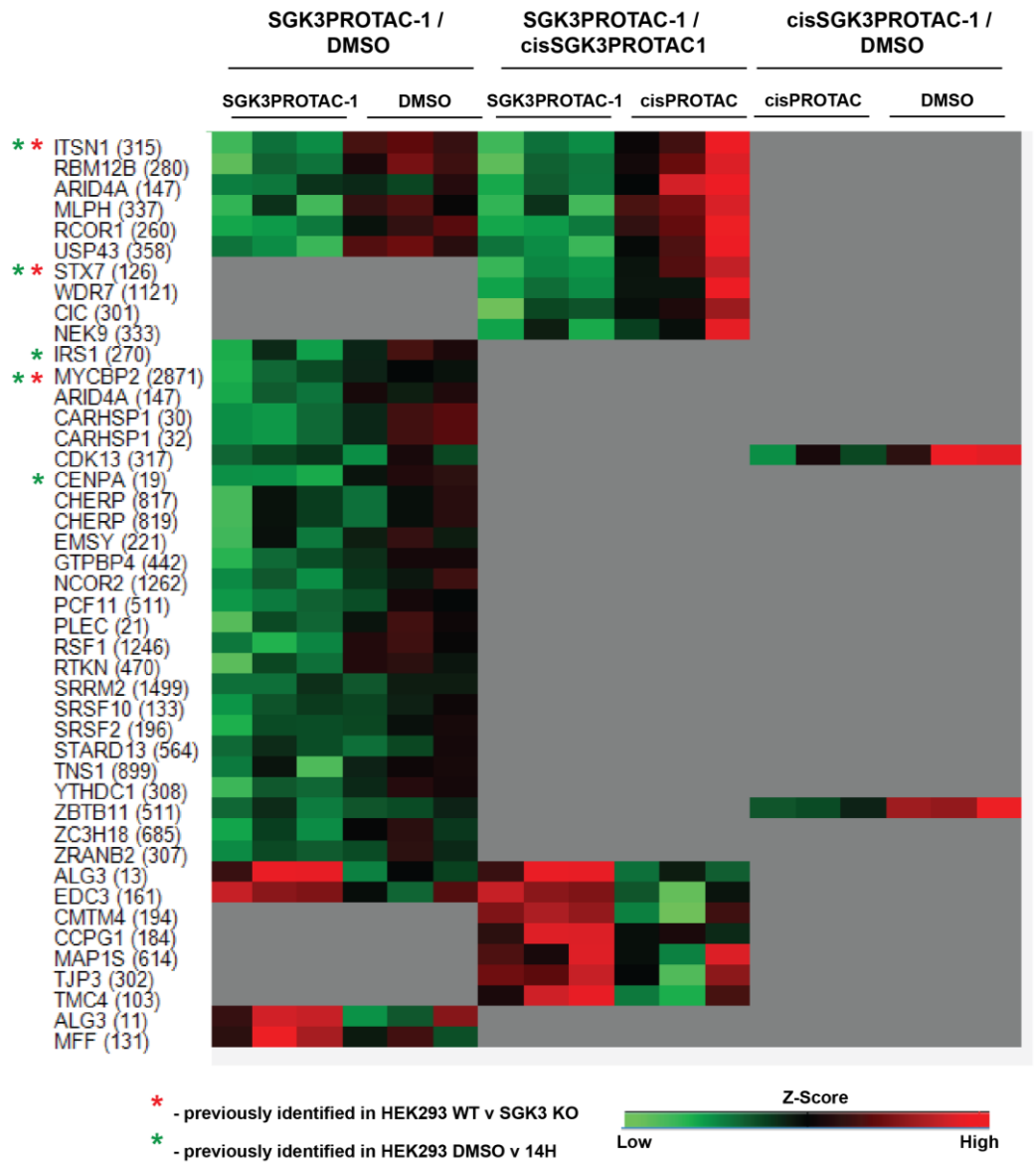

Figure 4.18 Heatmap of phosphorylation changes in RXRXXS/T sites across all 3 conditions.
Phosphoproteomic changes between SGK3-PROTAC1, cisSGK3-PROTAC1 and DMSO treatment were analysed by two-tailed t-test. Heatmap demonstrates significant (FC>1.5, p<0.05) changes in RXRXXS/T sites in each comparison. The log2 values of each of the RXRXXS/T phosphosite is Z-score normalized and generated the heat map using Perseus software.

Phosphorylation of WDR7 at Ser1121 was identified on 14H treatment in HEK293 cells. And ITSN1 is another protein identified both on SGK3 inhibition and knockout in HEK293 cells. Upon

further analysis, it was determined to be phosphorylated by both SGK3 and Akt *in vitro* (Karapetsas *et al*., unpublished).

The majority of modulated RXRXXS/T sites occur within potential 14-3-3 binding sites. Akt is known to modulate the activity of a range of proteins by phosphorylation on these sites, leading to protein sequestration in particular regions of the cell. As SGK3 is localised to endosomes, I analysed my data for any significantly modulated RXRXXpS/T sites on proteins annotated to have endosomal localisation. Apart from the previously discussed Syntaxins and Intersectin 1 (ITSN1), the only other significantly modulated protein was Melanophillin (MLPH). Melanophillin (also known as Synaptotagmin-like protein 2a) is an effector of Rab27-GTP and may regulate membrane trafficking. Therefore, the functional relevance of this site may be interesting to follow up in future work.

Only relatively minor changes in phosphorylation were detected in all these sites, with a threshold of 1.5fold change used for detection. However, at the basal level in ZR-75-1 cells SGK3 activity is very low. It would be important to repeat this assay under conditions inducing SGK3 activity, such as prolonged PI3K inhibition, in order to observe more profound changes in SGK3 substrates.

4.4.2 CCNY-CDK16 – a putative pathway downstream of SGK3.

Although I did not observe many significant changes in RXRXXS/T in these samples, there were several interesting phosphosites either up- or downregulated on SGK3-PROTAC1 treatment. Therefore, changes in these sites may, although not directly phosphorylated by SGK3, be downstream of a pathway regulated by SGK3.

The most significant and clear change in the phosphoproteomic data is a dramatic reduction in phosphorylation of CDK16 at Ser138. This phosphorylation occurs in a proline-directed pSP site typically phosphorylated by Cyclin Dependent Kinases (CDKs) or Mitogen activated protein kinases (MAPKs). Although not a predicted SGK3 phosphorylation site, it is of particular interest

as previous phosphoproteomic screens in HEK293 cells by former PhD student Nazma Malik, identified an SGK3-dependent phosphosite in the upstream effector CCNY. Therefore, my data, identifying a modulated site downstream of CCNY using a separate approach, reinforces a possible role for SGK3 in this pathway. It remains doubtful, however, that CDK16 is a direct SGK3 substrate.

In addition, both this experiment and previously performed phosphoproteomic analyses studying SGK3 knockout or 14H treatment identified a high number of modulated pS/TP sites (Figure 4.19), suggesting that signalling involving Cyclin Dependent Kinases is somehow modulated downstream of SGK3 knockdown or inhibition. In comparison of the SGK3-PROTAC1 and cisSGK3-PROTAC1 treated conditions, I detected 483 proline-directed Ser/Thr to be significantly modulated (FC>1.5, $p<0.05$). Of these, 57 sites were upregulated in response to SGK3-PROTAC1 treatment, and 426 were significantly downregulated.

In order to further investigate changes in putative CDK substrates, I analysed the data for changes within the typical CDK substrate motif (pS/T-P-X-K/R) and the CDK16 substrate motif. It was determined that CDK16 has a very different preferred substrate motif than other CDKs, preferring basic residues at the +2 and +4 positions, and a small aliphatic residue instead of acidic residues at the +2 site. Additionally, CDK16 has a significant preference for Ser over Thr (pS-P-K/R- φ-K/R/H) (Shehata *et al.*, 2012). From this analysis I found just 6 putative CDK16 sites modulated in response to SGK3-PROTAC1, and 66 sites within the canonical CDK motif.

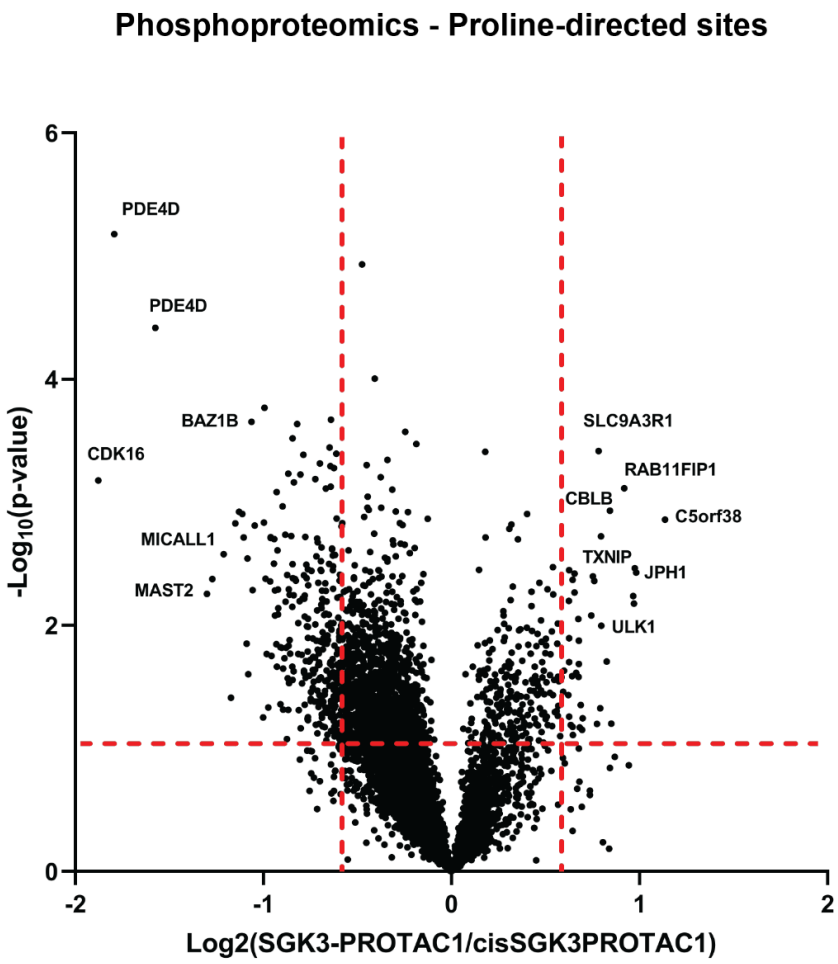

Figure 4.19 p***S/TP motif changes upon SGK3-PROTAC1 treatment, compared to cisSGK3PROTAC1.***
ZR-75-1 cells were treated for 6 h with SGK3-PROTAC1 (0.3 μM) or cisSGK3-PROTAC1 (0.3 μM), and cell lysates subject to quantitative mass spectrometry phosphoproteomic analysis after TiO_2 enrichment for phosphorylated peptides. Data are presented as a volcano plot

4.5 Discussion

Study of SGK3 degradation in ZR-75-1 cells revealed several possible novel roles for SGK3. The detection of PDE4D downregulation downstream of SGK3 was a surprising finding and may represent an exciting undiscovered axis by which PI3K signalling and the PKA pathway can interact. Although this was initially detected in ZR-75-1 cells, this effect could also be confirmed in HEK293 cells and appears to be a ubiquitous mechanism of PDE4D regulation. Conversely, an unexpected upregulation of Electron Transport Chain components was discovered to be specific to the SGK3-dependent cancer cell lines, and very little effect was seen in HEK293.

Downregulation of PDE4D in response to SGK3-PROTAC1

There are four subtypes of PDE4, namely PDE4A–PDE4D, which are highly specific for cAMP degradation but not for cGMP. PDE4 inhibition has been investigated as a potential therapeutic target in asthma, COPD and other inflammatory diseases (Li, Zuo and Tang, 2018). Inhibition of PDE4 results in accumulation of intracellular cAMP and activation of PKA, cyclic nucleotide gated ion channels and Epac1/2. Reactivation of the cAMP signaling pathway by PDE4D Inhibition has also been proposed as a novel druggable axis against tamoxifen resistance in ER+ breast cancer (Mishra *et al.*, 2018). Therefore, regulation of PDE4D downstream of SGK3 degradation is potentially an important component to this signaling axis in chemo-resistant breast cancer.

It is currently unclear from this data how PDE4D expression is reduced in response to SGK3-PROTAC1. PDE4D activity is spatially and temporally controlled by both extensive post-translational modification, and localization to 'cAMP signalosomes' in highly specific regions of the cell. Both methods of regulation are discussed regarding SGK3 degradation below.

It is possible that PDE4D stability is altered in some way by SGK3 degradation. A phosphodegron motif has been identified in the C terminus of PDE4D, leading to its ubiquitylation and degradation by the proteasome. This dual phosphorylation motif is regulated by CK1 and GSK3β. The motif is protected from phosphorylation by Calcineurin (Zhu *et al.*, 2010). Protein levels of PDE4D were not effective by SGK3 inhibition, and the phosphodegron motif lies outside of the RxRxxS/T SGK3 substrate motif, so it is unlikely to be a direct SGK3 substrate. However, SGK3 may act upstream on this motif, or alternatively act on another region of the protein. PDE4D expression can be induced in response to cAMP by cAMP response elements (CREs) in its gene promoter (Kim *et al.*, 2019). It has not been tested whether alterations in PDE4D expression are as a result of transcriptional/translation regulation, however as expression is reduced within 2 hours this is unlikely.

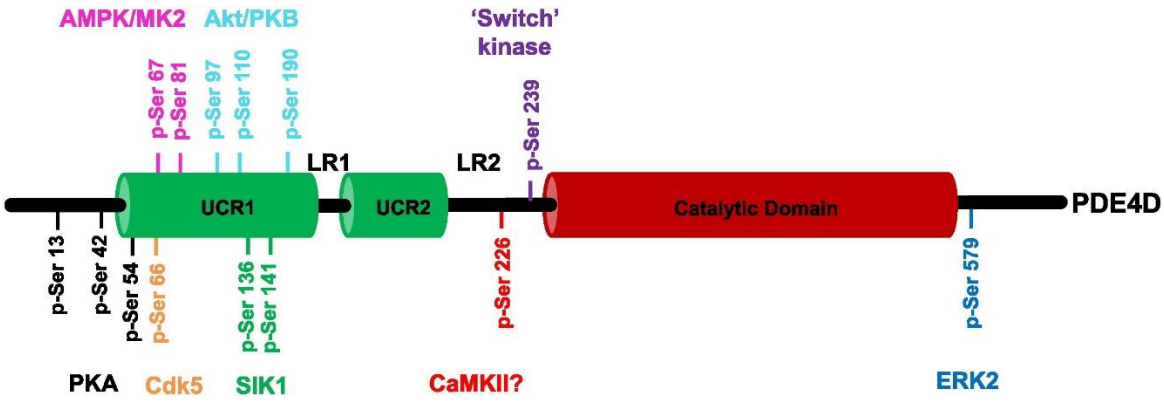

Figure 4.20 Domain structure of PDE4D and known regulatory posttranslational modification sites. *From (Mika and Conti, 2016)*

The PDE4D gene generates at least 9 isoforms through alternative splicing. All isoforms contain a shared C terminal catalytic domain and differ in their variable N terminus and splicing of the regulatory UCR1 and UCR2 domains. It was interesting to observe that only longer forms of PDE4D containing UCR1 were downregulated in response to SGK3-PROTAC1 treatment. The UCR1 and UCR2 domains of PDE4D have been proposed to be regulatory domains controlling PDE4D activity. UCR2 regulates the enzyme activity by opening and closing over the active site, controlling access of cAMP (Mika and Conti, 2016). UCR1 also forms contacts with UCR2 to modulate this regulation. UCR1 has also been proposed to be required for dimerization of PDE4D isoforms (Richter and Conti, 2002, 2004). Interaction of SGK3 with this UCR1 domain may therefore impact on stability, reveal a degron motif or otherwise trigger downregulation of PDE4D. UCR1 is also extensively decorated by posttranslational modifications, modulating the activity of PDE4D, as shown in Figure 4.20 above. For example, phosphorylation of S54 by PKA increases activity by 60% in a presumed negative feedback loop (Sette and Conti, 1996; Hoffmann *et al.*, 1998).

Interrogation of the phosphoproteomic data revealed no global changes in PKA substrate phosphorylation, suggesting global cAMP signaling is not impacted by SGK3-PROTAC1 treatment. However, adaptor proteins such as RACK1, AKAPs and SH3 domain-containing proteins are interacting modules which affect the intracellular localization and function of PDE4 isoforms.

This results in highly localized modulation of cAMP signaling through 'cAMP signalosomes' through combination with cAMP effectors such as PKA and Epac1/2 (Maurice *et al.*, 2014). This results in spatially and functionally distinct pools of cAMP. Therefore, reduction in PDE4D may result in modulation of very localized cAMP levels, not identified by a global phosphoproteomic approach.

PDE4D has been found in T-cells to be recruited to sites of PI3K activation through formation of a complex with Akt and B-arrestin (Bjørgo *et al.*, 2010). Co-recruitment to PIP_3 sites via the PH domain of Akt implicated PDE4D in shutting off T-cell activation signals. Similarly, in Cardiac Cells, PDE4D was recruited to sites of PTEN inactivation, and was involved in inhibiting calcium overload and mPTP opening upon cardiac ischemia, inhibiting necrotic cell death (Zheng *et al.*, 2014). No interaction has previously been demonstrated between SGK3 and PDEs. The interaction domain of Akt with B-arrestin was mapped to 429-441 of Akt and, while the majority of this sequence is well conserved between Akt and SGK3, the critical Tyrosine residue for binding in Akt is an asparagine in SGK3 (Bjørgo *et al.*, 2010). While the Akt complex forms via B-arrestin, phosphodiesterases are known to form complexes with several adaptors, therefore complex formation may occur via an adaptor other than B-arrestin, therefore not requiring this binding site. In future work, it would be interesting to determine whether SGK3 is forming a stable complex in cells with PDE4D, and whether downregulation of PDE4D is occurring through collateral ubiquitylation or destabilization due to loss of the complex.

Upregulation of electron transport chain components in response to SGK3-PROTAC1

While downregulation of PDE4D was reproducible across several cell lines, it was interesting that upregulation of mitochondria proteins was observed as a cancer cell line specific effect of SGK3-PROTAC1 treatment and could not be reproduced in HEK293 cells. This suggests a mitochondrial sensitivity of these ER+ breast cancer cell lines to degradation of SGK3.

Mitochondria are energy hubs to produce the majority of the cell's ATP. They also have roles in regulating cellular calcium, apoptosis and synthesis of macromolecules. Increased glucose uptake and metabolism, coupled to mitochondrial dysfunction, has been traditionally considered a hallmark of the Warburg effect in cancer. However, the role of mitochondrial metabolism in cancer is much more complex, with many cancers in fact becoming mitochondrially driven with a high reliance on oxidative phosphorylation (Solaini, Sgarbi and Baracca, 2011).

Mitochondrial function is known to be regulated downstream of PI3K. Akt phosphorylates Bcl2-family proteins in order to block the release of cytochrome c from mitochondria, inhibiting apoptosis (Datta *et al.*, 1997, 2000; del Peso *et al.*, 1997). As described above, Akt may also mediate necrotic cell death through regulation of mPTP opening via PDE4D control of cellular calcium (Fujio *et al.*, 2000; Murphy and Steenbergen, 2008). SGK1 has also recently been proposed to modulate mPTP opening through an interaction with mPTP and VDAC1, in a role not affected by PI3K inhibition and therefore possible a kinase-independent role of the SGKs (Zhou *et al.*, 2019). Further, inhibition of SGK1 was coupled with vulnerability to redox dysregulation. After inhibition or downregulation of SGK1, the authors found an increase in ROS and cytotoxicity upon H2O2 stress, mediated through NRF2 target gene expression (Wang *et al.*, 2019).

An increased expression of ETC genes, causing increased mitochondrial respiration, has been identified as a mechanism of resistance to BRAF inhibitors (Baenke *et al.*, 2016). However, increased expression of mitochondrial enzymes is observed within 30-60 minutes of SGK3-PROTAC1 treatment and therefore this effect is unlikely to be translational. Additionally, OxPhos proteins upregulated are transcribed from both mitochondrial and nuclear genes. Inhibition of complex 1 by Metformin has been shown to be anti-tumorigenic, and certain chemoresistant

cancers driven through mitochondrial metabolism become sensitized to combination treatment with metformin (Denise *et al.*, 2015; Vellinga *et al.*, 2015).

Crosstalk between PDE4D and Mitochondrial Metabolism

It is currently unclear whether the downregulation of PDE4D and the upregulation of ETC in cancer cell lines are linked. CAMA-1 cells presented the most mitochondrial sensitivity to SGK3-PROTAC1 treatment; however they lack the longer PDE4D isoforms downregulated upon SGK3 degradation.

cAMP is not a freely diffusible molecule within the cytosol, and cAMP signalling is therefore compartmentalised in the cell under the regulation of adenylyl cyclases (ACs) and phosphodiesterases such as PDE4D. PKA is one of a variety of kinases which translocate to mitochondria to modulate mitochondrial function downstream of cAMP signalling. AKAPs relocate endogenous PKA and cAMP modifiers such as phosphodiesterases to distinct subcellular compartments to strategically enhance cAMP regulated signalling pathways. PKA can be recruited to mitochondria by associating with 3 different AKAPS to regulate mitochondrial dynamics, structures and respiration. AKAP1 splice variants import and dock PKA to the outer mitochondrial membrane, and are also involved in transport of nuclear-encoded mRNA encoding mitochondrial proteins (Ginsberg *et al.*, 2003). Mitochondrial cAMP-PKA signalling has been shown to impact on OxPhos through phosphorylation of ETC components in complexes I, IV and V, impacting on both activity and protein stability. Therefore, via this mechanism downregulation of PDE4D may have an impact of PKA-controlled regulation of mitochondrial metabolism.

One of the first described mitochondrial targets of PKA is the nuclear-encoded 18-kDa subunit of complex I (NDUFS4) (Papa, 2002). Phosphorylation by PKA at S173 facilitates its interaction

with Hsp70 and its import into the mitochondria (Papa, 2002; De Rasmo *et al.*, 2008). cAMP-PKA signalling also modulates the stability of complex I by modulating degradation of its subunits by mitochondrial proteases. Inhibition of the mitochondrial adenylyl cyclase sAC, reducing cAMP signal within mitochondria, induces a decrease of complex I subunits (De Rasmo *et al.*, 2015). cAMP signalling triggered either in the cytosol or in the mitochondria both impact on complex IV stability and activity. During hypoxia, PKA phosphorylates complex IV subunits I, IV and Vb, inducing their degradation and decreasing complex IV activity (Prabu *et al.*, 2006; Shinzawa-Itoh *et al.*, 2007). Additionally, an increase in cAMP signalling induces tyrosine phosphorylation of complex IV subunit I (Lee *et al.*, 2005), inhibiting the complex's enzymatic activity. This effect has also been seen with the PDE4 inhibitor theophylline (Lee *et al.*, 2005). Finally, complex V can be modulated by PKA through phosphorylation of ATPase Inhibitory Factor AIF1 on Ser39, preventing binding to complex V and relieving inhibition of ATP synthase (García-Bermúdez *et al.*, 2015). Again, intramitochondrial cAMP signalling modulates complex V via mitochondrial proteases, as a depletion of cAMP in mitochondria decreases levels of complex V connecting subunits and complex V oligomerisation (De Rasmo *et al.*, 2016). The above describe a range of mechanisms by which a reduction of cellular or mitochondrial cAMP downstream of phosphodiesterases may impact on the stability and activity of ETC components. In particularly, the upregulation of ETC protein expression in response to SGK3-PROTAC1 treatment may lie downstream of inhibiting mitochondrial proteases against complexes I, IV and V.

Phosphoproteomic changes upon SGK3-PROTAC1 treatment

Complementary phosphoproteomic analysis revealed very few changes in RxRxxS/T motif phosphorylation sites. This was expected, as PI3K signaling through Akt is the primary driver of growth in these cells, and SGK3 is expressed at lower levels under basal conditions. However, identification of sites previously identified in HEK293 cells confirmed on target activity of the PROTAC and the potential to use this approach in SGK3-induced conditions to detect a range of

SGK3-dependent substrates. Of the modulated sites, many lie within 14-3-3 binding motifs. Akt phosphorylation of many of its substrates provides docking sites for binding of 14-3-3 proteins (Chen *et al.*, 2003), therefore phosphorylation of these sites by SGK3 may well provide docking sties for 14-3-3 proteins and modulate protein localization and function.

However, despite a relatively low number of changes in RxRxxS/T sites, many proteins did appear to be modulated at alternative sites. The reason for these changes is currently unclear. It is possible that degradation of SGK3 is regulating downstream kinases or phosphatases. No remarkable changes in the protein level or phosphorylation status of any protein kinases/phosphatases were detected in the proteomics, however a mild (20-25%) decrease was observed in the cyclin dependent kinases CDK18 and CDK17, and the CDK inhibitor CDKN1A. Additionally, such a large shift in mitochondrial proteins may result in modulation of further metabolic enzymes. Alternatively, these sites could be due to a currently unidentified off-target hit of SGK3-PROTAC1, or an unidentified substrate motif which can be phosphorylated by SGK3. A large number of modulated (S/T)P sites were also identified in previous phosphoproteomic screens (Malik *et al.*, 2019), therefore increasing confidence that these alterations are an on-target effect.

p(S/T)P sites were the most enriched throughout the sample set, representing 28% of the dataset and 23% of modulated sites. The p(S/T)P motif is a common substrate motif for many kinases, including the mitogen activated protein kinases (MAPKs) and cyclin dependent kinases (CDKs). Phosphorylation of many proteins is under the control of CDKs throughout the cell cycle, therefore this broad change in p(S/T)P sites may be a result of an impact on progress through the cell cycle in response to SGK3-PROTAC1 (Swaffer *et al.*, 2016).

In particular, the most downregulated phosphosite in response to SGK3-PROTAC1 treatment was phosphorylation of CDK16 and Ser138, which lies within a pSP site. Previous work from PhD student Nazma Malik and Postdoctoral researcher Athanasios Karapetsas has investigated the

interaction between CDK16 and Cyclin Y (CCNY). CCNY phosphorylation at Ser326 was identified in HEK293 cells as being reduced downstream of 14H treatment (Malik *et al.*, 2019). Their work has demonstrated that, *in vitro*, both SGK3 and Akt can phosphorylate CCNY at Ser326. Ser326 lies within an RXRXXS/T site, and alongside Ser100 phosphorylation leads to 14-3-3 binding of CCNY. 14-3-3 binding is critical for CCNY interaction with CDK16 and its subsequent activation. (Ou *et al.*, 2010; Mikolcevic *et al.*, 2012; Shehata *et al.*, 2012, 2015), (Karapetsas, unpublished) (Figure 4.22). Follow-up analysis in cells, however, revealed some possible functional redundancy, as the CCNY-CDK16 interaction was still present in SGK3 knockout cells, and treatment with the SGK3-PROTAC1 compound had only a partial effect.

Phosphorylation of CDK16 at Ser138 has not been studied in the literature, and the functional relevance of this site is not known. It is possible that the site is an autophosphorylation site upon CDK16 activation, or it is phosphorylated by an alternative upstream kinase. It would be interesting in future work to determine the kinase of this site, as it is unlikely to be mediated by SGK3 itself, and whether this site has any functional relevance for the activation of CDK16.

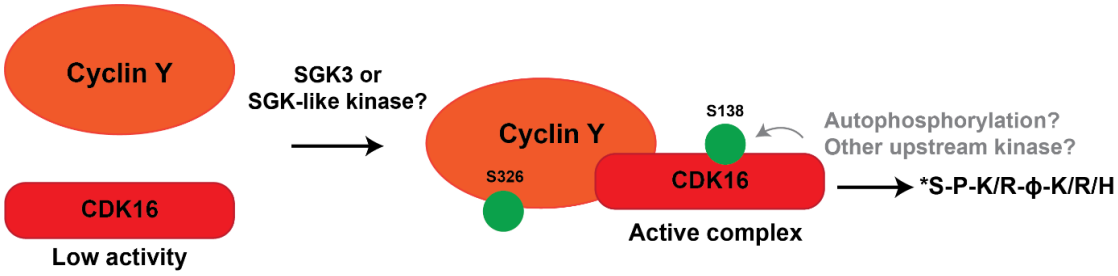

Figure 4.22 Current Model of CDK16 activation downstream of SGK3. *Phosphorylation of Cyclin Y (CCNY) at S326 promotes binding and activation of CDK16. Ser326 phosphorylation occurs in an RXRXXS/T motif site and can be phosphorylated by SGK3 and potentially other kinases. Phosphorylation of CDK16 at Ser138 may be a result of autophosphorylation or an alternative upstream kinase.*

Conclusion

Global proteomic and phosphoproteomic analysis of SGK3-PROTAC1 treatment in ZR-75-1 cells revealed several potential new roles for SGK3 in cancer metabolism. Downregulation of PDE4D upon SGK3 degradation implicates the kinase in modulation of the cAMP-PKA pathway. This may

in turn have a role in modulating the stability of electron transport chain components and other mitochondrial functions. As chemoresistance in cancer has been associated with mitochondrial function, knockout of SGK3 may target mTORC1 signalling and mitochondrial metabolism simultaneously, offering a therapeutic benefit over kinase inhibition alone. In further work, it would be important to further validate the mechanisms of PDE4D downregulation and ETC upregulation and determine whether these two processes are linked via SGK3.

Phosphoproteomic analysis revealed very few changes in SGK3 substrate RxRxxS/T motif sites. This was likely due to the activity of Akt in these cells in combination with relatively low expression of SGK3 in the unstimulated conditions. In future work this experiment could be improved by inducing SGK3 expression and activity with prolonged inhibition of PI3K or Akt, as described in Chapter 3. However, the findings of previously identified substrates STX7 and ITSN1 and WDR7 confirmed the success of SGK3-PROTAC1 in downregulating SGK3 substrate phosphorylation. Further the confirmation of these substrates in a second cell line increases confidence in these SGK3 substrates. In addition, phosphorylation of CDK16 at S138 was the most significantly downregulated phosphosite in the experiment, and although this isn't an SGK3 substrate motif site it reinforces a role for SGK3 in this pathway.

5. HaloPROTACs – a generalisable, targeted protein degradation approach

5.1 Targeting of proteins with no validated binding ligands

In the previous two chapters of this thesis I developed and validated SGK3-PROTAC1 and used this compound to directly target SGK3 for degradation. This compound was developed using known inhibitors of the SGK isoforms. PROTAC design, however, requires a ligand capable of interacting with the desired target, and high–affinity ligands are lacking for the vast majority of human proteins. In addition, detailed structural and biophysical analysis of the interaction between ligand and target protein is key for rational design of PROTAC compounds. In the case of SGK3, although we had known inhibitors of the kinase domain (Halland *et al.*, 2015), we currently lack information on protein structure, and how these ligands are binding.

In order to circumvent these issues, alternative strategies have been developed that involve attaching various tags to target proteins, to enable these to be targeted by a compound capable of inducing interaction with an E3 ligase machinery. One of the first approaches made use of the plant E3 ligase TIR1, exogenously expressed in non–plant cells, to trigger ubiquitylation and degradation of target proteins fused to an Auxin–Inducible Degron (AID) tag on addition of the plant hormone Auxin (Nishimura *et al.*, 2009; Natsume *et al.*, 2016; Nora *et al.*, 2017). A more recent approach exploits the ability of a phthalimide–based chimeric compound called dTAG-13 to bind proteins fused with a F31V mutant FKBP12 tag and induce degradation via the cereblon (CRBN) E3 ligase (Erb *et al.*, 2017; Weintraub *et al.*, 2017; Brunetti *et al.*, 2018; Nabet *et al.*, 2018). CRBN is endogenously expressed in most mammalian cells and therefore does not need to be overexpressed. Other methods include deGradFP and AdPROM, which rely on the overexpression of the von Hippel–Lindau (VHL) E3 ligase fused to a GFP binding nanobody capable of inducing degradation of GFP–tagged proteins (Caussinus, Kanca and Affolter, 2012; Caussinus and Affolter, 2016; Fulcher *et al.*, 2016), or the Trim–AWAY method that enables the TRIM21 E3 ligase to be recruited to targets via a specific antibody (Clift *et al.*, 2018).

Another example of this is the recently published HaloPROTAC approach (Buckley *et al.*, 2015). HaloPROTAC compounds contain a chloroalkane moiety conjugated to a ligand of an E3 ligase, typically VHL or cIAP1 (Buckley *et al.*, 2015; Tomoshige, Hashimoto and Ishikawa, 2016). These compounds are then targeted toward a modified bacterial dehalogenase HaloTag7 fusion to the target protein (Los *et al.*, 2008). HaloTag7 will covalently bind to the chloroalkane motif, and the fusion protein targeted for ubiquitylation and degradation (Fig 5.1).

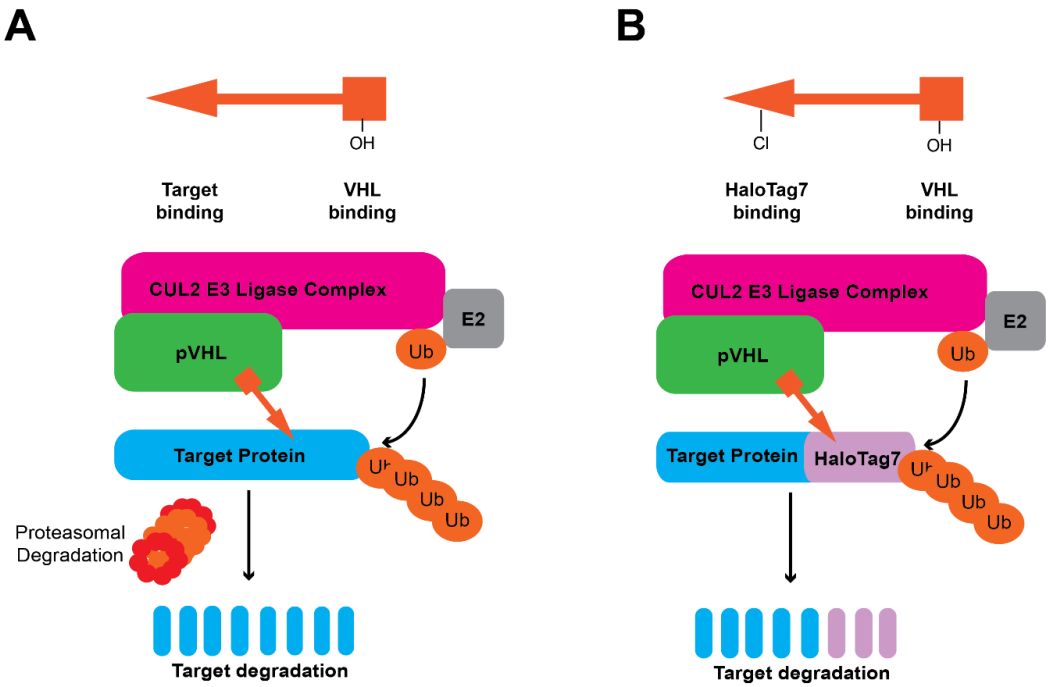

Figure 5.1 Mechanism of action of HaloPROTACs
A. *PROTACs are bivalent molecules, which bind to both the target protein of interest and an E3 ligase. These compounds function by recruiting the E3 ligase to the target protein, triggering polyubiquitylation and proteasomal degradation.* ***B.*** *HaloPROTAC compounds contain a chloroalkane motif which can be covalently targeted by HaloTag7. These compounds therefore target HaloTag7 fusion proteins for proteasomal degradation.*

At the time starting this study, previous HaloPROTAC studies had only been applied to exogenously overexpressed proteins, limiting their application to endogenous systems. In addition, the use of this method to degrade subcellularly localized proteins remains understudied. I therefore aimed to combine the HaloPROTAC approach with CRISPR/Cas9 to target endogenously labelled SGK3-Halo, and its upstream regulator Halo-VPS34. This project combined generation of novel HaloPROTAC compounds using previously described optimised

VHL ligands (Galdeano *et al.*, 2014; Frost *et al.*, 2016) with CRISPR/Cas9 to target and manipulate the endogenous hVPS34-SGK3 signalling axis.

5.2 Generation of SGK3-Halo and Halo-VPS34 KI cell lines by CRISPR/Cas9

In order to generate cell lines which could be targeted using the HaloPROTAC compounds, I first used CRISPR/Cas9 technology to endogenously knock in the HaloTag7 protein to the C-terminus of SGK3, or the N-terminus of VPS34 in HEK293 cells. The HEK293 cell line was chosen as these cells have previously been extensively used to study the hVPS34-SGK3 pathway (Malik *et al.*, 2018), and they are readily amenable to transfection and genetic alteration by CRISPR/Cas9, making them an ideal model cell line. The C-terminus of SGK3 was chosen as the protein contains an N-terminal Phox-homology (PX) domain critical for its localisation and activation, and SGK3 has previously tolerated well a GFP tag on its C terminus (Malik *et al.*, 2018). Similarly, VPS34 has previously been successfully tagged on its N terminus with no impact on activity or localisation (Fulcher *et al.*, 2016). VPS34 has previously been the subject of targeted degradation through the AdPROM system, which targets an exogenously overexpressed E3 ligase to a target protein via a fused nanobody. While this approach successfully degraded ~80% GFP-VPS34, the impact on SGK3 activity was only slight, although significant (Fulcher *et al.*, 2016; Malik *et al.*, 2018). Further, the AdPROM system described was expressed through viral transfection, and could be inducible only if expressed under a tetracycline-inducible promoter (Fulcher *et al.*, 2016).

Genome editing with CRISPR/Cas9

The clustered regularly interspaced short palindromic repeats (CRISPR)–CRISPR-associated protein 9 (Cas9) system evolved as a bacterial defence mechanism against phage infection and plasmid transfer. In recent years it has been repurposed in molecular biology as a RNA-guided DNA targeting platform for transcriptional perturbation, epigenetic modulation, genome imaging and, most commonly, genome editing (Jiang and Doudna, 2017).

For use in genome editing, the endonuclease enzyme Cas9 is targeted to a genomic target by a guide RNA (sgRNA). This sgRNA consists of a 20-nucleotide guide sequence within a scaffold which will bind to the Cas9 enzyme. The sgRNA guide sequence pairs with a DNA target directly upstream of a critical 5'-NGG adjacent motif (PAM site). The Cas9 enzyme then mediates a double strand break (DSB) ~3bp upstream of the PAM site (Ran, Hsu, Wright, *et al.*, 2013).

Following a DSB, the cell's DNA repair machinery will repair the break by one of 2 mechanisms, non-homologous end joining (NHEJ) or homology driven repair (HDR). The more common mechanism of DNA repair is through NHEJ, which often leaves insertion/deletion mutations (indels) in the genome. Such indels in a coding exon can result in frameshift mutations and premature stop codons, resulting in gene knockouts if targeted toward the start of the gene (Perez *et al.*, 2008). Alternatively, if a repair template is available, DNA repair may occur through HDR, although at a much lower frequency than NHEJ. HDR can be utilised to introduce defined modifications at the site of double strange breaks, for example specific point mutations, insertions, or addition of affinity tags such as GFP, RFP or HaloTag7. Repair templates consist of the desired DNA insertion flanked by short (~150bp) homology arms for integration into the target locus. Knock-in mutations mediated by CRISPR/Cas9 through HDR occur much less frequently than NHEJ knockout mutations, and HDR is generally only active in dividing cells (Saleh-Gohari and Helleday, 2004). Efficiency can also vary depending on cell type, and the genomic locus and template.

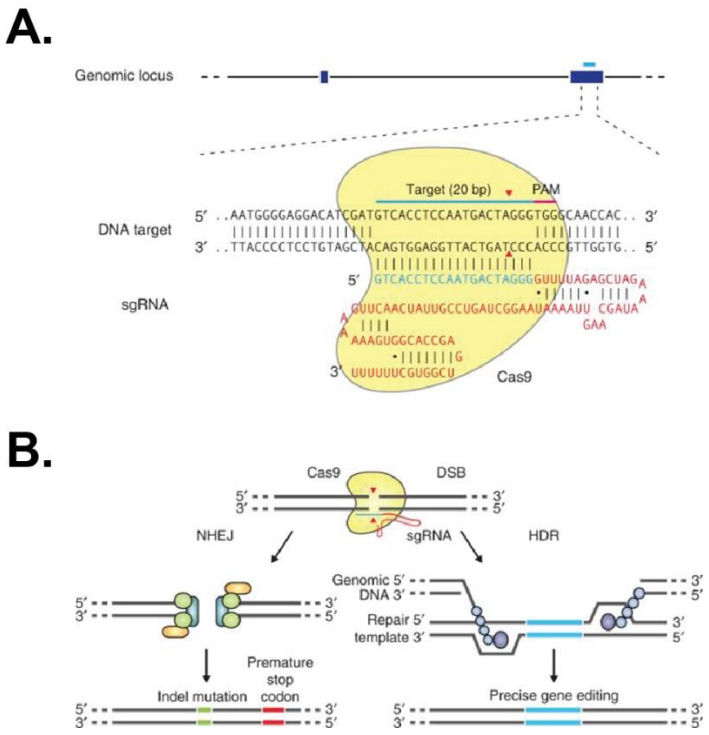

Figure 5.2 Mechanism of CRISPR/Cas9 mediated genome editing.
A. *The Cas9 endonuclease enzyme is targeted to the desired genomic locus by a guide RNA (sgRNA). This sgRNA targets a 20nt sequence upstream of a PAM site, targeted by the Cas9 enzyme. Cas9 mediates a double strand break (DSB).* ***B.*** *Cas9-mediated DSB is repaired by either non-homologous end joining (NHEJ) or homology driven repair (HDR). These two repair mechanisms can be utilized to generate knock-out or knock-in mutations respectively. For HDR, a repair template is also expressed with homology arms to target the desired genomic locus. From* (Ran, Hsu, Wright, *et al.*, 2013)

A common problem in CRISPR-Cas9 genome editing is the possibility of off-target genomic alteration by the Cas9 enzyme. In order the reduce this risk, in this study the D10A 'Nickase' form of Cas9 was utilised (Ran, Hsu, Lin, *et al.*, 2013). The D10A mutation in the active site of Cas9 removes the ability of the enzyme to form double strand breaks in DNA, instead generating single strand 'nicks'. Therefore combination of this form of Cas9 with 2 sgRNAs leads to more specific targeting of the desired locus (Ran, Hsu, Lin, *et al.*, 2013).

Despite improvements in the approach, knock-in (KI) efficiency by the CRISPR/Cas9 method and HDR is still fairly low (1-2%). Therefore, when generating SGK3-Halo KI clones, an IRES2-eGFP cassette was included in the SGK3-Halo Donor cDNA to increase the likelihood of selecting positive clones. The IRES2-GFP cassette encodes GFP expression downstream of a second start site, therefore successfully edited clones express GFP without tagging the GFP protein on to

SGK3. Hence, cells could be positively selected for GFP expression when performing single cell sorting. For Halo-VPS34, the chosen sgRNAs have previously been shown to generate a surprisingly high KI efficiency (Fulcher *et al.*, 2016), therefore these cells were selected by single cell sorting alone.

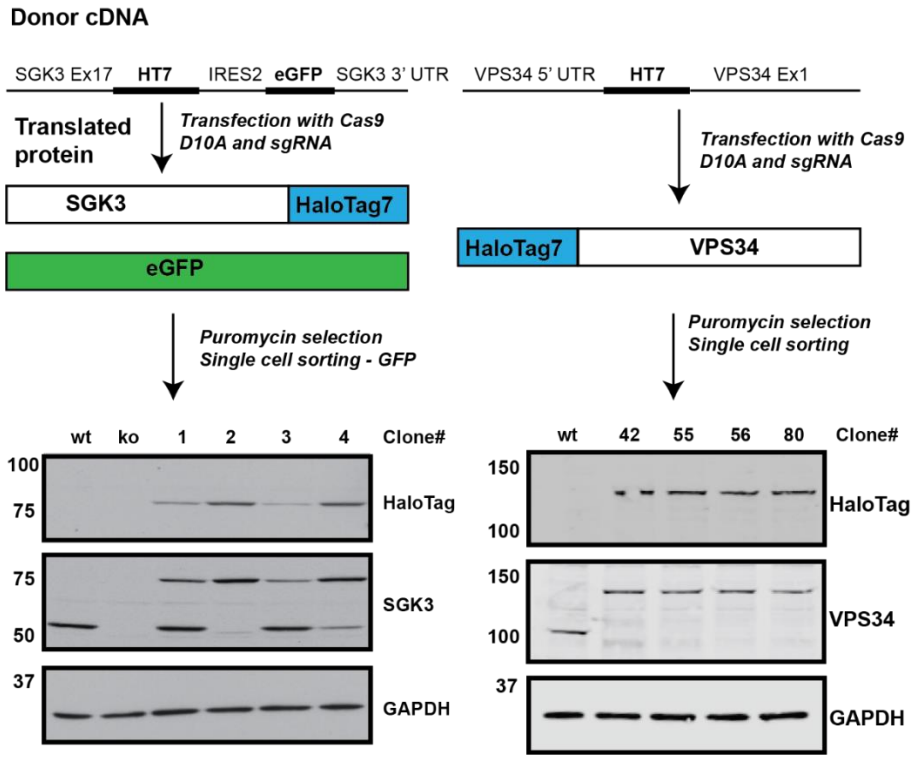

Figure 5.3 Generation of HaloTag7 endogenous fusion proteins by CRISPR/Cas9.
HEK293 cells were transfected with the D10A Nickase form of Cas9 and 2 sgRNAs and a HaloTag7 fusion donor targeted to each locus. The SGK3–Halo donor also included an IRES2–eGFP cassette, allowing successfully integrated cells to be selected for through FACs sorting for GFP positive cells. The Halo–VPS34 donor contained HaloTag7 only. Cells were selected through single cell sorting. Clones were selected and lysates screened by Immunoblot analysis, using antibodies against the endogenous proteins and a mouse monoclonal antibody against HaloTag7. The clones were characterized by DNA sequencing. Clone wt (wild type) refers to parental HEK293 cells, and ko (knockout) refers to previously described SGK3–knockout cell line (Malik *et al.*, 2018)

To confirm successful, in frame integration of HaloTag7 to the desired genetic locus, the selected clones were analysed by DNA sequencing analysis. HEK293 cells are pseudotriploid (Bylund *et al.*, 2004), and carry three copies of SGK3 and VPS34 (HEK293genome.org).Halo-VPS34 clone 56 was selected as a homozygous knock-in cell line. SGK3-Halo clone 2 was selected for the SGK3 studies. This cell line contained 2 alleles with in-frame insertions of the HaloTag7 protein to the SGK3 C terminus, and one large insertion, causing a frameshift and early truncation two residues

3’ of the critical hydrophobic motif activation residue Ser486, and is therefore predicted to produce an inactive protein.

Addition of HaloTag7 does not affect localisation or complex formation of SGK3 and VPS34

SGK3 and VPS34 are both localised to endosomal structures. SGK3 binds to PtdIns(3)P via its PX-domain, and VPS34 localises by forming a complex with VPS15, a PH-domain containing protein, which colocalises to the endosome. It was important to consider, before using these cell lines for further biological characterisation, whether the addition of a large 33kDa tag to these proteins would affect their localisation or complex formation. The colocalization of SGK3-Halo and Halo-VPS34 to early endosomal marker Rab5 was analysed by immunofluorescence, in comparison to wildtype HEK293 cells. These cells were seeded onto coverslips and stained with the HaloTag7-TMR ligand, which covalently couples the TMR fluorophore to HaloTag7 via a chloroalkane motif. This allows easy visualisation of HaloTag7 fusion proteins by fixed immunofluorescence or live cell imaging. Cells were then fixed with 4% Paraformaldehyde (PFA) and co-stained for the endosomal marker Rab5 (Figure 5.4). It was observed that both Halo-VPS34 and SGK3-Halo colocalised to Rab5-positive endosomal structures. As a negative control, analysis of HEK293 wildtype cells revealed no endosomal staining. On treatment with VPS34-IN1, which inhibits VPS34 and reduces endosomal PtdIns(3)P, SGK3-Halo became diffuse throughout the cell, as previously observed (Bago *et al.*, 2014; Malik *et al.*, 2018). Conversely, VPS34-IN1 treatment caused Halo-VPS34 to become more punctate on endosomal structures. This has not previously been observed and may give some further information on the mechanism of VPS34 inhibition and activity.

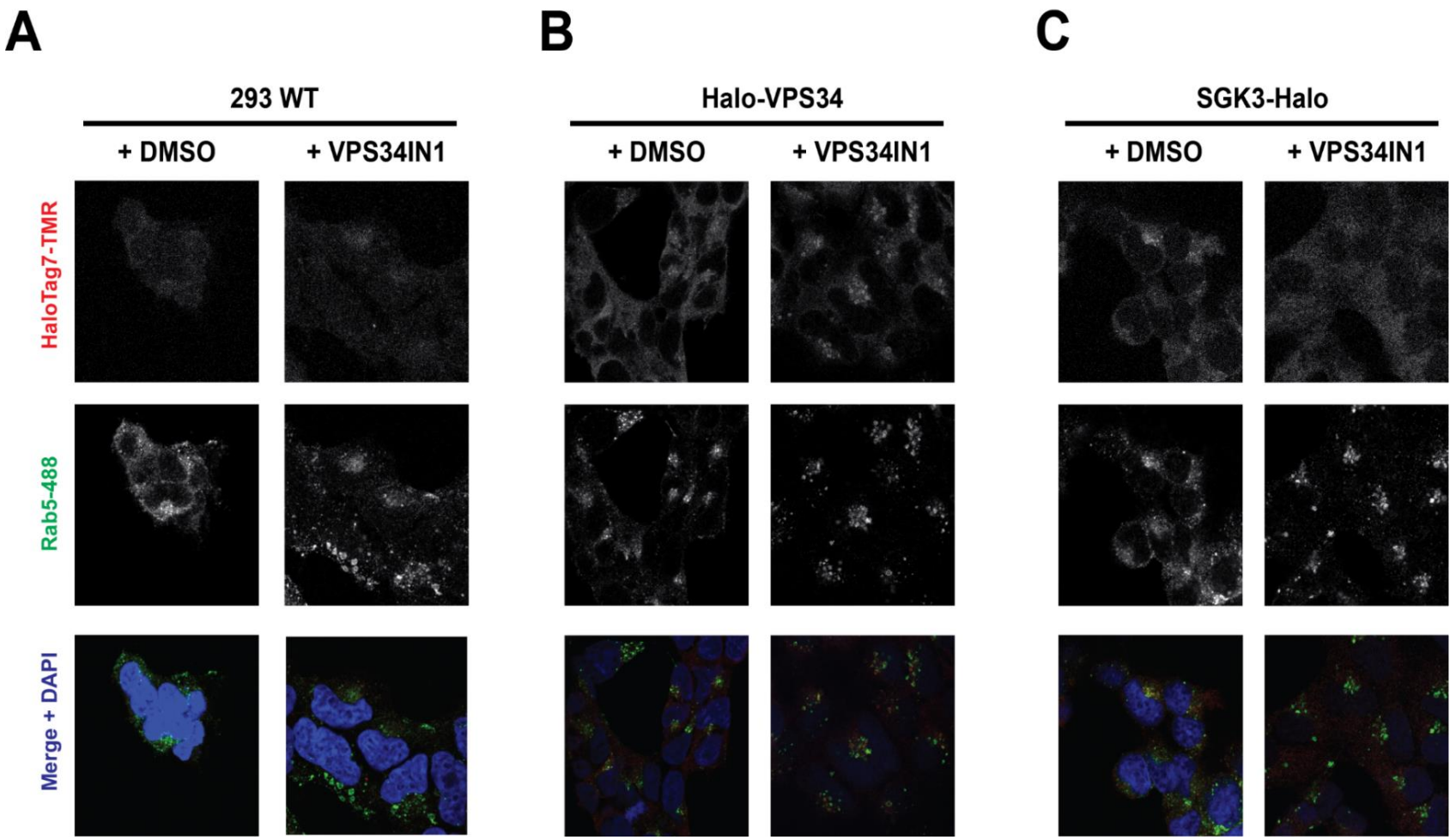

Figure 5.4 Endosomal localisation of SGK3 and VPS34 is unaffected by HaloTag7 fusion.
HEK293 wildtype (A), SGK3-Halo (B) and Halo-VPS34 (C) cells were treated with either DMSO or the VPS34 inhibitor VPS34-IN1. Cells were stained for HaloTag7 (TMR-594) and the early endosomal marker Rab5. Images are representative of n=10 images.

VPS34 forms a stable complex with VPS15 and Beclin1, either in complex I with UVRAG on Rab5-postive endosomes, or complex II with ATG14 on Rab7 positive endosomes. To ensure the stability of this complex was not affected by the tag on VPS34, I performed immunoprecipitation of VPS34 from wildtype and Halo-VPS34 KI HEK293 cells, and analysed coimmunoprecipitation of complex members by immunoblot. I observed that coimmunoprecipitation of VPS15, Beclin1, ATG14 and UVRAG was unchanged between the wildtype and KI cell line, suggesting the complex was unaffected

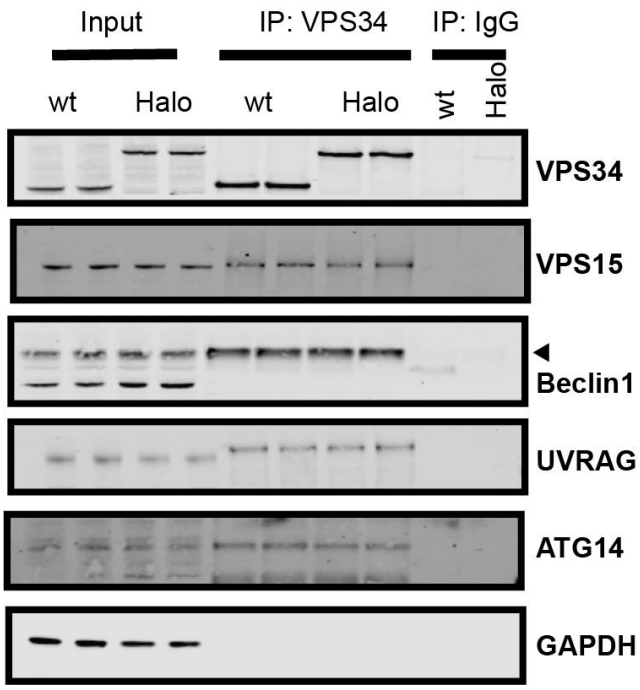

Figure 5.5 VPS34 complex stability is not affected by N-terminal HaloTag7 fusion.
Endogenous VPS34 was immunoprecipitated from HEK293 wildtype or Halo-VPS34 KI cells. Co-immunoprecipitation of complex members was detected by western blot.

Addition of HaloTag7 does not affect PtdIns(3)P production by VPS34

The critical role of VPS34 is to produce PtdIns(3)P from PtdIns on endosomal membranes. It was recently reported that this production of PtdIns(3)P was mediated in response to growth factor stimulation (Malik *et al.*, 2018). To ensure the activity of VPS34 was unaffected by addition of

HaloTag7, I compared and quantified the levels of PtdIns(3)P, measured by a previously published fluorescent probe binding PtdIns(3) via a recombinant 2XFYVE peptide from HRS, conjugated to an AlexaFluor-593 fluorophore. Again, in these cells, I observed no defect in PtdIns(3)P production, and the staining was sensitive to VPS34 inhibition by VPS34-IN1.

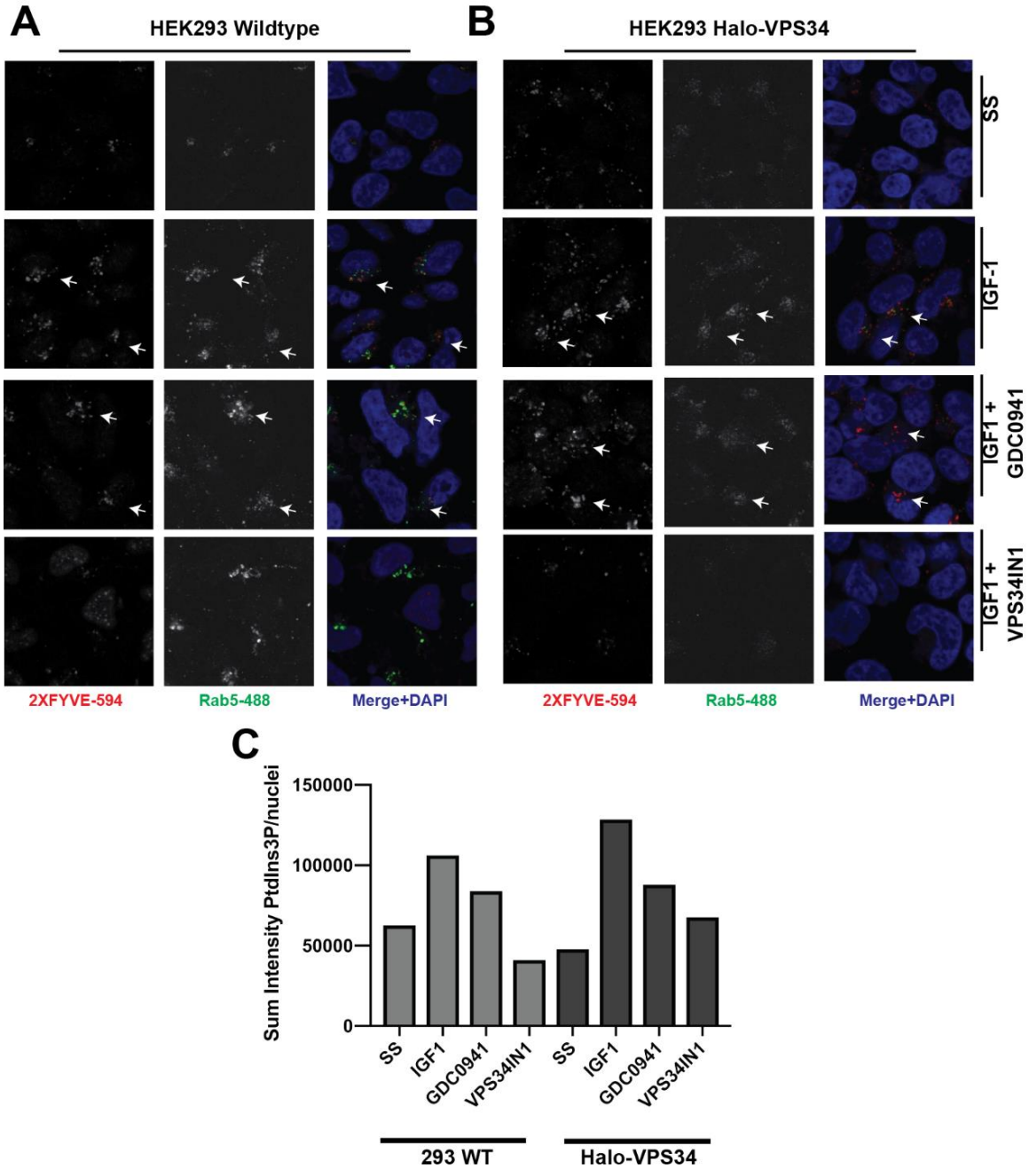

Figure 5.6 VPS34-mediated production of PtdIns(3)P is unaffected by HaloTag7 fusion.
*HEK293 wildtype **(A)** and HaloVPS34 **(B)** cells were stimulated with IGF1, after treatment with or without the Class I PI3K inhibitor GDC0941 or VPS34 inhibitor VPS34IN1. PtdIns(3)P production in these cells was measured with the 2XFYVE-AlexaFlour594 probe, and colocalised to the early endosomal marker Rab5. **C.** Quantification of PtdIns(3)P staining intensity/cell from n=10 images.*

SGK3-Halo cells have similar levels of NDRG1 phosphorylation to wildtype, and phosphorylation is sensitive to SGK3 inhibition.

In order to determine potential effects of the HaloTag7 fusion on SGK3 activity, I analyzed phosphorylation of the well characterized SGK3 substrate NDRG1 at Thr346 (Malik *et al.*, 2018) in HEK293 wildtype, SGK3-KO and SGK-Halo KI cells. NDRG1 is also phosphorylated at this site by the Akt kinases, therefore I assessed phosphorylation upon treatment with a selective Akt inhibitor (3 μM AZD5363 (Davies *et al.*, 2012)) in the presence or absence of a selective SGK3 inhibitor (1 μM 14H (Halland *et al.*, 2015)). This assay revealed that SGK3 mediated phosphorylation of NDRG1 in wild type and SGK3–Halo cells was similar and higher than observed in SGK3 knock–out cells (Fig 5.7). Taken together, this evidence suggested that the addition of HaloTag7 does not alter the function and activity of SGK3 within the cell.

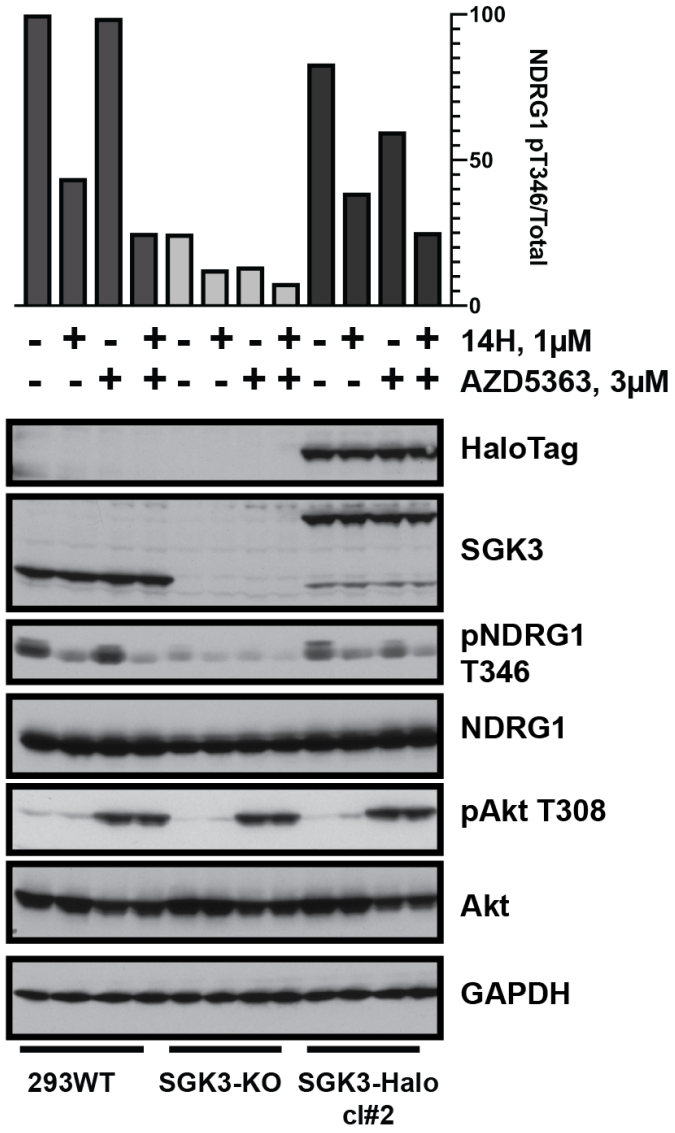

Figure 5.7 NDRG1 phosphorylation is equivalent in HEK293 wildtype and SGK3-Halo KI cells.
HEK293 wildtype, SGK3 KO and SGK3-Halo KI cells were treated with SGK inhibitor 14H or AZD5363 and SGK3 substrate NDRG1 phosphorylation measured by Western blot. Quantification of NDRG1 phosphorylation at Thr346 is shown above the blot.

***In vitro* SGK3 kinase Activity is altered by a C-terminal HaloTag7**

In order to determine the effect that addition of a C-terminal HaloTag7 has on SGK3 kinase activity *in vitro*, I performed an immunoprecipitation experiment to purify endogenous SGK3 from wildtype HEK293 and SGK3-Halo KI cells. The immunoprecipitated kinase was then subject to an *in vitro* kinase assay against the well characterised Crosstide peptide substrate. Efficiency of 32P-ATP incorporation into the substrate was then assayed by P81 paper assay (Fig 5.8). This

assay revealed that the activity of SGK3 immunoprecipitated from SGK3-Halo KI cells was much lower than that of the wildtype.

As described in figure 5.3, the SGK3-Halo KI clone #2 used in these experiments contained 2 KI alleles, and 1 allele harboured a predicted inactive truncation. SGK3-Halo KI clones #3 and #4 contained 1 and 2 KI alleles respectively, with the remaining alleles wildtype. I could therefore use these clones to determine whether the reduced activity in clone #2 is due to the HaloTag7 fusion, which would produce a 'dose-dependent' effect on SGK3 activity in the different cell lines, or a clonal effect of that cell line specifically. I therefore assayed the activity of each of these cell lines on stimulation with IGF1. This revealed that each SGK3-Halo KI allele reduced SGK3 activity by about 30% (Fig 5.9). This confirmed that reduction in SGK3 activity was likely due to the proximity of the tag, and not a clone-specific effect of the selected fusion clone. However, treatment with HaloPROTAC-A did reduce measured SGK3 kinase activity in clones 3 and 4, suggesting SGK3-Halo fusion protein does maintain some activity in these clones. The published SGK3-GFP KI cell line did exhibit reduced SGK3 activity, however responded normally to stimulation and inhibition of the pathway (Malik *et al.*, 2018). Therefore, the effect is likely due to a large tag being in close proximity to the critical hydrophobic motif activation residue Ser486, blocking phosphorylation of SGK3-Halo by mTORC2. Although *in* vitro activity was reduced, in figure 5.7, I have observed that SGK3-Halo KI cells maintain phosphorylation of NDRG1 at Thr346, which is sensitive to SGK3 inhibition. Therefore, it is possible that SGK3 activity is maintained in cells, however the protein in less stable when immunoprecipitated for an *in vitro* kinase assay, thus explaining this result.

In order to determine whether the proximity of HaloTag7 was blocking activation of SGK3, I performed an experiment overexpressing forms of SGK3-Halo in SGK3-KO 293 cells, with extended linkers from 5xGly to 20xGly, to determine if expanding the distance between SGK3 and HaloTag7 may reduce this interference and rescue activity of the kinase. This revealed that

extension of the linker up to 15xGly,modestly improved the activity of SGK3-Halo (Fig 5.10). However, the improvements in activity were very slight, and additionally the 20xGly linker construct did not have improved activity, and this was not followed up further in the study.

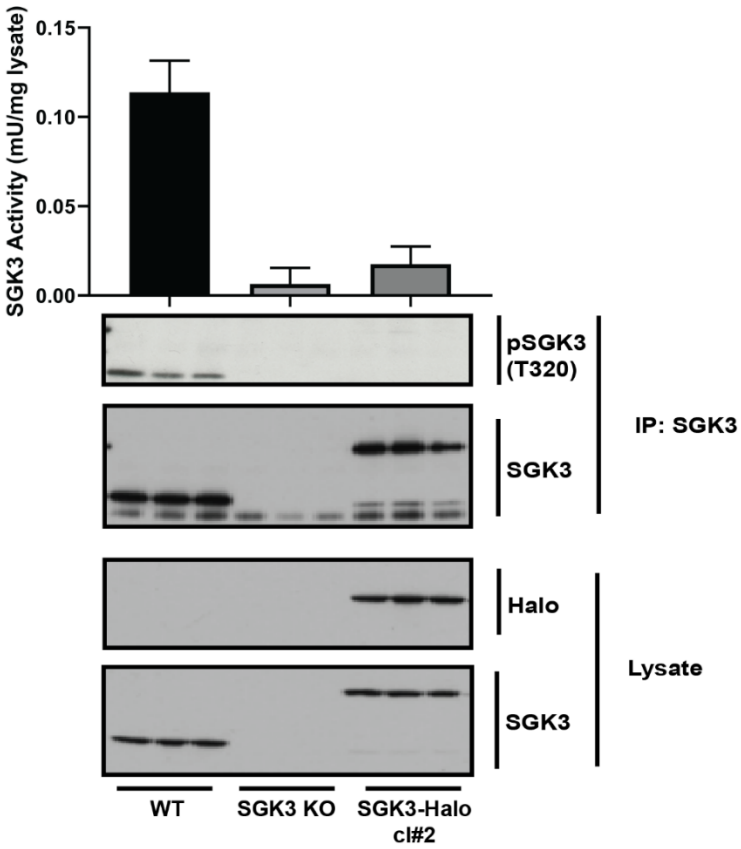

Figure 5.8 In vitro kinase activity of SGK3-Halo is substantially reduced.
3mg lysate of HEK293 wildtype, SGK3-KO or SGK3-Halo cells were immunoprecipitated for SGK3 , and subject to in vitro kinase assay against the Crosstide peptide, and incorporation of 32P γ-ATP measured. 1 unit of activity = incorporation of 1nmol γ-phosphate into substrate per mg lysate. Error bars = SD, n=3.

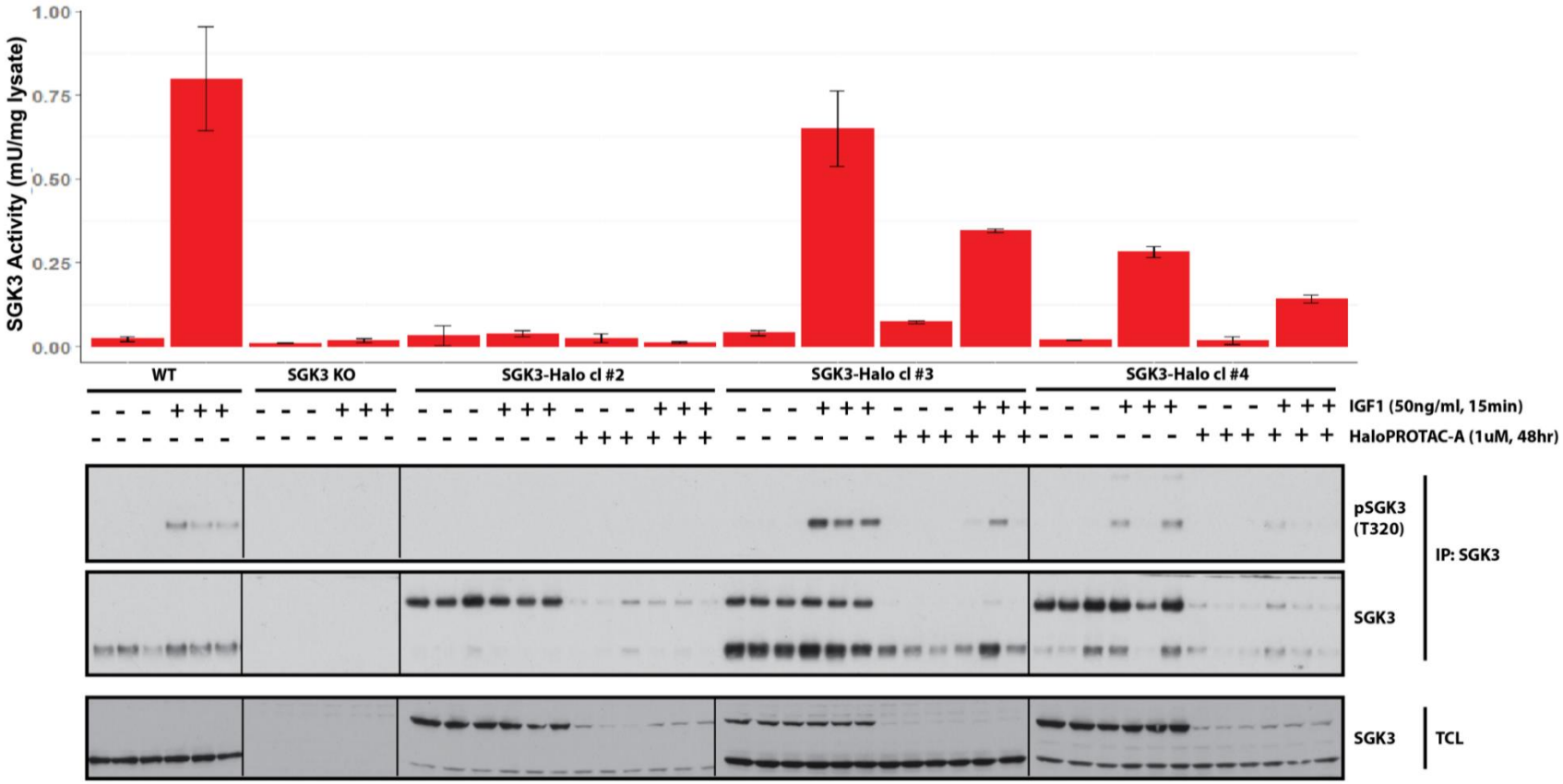

Figure 5.9 SGK3-Halo fusion causes loss of SGK3 in vitro kinase activity.

HEK293 wildtype, SGK3 KO or SGK3-Halo clones were treated with or without HaloPROTAC-A for 24 h, then serum-starved in empty DMEM overnight. Cells were harvested within or without prior stimulation with IGF-1 (50 ng/ml, 15 min). SGK3 was immunoprecipitated from 3 mg lysate, and subject to in vitro kinase assay against the Crosstide peptide, and incorporation of 32P γ-ATP measured. 1 unit of activity = incorporation of 1nmol γ-phosphate into substrate per mg lysate. Error bars = SD, n=3.

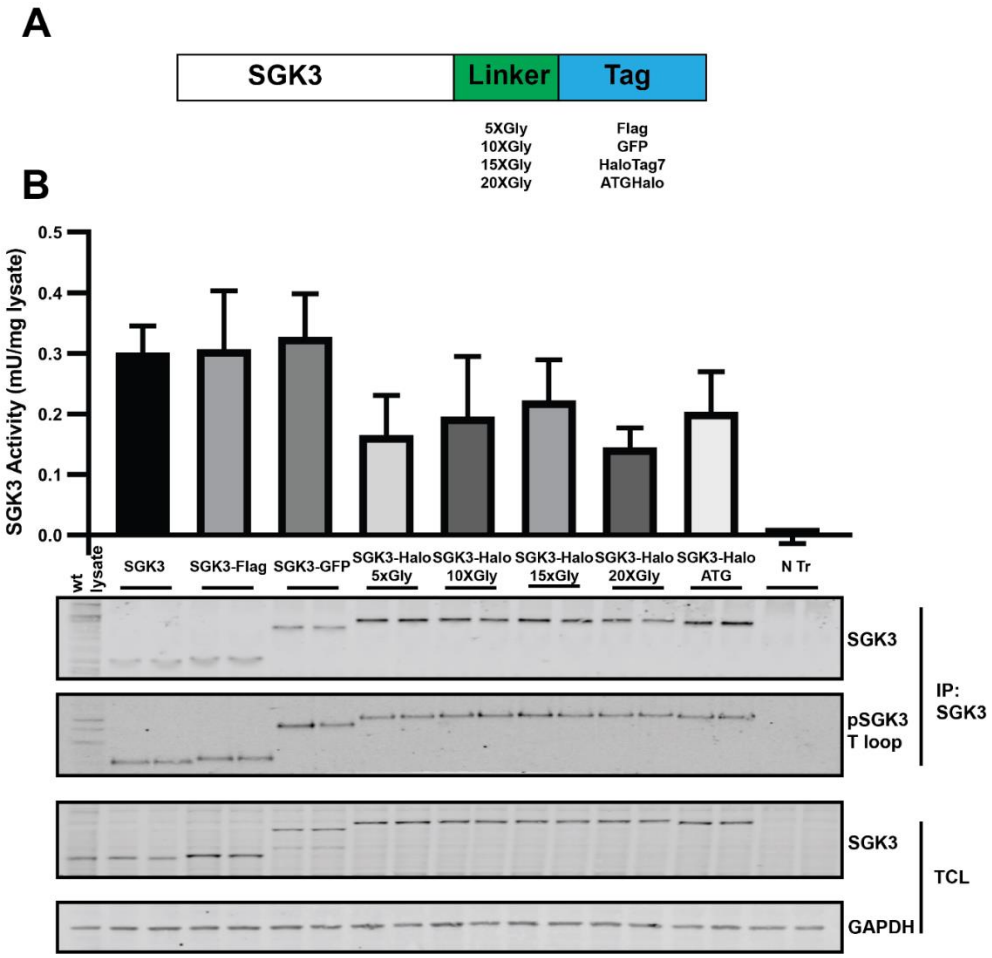

Figure 5.10 Extending the linker between SGK3 and HaloTag7 increases SGK3 in vitro kinase activity. ***A.*** *cDNA constructs were designed for transient transfection of SGK3 either alone of tagged with Flag, GFP or HaloTag7 with extending glycine linkers.* ***B.*** *SGK3-KO cells were transiently transfected with 30ng SGK3 cDNA described in B. SGK3 was immunoprecipitated from 3 mg lysate, and subject to in vitro kinase assay against the Crosstide peptide, and incorporation of 32P γ-ATP measured. 1 unit of activity = incorporation of 1nmol γ-phosphate into substrate per mg lysate. Error bars = SD, n=3.*

5.3 Compound design and screening

To generate novel HaloPROTAC probes, I collaborated with the Ciulli lab (BCDD, Dundee) to produce 6 new compounds. HaloPROTAC3, previously described by the Crews Lab, contained an isoindolinone–based VHL targeting group conjugated to the chloroalkane moiety (Fig 5.11a) (Buckley *et al.*, 2015). Based on recent publications from the Ciulli lab providing extensive understanding of structure–activity relationships and structure–based design of VHL ligands (Galdeano *et al.*, 2014; Frost *et al.*, 2016), it was hypothesized that substitution of the isoindolinone moiety of HaloPROTAC3 with other groups, optimized for VHL binding affinity could improve degradation activity (Fig 5.11b). In compounds A and B, the isoindolinone group

of HaloPROTAC3 was replaced with N–acylamides of L–*tert*–leucine on the left hand side of the molecule (as in VHL ligand VH032) (Galdeano *et al.*, 2014), maintaining the chloroalkane linker attachment point at the phenyl ring on the right hand side (Fig 5.11c). Compounds A and B contained linkers of 15 and 21 atoms respectively. In a second compound set, the acetyl group at the left hand side was replaced with a cyclopropylcyanoacetic moiety (as in VHL inhibitor VH298 (Frost *et al.*, 2016)) in compounds E and F, while maintaining chloroalkane linkers of the same length as compounds A and B (Fig 5.11c). Additionally, we prepared two HaloPROTACs (C, D) having linkers of 16 and 22 atoms length respectively attached at the N–terminal acyl amine moiety of VH032. This conjugation pattern had been explored previously albeit with different linker lengths (13 and 19 atoms) (Fig 5.11d) (Buckley *et al.*, 2015)

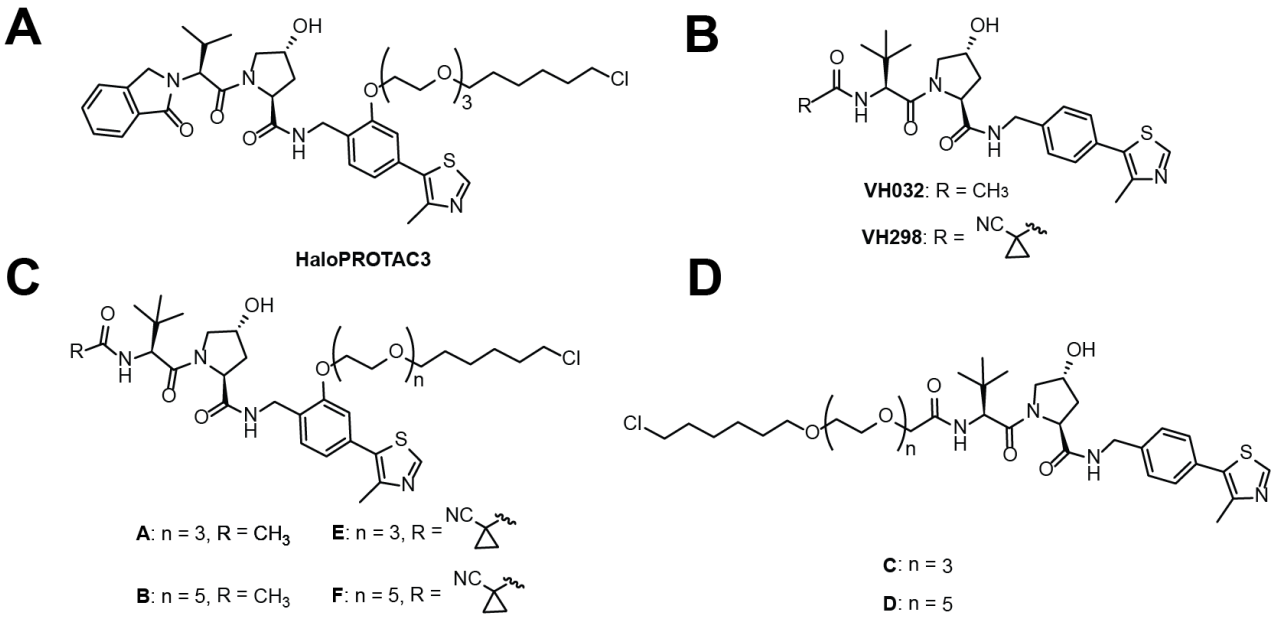

Figure 5.11 Design of HaloPROTAC compounds.
A. *Chemical structure of previously published HaloPROTAC3* (Buckley *et al.*, 2015). ***B.*** *New VHL inhibitors published by Ciulli lab* (Galdeano *et al.*, 2014; Frost *et al.*, 2016). ***C&D.*** *New HaloPROTAC compounds derived from phenyl position (**C**) or acetyl position (**D**) of VHL ligands.*

To determine the efficacy of each HaloPROTAC compound for degradation of HaloTag7 fusion proteins, I treated both SGK3-Halo and HaloVPS34 HEK293 cell lines with increasing concentrations of compound for 48h. This revealed that HaloPROTAC-E was the most potent compound, with a DC_{50} between 3-10nM and DC_{max} of 95% achieved by 300nM. Overall the

structure-activity relationship of the compounds was very interesting, with 15/16 atom linkers much more potent than the longer chain versions. Additionally, as observed in Buckley et al, the more potent compounds derived the chloroalkane moiety from the phenyl position of the VHL ligand. Finally, adaptation of the acetyl group to a cyclopropylcyanoacetic moiety in HaloPROTAC-E made it the most effective compound. This correlates with previous data that VH298, containing this cyclopropylcyanoacetic group is a much higher affinity ligand for VHL (Frost *et al.*, 2016).

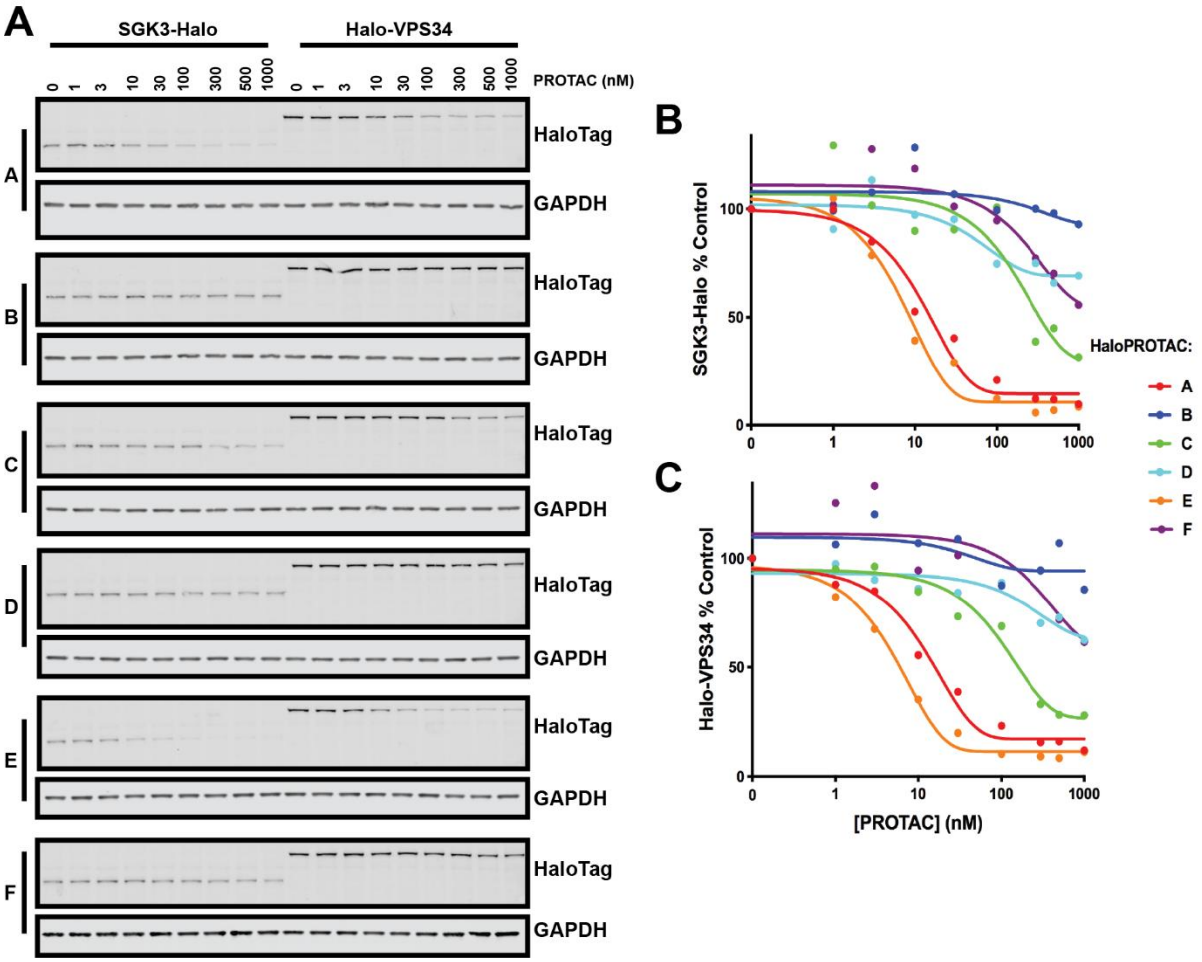

Figure 5.12 Cellular characterisation of HaloPROTAC compounds.
A*. SGK3–Halo and Halo–VPS34 cell lines were treated for 48h with increasing concentrations of each HaloPROTAC in parallel. Degradation of target protein measured by Immunoblot analysis for HaloTag7.* ***B&C.*** *Quantification of Western Blot intensity from A for SGK3–Halo (B) or Halo–VPS34 (C). Protein intensity was quantified and presented relative to an untreated control.*

5.4 Mechanistic characterisation of HaloPROTAC-E

It was important to fully characterise the kinetics and mechanism of degradation of HaloPROTAC-E. The above experiments demonstrated that HaloPROTAC-E mediated degradation was dose-dependent in HEK293 cells. I next demonstrated that degradation was time-dependent by treating SGK3-Halo and Halo-VPS34 cells with HaloPROTAC-E for up to 4 hours and measuring degradation of the target protein by western blot (Figure 5.13A). This revealed rapid degradation of both target proteins. 50% degradation of SGK3 was achieved within 30-40 minutes, and VPS34 within 1-2 hours. The slightly delayed degradation of VPS34 may be due to increased expression of VPS34 over SGK3, or due to the fact that VPS34 exists within a heterotetrameric complex. I also demonstrated HaloPROTAC-E mediated degradation to be reversible, as washout of the compound after 24h treatment resulted in rescued SGK3-Halo expression within 10h, nearing complete rescue within 24h (Fig 5.13b).

As in chapter 3, I used inhibitors of the ubiquitin-proteasome system to validate that this degradation occurred, as expected, via the $CUL2^{VHL}$ E3 Ligase complex and the proteasome. I pre-treated cells with various inhibitors of the pathway and measured blockade of HaloPROTAC-E induced degradation. In addition to the MLN4924 and MG132 inhibitors described in chapter 3, I also pre-treated cells with the VH298 high affinity, specific inhibitor of pVHL, recently published by the Ciulli lab (Frost *et al.*, 2016). As expected, pre-treatment with these inhibitors substantially blocked degradation of HaloTag7 fusion proteins (Fig 5.13c&d).

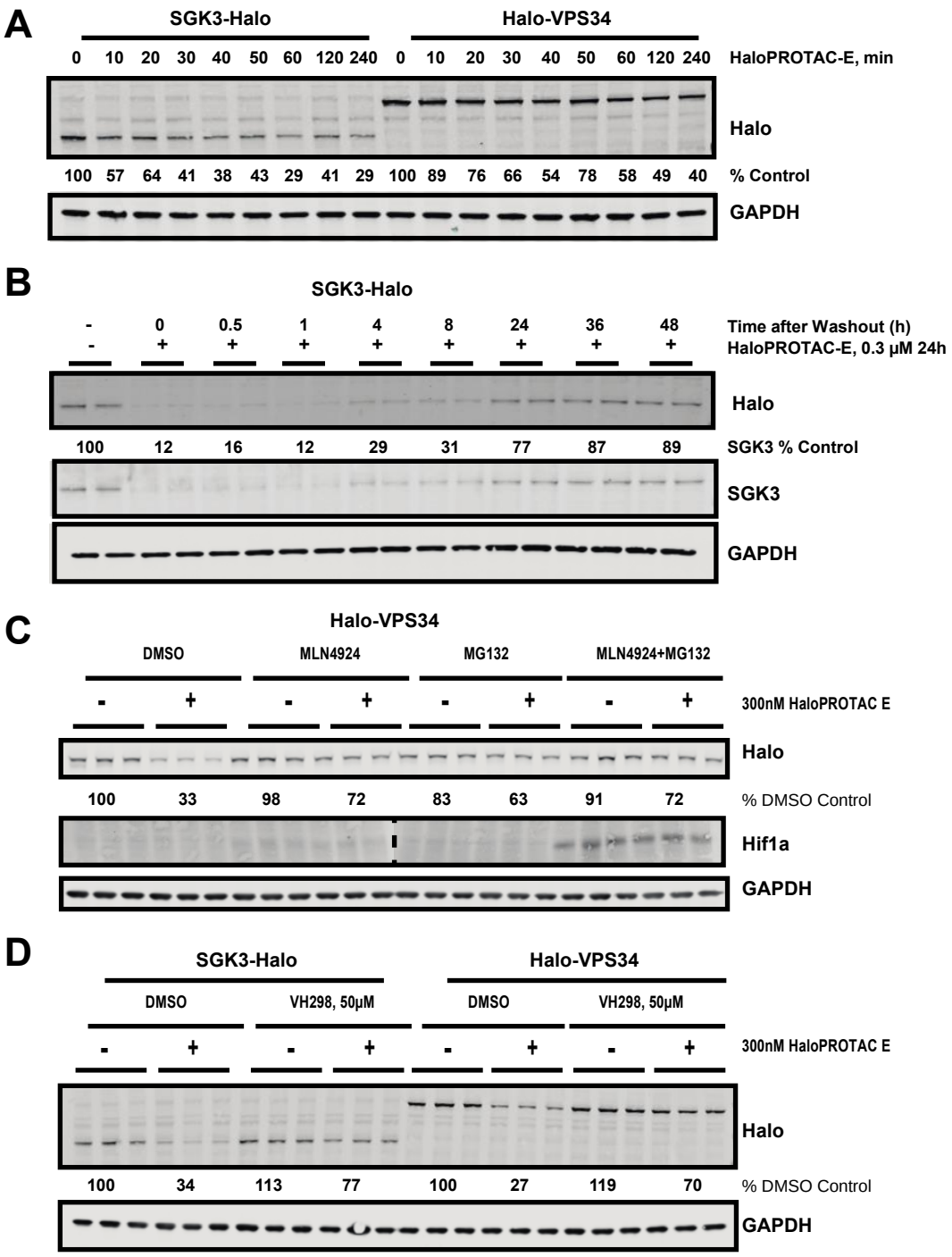

Figure 5.13 Mechanistic characterization of HaloPROTAC–E.

A. *SGK3–Halo and Halo–VPS34 cells were treated for up to 4h with 300 nM HaloPROTAC–E. Cells were lysed and probed by Western Blot for HaloTag7 and quantified for percentage of remaining HaloTag7 protein.* ***B.*** *SGK3–Halo cells were treated for 24h with 300 nM HaloPROTAC–E. After 24h, cells were washed 3 times with DMEM and replaced with fresh media for the times indicated. Recovery of SGK3–Halo was analyzed by Immunoblot* ***C.*** *Halo–VPS34 cells were treated for 6h with 300 nM HaloPROTAC–E, after pre–inhibition of Cullin Neddylation by MLN4924 (3 µM for 3h) or Proteasome by MG132 (50 µM for 30 minutes). Cells were lysed and remaining HaloTag7 fusion protein was analyzed by Immunoblot.* ***D****. SGK3–Halo and HaloVPS34 cells were treated for 6h with 300 nM HaloPROTAC–E, after pre–inhibition of VHL by 50 µM VH298 for 15 minutes.*

SGK3 and VPS34 are both endosomally-localised, as demonstrated in Figure 5.4. It was of particular interest whether these proteins could be easily degraded on the endosome, or if they were degraded in the cytosol. I therefore treated SGK3-Halo HEK293 cells with HaloPROTAC-E in the presence or absence of the VPS34 inhibitor VPS34-IN1. Inhibition of VPS34 results in a reduction of endosomal PtdIns(3)P and translocation of SGK3-Halo to the cytosol. Therefore, studying the degradation rates of SGK3-Halo in the presence of absence of VPS34-IN1 revealed whether this protein was more rapidly degraded when diffuse in the cytosol. I observed no difference between these two conditions (Figure 5.14), suggesting SGK3-Halo can be degraded on endosomes.

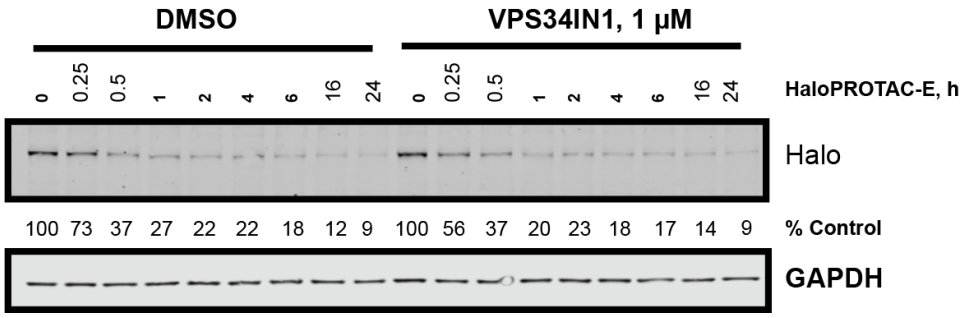

Figure 5.14 SGK3 is degraded when localised both on endosomes and in the cytosol.
SGK3-Halo HEK293 cells were treated for up to 24 h with HaloPROTAC-E, with or without treatment with VPS34-IN1 (1 µM). Cells were lysed and subject to immunoblot analysis with the indicated antibodies.

It was important to directly compare our new compound HaloPROTAC-E to the previously published HaloPROTAC3 (Buckley *et al.*, 2015). The publication reported a DC_{max} of 90% could be achieved 625nM HaloPROTAC3, however this was performed against exogenously expressed HaloTag7 protein. Both timecourse analysis and dose-response curves demonstrated an improved potency and efficacy of HaloPROTAC-E in inducing degradation of Halo-VPS34 (Figure 5.15).

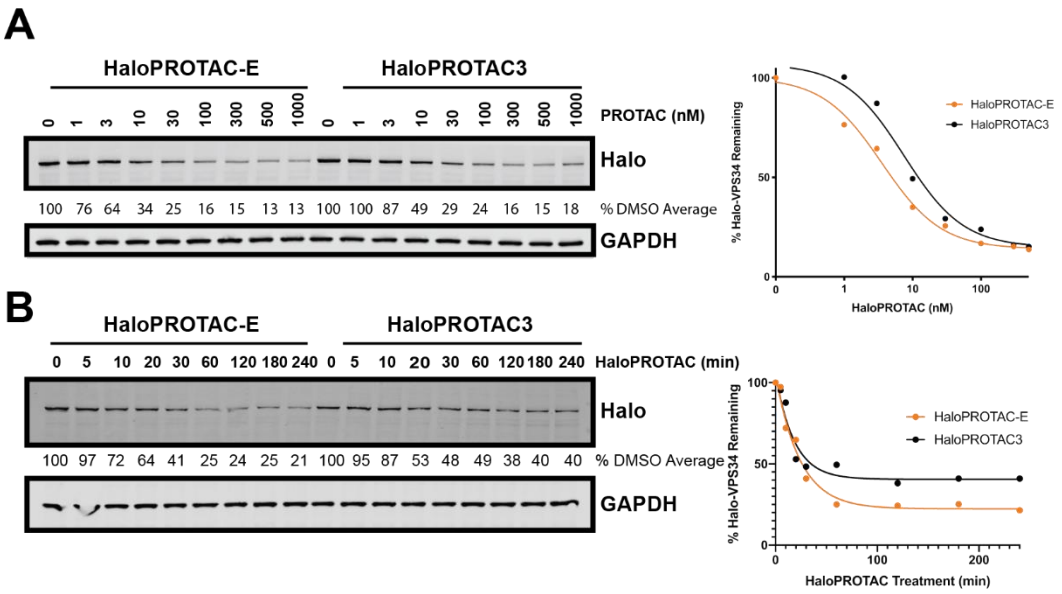

Figure 5.15 Comparison of HaloPROTAC–E to previously characterized HaloPROTAC3.
A. *Halo–VPS34 cells were treated in parallel for 24h with 1–1000 nM HaloPROTAC–E or HaloPROTAC3. Cells were lysed and remaining HaloTag7 fusion protein was analyzed by Immunoblot.* ***B.*** *Halo–VPS34 cells were treated for up to 4h with 300 nM HaloPROTAC–E or HaloPROTAC3. Cells were lysed and probed by Western Blot for HaloTag7, and quantified for percentage of remaining HaloTag7 protein.*

5.5 Global proteomic analysis for specificity of compound

The global specificity of HaloPROTAC-mediated degradation has yet to be determined in the published literature. Therefore, to answer this, I performed a quantitative Tandem-Mass-Tag(TMT)-labelled global proteomic analysis of Halo-VPS34 cells, treated in the presence or absence of 300nM HaloPROTAC-E for 4 hours. This experiment was undertaken in quadruplicate, and analysis in Proteome Discoverer v2.2 using Mascot search engine allowed relative quantification of 9786 proteins. This unbiased approach revealed that HaloPROTAC–E was remarkably selective. Halo-VPS34 was the most substantially and significantly degraded protein, with a 70% reduction in detected protein levels. The only other proteins with a significant reduction in protein levels were the known regulatory subunits of the VPS34 complex. VPS15 (50%), Beclin1 (20%), ATG14 (30%) and UVRAG (15%) were all reduced to a statistically significant value ($p<10^{-4}$) (Figure 5.16a). This exquisite selectivity is a clear advantage of the HaloPROTAC approach. This reduction in associated complex members has previously been observed when VPS34 was degraded constitutively in cells via the AdPROM method (Fulcher *et*

al., 2016; Malik *et al.*, 2018), and was confirmed by Immunoblot analysis (Fig 5.16b). As HaloPROTAC-mediated degradation offers temporal control, I next analysed whether expression of these components was lost in parallel to VPS34, or followed at a later timepoint due to loss of complex stability. Time course analysis of VPS34 degradation revealed that at very early time points of 10–20 minutes, VPS15 was reduced at a similar rate to VPS34, whereas the reduction in Beclin1 expression was slower (Fig 5.16c&d).

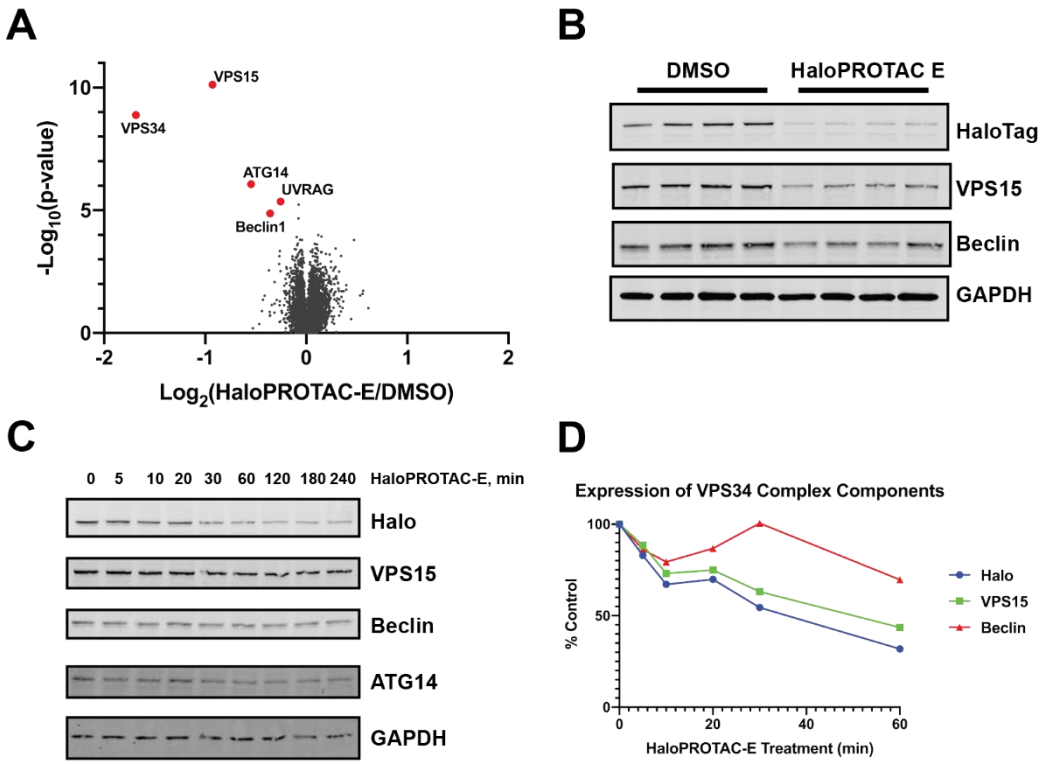

Figure 5.16 Degradation of HaloTag7 fusions is highly specific and has a biological impact.
A. *Volcano plot quantifying proteins significantly downregulated on 4h HaloPROTAC–E treatment in Halo–VPS34 cells.* ***B.*** *Immunoblot analysis of lysates taken for Mass Spectrometry analysis* ***C&D****. HaloVPS34 cells were treated with 0.3 μM HaloPROTAC–E for up to 4 hours.* ***C.*** *Immunoblot analysis of these lysates for VPS34 complex members.* ***D.*** *Quantification of relative protein levels of VPS34 complex members from 5.16C.*

5.6 Biological impact of HaloPROTAC-E mediated degradation of target proteins

The advantage of combining a HaloPROTAC approach with CRISPR/Cas9 is that these tools can be deployed to investigate the endogenous roles of a protein. Additionally, this approach can be used to validate potential targets for PROTAC development and support the rationale for

targeted degradation. I therefore investigated known roles of SGK3 and VPS34, and the impact on these pathways by targeted degradation.

Degradation of SGK3-Halo and Halo-VPS34 results in reduced phosphorylation of the SGK3 substrate NDRG1.

The best validated substrate of SGK3 is phosphorylation of NDRG1 at its Thr346 residue. This site is also shared with SGK1 and Akt. VPS34 acts upstream of SGK3, generating PtdIns(3)P on early endosomal membranes, triggering SGK3 activation. I chose to investigate whether degradation of Halo-VPS34 or SGK3-Halo was able to downregulate the hVPS34-SGK3 signaling axis and inhibit the phosphorylation of NDRG1. In order to remove the effect of Akt activity on NDRG1 phosphorylation, all conditions were performed in the presence of Akt inhibitor AZD5363. A timecourse analysis of HaloPROTAC-E mediated protein degradation revealed that degradation of both proteins induced dephosphorylation of NDRG1. Degradation of SGK3 reduced NDRG1 phosphorylation within 4 h, whereas dephosphorylation of NDRG1 through VPS34 degradation took up to 24h (Figure 5.17).

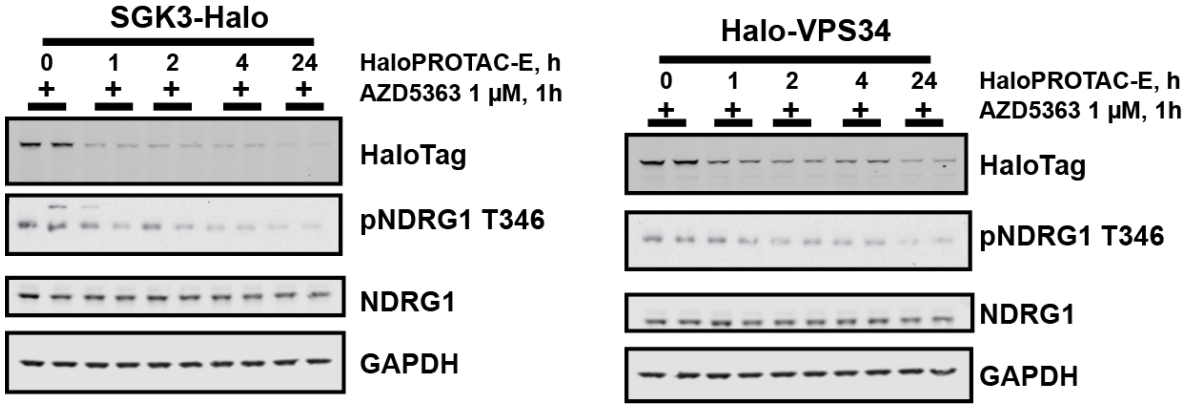

Figure 5.17 NDRG1 phosphorylation is reduced on degradation of SGK3-Halo and HaloVPS34.
SGK3-Halo and Halo-VPS34 HEK293 cell lines were treated for up to 24h with HaloPROTAC-E to induce degradation of HaloTag7 target proteins. In the final hour before lysis, cells were treated with Akt inhibitor AZD5363 (1 µM). Phosphorylation of the SGK3 substrate NDRG1 at Thr346 was measured by western blot.

in vitro studies of SGK3 activity had revealed a significant reduction in SGK3 kinase activity on addition of a C-terminal HaloTag7 fusion (figures 5.8-5.10). However, this data reveals that

NDRG1 phosphorylation is still mediated by SGK3 activity, and degradation of SGK3 reduces phosphorylation of its substrate.

Degradation of HaloVPS34 marginally impacts on known VPS34 functions

VPS34 is known to play a number of important roles in the cell. It catalyses the phosphorylation of PtdIns in order to produce PtdIns(3)P on endosomal membranes. This PtdIns(3)P is critical in the formation of authophagosomal vesicles in autophagy, and also the recruitment of PX containing effector proteins such as SGK3, stimulating its activation. I therefore used my Halo-VPS34 cells to investigate whether degradation of VPS34 via HaloPROTAC-E has an impact on these biological readouts

First, I used Halo-VPS34 KI cells to assay the activity of SGK3 on degradation of VPS34. Inhibition of this lipid kinase with VPS34-IN1 results in a substantial reduction in SGK3 activity, as PtdIns(3)P is reduced on endosomal membranes (Bago *et al.*, 2014). I therefore compared SGK3 activity in the immunoprecipitation assay described above, on inhibition or degradation of Halo-VPS34. I also combined these treatments with the Class I PI3K inhibitor GDC0941 (0.5 μM), to remove the effect of SGK3 activation through the Class I PI3K pathway (Malik *et al.*, 2018). I unveiled a slight, although statistically significant, reduction in SGK3 activity on HaloPROTAC-E treatment, however not as great an effect as seen on inhibition (Figure 5.18). This is in line with what was previously observed when degrading VPS34 via the AdPROM system (Fulcher *et al.*, 2016; Malik *et al.*, 2018).

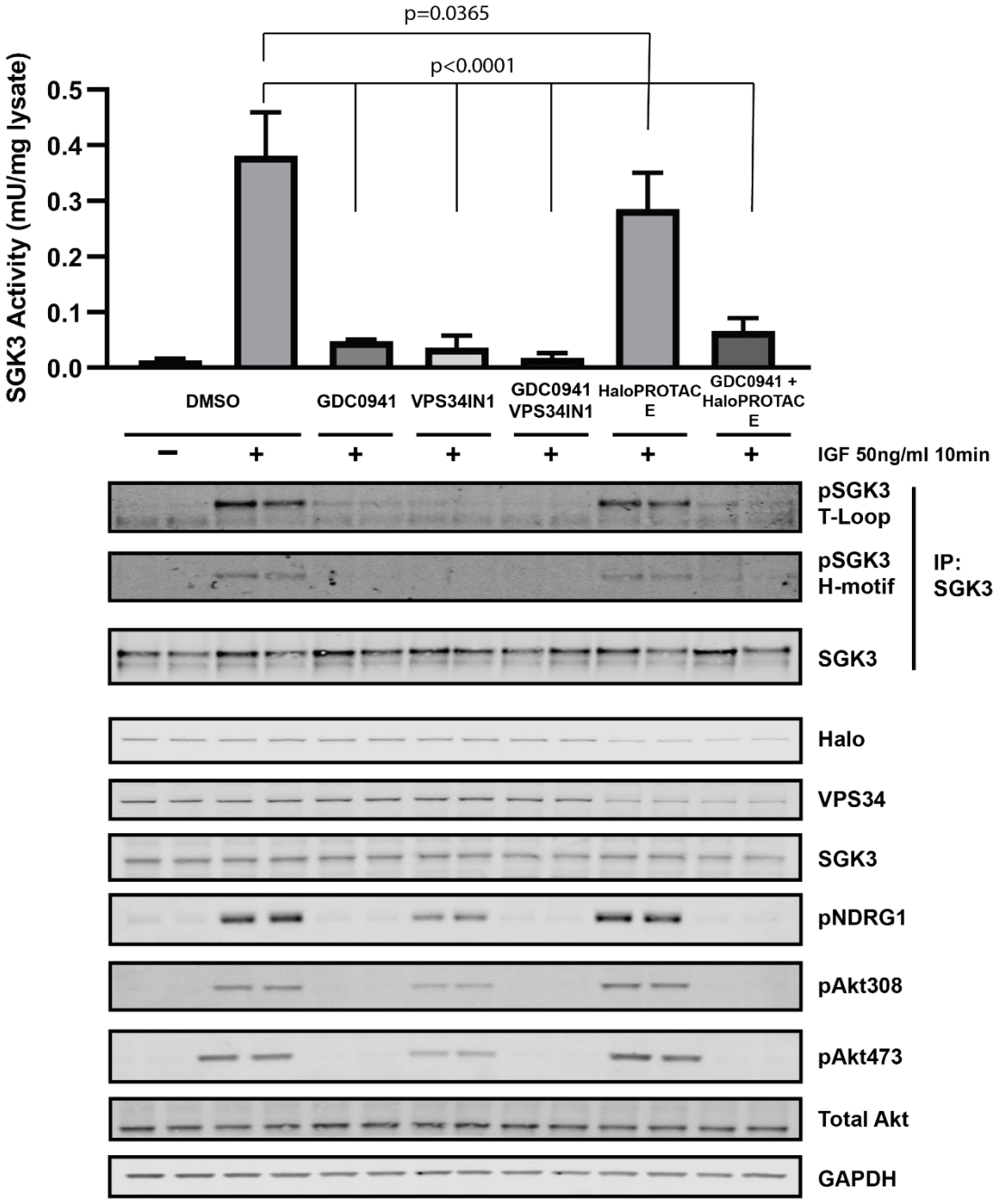

Figure 5.18 SGK3 activation in response to growth factors is marginally reduced by Halo-VPS34 degradation.

HEK293 Halo-VPS34 cells were treated with or without HaloPROTAC-E for 24 h, then serum-starved in empty DMEM overnight. Prior to stimulation with IGF-1 (50 ng/ml, 10 min), cells were treated with DMSO, GDC0941 (0.5 µM) or VPS34IN1 (1µM). SGK3 was immunoprecipitated from 3 mg lysate, and subject to in vitro kinase assay against the Crosstide peptide, and incorporation of 32P γ-ATP measured. 1 unit of activity = incorporation of 1nmol γ-phosphate into substrate per mg lysate. Error bar = SD, n=3. Statistical analysis 2-way ANOVA with posthoc Tukey multiple comparisons test.

However, a caveat of this assay is that long-term degradation of VPS34 (24 h degradation before 16 h serum starvation), was being compared to short-term inhibition (1 h inhibition before IGF-1 stimulation). I therefore performed a second assay to determine the immediate effect of

VPS34 degradation, and whether the cells react and compensate for loss of VPS34. I also performed this assay under basal conditions to remove the effect of growth factor stimulation of the Class I PI3K pathway. I observed that 1 h degradation of VPS34 caused an immediate reduction in SGK3 activity, but that this activity was then recovered after 24 h. Further, I observed that co-treating with VPS34-IN1 in the final hour before lysis was now unable to further reduce SGK3 activity (Fig 5.19). This suggests that a compensatory mechanism, perhaps via Class II PI3K or lipid phosphatases, may be responsible for this SGK3 activity, and that activity was being mediated independently of VPS34.

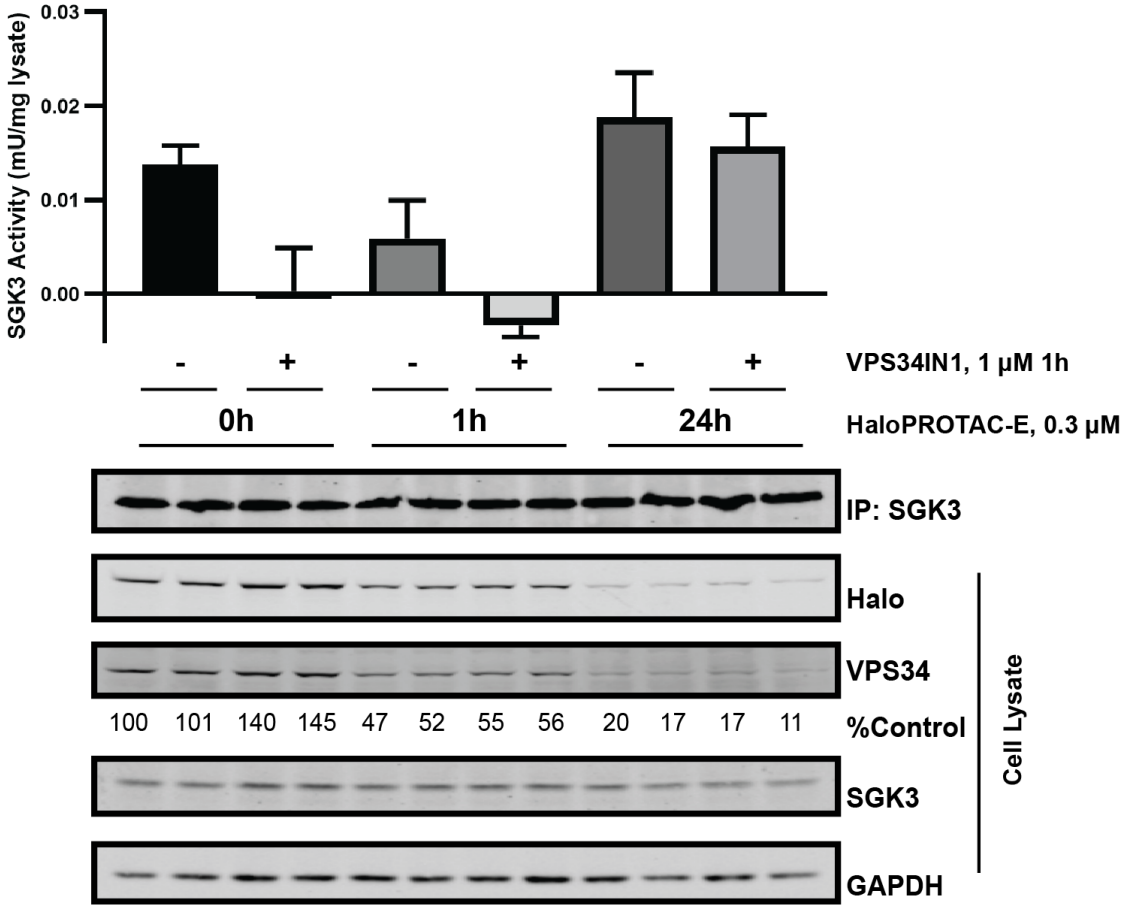

Figure 5.19 After prolonged Halo-VPS34 degradation, SGK3 activity is not mediated by VPS34.
HEK293 Halo-VPS34 cells were treated with or without HaloPROTAC-E for 1 or 24 h. Prior to lysis, cells were additionally treated with VPS34IN1 (1 µM) for 1 h. SGK3 was immunoprecipitated from 3 mg lysate, and subject to in vitro kinase assay against the Crosstide peptide, and incorporation of 32P γ-ATP measured. 1 unit of activity = incorporation of 1nmol γ-phosphate into substrate per mg lysate. Error bars = SD, n=3.

Given this response in SGK3 activity, I decided to assess the impact of HaloPROTAC-E mediated degradation of HaloVPS34 on production of endosomal PtdIns(3)P, as described in section 5.2 (Figure 5.6). However, I only observed a very mild decrease in PtdIns(3)P on treatment with HaloPROTAC-E. Whereas in the SGK3 activity assay I observed a resistance to VPS34IN1 treatment after degradation, when analysing PtdIns(3)P I could observe phospholipid levels were still sensitive to VPS34 inhibition after 24 h of degradation (Figure 5.20). Therefore, PtdIns(3)P production is still under the control of the remaining ~15% VPS34 in these cells.

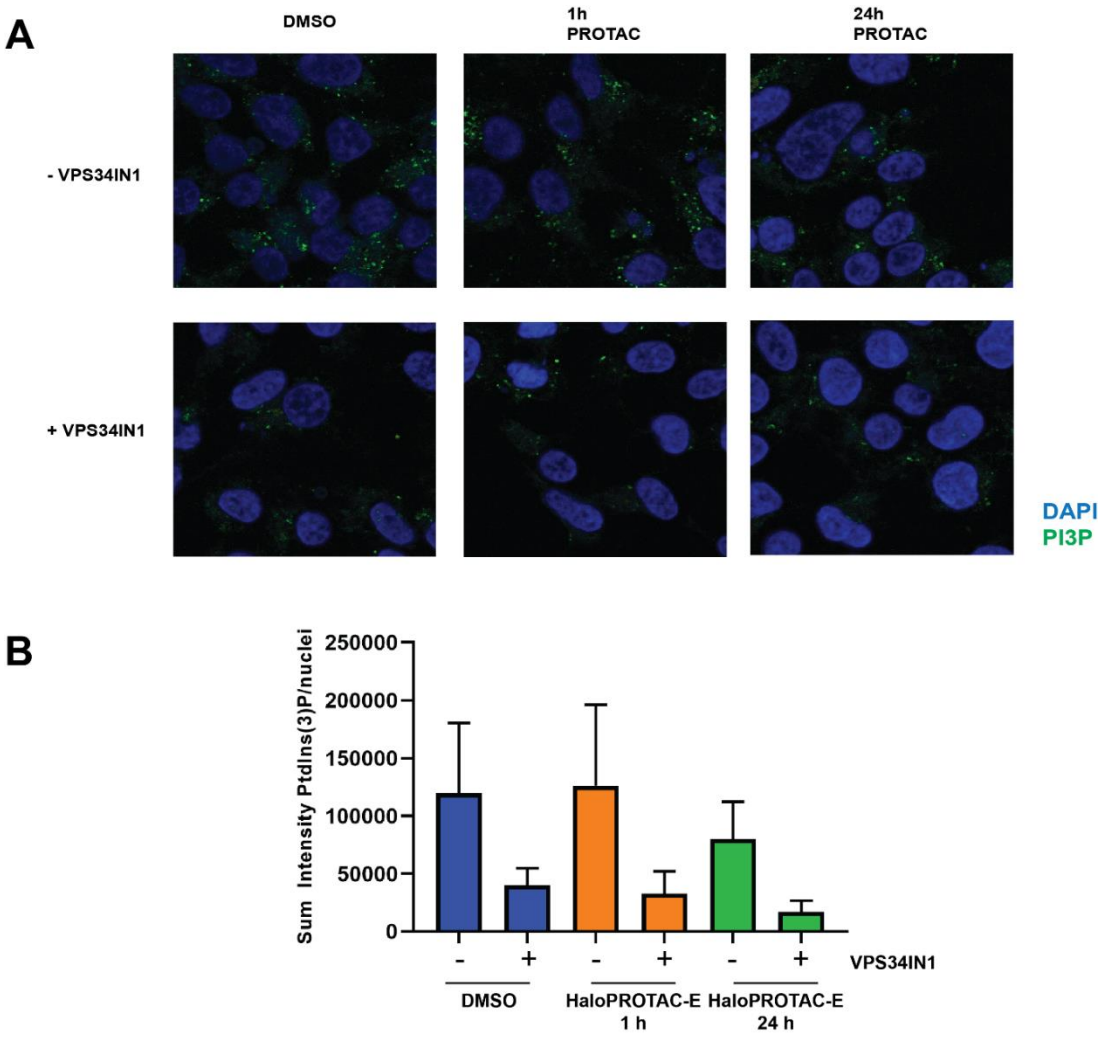

Figure 5.20 Production of PtdIns(3)P on endosomes is marginally decreased on Halo-VPS34 degradation. ***A.*** *HEK293 Halo-VPS34 cells were seeded onto coverslips and allowed to adhere overnight. Cells were then treated for 1 or 24 h with HaloPROTAC-E and treated with or without VPS34IN1 (1 µM) 1h before lysis. Production of PtdIns(3)P on endosomal membranes was measured with the 2XFYVE-AlexaFlour488 PtdIns(3)P probe.* ***B.*** *Quantification of PtdIns(3)P intensity/nuclei. Error bars = SEM, n=10*

Aside from the activation of SGK3, VPS34 is more commonly associated with an important role in regulating autophagy. PtdIns(3)P production in response to, for example, nutrient starvation is critical for the formation of autophagosomes. I therefore chose to investigate the effect of Halo-VPS34 degradation has on autophagic flux. This can be measured by inducing autophagy by total nutrient starvation with EBSS, and blocking fusion of autophagosomes to lysosomes with the inhibitor Bafilomycin A (Ohkuma *et al.*, 1993). Under these conditions, levels of lipidated LC3 can be measured by Western Blot, as a measure of autophagosomes formed. Under these conditions, I was able to observe a slight decrease in lipidated LC3 on HaloVPS34 degradation, however not as much as was observed upon VPS34 inhibition by VPS34-IN1 (Figure 5.21). More specifically, while basal autophagy appeared to be substantially inhibited, induction of high levels of autophagy by serum and amino acid starvation with EBSS could still occur after VPS34 degradation. However, as with the previous kinase assay, this assay was performed after 24 h of VPS34 degradation, in comparison to short term inhibition. Therefore, this pathway may have been subject to compensatory mechanisms. If repeated at earlier timepoints, a greater effect may be observed.

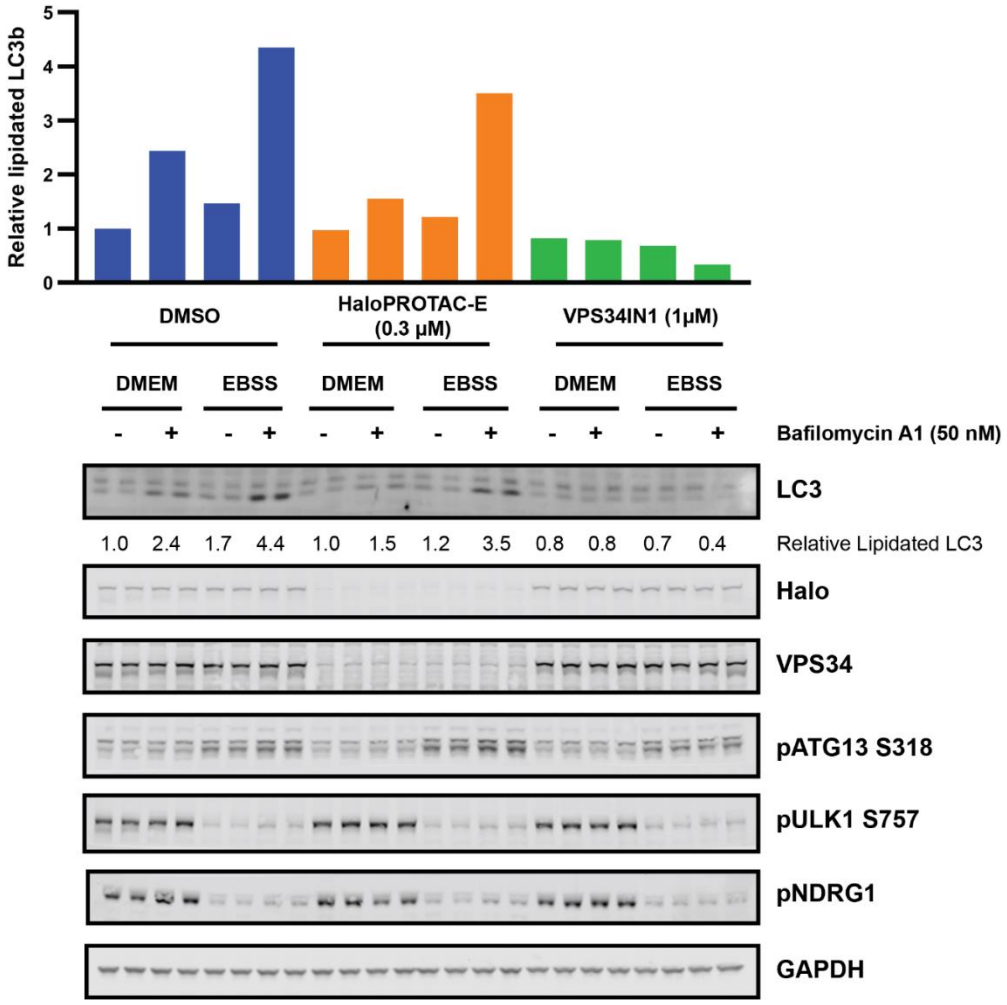

Figure 5.21 Autophagic flux is mildly inhibited on degradation of Halo-VPS34.
HEK293 HaloVPS34 cells were treated for 24h with DMSO or HaloPROTAC-E to induce degradation of VPS34. 2h before lysis, cells were washed twice with EBSS and media replaced with either DMEM or EBSS to induce autophagy. At this point, cells were treated with out without VPS34IN1 (1 µM) to inhibit VPS34, and Bafilomycin A (50nM) to block lysosome fusion of autophagosomes. Autophagic flux was measured by quantification of lipidated LC3b (lower band).

5.7 Mutation of surface lysines of HaloTag7 does not significantly impact on the rate of degradation

Proximity-driven ubiquitylation occurs on surface lysines of the target protein. In an attempt to increase the rate of ubiquitylation and therefore proteasome-mediated degradation of SGK3, I generated several mutant forms of SGK3-Halo, in which positive surface residues were mutated to extra lysines on the surface of HaloTag7. These residues were selected by inspection of the X-ray crystal structure of HaloTag7 (PDB: 4KAF) and selecting Arginine or Histidine residues on

the surface which were predicted to tolerate mutation to lysine without altering the properties of the protein surface (Figure 5.22). I also investigated swapping the 5XGly Linker between SGK3 and HaloTag7 to 5XLys, to see if this would increase proteasomal degradation further. These proteins were overexpressed in HEK293 FlpIn cells by 24 h doxycycline induction, then rate of degradation measured after up to 16 h treatment with HaloPROTAC-A. These experiments were performed with HaloPROTAC-A as the final HaloPROTAC-E compound had not yet been optimised at the time of performing the experiments. It would be interesting to repeat these experiments with HaloPROTAC-E and determine any differences with an optimised compound.

The exchange of a 5XGly linker for 5XLys showed no significant increase in the rate of degradation (Figure 5.23), in fact early timepoints of degradation were marginally slower. The first set of mutations, summarised as ‘MUT1’ partially increased the rate of degradation, and total degradation achieved within 16 h. However, any further mutations did not increase the rate of degradation. These mutations may have destabilized the protein or impacted on its catalytic activity, as degradation was often seen on addition of further mutations (Figure 5.23).

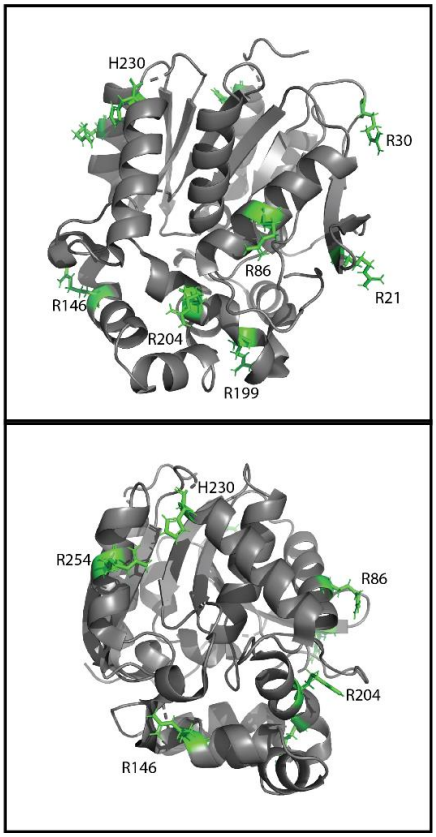

Cell Line	Mutation in HaloTag7	Desired Effect
SGK3-Gly$_5$-Halo	-	-
SGK3-Gly$_5$-Halo^{MUT1}	R21K, R86K, R204K, R254K, R288K	Addition of surface lysines to increase ubiquitylation
SGK3-Gly$_5$-Halo^{MUT2}	MUT1 + R30K, R146K, H230K	Addition of surface lysines to increase ubiquitylation
SGK3-Gly$_5$-Halo^{MUT3}	MUT2 + R199K	Addition of surface lysines to increase ubiquitylation
SGK3-Gly$_5$-Halo^{D106A}	D106A	Mutation of catalytic residue to prevent PROTAC binding
SGK3-Lys$_5$-Halo	-	-
SGK3-Lys$_5$-Halo^{MUT1}	R21K, R86K, R204K, R254K, R288K	Addition of surface lysines to increase ubiquitylation
SGK3-Lys$_5$-Halo^{MUT2}	MUT1 + R30K, R146K, H230K	Addition of surface lysines to increase ubiquitylation
SGK3-Lys$_5$-Halo^{MUT3}	MUT2 + R199K	Addition of surface lysines to increase ubiquitylation
SGK3-Lys$_5$-Halo^{D106A}	D106A	Mutation of catalytic residue to prevent PROTAC binding

Figure 5.22 Design of HaloTag7 surface mutants.
A series of SGK3-Halo surface mutants were designed by Alessio Ciulli (BCDD), to increase lysine residues on the surface of the protein. Residues were selected based on the crystal structure of HaloTag7 (PDB: 4KAF), to reduce impact on surface characteristics.

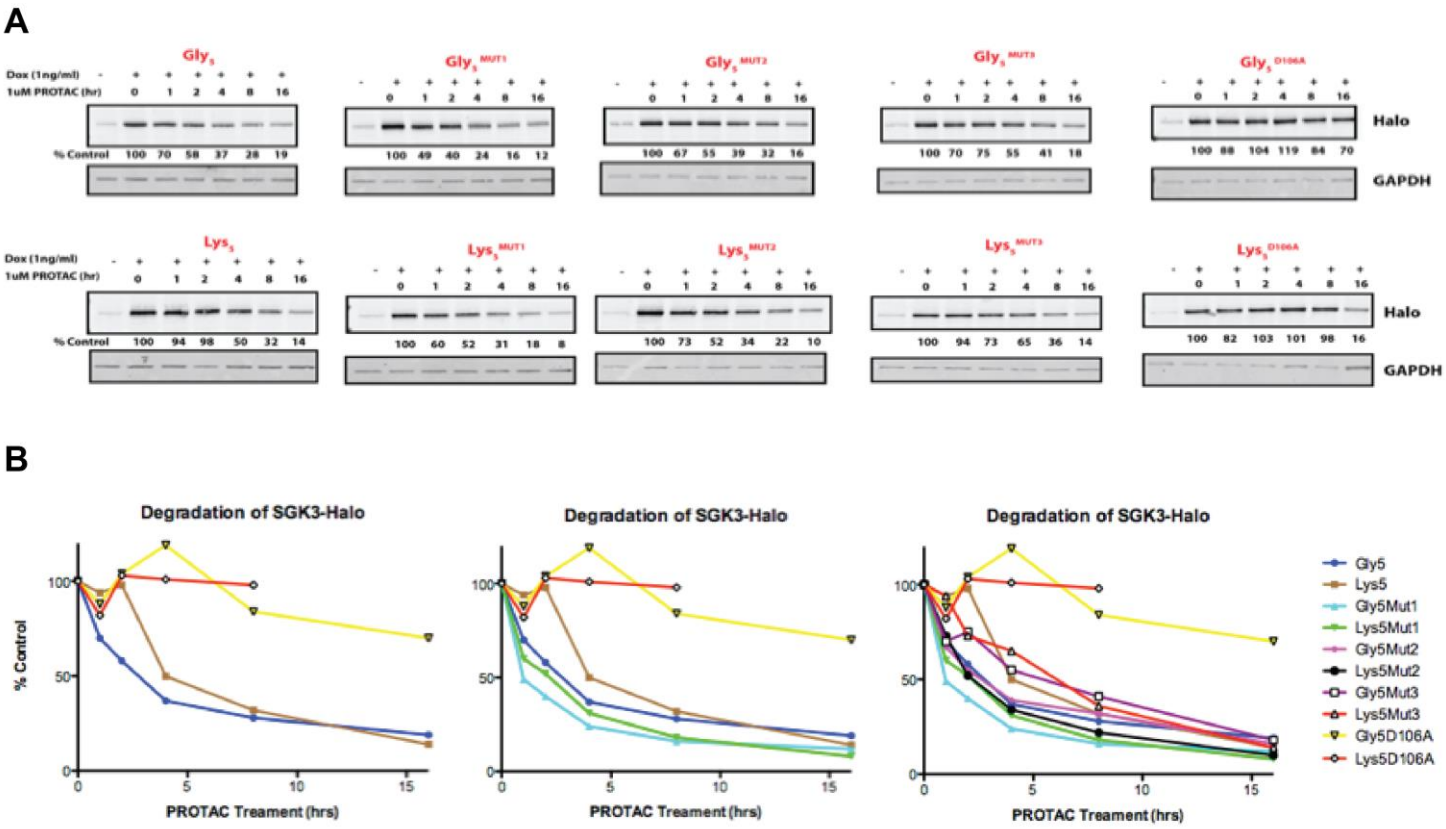

Figure 5.23 Addition of surface lysines to HaloTag7 does not significantly increase the rate of HaloPROTAC induced degradation.
HEK293 FlpIn cell lines were produced expressing SGK3-Halo with a range of modifications, with the aim to induce more rapid degradation of SGK3-Halo protein. These changes included exchange of the 5XGly linker for 5XLys, and a series of surface mutations to decorate the protein surface with lysines to increase potential ubiquitylation. Expression of SGK3-Halo was induced with doxycycline (0.1 µg/ml) and degradation induced with HaloPROTAC-A for up to 16h. Degradation of SGK3-Halo was measured (A) and quantified (B) by western blot

5.8 Discussion

In this chapter, I present the design and synthesis of a new, potent HaloPROTAC compound, termed HaloPROTAC–E. More specifically I generated CRISPR/Cas9 KI cell lines of both SGK3 and its upstream regulator VPS34, and show that HaloPROTAC-E induces the rapid and efficient degradation of both target proteins. HaloPROTAC–E induced potent degradation, with a DC_{50} between 3–10 nM. Both SGK3 (20–30 min for 50% degradation) and VPS34 (1–2 h for 50% degradation), which forms part of a complex, were rapidly degraded. A direct comparison revealed the HaloPROTAC compound described in this study was more effective than the previously reported compound HaloPROTAC3. The design and publication of HaloPROTAC-E is therefore an important addition to the field for the validation of potential PROTAC targets. As SGK3 and VPS34 are both endosomally localised, I have demonstrated in this study that the HaloPROTAC approach is capable of inducing degradation of both endosomally localised and cytosolic proteins. Treatment of SGK3-Halo cells with VPS34-IN1, to reduce endosomal PtdIns(3)P and move SGK3 to the cytosol, had no impact on the rate at which SGK3-Halo could be degraded. This is of great importance to the field as it demonstrates that subcellularly localised proteins can be targeted for degradation.

The goal of this project was to target the HaloPROTAC approach towards endogenous proteins, and therefore manipulate an endogenous signalling pathway. Phosphorylation of the SGK3 substrate NDRG1 at Thr346 was substantially reduced on degradation of either SGK3-Halo or Halo-VPS34. This demonstrated the ability of this approach to target endogenous proteins, and act as validation for the selection of target proteins for PROTACs or other chemical modulation approaches. Quantitative mass spectrometry studies also revealed that degradation mediated by HaloPROTAC-E is strikingly selective, not degrading any other proteins in the Halo-VPS34 cell line other than Halo-VPS34 itself and its known regulatory subunits. Again, this is a clear strength for the use of this approach in understanding and manipulating endogenous systems. It is unclear from these studies whether the reduction in VPS34 complex members is due to loss of

stability of the complex upon VPS34 degradation, a hypothesis that is supported by previous siRNA knock–down data (Itakura *et al.*, 2008). Alternatively, these subunits could be degraded through a "by–stander" effect, receiving collateral ubiquitination by the VHL ligase as a result of being part of the same complex (Maniaci *et al.*, 2017).

While NDRG1 phosphorylation was clearly impacted on degradation of SGK3-Halo and Halo-VPS34, other biological readouts of VPS34 activity gave only marginal or conflicting results on degradation of Halo-VPS34. Only a mild reduction in autophagic flux, measured by production of lipidated LC3b, was observed after Halo-VPS34 degradation. It is possible that this milder effect may be due to the remaining VPS34 being sufficient to carry out necessary functions. Alternatively, compensatory pathways could be activated on degradation of VPS34, for example generating PtdIns(3)P from PtdIns(3,4,5)P_3 via the lipid phosphatases INPP4B and SHIP2 (Malik *et al.*, 2018). As VPS34 is an essential gene and cannot be knocked out at the genome level, relatively little is known about compensatory pathways which may occur in the absence of VPS34. A mechanism for inducible reduction in VPS34 expression in cells is therefore a very powerful tool.

Similarly, after 24h degradation of Halo-VPS34, *in vitro* SGK3 kinase activity was only marginally reduced. This was also observed when constitutively degrading GFP-VPS34 using the AdPROM system, which resulted in only a mild reduction in SGK3 activity (Fulcher *et al.*, 2016; Malik *et al.*, 2018). However, an advantage of the HaloPROTAC system is temporal control of protein expression, as degradation is both inducible and reversible. Using shorter HaloPROTAC treatments, I was able to demonstrate that short-term loss of VPS34 significantly reduced SGK3 *in vitro* kinase activity, however after 24 h SGK3 activity was rescued, and could no longer be modulated by VPS34 inhibition. However, conflictingly, I also demonstrated by western blot that SGK3-mediated phosphorylation of NDRG1 is not rescued at this timepoint, and by immunofluorescence that PtdIns(3)P is still under the control of remaining VPS34. The biological

explanation behind these apparently conflicting results is still unclear, and merits further investigation. Perhaps, SGK3 activated independently of PtdIns(3)P is incorrectly localised for phosphorylation of its substrate NDRG1. Alternatively, an autoinhibition mechanism may inhibit its activity in cells, but kinase activity can still occur *in vitro*.

Because the chloroalkane handle reacts covalently with HaloTag7, a potential limitation of the HaloPROTAC approach is that stoichiometric occupancy of the tagged protein is required to achieve complete degradation of the target protein. A key advantage to PROTACs bearing non–covalent target ligands is that they can function catalytically at sub–stoichiometric concentrations relative to the target protein. Despite the clear strengths of non–covalent protein degradation modalities, potent ligands are often required and structure–guided PROTAC design requires structural information on ternary complexes (Gadd *et al.*, 2017). Even with this knowledge, many variables affecting efficacy of PROTACs are still not thoroughly understood, and are highly target dependent. The HaloPROTAC approach removes these issues, allowing for exquisite selectivity and high affinity.

A caveat to the HaloPROTAC approach is the size of the required HaloTag7 fusion onto the target of interest. Such a large tag may interfere with the activation, complex formation or function of a target protein. This study demonstrates that both N- and C-terminal fusions can be degraded using HaloPROTAC-E, and the kinetics of degradation was similar for both proteins. Therefore, for most proteins with a regulatory terminal domain this issue can be avoided. However, the addition of a large 33kDa tag may impact on protein function and should always be evaluated. In the case of SGK3-Halo, we observed a significant reduction in its *in vitro* kinase activity on addition of the HaloTag7 fusion. This is likely due to the proximity of such a large tag to the critical hydrophobic motif activating residue, therefore blocking SGK3's phosphorylation by mTORC2. As both the N- and C- terminus are critical for SGK3 activation, this has limited the HaloPROTAC approach for further use targeting SGK3 in this thesis. Preliminary data suggested

that extending the linker between SGK3 and HaloTag7 began to rescue the activity of SGK3, however this was not followed up in this study. For this reason, I therefore continued with the approach described in Chapter 4, with the development of an inhibitor derived PROTAC against SGK3, which interacts with the protein directly in its kinase domain. This approach requires a more intensive optimization of compounds, however removes the caveats of placing a large tag on the protein. An advantage of having tried both approaches is that HaloPROTAC-E could be used to determine the specificity and any off-target effects of SGK3-PROTAC1, by treatment of SGK3-Halo cells with both compounds. Overall this optimized HaloPROTAC approach, combining HaloPROTAC–E with CRISPR/Cas9 mediated endogenous protein tagging, has been demonstrated to provide a useful tool to interrogate an endogenous system and validate the therapeutic potential of degrading its protein target.

6. How is SGK3 activated in the context of PI3K Inhibition?

6.1 Activation of SGK3 by Class I and Class III PI3K

In common with other AGC protein kinases, SGK3 is activated by phosphorylation on its hydrophobic motif by mTORC2, and T-loop by PDK1. This activation has been demonstrated to also be dependent on the PX domain of SGK3, which recruits the kinase to PtdIns(3)P on endosomal membranes. In the case of Akt, this activation mechanism is dependent on the activity of Class I PI3K generating PtdIns(3,4,5)P_3 on the plasma membrane. Recent work published by the lab has demonstrated that SGK3 can be activated by Class I PI3K, possibly through the action of lipid phosphatases INPP4B and SHIP2 (Malik *et al.*, 2018), however it can also be activated by alternate mechanisms in the context of prolonged PI3K inhibition. Bago *et al.*, demonstrated that SGK3 is activated by the activity of Class III PI3K VPS34, which generates PtdIns(3)P on endosomal membranes (Bago *et al.*, 2014, 2016). Malik *et al* went on to demonstrate that activation via VPS34 could be stimulated by growth factors, similarly to Class I PI3K. However, the mechanism by which VPS34 is activated by growth factors in yet to be determined, as the paper demonstrated IGF stimulation did not increase *in vitro* kinase activity of VPS34, or the amount of VPS34 localised to endosomal membranes (Malik *et al.*, 2018). Therefore, as part of my thesis I decided to investigate how VPS34 was activated by growth factors, and consequently activated SGK3.

VPS34 exists in the cell in 2 complexes. The core VPS34 complex of VPS34, VPS15 and Beclin1 can be found in complex I, with ATG14 on Rab7 containing membranes, commonly involved in nutrient sensing and autophagy. Alternatively, Complex II contains UVRAG in the place of ATG14 and is found primarily on Rab5 containing membranes. A number of more transient accessory interactors bind to these complexes and modulate VPS34 activity. I was interested to determine whether complex composition of VPS34 was altered on growth factor stimulation, and whether interaction with known or unknown effectors may be altered on IGF1 stimulation, impacting on VPS34's activity and generation of PtdIns(3)P. I therefore undertook a proximity biotinylation

approach, TurboID, to selectively biotinylate and identify interactors of GFP-VPS34 , in the case of serum starvation or IGF1 stimulation.

Bago *et al*. demonstrated that when cancer cell lines activate SGK3 in the context of PI3K inhibition, this activation still occurs via mTORC2, as demonstrated by shRNA experiments against the mTORC2 component Rictor which blocked SGK3 activation (Bago *et al.*, 2016). Under these conditions, mTORC2-dependent phosphorylation of SGK3 is observed, but not of Akt, which remained dephosphorylated at S473. This finding suggested differential mechanisms by which SGK3 and Akt can be recognised and phosphorylated my mTORC2, which would be an important mechanism to understand in preventing PI3K-inhibitor resistance in breast cancer.

It was recently proposed by Liu *et al* that mTORC2 activity was determined by the complex member mSin1, in particular the PH domain binding $PI(3,4,5)P_3$ on the plasma membrane (Liu *et al.*, 2015). However, under conditions of Class I PI3K inhibition, SGK3 was targeted by mTORC2 independently of $PtdIns(3,4,5)P_3$. I therefore chose to investigate how SGK3 phosphorylation by mTORC2 was regulated, and how this regulation differed from Akt. I also chose to focus on mSin1 as a regulatory component of mTORC2 and generated various truncations and mutants of mSin1 to determine which elements were required for activation of Akt and SGK3 respectively.

6.2 PI3K-independent activation of mTORC2 mediated by mSin1

6.2.1 SGK3 activation is mediated by mTORC2, and reliant on mSin1.

I first aimed to generate CRISPR/Cas9 knockout of mSin1 in HEK293 TREx and U2OS TREx cells. The purpose of this was to remove endogenous mSin1, therefore any activity of mTORC2 should be mediated by the mSin1 mutants introduced to the cells via the Flp-In™ T-REx™, Doxycycline-inducible system. Using the D10A Nickase form of Cas9 described in Chapter 5, mSin1 gRNAs were designed targeting Exon 5. As generation of gene knockouts occurs by non-homologous end joining (NHEJ) rather than homology driven repair (HDJ) a donor template was not required. Exon 5 was chosen as this is the first common exon between all known transcript variants, and

therefore all isoforms of mSin1 should be affected. Using this approach, I generated 9 mSin1 KO clones in HEK293 TREx cells, and 3 knockout clones in U2OS TREx (Figure 6.1). The entire gel was analysed to ensure no expression of truncated forms of mSin1 remained. All U2OS clones and 4 HEK293 clones were confirmed by Sanger sequencing.

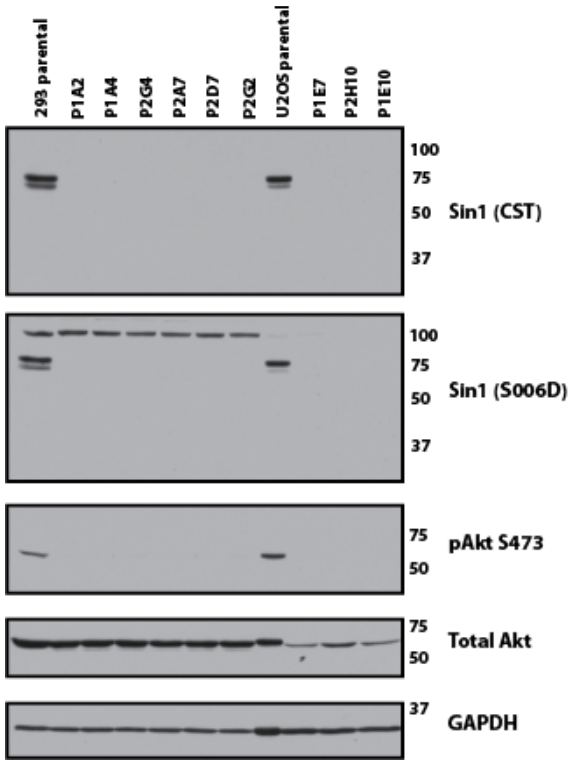

Figure 6.1 CRISPR/Cas9 KO of mSin1 from HEK293 TREx and U2OS TREx cells.
CRISPR/Cas9-mediated knockout of mSin1 was performed in HEK293 TREx and U2OS TREx cells by sgRNA targeting exon 5 of the MAPKAP1 gene. Successful knockout clones were subject to immunoblot analysis with the given antibodies before confirmation by Sanger Sequencing.

I first studied the mSin1 KO cells in comparison to parental cells to confirm that knockout of mSin1, and therefore loss of mTORC2 activity, blocks phosphorylation and activation of SGK3. I used 2 HEK293 mSin1 KO clones and performed a comparison with the parental cell line. Cells were serum starved overnight then stimulated with IGF1 for 10' at 50 ng/ml. This revealed strong activation of SGK3 and an increase in its phosphorylation at T320 on stimulation with IGF in the parental cell line, but not in the 2 knockout clones (Figure 6.2).

Similarly, phosphorylation of Akt at S473 which is also modulated by mTORC2 was fully blocked by mSin1 KO, and phosphorylation of the shared substrate NDRG1 was significantly reduced, although could still be partially induced by IGF1 stimulation.

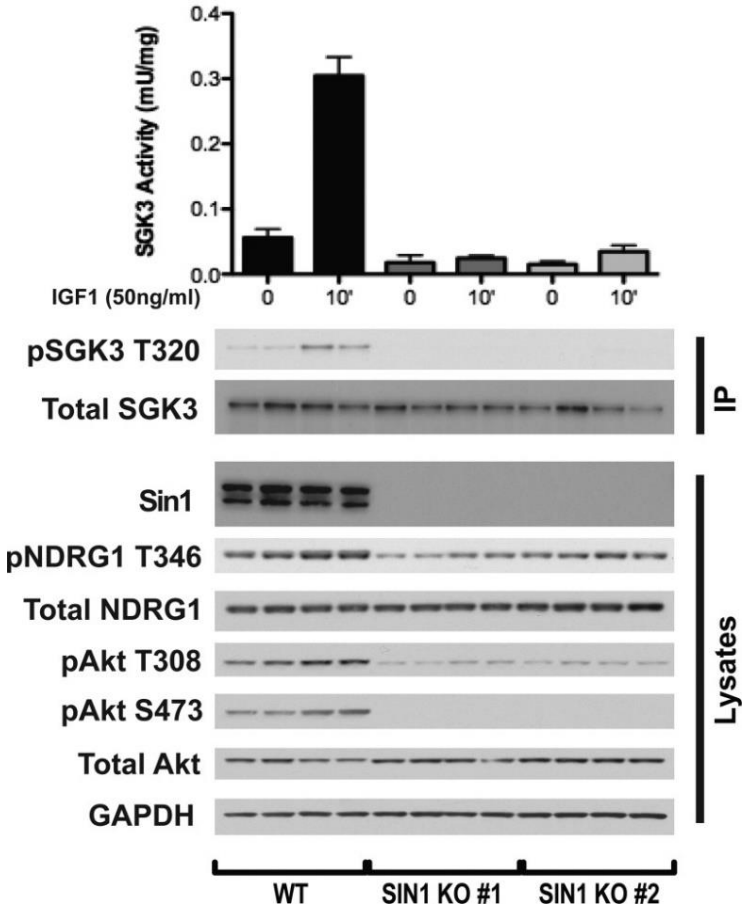

Figure 6.2 CRISPR/Cas9 knockout of mSin1 in HEK293 ablates activation of SGK3 and phosphorylation of its activation site.
Parental U2OS TREx cell lines and 2 mSin1 KO clones were serum starved overnight and stimulated with 50 ng/ml IGF1 10 minutes before lysis. SGK3 activity was measured by immunoprecipitation of SGK3 from 3 mg lysate and in vitro kinase assay against a peptide substrate. Lysates and eluted immunoprecipitated proteins were also subjected to immunoblot analysis using the antibodies specified. Error bars = SD, n=3.

6.2.3 Development of tools to study hydrophobic motif phosphorylation of SGK3

In order to robustly detect and study phosphorylation of SGK3 on its hydrophobic motif, it was necessary to develop a set of tools to assay this function. I first tested and optimised antibodies against both (a) Total SGK3 (S848D) and (b) the S486 hydrophobic motif site of SGK3 (LGF*SYAP) developed with MRCPPU Reagents and Services. As hydrophobic motif phosphorylation is necessary for activation of SGK3, I also assayed SGK3 phosphorylation by measuring (c) SGK3 *in*

vitro kinase activity as well as phosphorylation of its substrates in cells. In addition, I optimised (d) an *in vitro* mTORC2 kinase assay, by co-immunoprecipitating mTORC2 via HA-mSin1, to determine whether mSin1 mutations altered the ability of mTORC2 to phosphorylate SGK3 directly *in vitro,* or just in cells.

a. Total SGK3 antibody S848D

One of my first tasks in the lab was to develop a new polyclonal antibody against SGK3. The aim was to produce an antibody which could detect SGK3 by western blot, and also immunoprecipitate it from cells. In order to obtain an antibody specific for SGK3 over the other isoforms, the antibody was raised against a peptide corresponding to the N-terminal PX-domain of SGK3 (Residues 1-130, DU2034, Figure 6.3A). I tested the specificity of 7 bleeds of the antibody for western blot by comparing 10 µg HEK293 WT lysate with 10 µg lysate from SGK3-KO HEK293 cells. I determined from this assay that the 6th Bleed of the S848D antibody gave a very clean, specific signal, which was stronger than the previous S037D antibody (Figure 6.3B).

I also tested the ability of all bleeds to immunoprecipitate SGK3. Immunoprecipitation of SGK3 is critical for detection of SGK3's activation sites, T320 and S486 phosphorylation, and *in vitro* kinase assays against a peptide substrate. For each bleed of the antibody, I immunoprecipitated from 3 mg HEK293 lysate using a ratio of 1 µg antibody to 1 mg lysate. I compared the ability of these antibodies to immunoprecipitate SGK3 to the previous S037D antibody and a pre-immune IgG antibody as a negative control. I determined that all bleeds of the antibody were capable of immunoprecipitating SGK3 and, although none of the antibodies were able to fully deplete SGK3 from the supernatant, the best immunodepletion was again from the 6th bleed of S848D (Figure 6.3C). In this experiment I blotted with the panSGK antibody from Sigma Aldrich and found that only SGK3 was pulled down over the other isoforms, as expected. I also performed an *in vitro* kinase assay as a quantitative measure of immunoprecipitation and to confirm immunoprecipitated SGK3 still maintained kinase activity, and found bleeds 2-7 to give very

similar readouts, with substantially better activity than S037D (Figure 6.3D). I therefore used bleed 6 of the S848D anti-SGK3 antibody for the rest of this project.

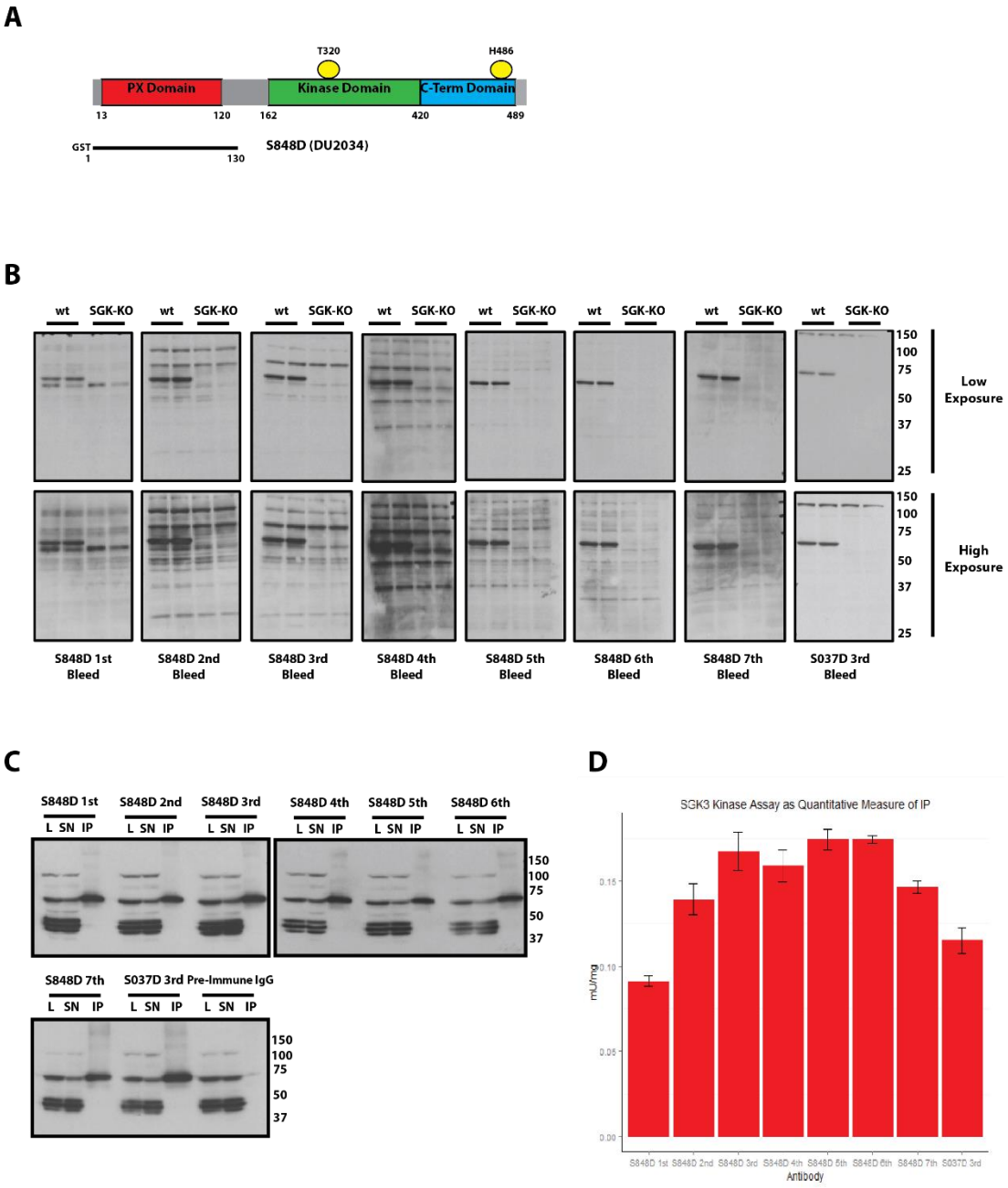

Figure 6.3 Characterisation of SGK3 antibody S848D.
A. *S848D was raised against residues 1-130 covering the PX domain of SGK3.* ***B.*** *7 bleeds of S848D were tested for their ability to detect SGK3 in 10 µg HEK293 lysate compared to an SGK3-KO control.* ***C.*** *7 bleeds of S848D were tested for their ability to immunoprecipitate SGK3 from HEK293.* ***D.*** *in vitro kinase assay of SGK3 immunoprecipitated using S848D antibody bleeds 1-7. Error bars = SD, n=3.*

b. Hydrophobic Motif antibody

To understand regulation of hydrophobic motif phosphorylation of SGK3, an antibody to detect phosphorylation of this site is critical for the progress of the project. Previous work in the lab has used a SGK1 pSer422 antibody to study this site, as after immunoprecipitation of SGK3 this antibody can cross-react to detect SGK3 phosphorylation. However, the cross-reactivity is very weak for SGK3, therefore this signal is not robust or reliable to assay hydrophobic motif phosphorylation. I therefore tested several antibodies against this site in order to generate a more robust readout of SGK3 phosphorylation.

I first tested 2 commercial antibodies, 1 SGK1 pS422 antibody from Abcam, and a PDK1-docking motif antibody from Cell Signalling Technology. This PDK1-Docking motif antibody is designed to recognise the hydrophobic FXXpS/TY/F motif which docks into the PIF-Pocket of PDK1. I tested the ability of these antibodies to detect SGK3 phosphorylation after serum starvation, stimulation of SGK3 phosphorylation with IGF1 and blockade of SGK3 phosphorylation by treatment with mTOR inhibitor AZD8055. In parallel, I also overexpressed SGK3 and stimulated with IGF as a positive control. Testing these antibodies against either 10 µg lysate or after immunoprecipitation of SGK3 from 3 mg lysate, I determined that these antibodies detected overexpressed, phosphorylated SGK3, but not the endogenous protein (Figure 6.4).

While the commercial antibodies were able to detect phosphorylation of overexpressed SGK3, I was interested in this project in analysing phosphorylation and activation of the endogenous protein. I therefore generated an antibody with MRCPPU Reagents and Services raised against the Hydrophobic motif site of SGK3. Antibody SA517 was raised against the sequence indicated in the sequence alignment below (Figure 6.5). In order to generate the antibody, 2 immunogenic peptides were produced of this sequence, tagged with an Ahx-Cys motif in either terminus for purification purposes.

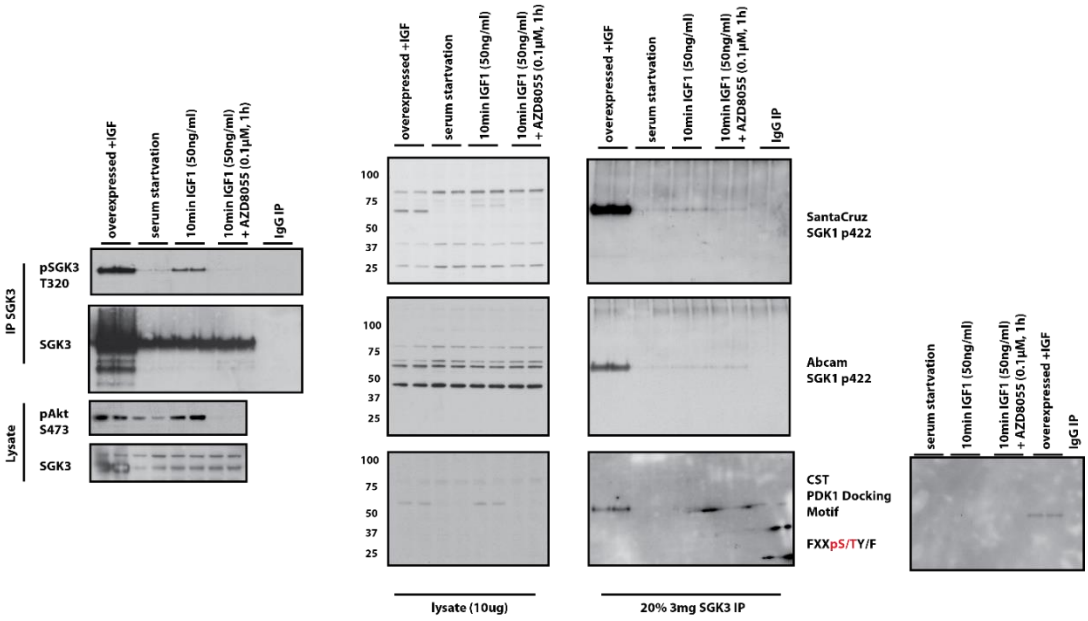

Figure 6.4 Commercial antibodies tested do not recognise S486 phosphorylated endogenous SGK3.
HEK293 cells were serum starved overnight, before stimulation with 50 ng/ml IGF1 for 15 minutes before lysis. mTORC2 activity was modulated by treatment with and without mTOR inhibitor AZD8055 (0.1 μM, 1h) and IGF1 stimulation (50 ng/ml, 10 min). Ability of antibodies to detect immunoblot was tested from 10 μg lysate or after a 3mg IP of SGK3.

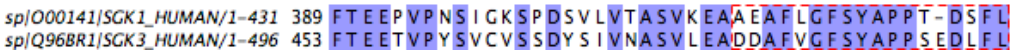

Figure 6.5 Sequence alignment of the SGK1 and SGK3 hydrophobic motif sites.
Antibody SA517 was raised against the residues indicated in the alignment.

The resultant antibody was then purified using either the N-terminally tagged Peptide A or the C-terminally tagged Peptide B. In order to determine the sensitivity and selectively of these antibodies, I first tested their ability to recognise overexpressed SGK3. As before, I serum starved cells overnight, then stimulated SGK3 phosphorylation by addition of IGF1, in the presence or absence of an mTOR inhibitor. Figure 6.6 shows the results for Bleeds 1 and 5. Antibodies were dissolved to 1 μg/ml in the presence of 10 μg/ml non-phosphorylated peptide. While all bleeds of the antibody were able to detect overexpressed SGK3, this detection was found not to be phospho-specific, as detection was equal across all conditions (Figure 6.6).

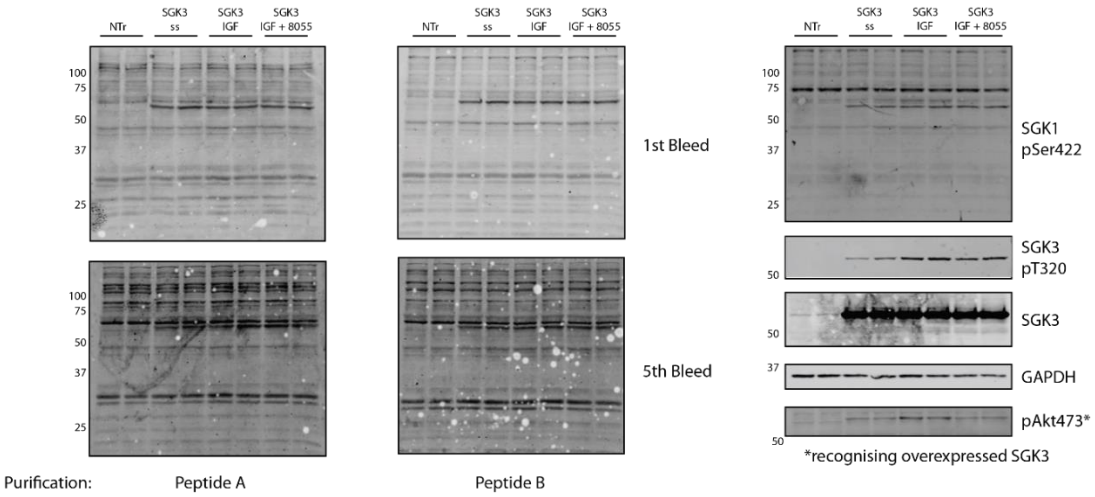

Figure 6.6 SA517 recognises overexpressed SGK3, however is not phosphospecfic.
SGK3 was exogenously overexpressed in HEK293 cells for 24 h. Following transfection, cells were serum starved overnight before treatment with or without mTOR inhibitor AZD8055 (0.1 µM, 1 h) and IGF1 (50 ng/ml, 10 min). Lysates were subject to immunoblot analysis with the indicated antibodies. SGK3 pS486 antibodies were incubated with 10 µg/ml non-phosphorylated peptide corresponding to the phosphosite.

It was possible that this lack of phosphospecificity was due to the large amounts of protein being detected, masking a phospho-specific signal. I therefore used the best antibody from this screen, Bleed 1 purified by peptide B, to probe the phosphorylation of endogenous SGK3. In this experiment I found that, even after immunoprecipitation, this antibody was unable to detect phosphorylation of endogenous SGK3, although again it could recognise overexpressed protein (Figure 6.7)

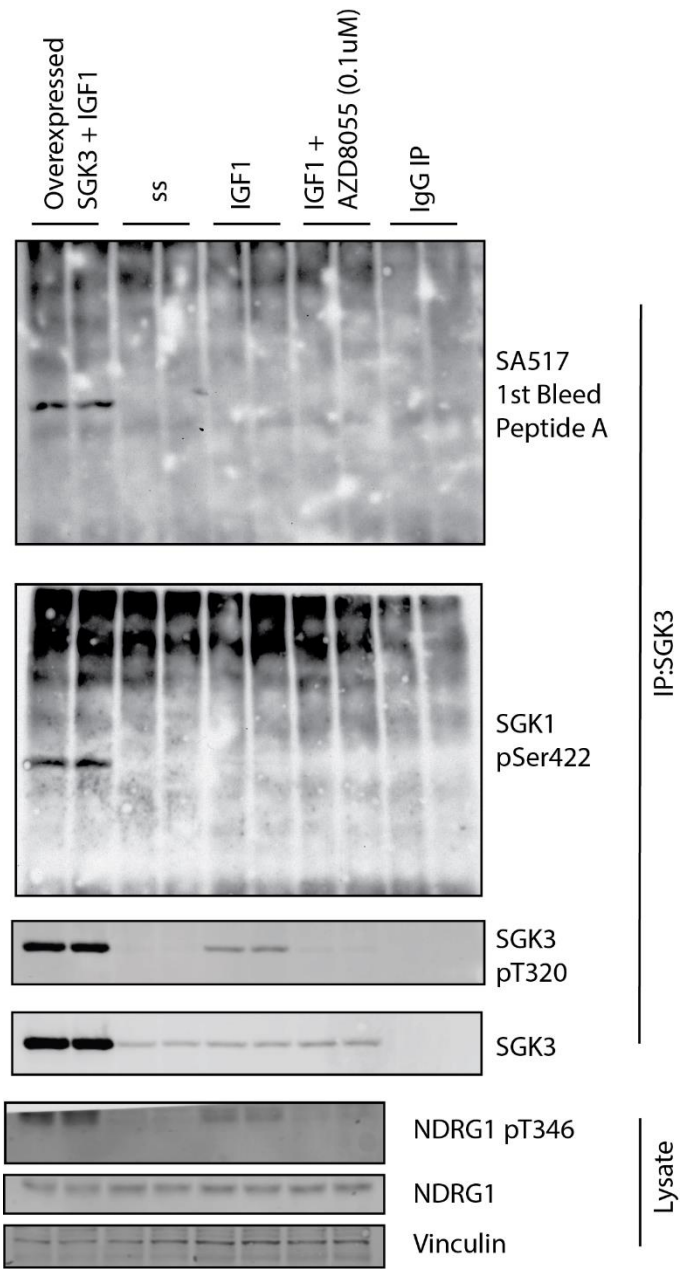

Figure 6.7 SA517 does not recognise endogenous phosphorylated SGK3.
Endogenous or exogenously overexpressed SGK3 was immunoprecipitated from HEK293 cells, which had been starved of serum for 16 h. Before lysis, cells were treated with or without mTOR inhibitor AZD8055 (0.1 µM, 1 h) and IGF1 (50 ng/ml, 10 min). Immunoprecipitated SGK3 and whole cell lysate were subject to immunoblot analysis with the antibodies shown.

c. Substrate phosphorylation

Another readout for studying the activation of SGK3 is through analysing phosphorylation of its substrates. NDRG1 phosphorylation at Thr346 has been extensively used in our lab as a readout of SGK3 phosphorylation, however use of this substrate is complicated by the fact NDRG1 phosphorylation is also carried out by Akt and SGK1. I have used phosphorylation of NDRG1 as

a readout in my assays however this will be confounded by Akt-driven phosphorylation. As described in Chapter 4, two members of the Syntaxin family, STX7 and STX12 appear to be specifically phosphorylated by SGK3, and PostDoc Athanasios Karapetsas has developed a robust PhosTag assay for detection of Syntaxin phosphorylation (Malik *et al.*, 2019). This assay will provide a useful tool in assaying SGK3 activity, and therefore hydrophobic motif phosphorylation, and will be used in future assays. In addition, a phospho-specific antibody for detection of STX12 phosphorylation by SGK3 is in development. I also measure *in vitro* kinase activity of SGK3 against a peptide substrate Crosstide after immunoprecipitation from cells.

d. mTORC2 *in vitro kinase assay*

In order to determine whether mSin1 variations impacted on the ability of mTORC2 to phosphorylate SGK3, SGK1 or Akt *in vitro*, I developed an *in vitro* mTORC2 kinase assay via immunoprecipitation of HA-mSin1 constructs and incubation with recombinantly expressed substrate SGK3, SGK1 and Akt protein.

To produce recombinant substrate protein, I expressed GST-tagged kinase inactive (KI) SGK3, Akt and SGK1 in HEK293 cells. Kinase inactive constructs were chosen to remove the chance of autophosphorylation of the site in *in vitro* conditions. To ensure full dephosphorylation of the hydrophobic motif site, I serum starved cells overnight and treated with mTOR inhibitor AZD8055 for 1 h before lysis. By GST purification I was able to produce large amounts of relatively pure substrate protein, as shown in figure 6.8

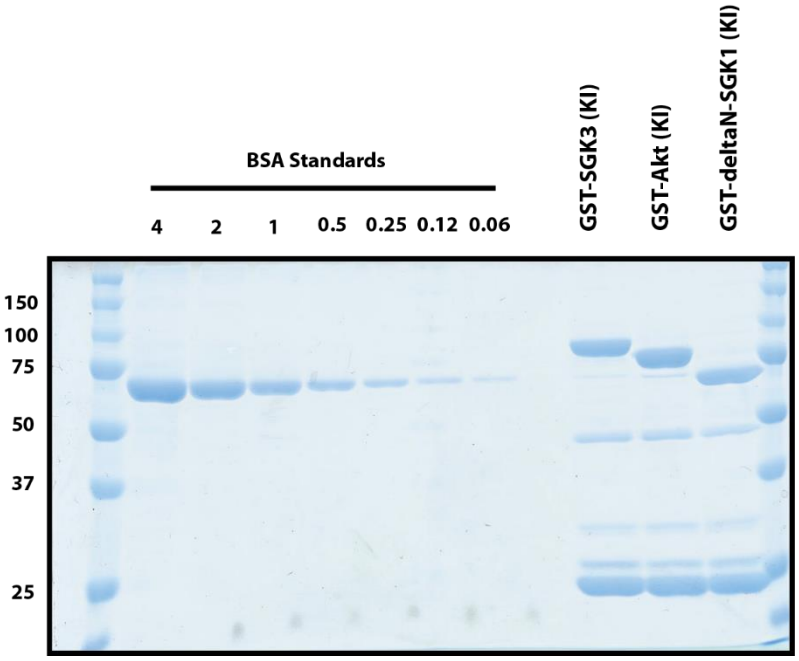

Figure 6.8 Substrate purification of GST-SGK3, GST-Akt and GST-deltaN SGK1.
Kinase-inactive (KI) GST-SGK3, GST-Akt and GST-(60-end)-SGK1 were transiently expressed in HEK293 cells. 24 h after transfection, cells were serum starved overnight, and treated with mTOR inhibitor AZD5363 (0.1 μM, 1 h) before lysis, to remove any hydrophobic motif phosphorylation of the substrate protein.

I then used Akt as a positive control substrate and was able to robustly detect phosphorylation of Akt after immunoprecipitation from HA-mSin1 cells, but not the mSin1 KO cells, as expected. This *in vitro* phosphorylation was also blocked by mTOR inhibitor AZD8055 (Figure 6.9A). Phosphorylation of Akt could be specifically detected by both the specific Akt p473 antibody and the pPDK1-Docking Motif antibody (Figure 6.9A).

Using these same conditions against substrate SGK1 and SGK3, I was again able to produce specific phosphorylation of substrate protein at the hydrophobic motif site, as measured by the SGK1 p422 antibody from Sigma Aldrich. Unfortunately, the pPDK1-Docking Motif antibody displayed poor recognition of the phosphorylated SGK isoforms, and therefore could not be used as a readout for all substrate proteins (Figure 6.9B). However, it was evident from this experiment that detection of SGK3 phosphorylation with the pSer422 antibody was very weak, so I therefore optimized these blotting conditions and determined that a 1:1000 dilution of the pSGK antibody specifically detected 40ng of phosphorylated SGK3 (Figure 6.9C). Meanwhile,

phosphorylated SGK1 was better detected using a 1:2000 dilution of the antibody against 10ng substrate protein (Figure 6.9C).

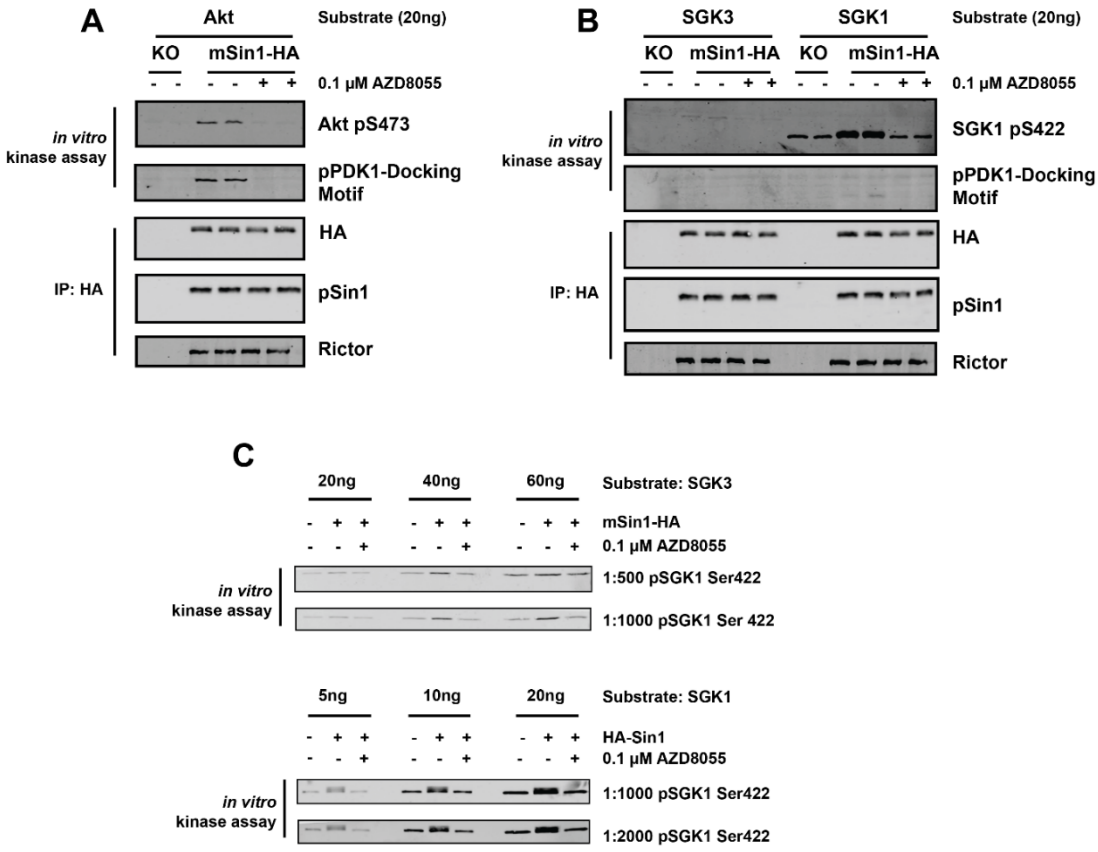

Figure 6.9 Development of an mTORC2* in vitro *kinase assay.
A. *mTORC2 immunoprecipitated from HA-mSin1 expressing cells phosphorylated substrate Akt in vitro.* ***B.*** *in vitro kinase assay against SGK3 and SGK1* ***C.*** *Optimisation of antibody concentration and protein loading for specific identification of substrate phosphorylation*

6.2.4 Reintroduction of mSin1 variants

I next proceeded to generate a series of stable cell lines expressing mSin1 variants (described in Fig 6.10) from a doxycycline-inducible promotor in the TREx mSin1 KO cells. Information from these cell lines could determine the ability of mSin1 variants to activate mTORC2 against SGK3 or Akt and therefore determine the functional role of different regions of mSin1.

Several functional domains have been annotated within the sequence of mSin1, as shown in figure 6.10. Incorporation of mSin1 into mTORC2 is mediated by the N-terminal sequence (Yao *et al.*, 2017). Evolutionary sequence analysis also revealed a Raf-like Ras-binding domain, with the ability to bind activated Ras, and a Pleckstrin-Homology (PH) domain, which mediates

membrane and lipid binding (Schroder *et al.*, 2007). The Conserved Region in the Middle (CRIM) domain is less well characterised, but may play a role in mTORC2 substrate recognition (Tatebe *et al.*, 2017).

I first introduced the 5 known transcript variants of mSin1. If activation of SGK3 in the absence of PI3K is mediated by mSin1, one naturally occurring form of mSin1 would theoretically be responsible. These transcript variants are shown in Figure 6.10. The most highly expressed variants of mSin1 are the full length TV1 and TV2, which contains a small deletion in the RBD. TV3-5 are less commonly expressed. All variants except TV4 are believed to be able to form a complex with mTORC2, whereas TV4 lacks the N-terminal domain critical for binding the complex. TV5 carries a C-terminal variant which lacks the PH domain proposed to be critical for activity of mTORC2 (Liu *et al.*, 2015).

I also generated point mutations and truncations designed to disrupt the RBD and PH Domain. The point mutations in the mSin1-PHmut construct are R393C K428A K464A, as described in Liu *et al*., 2015. These residues were predicted by modelling against the PH domain of Akt to disrupt binding to PtdIns(3,4,5)P_3. The mSin1-RBD mutant sequence carries an R312L mutation, which I designed by sequence alignment and homology to the R89L inactivating mutant of cRAF (Zeng *et al.*, 1999). These mutants are also shown in Figure 6.10

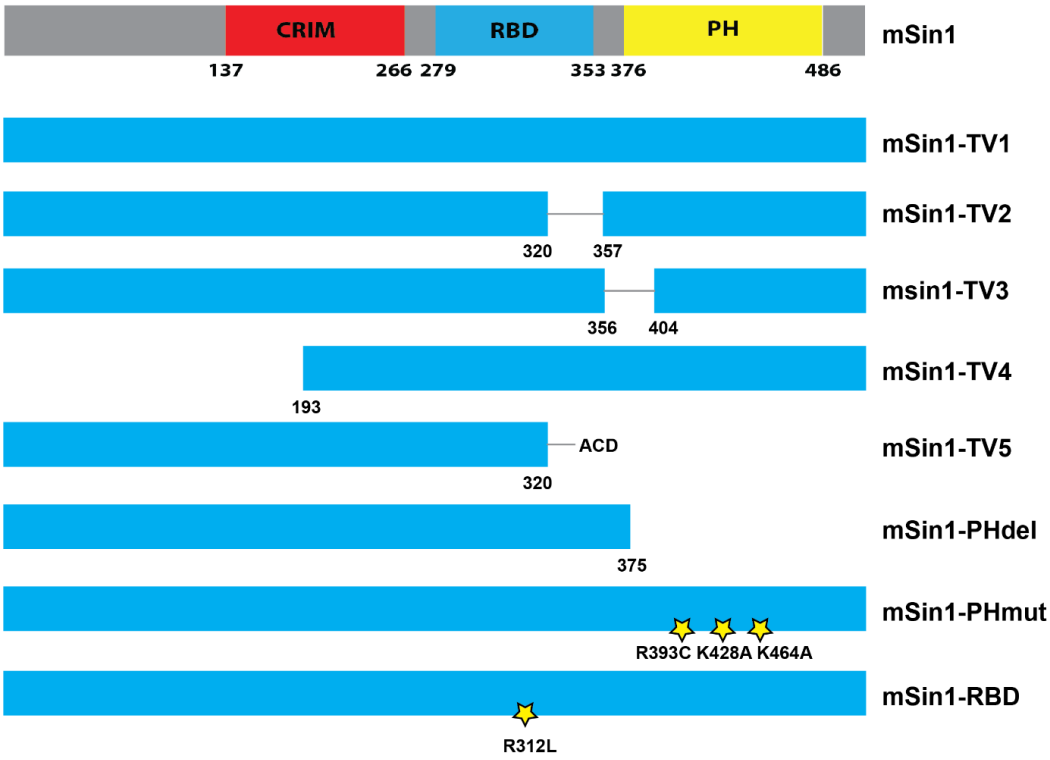

Figure 6.10 Transcript variants and mutants of mSin1 used in this study.
Variants were incorporated in TREx cells with a C terminal HA tag.

Figure 6.11 shows the re-expression of these constructs under the doxycycline-inducible system in the U2OS mSin1 KO clone P1E7. With the exception of Transcript Variant 4 (TV4) which does not incorporate into mTORC2, all variants rescued turn motif phosphorylation of Akt, which occurs cotranslationally and is not under the control of growth factor signalling. I proceeded to use these cell lines to perform initial assays to survey the effects of each of the variants and mutants on SGK3 and Akt phosphorylation.

As an initial screen of these mSin1 variants, and their ability to mediate phosphorylation of Akt and SGK3, all cell lines were stimulated with IGF1 following serum starvation and assayed for SGK3 kinase activity and Akt Hydrophobic motif phosphorylation (Figure 6.12). This screen revealed a number of interesting results for further investigation. The full-length variant TV1 and near-full length TV2 both showed activity comparable to the parental cell line. As expected TV4, lacking the N-terminal domain is unable to mediate activation of Akt or SGK3. This agrees

with previous published data suggesting TV4 cannot integrate into an active mTORC2 complex as this occurs through the N-terminus of mSin1.

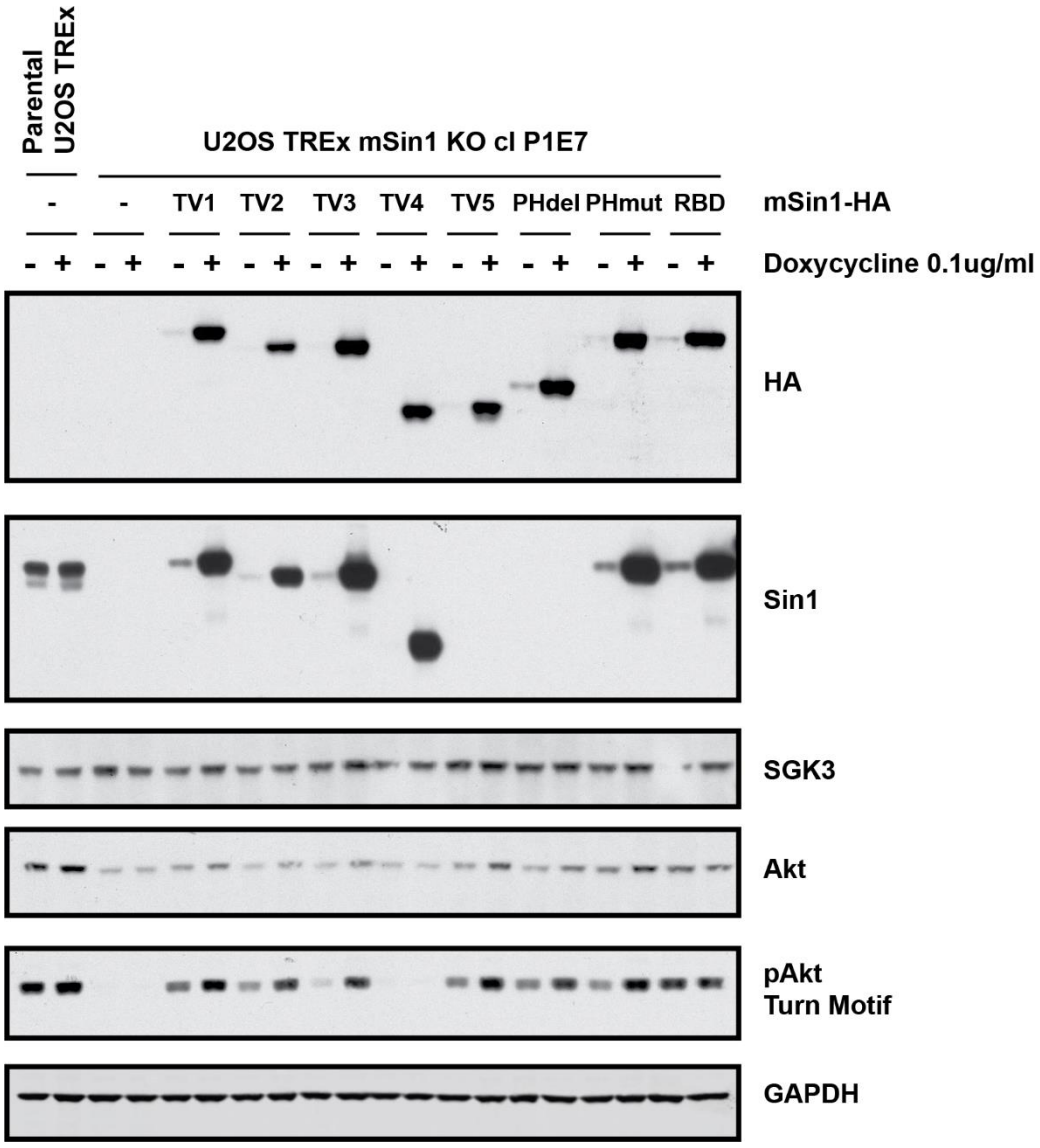

Figure 6.11 Doxycycline-induced re-expression of mSin1 variants in U2OS mSin1 KO cells.
Stable cell lines were generated to express mSin1 variants under a doxycycline-inducible promotor. Cells were stimulated in the presence or absence of 0.1 µg/ml Doxycycline for 24 h, and after lysis were subject to immunoblot analysis with the specified antibodies.

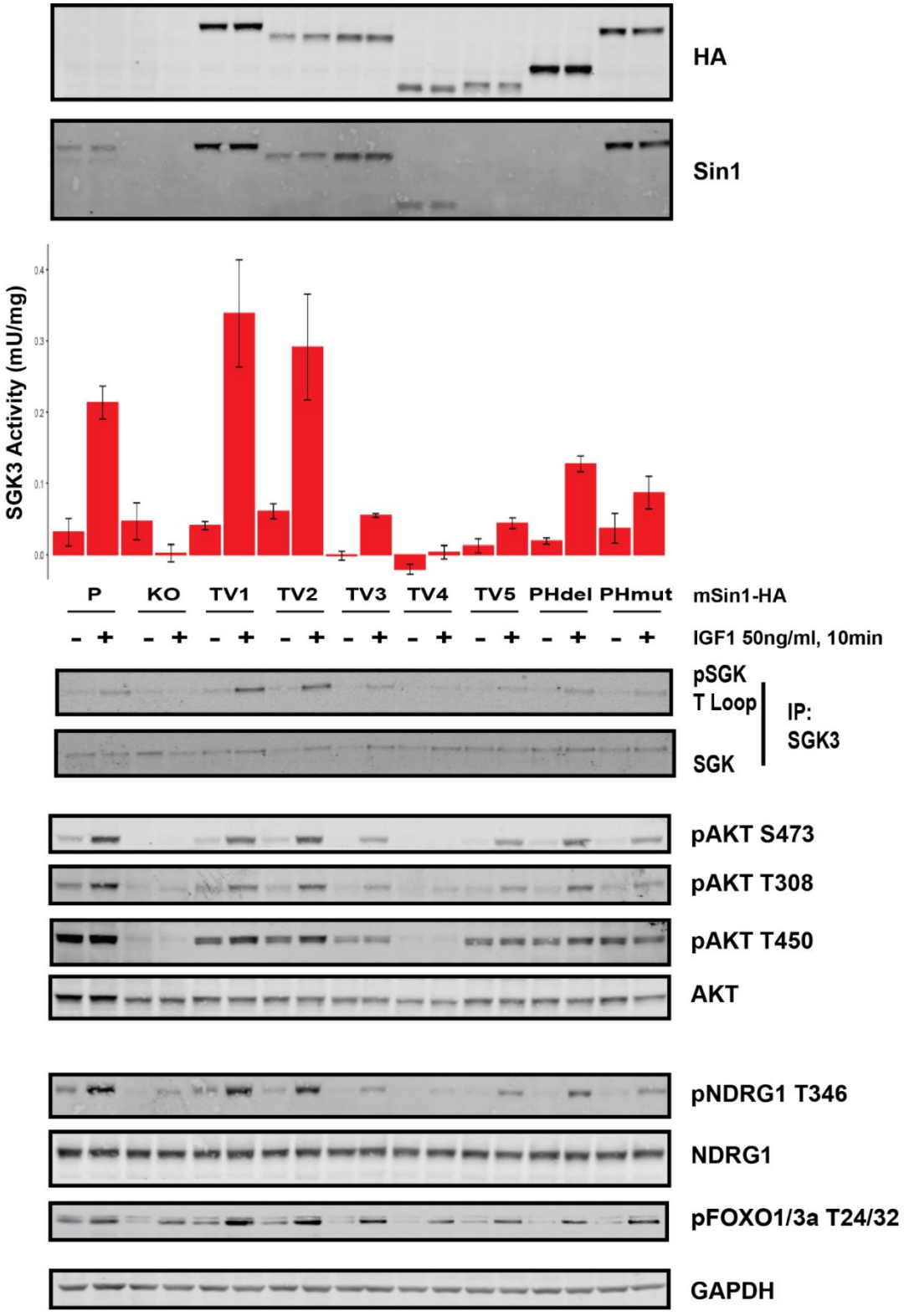

Figure 6.12 Reexpression of mSin1 in KO cells rescues phosphorylation and activation of SGK3.
The mSin1-HA variants were expressed in mSin1-KO U2OS cells by induction with 0.1 µg/ml Doxycycline. These cells, alongside parental (P) and mSin1-KO (KO) cells were serum starved overnight, before stimulation with or without IGF1 and cell lysis. SGK3 was immunoprecipitated from 3 mg lysate for in vitro kinase assay against Crosstide substrate, and immunopreciptates and whole cell lysate subject to immunoblot analysis with the antibodies indicated. Error bars = SD, n=3

Previous data from, for example Liu *et al*, suggested that the PH domain of mSin1 is critical for mTORC2 activity against Akt, and that this activity is mediated via $PI(3,4,5)P_3$. However, in this assay, both Akt and SGK3 could be partially activated by the PH-domain deletion and binding-mutant mSin1 cell lines, although not to the same extent as the full-length version. This suggests that a second mechanism aside from the PH domain may play a secondary role in Akt/SGK3 activation. Another interesting result was that both TV3 and TV5 mSin1 were able to mediate activation of Akt, but not SGK3, suggesting a differing mechanism of substrate recognition of SGK3 and Akt by mTORC2.

6.2.5 Full length mSin1 does not fully reactivate SGK3

Although the initial screen using these cells revealed full phosphorylation and activation of SGK3, in this assay TV1 was very highly expressed in comparison to the parental cell line and many of the other mSin1 variants. In figure 6.13, I repeated this assay with expression of mSin1 normalised to parental expression. I determined in this assay that full length mSin1 only partially rescues the phosphorylation and activation of SGK3. I also repeated this assay in 2 independent HEK293 KO clones and found similar results (Figure 6.14)

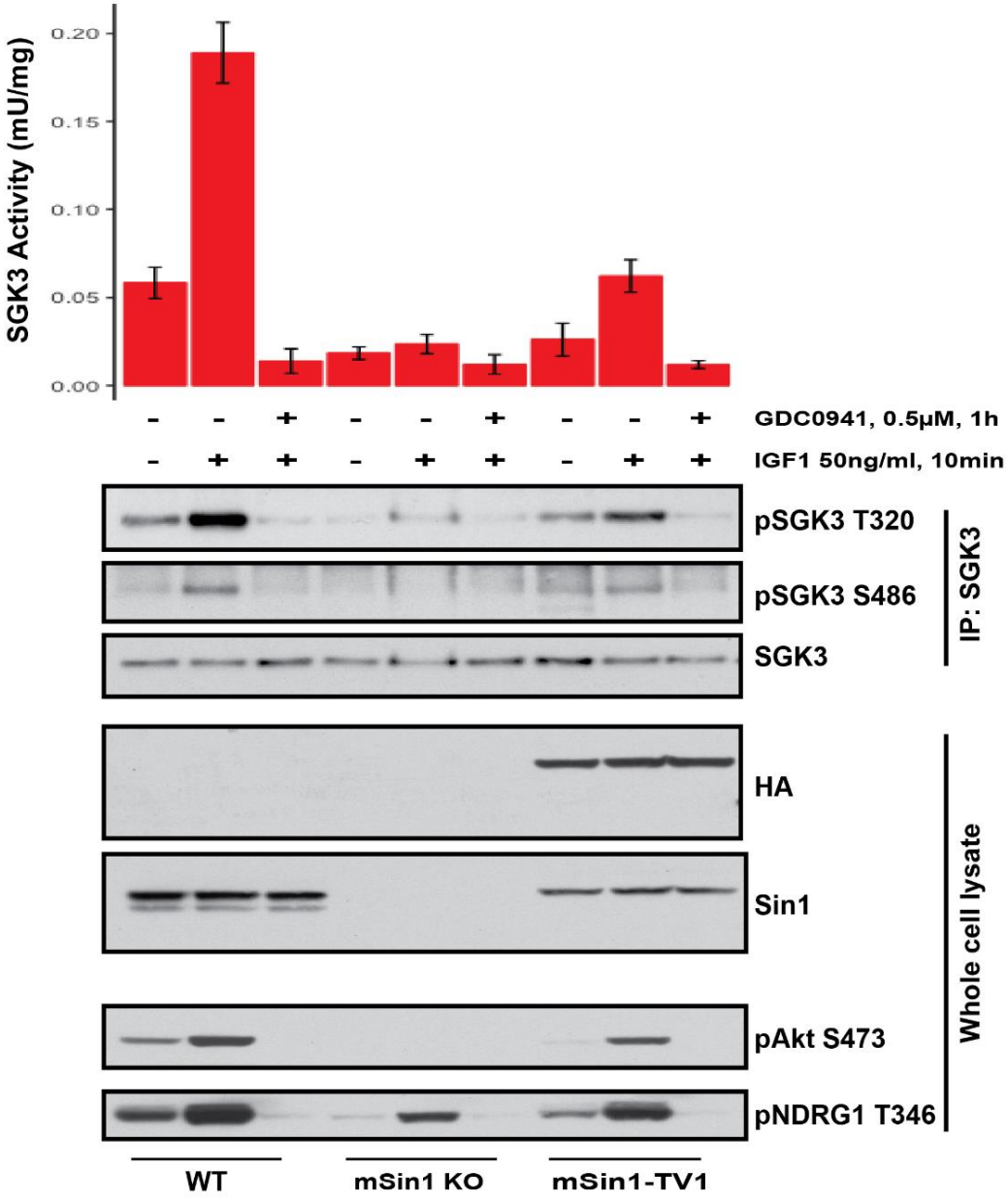

Figure 6.13 Reexpression of full length mSin1 does not fully rescue SGK3 phosphorylation in mSin1 knockout cells.

Full length mSin1-HA (mSin1-TV1) was expressed in mSin1-KO U2OS cells by induction with 0.1 μg/ml Doxycycline. These cells, alongside parental (P) and mSin1-KO (KO) cells were serum starved overnight, before stimulation with or without IGF1 and cell lysis. Endogenous SGK3 was immunoprecipitated from 3 mg lysate for in vitro kinase assay against Crosstide substrate, and immunopreciptates and whole cell lysate subject to immunoblot analysis with the antibodies indicated. Error bars = SD, n=3

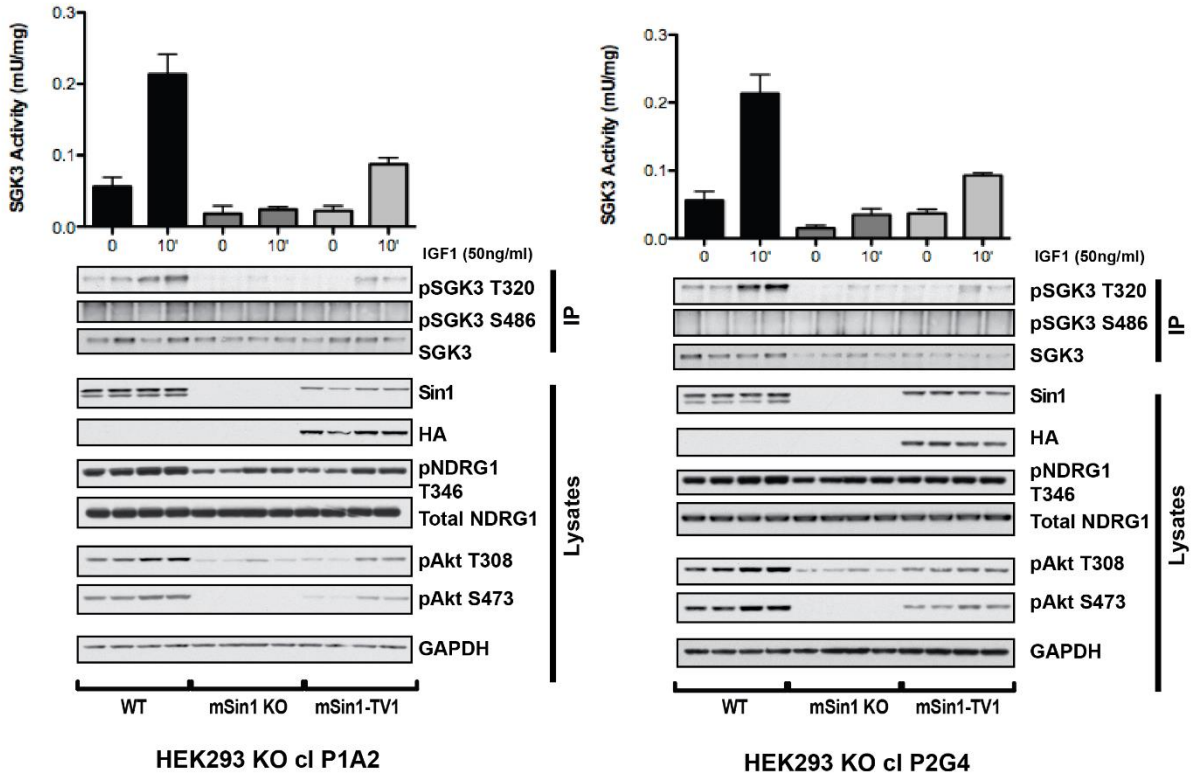

Figure 6.14 In 2 HEK293 mSin1 KO clones, re-expression of mSin1 only partially rescues the phenotype. *Full length mSin1-HA (mSin1-TV1) was transiently overexpressed in 2 independent mSin1-KO HEK293 cells. These cells, alongside parental (P) and the relevant mSin1-KO (KO) cells were serum starved overnight, before stimulation with or without IGF1 and cell lysis. Endogenous SGK3 was immunoprecipitated from 3 mg lysate for in vitro kinase assay against Crosstide substrate, and immunopreciptates and whole cell lysate subject to immunoblot analysis with the antibodies indicated. Error bars = SD, n=3*

However, I determined that when expressing mSin1-TV2 in these cells, SGK3 phosphorylation and activity was fully rescued. Interestingly, I also saw full rescue of activity from the mSin1-RBD binding mutant. This is interesting as mSin1-TV2 differs from the full length transcript of mSin1 through a short deletion within the RBD. As mutation of this domain has the same effect on activity, this therefore suggests this region of the protien is important in regulating SGK3 phosphorylation and activation.

However, a caveat to this experiment is that both TV2 and RBD expressed much higher than parental levels and TV1 expression, and therefore cannot be directly compared. Akt rescue is also deficient in TV1 in this experiment but not rescues in Figure 6.13 and 6.14. Experiment ought to be repeated with equalised expression. An alternative to avoid unequal expression would be to restore variants at the native mSin1 locus by CRISPR/Cas9.

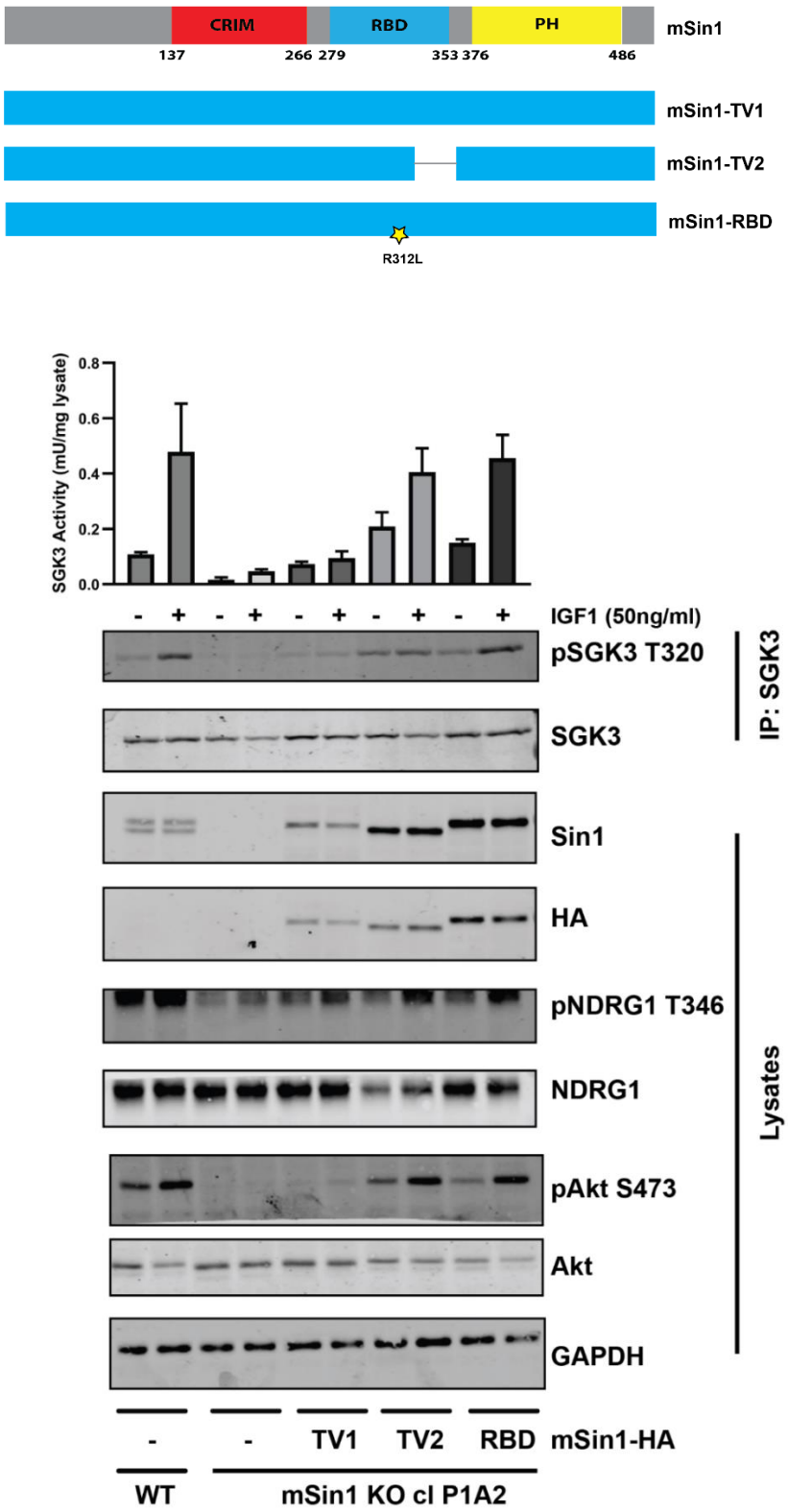

Figure 6.15 TV2 and RBD fully rescues SGK3 phosphorylation and activity.
The indicated *mSin1-HA variants were transiently overexpressed in mSin1-KO HEK293 clone P1A2. These cells, alongside parental (P) and mSin1-KO (KO) cells were serum starved overnight, before stimulation with or without IGF1 and cell lysis. Endogenous SGK3 was immunoprecipitated from 3 mg lysate for in vitro kinase assay against Crosstide substrate, and immunopreciptates and whole cell lysate subject to immunoblot analysis with the antibodies indicated. Error bars = SD, n=3*

6.2.6 How is the mSin1 PH domain impacting on phosphorylation of SGK3.

In my initial screen (figure 6.12) I identified that, although reduced, SGK3 and Akt phosphorylation and activation could still occur upon mutation or deletion of the mSin1 PH domain. This is in contradiction of previous literature (Liu *et al*, 2015), which proposed that PH domain binding to PtdIns(3,4,5)P_3 was critical for activity of mTORC2 against Akt. I therefore repeated expression of mSin1-TV1, mSin1-PHdel and mSin1-PHmut in U2OS mSin1 KO cells to validate the result. Again, I found that, although phosphorylation was impacted, SGK3 phosphorylation and activation could still occur. Conversely, Akt phosphorylation at its Ser473 site was relatively unaffected (Figure 6.16).

In this and future experiments, I also measured phosphorylation of mSin1 at T86 using a phospho-specific antibody. The role of this phosphorylation site is unclear, it lies within the canonical RxRxxS/T motif, and has previously been associated with positive feedforward phosphorylation by Akt or negative feedback regulation by S6K1 in different cell types (Liu *et al.*, 2014; Humphrey, Azimifar and Mann, 2015; Yang *et al.*, 2015). I therefore was interested in any association with this phosphorylation site and SGK3 phosphorylation and activation downstream of mTORC2. In this experiment, I observed that T86 phosphorylation was reduced in the PH-domain mutation and deletion mutants, which were deficient in SGK3 activation, despite fairly equal expression of mSin1.

As these mutants are deficient for phosphorylation of SGK3 in cells, I decided to study the effect these mutations had on mTORC2 function *in vitro*. I therefore immunoprecipitated the same mSin1-HA variants from cells and performed an *in vitro* mTORC2 kinase assay against SGK3. In this *in vitro* assay, mTORC2 immunoprecipitated by these constructs showed no defect in phosphorylation of SGK3, in fact phosphorylation appeared to be enhanced (Figure 6.17).

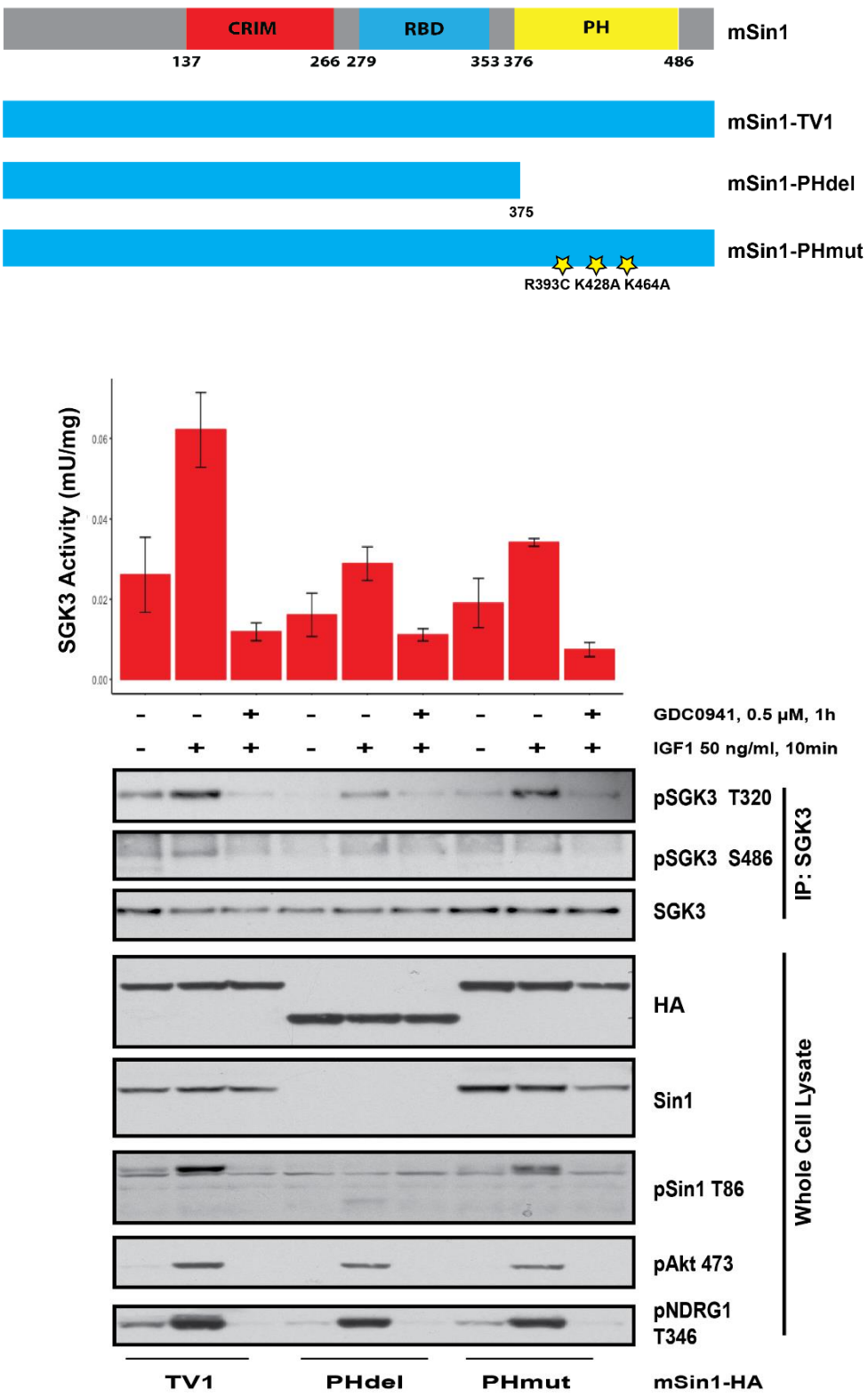

Figure 6.16 PH deletion and mutation constructs still maintain partial activity against SGK3 and Akt. *Full length mSin1 (TV1) and PH-domain deletion and mutation variants were re-expressed in mSin1 KO U2OS cells. SGK3 was immunoprecipitated from cells and assayed for its in vitro kinase activity, alongside blotting for the T320 and S486 phosphorylation sites. Error bars = SD, n=3*

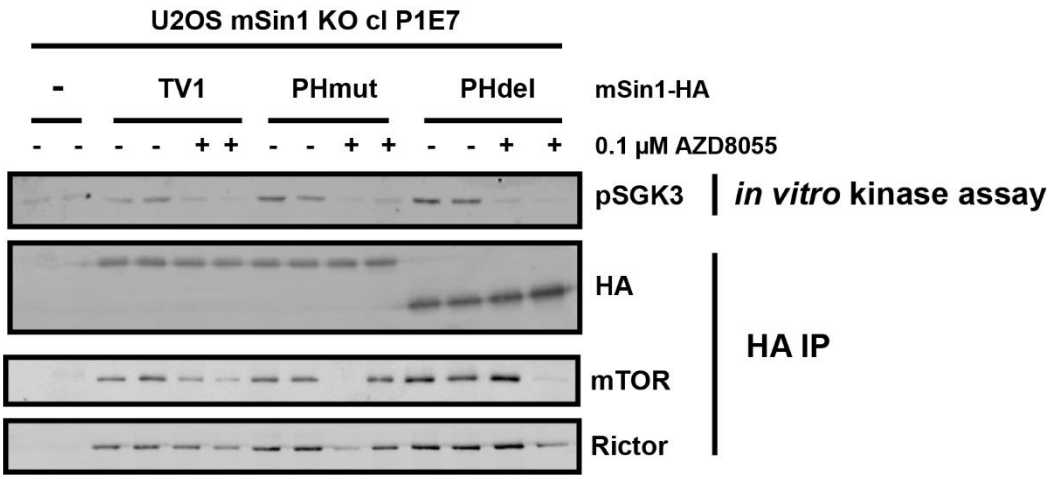

Figure 6.17 PH deletion and mutation have no effect on ability of mTORC2 to phosphorylate SGK3 in vitro.
mTORC2 was immunoprecipitated from mSin1 KO cells expressing full length (mSin1-TV1), or PH-domain deletion and mutation variants. Immunopreciptates were assayed against recombinantly expressed SGK3 in an in vitro kinase assay. The resulting protein was blotted for phosphorylation on its hydrophobic motif. Immunoprecipitates from mSin1 KO cells not expressing mSin1-HA and mTOR inhibitor AZD8055 were used as negative controls

6.2.7 How is the mSin1 Ras Binding Domain (RBD) impacting on activation of SGK3?

Given that PH-binding deficient variants of mSin1 were still able to partially lead to phosphorylation of SGK3, I next tested whether this deficiency could be compensated for the Ras Binding Domain (RBD) of mSin1. Therefore, I generated a double mutant cell line carrying both the PH-binding point mutations and mutation of the Ras Binding Domain. Unexpectedly, instead of this second mutation further inactivating mTORC2 and reducing SGK3 activation, I discovered a recovery of activity upon inactivation of the RBD (Figure 6.18). This therefore suggests that the RBD may be a negative regulator of SGK3 phosphorylation by mTORC2 and warrants further investigation. Additionally, it will be interesting to measure the effect of PH-domain mutations in mSin1 TV2, which carries a deletion of the Ras Binding Domain. It is possible that, without the Ras binding activity, TV2 is not reliant on the PH domain and is therefore not subject to PtdIns lipid regulation and may therefore be responsible for activation of SGK3 in the absence of Class I PI3K activity. Sequence analysis predicted the RBD of mSin1 to be a Raf-like RBD, which is able to bind to bind to activated Ras (Schroder *et al.*, 2007). It has been previously demonstrated that activating mutations in Ras can activate SGK3 (Malik *et al.*, 2018).

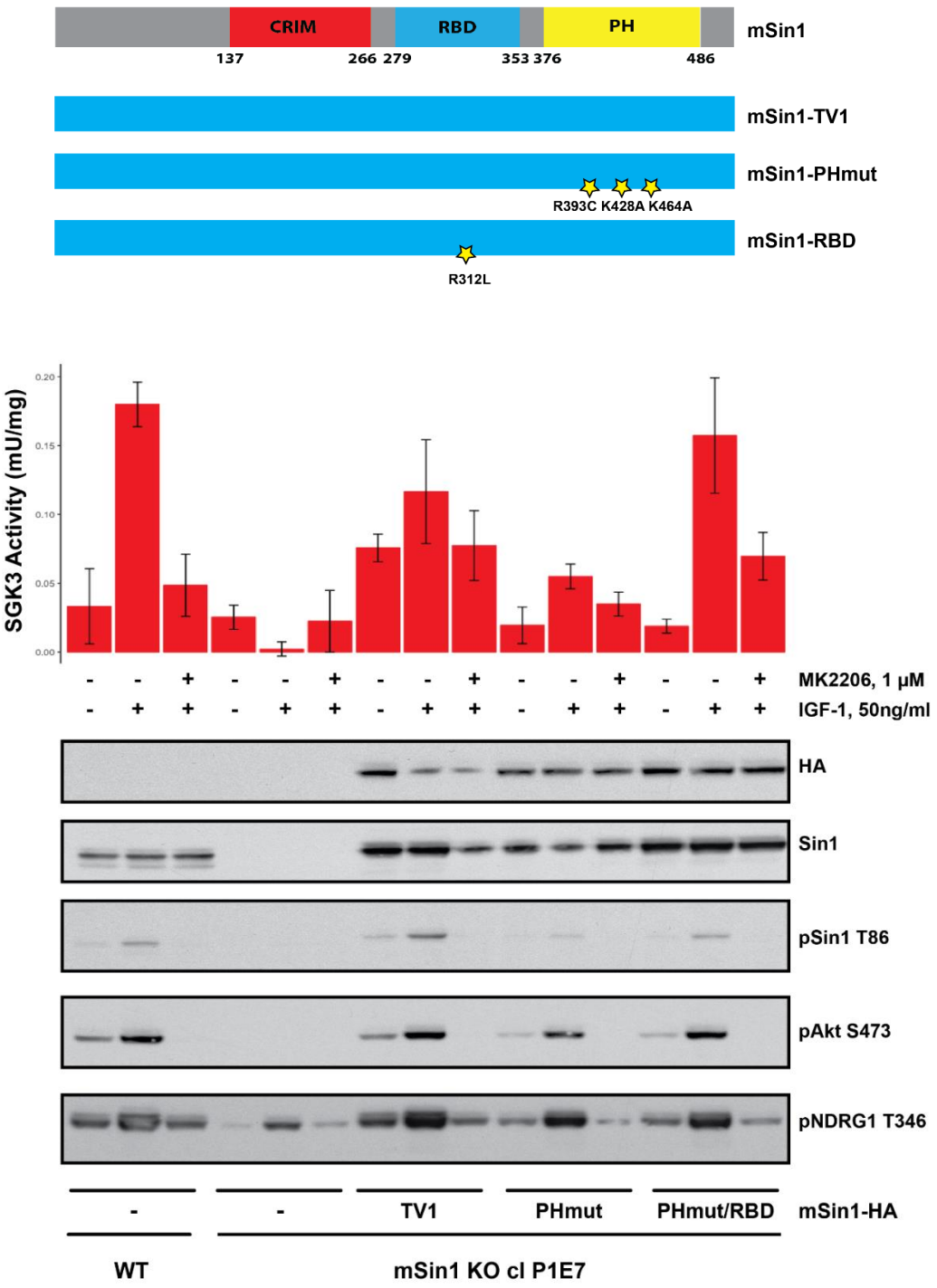

Figure 6.18 Reexpression of TV1,PHmut and PH/RBD double mutant in mSin1 KO cells.
U2OS mSin1 KO cells reexpressing mSin1 under a doxycycline-inducible system were analysed for their ability to activate SGK3. mSin1_TV1, mSin1_PHmut and mSin1_PHmut/RBDmut were expressed, cells were serum starved overnight and stimulated with 50 ng/ml IGF1 for 15 minutes, in the presence or absence of Akt inhibitor MK2206. SGK3 activity upon IGF1 stimulation was measured by immunoprecipitation and in vitro kinase assay. Error bars = SD, n=3

Again, in this experiment I observed that T86 phosphorylation was reduced in the PHmut form of mSin1, which was partially rescued by the PH/RBD double mutant. Additionally, treatment

with the Akt inhibitor MK2206 reduced T86 phosphorylation in these cells, suggesting in U2OS T86 is a substrate of Akt, and may mediate the observed downregulation of SGK3 activity in these cells upon MK2206 treatment.

6.2.8 What is the significance of mSin1 T86 phosphorylation?

As mentioned above, I observed in several experiments that phosphorylation of Thr86 of mSin1 was substantially reduced in variants of mSin1 which are less able to induce phosphorylation of SGK3. This site lies within the canonical RxRxxS/T motif, and has previously been proposed to be phosphorylated by Akt and S6K1 in different cellular contexts (Liu *et al.*, 2014; Humphrey, Azimifar and Mann, 2015; Yang *et al.*, 2015). While I could observe a defect in phosphorylation of this site, it could not be determined from this data whether T86 phosphorylation was a necessary upstream regulator for SGK3 phosphorylation or was itself a substrate of SGK3.

In order to answer these questions, I have generated cell lines expressing both mSin1-TV1 and mSin1-TV2 carrying T86A and T86E mutations. In future work it will be important to use these cell lines in order to study the effect of these mutations on SGK3 phosphorylation and whether T86 phosphorylation was required for activity.

I additionally studied phosphorylation of mSin1 downstream of SGK3, by inducing SGK3 activity in ZR-75-1 cells with 5 day Akt inhibitor treatment (MK2206, 1 µM). As described in previous chapters, prolonged treatment of ZR-75-1 cells with MK2206 results in a transcriptional upregulation and activation of SGK3, and the protein kinase can substitute for Akt activity in the phosphorylation of substrates.

Under basal and prolonged inhibitor conditions, I treated cells for 1 h before lysis with the MK2206 (1 µM) or the SGK inhibitor 14H. In basal conditions, as in the U2OS cells, treatment with the Akt inhibitor reduced phosphorylation of mSin1 at T86. However, treatment with the 14H inhibitor had no effect. Therefore, mSin1 is likely a substrate of Akt and not significantly

phosphorylated by SGK3 under these conditions. Upon 5 day treatment with MK2206, phosphorylation of mSin1 and the common substrate NDRG1 was recovered. Under these conditions I observed that Sin1 phosphorylation was not reduced by treatment with SGK3 inhibitor 14H, whereas SGK3 substrate NDRG1 phosphorylation was affected (Figure 6.19). Therefore, mSin1 is likely not a direct substrate of SGK3. It would be of interest to further characterise this phosphorylation site in future work, to determine its relevance to phosphorylation and activation of SGK3 by mTORC2.

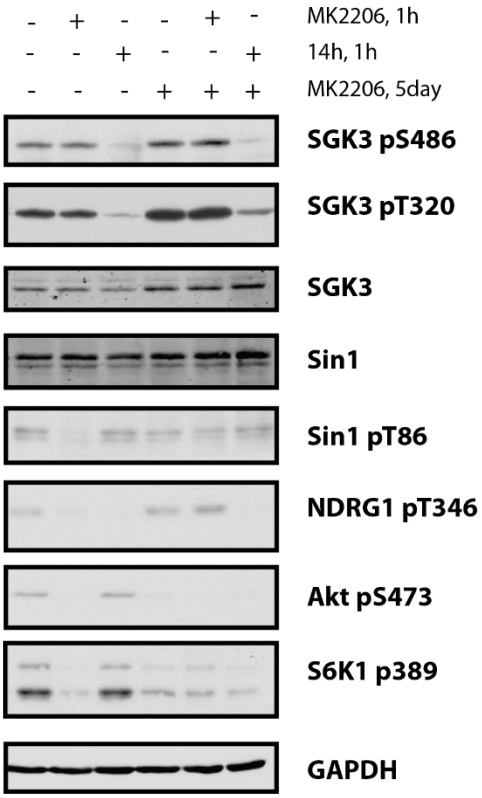

Figure 6.19 mSin1 phosphorylation is not downstream of SGK3 in Akt inhibitor-induced ZR-75-1 cells. *ZR-75-1 cells were treated for 5 days in the presence or absence of Akt inhibitor MK2206 (1 µM). 1 h before lysis, cells were treated with MK2206 (1 µM) or SGK3 inhibitor 14H (1 µM). Cell lysates were subject to immunoblot analysis with the indicated antibodies.*

6.2.9 Q68H mutation has no effect on SGK3 activation

It has previously been reported that a Q68H mutation in mSin1 completely ablates phosphorylation of SGK1 but not Akt (Lu *et al.*, 2011).This was proposed to be due to a direct interaction with SGK1 via this residue determining substrate specificity. I was therefore very interested to test whether this mutation impacts on SGK3 phosphorylation downstream of

mTORC2. I introduced this mutation in full length mSin1 and tested the ability of this construct to mediate SGK3 phosphorylation at S486 in comparison to mSin1-TV1 and mSin1-PHmut as a negative control. Immunoprecipitation and immunoblot of SGK3 for the T320 and S486 sites revealed no defect in phosphorylation of SGK3 upon Q68H mutation (Figure 6.20).

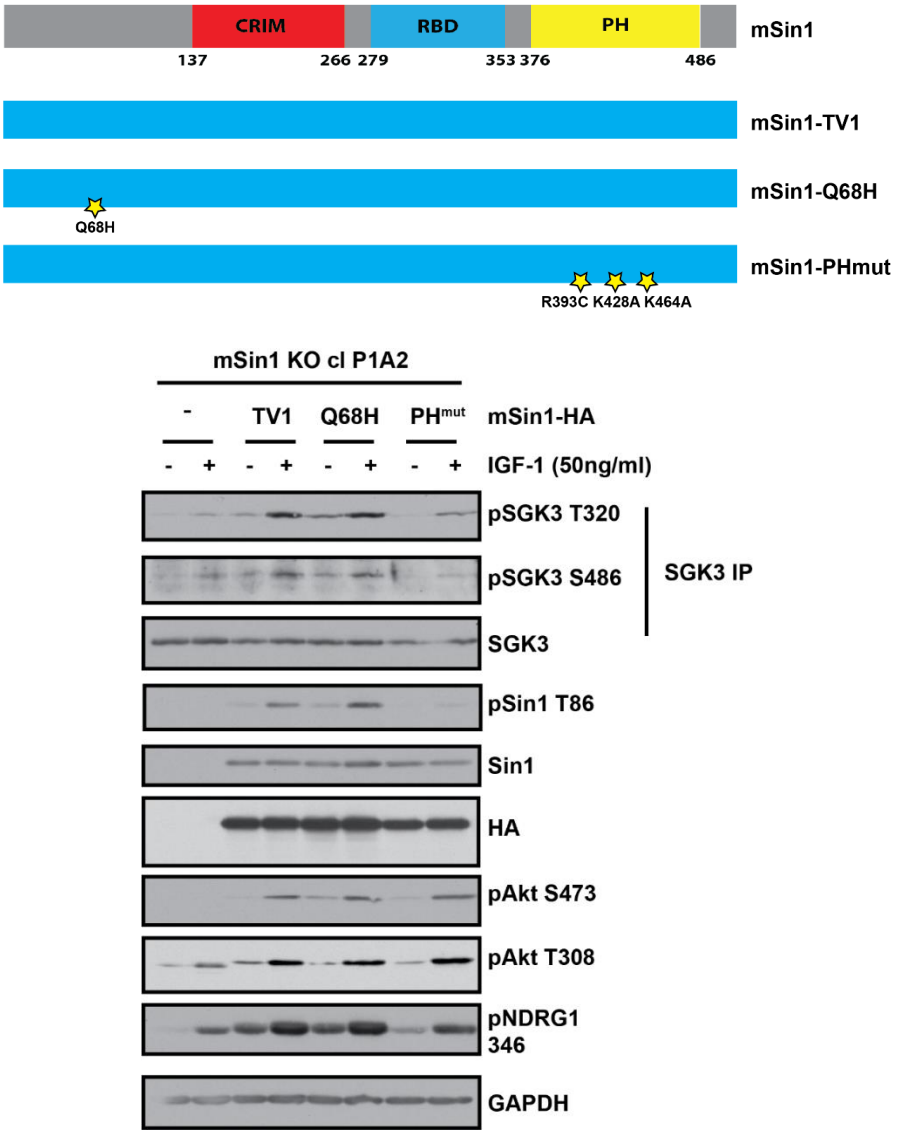

Figure 6.20 *Q68H mutation does not impact on hydrophobic motif phosphorylation of SGK3.*
A. *Domain structure of Q68H and PH domain mutants of mSin1.* ***B.*** *Full Length (TV1), Q68H mutant and PH-domain mutant mSin1 were transfected into mSin1 KO cells. Cells were serum starved overnight then stimulated with IGF-1 (50 ng/ml). SGK3 was immunoprecipitated and blotted for S486 and T320 phosphorylation.*

6.2.10 Localisation of mSin1 in U2OS

I was interested to determine the cellular localisation of various mSin1 transcripts. Further, functional information could be gained by analysing how localisation changes upon activation

and inhibition of the PI3K signalling pathway. It was hypothesised that different variants or mutants of mSin1 may alter SGK3 activation by changing localisation of mTORC2 in the cell. It has been reported that mSin1 is localised to the plasma membrane, through binding of its PH domain to PtdIns(3,4,5)P_3 generated in response to growth factors. I therefore expressed different transcript variants of HA-mSin1 and stained by immunofluorescence for HA and costained using Wheat Germ Agglutin (WGA) conjugated to Alexa Fluor 594 to identify the plasma membrane. mSin1 stably expressed in the TREx system revealed mSin1 to be largely cytoplasmic, with some localisation to the plasma membrane and intracellular vesicles (Figure 6.21). This is in agreement with Ebner et al, who studied the localisation of GFP-tagged mSin1 in cells, and similarly determined that mSin1 was localised to the cytoplasm and endosomal vesicles. Transcript Variant 5 (TV5), which lacks a PH domain, was discovered to be primarily localised in the nucleus. It would be interesting to continue this analysis of the PH-domain mutant constructs, as presumably these mutations would affect cellular localisations. Further, mutation of the Ras Binding Domain or the T86 phosphorylation site may also have an impact on cellular localisation.

As mSin1 Transcript Variant 2 (TV2) and others presented possible localisation to intracellular vesicles, I decided to study colocalization with early endosomal marker Rab5. In this experiment, I used a freeze-thaw method of permeabilization to remove cytosolic protein and therefore only membrane-bound proteins remained in the sample. I determined that HA-mSin1 did localise to internal membranes, however surprisingly did not colocalise with the Rab5 marker as expected (Figure 6.22). It would therefore be important to continue this analysis with further markers of internal membranes, such as EEA1 as another early endosomal marker, Rab7 as a late endosomal marker, as well as mitochondrial and lysosomal trackers. Surprisingly, the full length TV1 was not observed to stain to many internal structures.

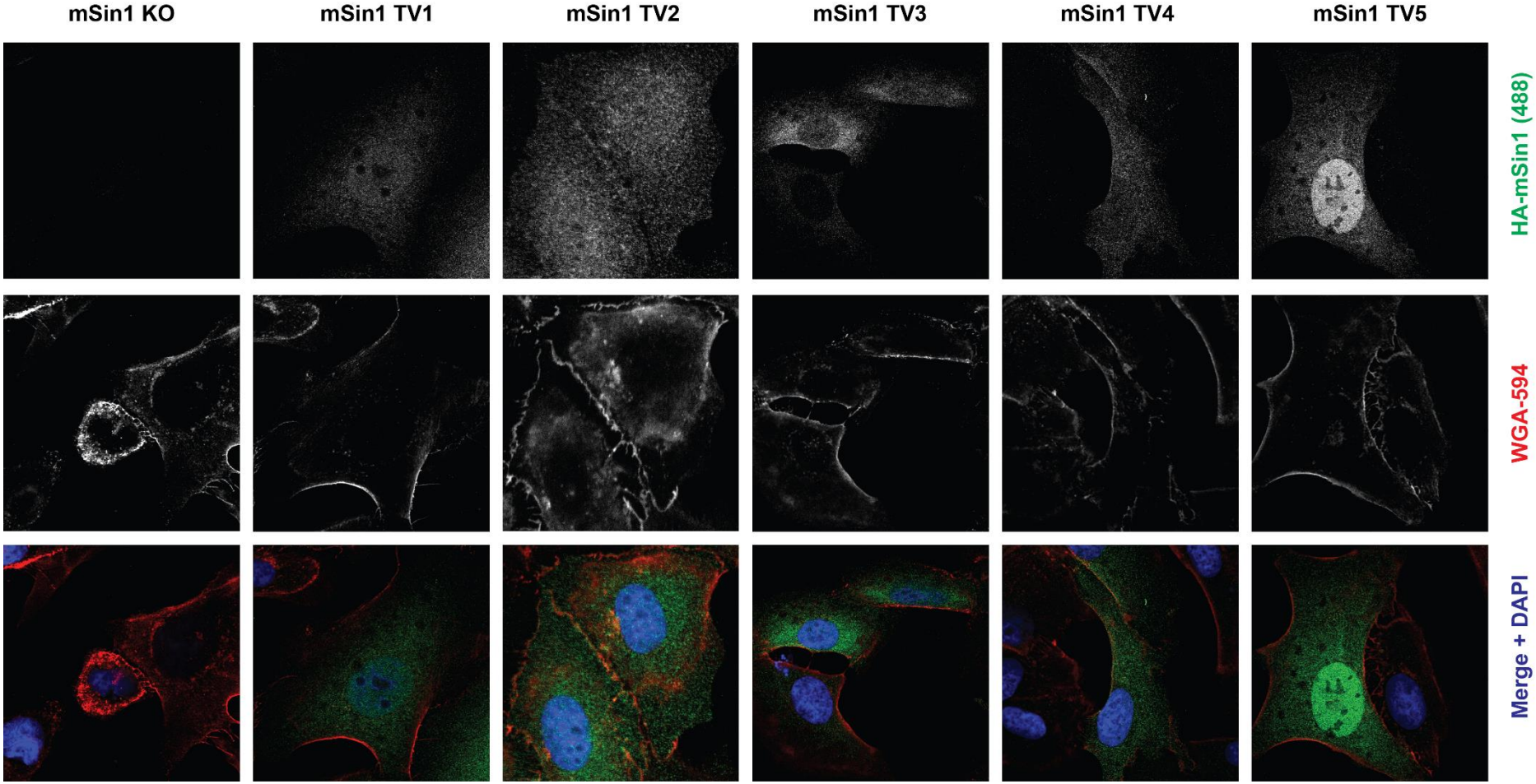

Figure 6.21 mSin1 variants are cytosolically diffuse through throughout cell.
mSin1 transcript variants were expressed under a Doxycycline-inducible system in U2OS cells. Localisation of mSin1 was analysed by immunofluorescence and compared to WGA staining of the plasma membrane. Images are representative of n=10 images.

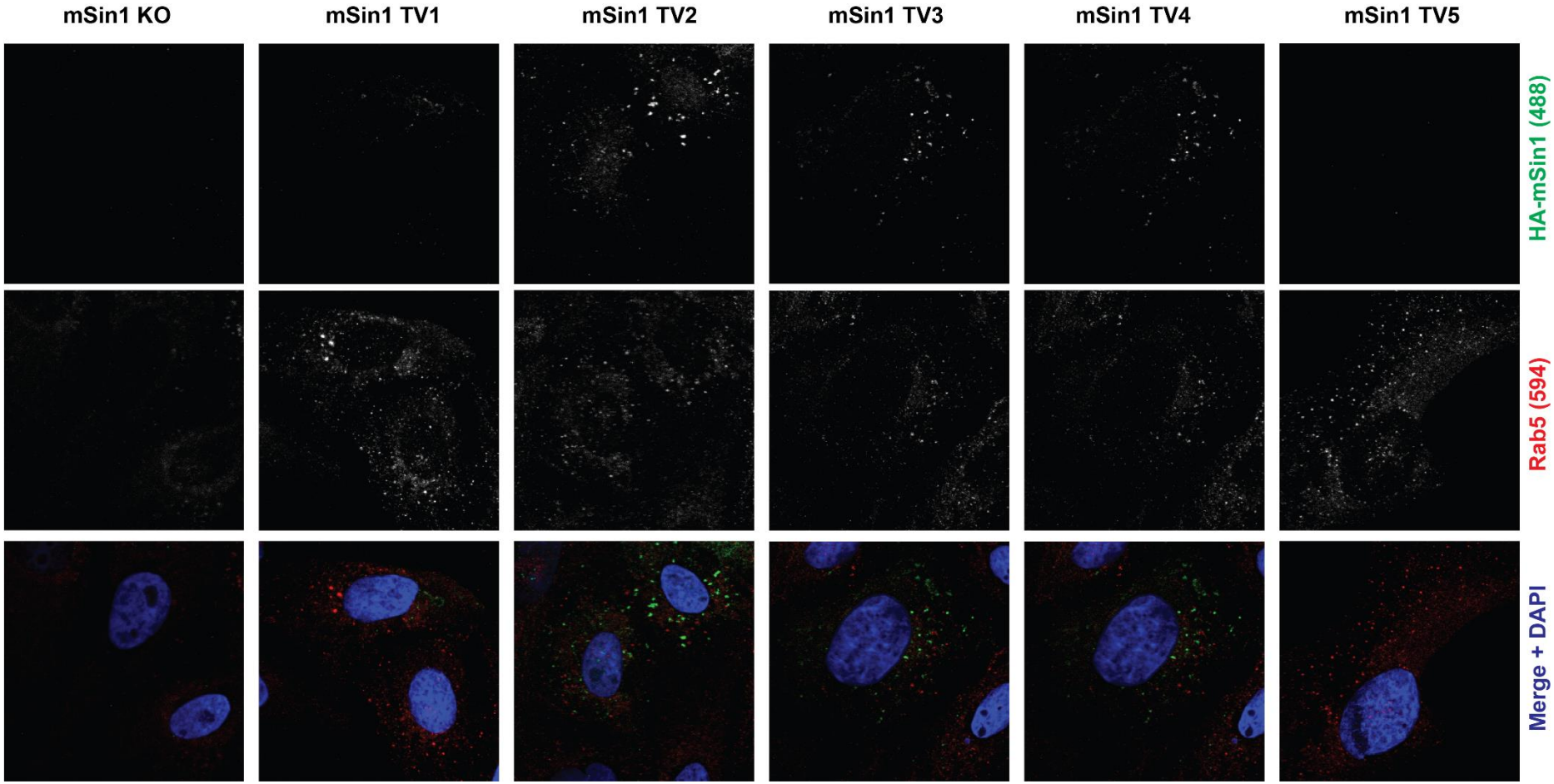

Figure 6.22 mSin1 Transcript variants localised to intracellular membranes, which do not colocalise with Rab5.
mSin1 transcript variants were expressed under a Doxycycline-inducible system in U2OS cells. Cells were subject to freeze-thaw permeabilization to remove diffuse cytosolic proteins. Localisation of mSin1 was analysed by immunofluorescence and compared to anti-Rab5 staining of early endosomal membranes. Images are representative of n=10 images.

Additionally, these analyses were undertaken under basal signalling conditions. It would be interesting to use this assay to determine how localisation of various mSin1 variants differ upon stimulation with growth factors or inhibition of the PI3K pathway.

Despite some information on subcellular localisation of cells, a large proportion of the mSin1 protein was cytoplasmic. This is in agreement with previous literature (Ebner et al., 2017). If mTORC2 is present and active all over the cytoplasm, these localisation differences may not be as important. However, as this study, and previous literature, was performed using overexpressed proteins, it may be the case that this cytoplasmic localisation is an artefact of this overexpression system. However, during amino acid starvation mTORC1 is diffuse in the cytosol (Laplante and Sabatini, 2012; Jewell, Russell and Guan, 2013), therefore this may also be true of mTORC2. I have therefore generated endogenous GFP knockins to Rictor and mSin1 by CRISPR/Cas9 to investigate endogenous localisation in future work.

6.3 Activation of VPS34 by growth factors

6.3.1 Proximity-driven Biotinylation to identify interactors of VPS34 upon IGF1 stimulation.

Co-immunoprecipitation has been extensively used for identification of interactors of a protein of interest for decades. In this approach, a target protein is subject to immunoprecipitation and any co-eluting proteins measured by western blot or by mass spectrometry analysis. This powerful technique has led to a number of important discoveries and enhanced our understanding of major protein complexes such as mTOR and identification of high affinity binding protein kinase substrates. However, a caveat to this approach is that co-immunoprecipitation relies upon a stable, high affinity interaction with effectors, as more weakly associated, transient interactors may not immunoprecipitate with the target protein, or may be lost through extensive wash steps during the purification process. Therefore recently, Proximity-based Biotinylation techniques, such as BioID, APEX2 and TurboID, have been developed as an alternative to co-immunoprecipitation for identification of co-localised or

interacting proteins (Burke *et al.*, 2013; Han *et al.*, 2017; Branon *et al.*, 2018). These approaches work by either endogenously expressing a target protein in tandem with a biotin ligase or expressing a biotin ligase targeted to the endogenous target protein by, for example, a GFP tag (Branon *et al.*, 2018). In this approach, activation of the biotin ligase, in proximity to the target protein, leads to biotinylation of any nearby, interacting proteins. Biotinylated proteins can then be isolated by streptavidin pulldown and identified by mass spectrometry. This approach has an advantage over classical co-immunoprecipitation for identification of interactors, as more transient interactors can be permanently biotinylated and identified, rather than relying upon a stronger, high affinity interaction.

The hypothesis of this study was that, upon stimulation with growth factors, a transient change in VPS34 complex members could occur to increase the capability of VPS34 to phosphorylate PtdIns. The APEX2 approach allows for rapid labelling of interacting proteins within 1 minute, however is reliant upon Biotin phenol and requires activation with H_2O_2 (Han *et al.*, 2017). This approach was unsuitable for study of VPS34, as previous work as shown that H_2O_2 leads to inhibition of lipid phosphatases and significantly alters proteins on the plasma membrane within 1 minute (Cheung *et al.*, 2007). BioID uses Biotin as a substrate and does not require hydrogen peroxide for activation, however the labelling kinetics are very slow, requiring 18-24 hrs and are not suitable for dynamic processes such as VPS34 activation (Burke *et al.*, 2013). TurboID was recently developed through targeted evolution as an optimized biotin ligase, with the simplicity of BioID, but with decreased labelling times. I therefore chose this technique for studying any rapid changes in VPS34 complexes in response to growth factors.

I therefore generated cell lines stably expressing TurboID biotin ligase targeted against GFP-tagged VPS34. I could therefore then stimulate these cells in the presence or absence of IGF1, to identify any differential interactors of VPS34 under these conditions (Figures 6.23, 6.24).

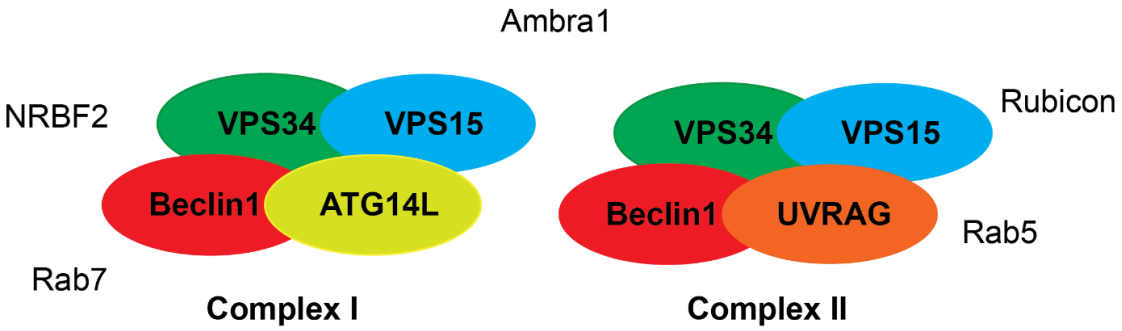

Figure 6.23 VPS34 Complexes in cells.
VPS34 is found in 2 stable complexes in cells. Both complexes contain VPS34, VPS15 and Beclin1, while complex I is formed with ATG14L and complex II is formed with UVRAG. Other transiently binding proteins interact with these complexes to modulate VPS34 activity.

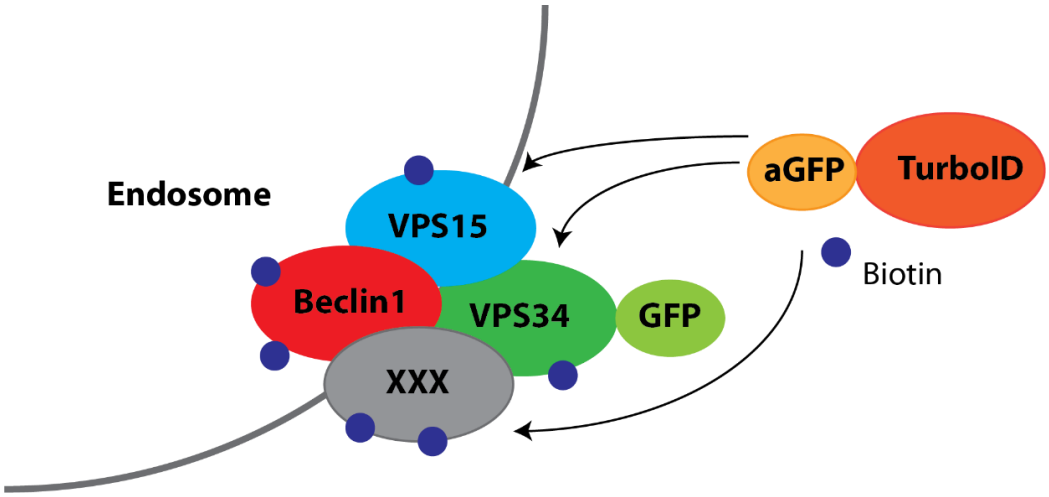

Figure 6.24 TurboID Mechanism of action.
TurboID Biotin ligase is targeted to the substrate GFP-VPS34 by an anti-GFP nanobody (aGFP). Interacting proteins are biotinylated by the enzyme and can be isolated using streptavidin-conjugated beads.

6.3.2 Viral generation of TurboID into GFP-VPS34 cell lines

HEK293 cell lines expressing GFP-VPS34 had been generated in the lab previously by bachelor's student Annika Hornberger. These were fully characterised and the GFP-tag demonstrated not to impact on VPS34 activity (Malik *et al.*, 2018). I therefore chose these cells to virally transfect aGFP-TurboID, and study interactors of VPS34.

The TurboID construct used in this study is targeted by a destabilised anti-GFP nanobody. Therefore, in the presence of GFP, the biotin ligase will be targeted towards GFP and stabilized on GFP binding. In the absence of GFP, for example in control, wildtype HEK293 cells or regions

of the cell not expressing GFP, the ligase will be unstable and rapidly degraded and turned over. This reduces non-specific off target biotinylation which could be observed when exogenously overexpressing a biotin ligase. I therefore transfected this construct into wildtype, 5 GFP-VPS34, and 3 Beclin1-GFP HEK293 cell lines, and selected for TurboID integration by puromycin resistance. Of these transfections, 2 Beclin1-GFP and 3 GFP-VPS34 cell lines survived transfections and expressed the TurboID Biotin Ligase. The wildtype cell line was designed to be a negative control to account for any remaining off-target biotinylation.

Figure 6.25 demonstrates the resultant cell lines from this transfection and selection process, with or without stimulation with 500 µM Biotin. First, the untransfected wildtype, Beclin1-GFP and GFP-VPS34 cell lines are shown with only biotinylation of the native carboxylases recognised by Streptavidin-HRP. The wildtype TurboID transfected cell line presents with a smear of biotinylated proteins which is increased on addition of Biotin. The Beclin1-GFP cell lines did not have any appreciable increase in biotinylation, likely due to relatively low expression of GFP-tagged protein and, upon streptavidin pulldown of biotinylated proteins, there was only weak detection of VPS34 complex members. Comparatively, GFP-VPS34 cell lines expressed increased general biotinylation. In addition, additional bands appeared in the streptavidin blot specifically in the GFP-VPS34 TurboID samples, representing target proteins which were specifically biotinylated when TurboID is targeted toward VPS34. Upon streptavidin pulldown, all core VPS34 complex members could be detected by western blot, with greater efficiency than the Beclin1-GFP TurboID cell lines. Further, both ATG14 forming complex I, and UVRAG forming complex II could be detected. While all complex members were identified by streptavidin pulldown, the VPS34 core complex forms a very tight high affinity complex, therefore this does not necessarily mean the entire complex is being biotinylated. Since GFP-VPS34 TurboID clone #1 cell line gave the strongest biotinylation of VPS34, I selected this cell line for further investigation.

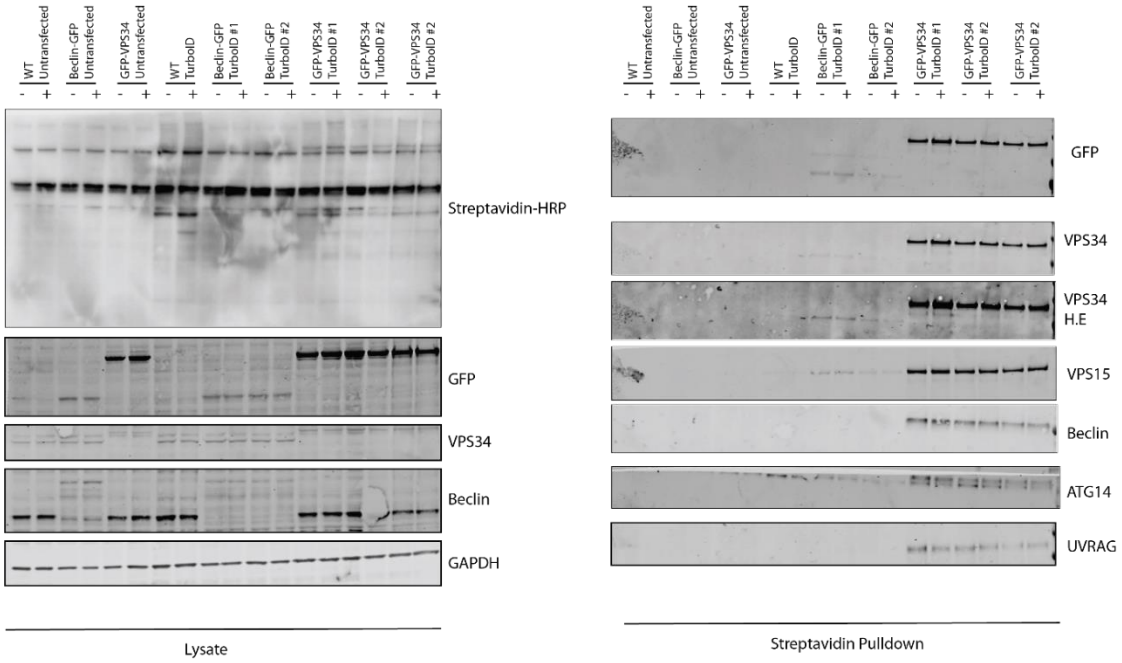

Figure 6.25 Screening of TurboID cell lines.
TurboID constructs were transfected into wildtype HEK293 cells and Beclin1-GFP and GFP-VPS34 cell lines. Cells were stimulated with 500 µM Biotin and analysed for global biotinylation. Biotinylated proteins were isolated by Streptavidin-conjugated sepharose beads and eluted for analysis by immunoblot. Global biotinylation was also analysed in cell lysates using Streptavidin-HRP. Lysates and biotinylated proteins were analysed by immunoblot with the indicated antibodies.

Optimisation of TurboID stimulation conditions

In figure 6.25 above I used a 15 minute standard stimulation time with 500 µM Biotin to stimulate biotinylation of colocalising proteins by TurboID. However, in the cell line screen I noted only a slight increase in general biotinylation in the GFP-VPS34 cell line after stimulation. I therefore next tested a timecourse of Biotin treatments up to an hour to determine the best time point to detect specific biotinylation. I observed that, although non-specific biotinylation in the wildtype cell line increase over time, I only observed a slight increase in specific biotinylation at 15 minutes in the VPS34 cell line which did not increase further (Figure 6.26). This result was surprising, as the nanobody is stabilized in the GFP-VPS34 cell line, but not in the wildtype. However, this result is possibly due to the stabilized nanobody being highly localised to VPS34 on endosomes, while the destabilized nanobody is diffuse in the cytosol and therefore able to

biotinylate more substrate proteins. This could be investigated further by immunofluorescent analysis either against FLAG to determine the localisation of the nanbody or with fluorescently labelled biotin to determine where biotinylation is occurring in the cell.

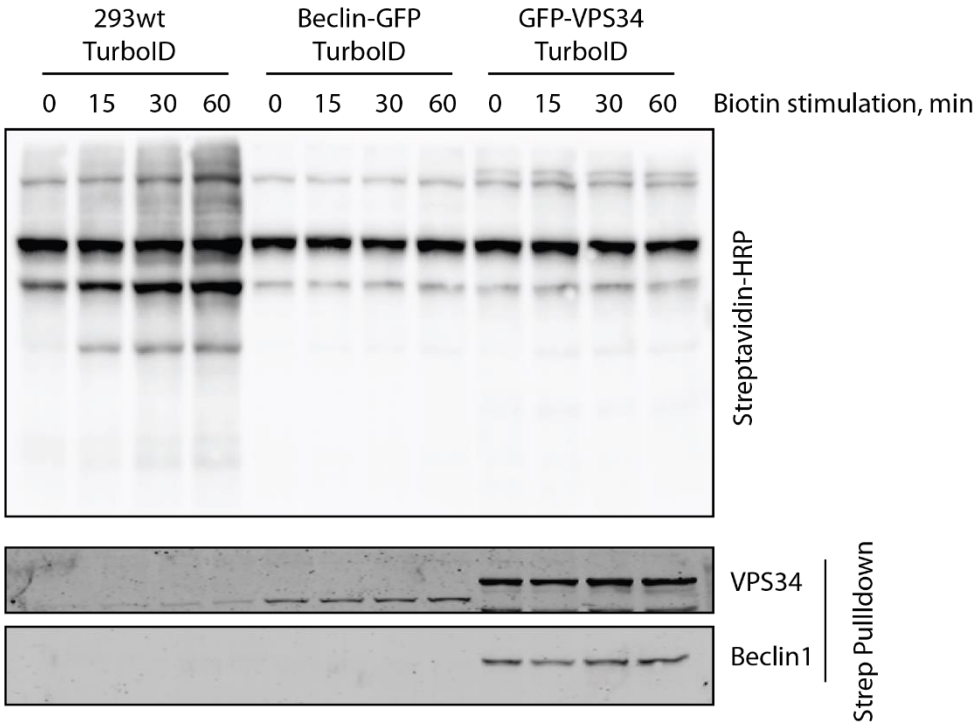

Figure 6.26 Timecourse of Biotin stimulation in TurboID cell lines.
HEK293 WT, Beclin1-GFP or GFP-VPS34 cells expressing TurboID Biotin Ligase were stimulated for up to 60 minutes with 500 µM Biotin before cell lysis. Biotinylated proteins were isolated by Streptavidin-conjugated sepharose beads and eluted for analysis by immunoblot analysis with the indicated antibodies. Global biotinylation was also analysed in cell lysates using Streptavidin-HRP.

Biotinylation of substrate proteins by the TurboID biotin ligase is an ATP-dependent process. Therefore, it was important to determine, before moving further with the assay, whether serum starvation of cells or stimulation with IGF1 would impact on biotinylation efficiency. An increase in biotinylation efficiency on IGF1 stimulation could result in false positives, as increased biotinylation in the IGF1 stimulated samples would not necessarily represent increased interaction with the VPS34 complex. I therefore studied stimulation of wildtype and GFP-VPS34 TurboID cell lines with IGF1, either from a serum starved or basal state, and assayed overall biotinylation by the Streptavidin-HRP blot, and also specific biotinylation of the VPS34 complex. I observed that, although there was a very slight decrease in general biotinylation upon serum

starvation the complex could still be readily detected by streptavidin pulldown. In addition, IGF1 stimulation did not impact on global biotinylation changes (Figure 6.27).

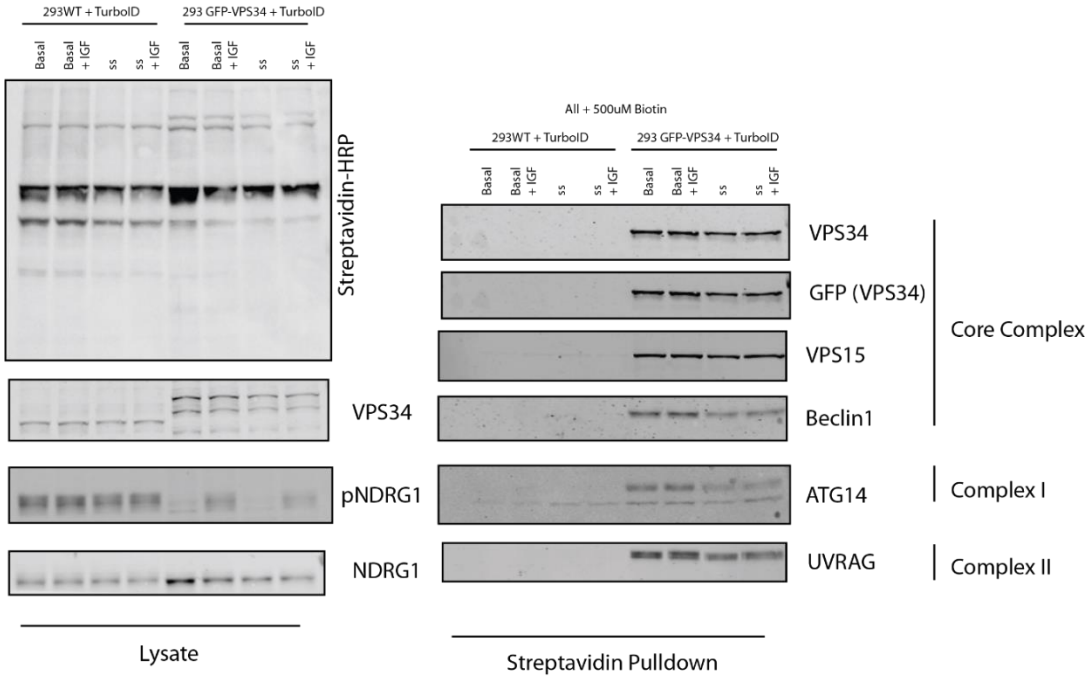

Figure 6.27 Serum starvation and IGF1 stimulation do not impact on TurboID-induced biotinylation. *HEK293 WT or GFP-VPS34 cells expressing TurboID Biotin Ligase were either grown in serum or serum starved overnight. Cells were then stimulated for 15 minutes with 500 µM Biotin in the presence or absence of IGF before cell lysis. Biotinylated proteins were isolated by Streptavidin-conjugated Sepharose beads and eluted for analysis by immunoblot analysis with the indicated antibodies. Global biotinylation was also analysed in cell lysates using Streptavidin-HRP.*

6.3.3 Mass Spectrometry Analysis of Streptavidin pulldown

Based on the results above, I set up an assay to compare GFP-VPS34 TurboID cells by TMT-labelled Mass Spectrometry in triplicate, stimulated with or without IGF1 (50 ng/ml, 15 minutes), in parallel with 15 minutes Biotin Stimulation. These were compared to the wildtype TurboID cell line also stimulated with IGF1 as a negative control for off-target biotinylation. Cells were serum starved overnight, stimulated with IGF1 and Biotin and washed 5 times with PBS before lysis in RIPA buffer, to remove any exogenous Biotin which would reduce the efficiency of the streptavidin pulldown. I performed a pulldown of biotinylated proteins overnight from 500 µg lysate using Agarose-conjugated streptavidin, and digested peptides from the beads by trypsin

digestion. The resultant peptides were then labelled using TMT labelling reagents for quantitative mass spectrometry.

In order to determine the efficiency of the streptavidin pulldown ahead of TMT labelling, I performed a streptavidin blot on the lysates, supernatant and pulldown of this experiment. I determined that the pulldown was largely efficient with most biotinylated proteins removed from the supernatant (Figure 6.28). However, while in the lysate I observed slightly higher biotinylation levels in the wildtype cell line compared to the GFP-VPS34, upon streptavidin pulldown I noticed substantially higher levels of general biotinylation. However, IGF1 stimulation in the GFP-VPS34 cell line resulted in no noticeable changes in general biotinylation.

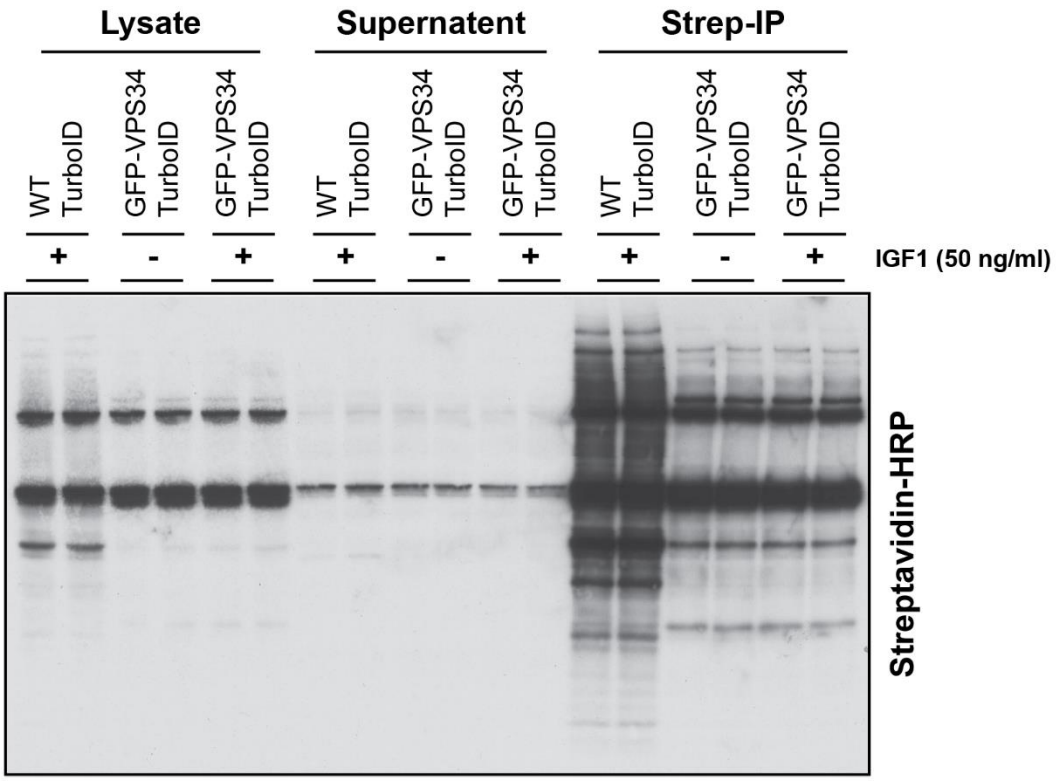

Figure 6.28 Many more biotinylated proteins are detected in HEK293 WT TurboID cells than GFP-VPS34 TurboID.

HEK293 WT or GFP-VPS34 cells expressing TurboID Biotin Ligase were serum starved overnight, then stimulated for 15 min with 500 µM Biotin in the presence or absence of IGF1 stimulation before cell lysis. Biotinylated proteins were isolated by Streptavidin-conjugated sepharose beads and analysed by mass spectrometry. Global biotinylation in lysates, streptavidin immunoprecipitation and the resulting supernatant was analysed using Streptavidin-HRP.

I also observed, upon analysis of the quantified mass spectrometry data, that many more non-specific biotinylated peptides were identified in the wildtype samples compared to the GFP-VPS34 samples (Figure 6.29). The excessive number of non-specific peptides impacted on the sensitivity of the mass spec approach, as only PIK3C3 (VPS34) and PIK3R4 (VPS15) were detected in the GFP-VPS34 samples.

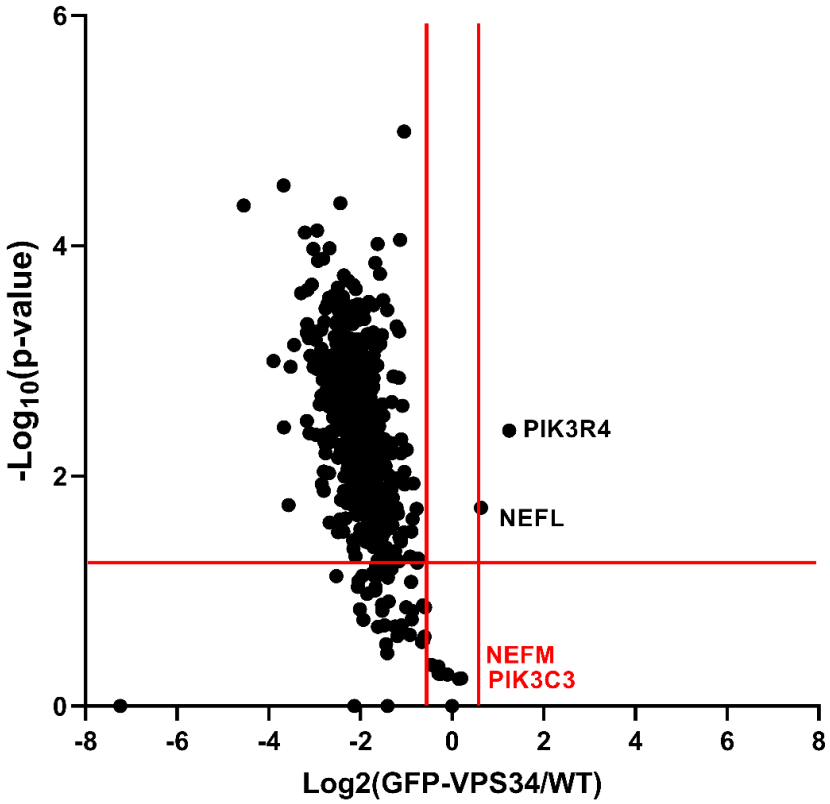

Figure 6.29 Comparison of Biotinylated proteins in GFP-VPS34 and WT TurboID cells
Biotinylated proteins from HEK293 WT or GFP-VPS34 cells expressing TurboID were isolated using streptavidin-conjugated sepharose beads. Peptides were eluted from beads by Trypsin Digestion overnight and the resultant peptides analysed by TMT-labelled quantitative mass spectrometry. Data comparing GFP-VPS34 and WT HEK293 cells is demonstrated by Volcano plot. Full dataset available in Appendix Table 5.

This low sensitivity resulted in very few changes being observed when comparing the IGF1 stimulated cell to serum starvation (Figure 6.30). I observed, as expected, that amounts of VPS34 and VPS15 were not affected by IGF1 stimulation. This is in agreement with previous literature than VPS15 is an obligate dimer with VPS34 and this interaction is not impacted by external signals. However, very few changes were observed between the two conditions. It was however

promising that I identified the autophagy-related protein ATG2B to be enriched in the serum starved condition in comparison to IGF stimulation. However, changes were very slight due to low sensitivity of the experiment. This experiment should therefore be repeated without the wildtype control samples, as in this case the cell line does not serve well as a negative control.

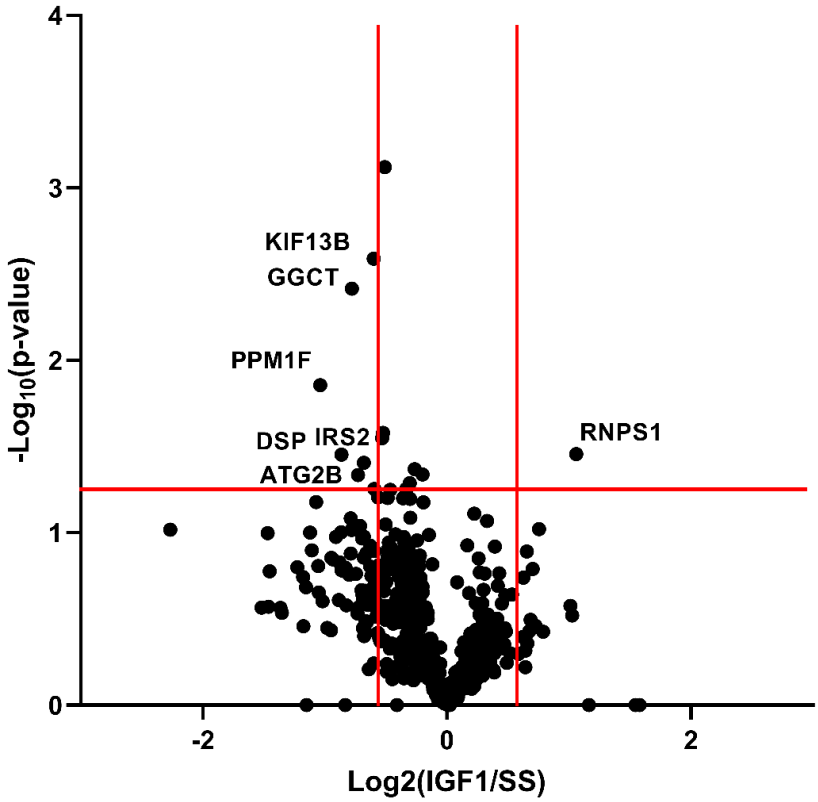

Figure 6.30 Comparison of Biotinylated proteins in GFP-VPS34 TurboID cells
Biotinylated proteins from GFP-VPS34 cells expressing TurboID in the presence or absence of IGF1 stimulation were isolated using streptavidin-conjugated sepharose beads. Peptides were eluted from beads by Trypsin Digestion overnight and the resultant peptides analysed by TMT-labelled quantitative mass spectrometry. Data comparing IGF1-stimulation and serum starvation in GFP-VPS34 cells is demonstrated by Volcano plot.

6.4 Discussion

In this chapter, I present preliminary experiments investigating how SGK3 is activated under prolonged Class I PI3K inhibition. Current understanding in the field is that SGK3 is recruited to PtdIns(3)P produced on early endosomes by VPS34 and is there phosphorylated by mTORC2 and PDK1 for its activation. However, questions still remain over how mTORC2 is directed to SGK3 under these conditions, as compared to mTORC1 this complex is relatively poorly studied and

most literature relates its activity to PI3K activation. Additionally, our current data does not explain how VPS34 is activated by growth factor signals.

In order to further understand mTORC2 activation and targeting towards SGK3, I performed genome level knockout of the critical mTORC2 component mSin1 in HEK293 and U2OS TREx cells, and re-expressed several isoform variants and mutants under a doxycycline-inducible promotor.

I first confirmed that my knockout of mSin1 inactivated mTORC2, as observed by a loss of Akt phosphorylation at Ser473, and that this loss of mTORC2 activity resulted in lost SGK3 activation and phosphorylation of its activation loop residue T320 (published in Malik et al., 2018). This confirmed previously published data using shRNA knockdown of Rictor that demonstrated activation of SGK3 was reliant on mTORC2 (Bago *et al.*, 2016). Re-expression of the 5 transcript variants of mSin1 also reproduced current literature proposing that transcript variant 4, carrying an N-terminal truncation, cannot integrate into and activate mTORC2, and as such SGK3 was not activated in response to IGF1 stimulation in this cell line. This increases confidence in my chosen model for studying SGK3 activation by mTORC2 as these results agree with current literature.

A key limitation to this study was that the chosen antibody for detecting SGK3 hydrophobic motif phosphorylation, raised against pSer422 of SGK1, had limited sensitivity for detecting pSer486 of SGK3, and therefore this assay was not robust enough for detection in every experiment described. Although Thr320 phosphorylation and SGK3 *in vitro* activity could be used as a proxy for hydrophobic motif phosphorylation, to truly study phosphorylation of SGK3 by mTORC2 an improved tool would be required to detect this site. In this study, I tested several antibodies against the hydrophobic motif site, however none offered any improvement over the current pSer422 antibody, including a sheep polyclonal antibody raised in house. The development of a PhosTag assay for monitoring the phosphorylation of SGK3-specific substrates by Athanasios Karapetsas. will also be a powerful tool in continuing this project

In this model, phosphorylation and activation of SGK3 could be rescued by mSin1 with a deletion of binding mutations in the PH domain. This is in contrast with Liu et al., who published that the PtdIns(3,4,5)P_3 binding was critical for activation of mTORC2 and phosphorylation on the hydrophobic motif of Akt. The model proposed in the paper was that the PH domain acts by autoinhibition of the kinase domain of mTOR, which is released upon PtdIns(3,4,5)P_3 binding (Liu *et al.*, 2015). Within this model, it would make sense for the PH deletion mutant to be active, if mislocalised, as this inhibition is released, however it does not explain the activity of the PtdIns(3,4,5)P_3-binding deficient mutant, which would still be autoinhibitory in the mTOR active site. Additionally, the PH-domain is not performing any auto-inhibitory roles by *in vitro* kinase assay. My data also propose a possible inhibitory role of the Ras-Binding domain of mSin1. Mutation of this domain appeared to rescue the decreased activity of the PH-domain mutant, and additionally this mutation in the full-length protein further increased its activity. It is possible that transcript variant 2, lacking this region of the RBD is not affected by the autoinhibitory effects of the PH-domain, and therefore is capable of activating mTORC2 in the absence of PI3K signals. This would provide a mechanism by which SGK3 could be activated by mTORC2 under prolonged Class I PI3K inhibition, however further experiments would be required to validate this mechanism. In order to fully characterise these effects, I would further analyse the ability of Ras Binding mutant or Isoform 2 of mSin1 to initiate phosphorylation and activation of SGK3. This would include combinations of the PH-domain mutations in TV2 to determine if the mutations have an effect in this cell line. It would also be interesting if the Ras Binding domain mutation altered the localisation of full length Sin1, and whether this was affected by PH domain mutations. Sequence analysis predicted the RBD of mSin1 to be a Raf-like RBD, which is able to bind to activated Ras (Schroder *et al.*, 2007). This study also suggested the RBD acted as an inhibitor or Ras signalling. It would be interesting to follow up this work by comparing Ras-like effectors which bind the mSin1 in the presence or absence of IGF1 stimulation or prolonged inhibition of the PI3K pathway.

Analysis of the cellular localisation of HA-mSin1 revealed a largely diffuse, cytoplasmic localisation of mSin1. However, it was unclear from these experiments whether this is representative of the true localisation of the endogenous protein or an artefact of the overexpression approach. mTORC1 has been shown to be diffuse in the cytosol upon amino acid starvation (Jewell, Russell and Guan, 2013). I therefore decided to generate endogenous CRISPR/Cas9 knockin cell lines of mSin1-GFP and GFP-Rictor, another mTORC2 component, and use these cells to study endogenous localisation. While these experiments do not allow the analysis of different variants and mutants of mSin1, they provide an overview of endogenous subcellular localisation, and the response to stimulation and inhibition of the pathway.

Several recent papers have proposed mechanisms by which mTORC2 could be activated independently of PI3K, and propose independent pools of mTORC2 with differing sensitivity to modulation of the PI3K pathway. Ebner *et al*., used a fluorescent biosensor of mTORC2 activity tethered to different cellular compartments to investigate independent mTORC2 pools. They determined that mTORC2 activity was most prominent at the plasma membrane, followed by the late and early endosomes. It is therefore surprising that I did not detect any strong localisation to either the plasma membrane or Rab5-positive early endosomal membrane structures. Using this system they determined that pools of active mTORC2 are present on the plasma membrane and mitochondria which are unaffected by GDC0941 treatment and are therefore regulated in a PI3K-independent manner (Ebner, Sinkovics, *et al.*, 2017). Two recent papers have suggested mechanisms by which mTORC2 can be regulated independently of PI3K activity. Further, Jia *et al* recently published data suggesting that, as with mTORC1, lysosome positioning had an impact on reactivation of certain pools of mTORC2 after serum starvation (Jia and Bonifacino, 2019). Given evidence that pools of mTORC2 are regulated independently, it is reasonable that an endosomal pool of mTORC2 could be activated to phosphorylate SGK3 independently of Class I PI3K signals. Kazyken *et al*. have recently described that mTORC2 can

be activated by phosphorylation of mTOR and Rictor by AMPK in response to a range of AMPK agonists (Kazyken *et al.*, 2019).

In this chapter I also set up an assay for studying how VPS34 is activated to produce further PtdIns(3)P in response to growth factor stimulation. Using the TurboID Proximity-based Biotinylation system. I was able to set up a cell line in which the VPS34 complex was specifically biotinylated in GFP-VPS34 cells. However, a high degree of background biotinylation limited the depth of analysis, and detection of specifically biotinylated peptides. Therefore, in future work this system can be used to modify conditions and determine changes in complexes in response to stimuli. Further controls should also be used to optimise the TurboID system before proceeding to mass spectrometry analysis. The increased biotinylation in the wildtype cell line may be due to increased viral load on transfection of these cells. Additionally, immunofluorescent analysis can be used to ensure correct colocalization of GFP-VPS34 and the Flag-aGFPTurboID. By a similar method, streptavidin staining can be applied to ensure biotinylation is colocalised to GFP-VPS34.

Additionally, a miniTurbo biotin ligase was also published to be 1.5-fold less active than TurboID but exhibit less labelling before addition of exogenous biotin. This construct would potentially allow for more precise temporal control of labelling in highly dynamic processes (Branon *et al.*, 2018). In my samples, biotinylation in the VPS34-TurboID cell line only slightly increased on biotin stimulation compared to labelling from endogenous biotin. Therefore, changes within a 15-minute stimulation may not be detected as easily. Therefore, repeating this process with the miniTurbo construct may allow for more sensitive detection of any potential changes in response to growth factors.

Another interesting area to study would be whether post-translational modification of VPS34 is affected by prolonged PI3K inhibitor treatment. For example, VPS34 activity is known to be modulated by acetylation at K29, K771 and K781 by p300, and p300 is also regulated

downstream of Akt (Huang and Chen, 2005; Su *et al.*, 2017). Additionally, Beclin1 is heavily decorated with posttranslational modifications which modulate VPS34 complex activity (Hill, Wrobel and Rubinsztein, 2019). It is therefore possible that phosphorylation or acetylation changes occur over prolonged PI3K inhibition which impact on VPS34 activity. To answer this question, I would perform acetylation mapping and phosphosite mapping of VPS34 from ZR-75-1 cells in the presence or absence of Class I PI3K inhibition for 5 days. Any identified changes in acetylation or phosphorylation sites could then be followed up to determine whether they have any impact on activity.

7. General Discussion and Future Directions

Prior to the start of my PhD, SGK3 had been demonstrated to lie downstream of PI3K signalling and play a key role in resistance to PI3K-Akt pathway inhibitors in breast cancer. It is therefore critical to develop tools to modulate and understand this resistance pathway.

In this study I generated 2 tool compounds for studying the biology of SGK3. SGK3-PROTAC1 rapidly and specifically induced degradation of SGK3 from a range of cancer cell lines allowing modulation of downstream signalling. Importantly, degradation of SGK3 was observed to have a greater effect on inhibiting growth of cancer cells in the context of PI3K-Akt pathway inhibition. PROTAC compounds have recently grown in use to study the non-enzymatic functions of proteins, for example studying the non-kinase functions of FAK or CDK6. That degradation of SGK3 can have a greater impact on PI3K inhibitor resistance than inhibition of its activity suggests that SGK3 may have cellular roles beyond its kinase activity.

Further to this hypothesis, mass spectrometry analysis of SGK3 degradation in ZR-75-1 cells revealed surprisingly cellular effects not observed upon SGK3 inhibition. I first demonstrated the degradation of SGK3 resulted in reduced expression of the phosphodiesterase PDE4D. As PDE4D acts in signalling complexes to mediate highly localised pools of cAMP, it may therefore form a complex with SGK3 to mediate endosome-localised cAMP. Further work would be required to determine the functional impact and mechanism by which PDE4D is downregulated. I also found a surprising upregulation of proteins forming the electron transport chain complexes in mitochondria. This could represent an exciting role for SGK3 in mediating cancer cell metabolism and warrants further investigation in future work. Importantly, in this study I have not functionally characterised the mechanism leading to the upregulation of these proteins, and whether mitochondrial function is being activated or inhibited in response to SGK3 degradation, and this would be an important future experiment to follow up from this work. Overall, SGK3-PROTAC1, developed and characterised in this thesis, is a powerful tool for the further investigation of SGK3 signalling in cancer resistance.

In addition to the specific SGK3-PROTAC1, I worked with Alessio Ciulli's lab to develop HaloPROTAC-E. This compound utilizes the bacterial dehalogenase activity of HaloTag7 to specifically induce degradation of any endogenously Halo-tagged protein. I demonstrated that HaloPROTAC-E was able to induce degradation of the entire VPS34 complex to impact on downstream biology. The compound can also be used in future work to determine the specificity and off-target effects of SK3-PROTAC1, by comparing the effects of both compounds on the SGK3-Halo cell line. This compound will be a useful tool within the unit and wider field to study proteins with no known ligands or validate target proteins for potential PROTAC development.

I also set up assays to study the upstream regulation of SGK3 and determine how SGK3 can be activated in PI3K inhibitor resistance. I generated mSin1 KO cell lines and used these tools to set up a range of assays to study phosphorylation of SGK3 by mTORC2. The data generated from this model system demonstrated that the PH domain of mSin1 is dispensable for the phosphorylation and activation of SGK3, in contradiction with previous literature (Liu *et al.*, 2015). Additionally, the data suggests a negative regulatory role of the Ras Binding Domain of mSin1. Given that mTORC1 is regulated by the Rag GTPases it would be interesting if activation of mSin1 was regulated by G protein binding of the Ras Binding Domain of mSin1. Further work would involve further investigating the effect of PH domain and RBD mutations on the localisation of mSin1, and how these change in response to pathway stimulation and inhibition. It would also be interesting to combine my model with biosensors of mTORC2 activity such as in Ebner *et al*., 2017, to determine if stimulation and inhibition alters the activity of mTORC2 in particular cellular compartments. For the study of VPS34 regulation by growth factors, I have developed a proximity based Biotinylation assay to identify novel interactors of VPS34, and how these interactions change in response to growth factor stimulation. It is important to understand regulation of VPS34 as this is a key component in the activation of SGK3 in inhibitor resistance. The system I have set up in preliminary experiments will be an important tool in investigating VPS34 protein function.

To conclude, the aim of my PhD was to develop tools to dissect the roles of SGK3 in PI3K-Akt inhibitor resistance. As such, I developed 2 compounds, SGK3-PROTAC1 and HaloPROTAC-E, which were able to induce rapid, reversible degradation of SGK3 in a variety of cell lines. From this work, I identified 2 potential new roles for SGK3 in cancer cells, possibly modulating cAMP signalling through the phosphodiesterase PDE4D, and mitochondrial metabolism. Important future work would determine the functional impact of these alterations and whether they have a relevant regulatory role in cancer progression. I also developed tools to study the mechanisms by which SGK3 can be activated upon Class I PI3K inhibition. These tools will be useful to the field to further understand SGK3 activation and therefore determine methods to modulate its activity in the cancer setting.

8. Appendix Tables

Appendix Tables are held online and are available at:

https://benchling.com/s/etr-D7NWzXp03rRSWREFOqeH

9. References

Addie, M. *et al.* (2013) 'Discovery of 4-amino-N-[(1S)-1-(4-chlorophenyl)-3-hydroxypropyl]-1-(7H-pyrrolo[2,3-d]pyrimidin -4-yl)piperidine-4-carboxamide (AZD5363), an orally bioavailable, potent inhibitor of Akt kinases.', *Journal of medicinal chemistry*. United States, 56(5), pp. 2059–2073. doi: 10.1021/jm301762v.

Alessi, D. R. *et al.* (1996) 'Molecular basis for the substrate specificity of protein kinase B; comparison with MAPKAP kinase-1 and p70 S6 kinase.', *FEBS letters*. England, 399(3), pp. 333–338.

Alessi, D. R., Deak, M., *et al.* (1997) '3-Phosphoinositide-dependent protein kinase-1 (PDK1): structural and functional homology with the Drosophila DSTPK61 kinase.', *Current biology : CB*. England, 7(10), pp. 776–789.

Alessi, D. R., James, S. R., *et al.* (1997) 'Characterization of a 3-phosphoinositide-dependent protein kinase which phosphorylates and activates protein kinase Balpha.', *Current biology : CB*. England, 7(4), pp. 261–269.

Alessi, D. R. and Sammler, E. (2018) 'LRRK2 kinase in Parkinson's disease', *Science*. American Association for the Advancement of Science, pp. 36–37. doi: 10.1126/science.aar5683.

Alliouachene, S. *et al.* (2015) 'Inactivation of the Class II PI3K-C2beta Potentiates Insulin Signaling and Sensitivity.', *Cell reports*. United States, 13(9), pp. 1881–1894. doi: 10.1016/j.celrep.2015.10.052.

Alonso, L. *et al.* (2005) 'Sgk3 links growth factor signaling to maintenance of progenitor cells in the hair follicle', *The Journal of Cell Biology*, 170(4), pp. 559 LP – 570. doi: 10.1083/jcb.200504131.

Alvarez de la Rosa, D. *et al.* (2003) 'Distribution and regulation of expression of serum- and glucocorticoid-induced kinase-1 in the rat kidney', *The Journal of physiology*. 2003/06/19. Blackwell Science Inc, 551(Pt 2), pp. 455–466. doi: 10.1113/jphysiol.2003.042903.

André, F. *et al.* (2019) 'Alpelisib for PIK3CA-Mutated, Hormone Receptor–Positive Advanced Breast Cancer', *New England Journal of Medicine*. Massachusetts Medical Society, 380(20), pp. 1929–1940. doi: 10.1056/NEJMoa1813904.

Antonioli, M. *et al.* (2014) 'AMBRA1 interplay with cullin E3 ubiquitin ligases regulates autophagy dynamics.', *Developmental cell*. United States, 31(6), pp. 734–746. doi: 10.1016/j.devcel.2014.11.013.

Arroyo, J. P. *et al.* (2011) 'Nedd4-2 modulates renal Na+-Cl- cotransporter via the aldosterone-SGK1-Nedd4-2 pathway', *Journal of the American Society of Nephrology : JASN*. American Society of Nephrology, 22(9), pp. 1707–1719. doi: 10.1681/ASN.2011020132.

Aung, K. T. *et al.* (2019) 'The class II phosphoinositide 3-kinases PI3K-C2$α$ and PI3K-C2$β$ differentially regulate clathrin-dependent pinocytosis in human vascular endothelial cells', *The Journal of Physiological Sciences*, 69(2), pp. 263–280. doi: 10.1007/s12576-018-0644-2.

Aylett, C. H. S. *et al.* (2015) 'Architecture of human mTOR complex 1 (Supplementary Materials)', *Science*, 351(6268), pp. 48–52. doi: 10.1126/science.aaa3870.

Baenke, F. *et al.* (2016) 'Resistance to BRAF inhibitors induces glutamine dependency in melanoma cells.', *Molecular oncology*. United States, 10(1), pp. 73–84. doi: 10.1016/j.molonc.2015.08.003.

Bago, R. *et al.* (2014) 'Characterization of VPS34-IN1, a selective inhibitor of Vps34, reveals that the phosphatidylinositol 3-phosphate-binding SGK3 protein kinase is a downstream target of class III

phosphoinositide 3-kinase', *Biochemical Journal*. Portland Press Ltd., 463(Pt 3), pp. 413–427. doi: 10.1042/BJ20140889.

Bago, R. *et al.* (2016) 'The hVps34-SGK3 pathway alleviates sustained PI3K/Akt inhibition by stimulating mTORC1 and tumour growth.', *The EMBO journal*. England, 35(17), pp. 1902–1922. doi: 10.15252/embj.201693929.

Bain, J. *et al.* (2007) 'The selectivity of protein kinase inhibitors: a further update', *The Biochemical journal*. Portland Press Ltd., 408(3), pp. 297–315. doi: 10.1042/BJ20070797.

Bar-Peled, L. *et al.* (2012) 'Ragulator is a GEF for the rag GTPases that signal amino acid levels to mTORC1.', *Cell*. United States, 150(6), pp. 1196–1208. doi: 10.1016/j.cell.2012.07.032.

Bar-Peled, L. *et al.* (2013) 'A tumor suppressor complex with GAP activity for the Rag GTPases that signal amino acid sufficiency to mTORC1', *Science*. American Association for the Advancement of Science, 340(6136), pp. 1100–1106. doi: 10.1126/science.1232044.

Baselga, J. *et al.* (2018) 'Phase III study of taselisib (GDC-0032) + fulvestrant (FULV) v FULV in patients (pts) with estrogen receptor (ER)-positive, PIK3CA-mutant (MUT), locally advanced or metastatic breast cancer (MBC): Primary analysis from SANDPIPER.', *Journal of Clinical Oncology*. American Society of Clinical Oncology, 36(18_suppl), pp. LBA1006–LBA1006. doi: 10.1200/JCO.2018.36.18_suppl.LBA1006.

Baskaran, S. *et al.* (2014) 'Architecture and dynamics of the autophagic phosphatidylinositol 3-kinase complex.', *eLife*. England, 3. doi: 10.7554/eLife.05115.

Besant, P. G. and Attwood, P. V (2012) 'Histone H4 histidine phosphorylation: kinases, phosphatases, liver regeneration and cancer.', *Biochemical Society transactions*, 40(1), pp. 290–3. doi: 10.1042/BST20110605.

Bhalla, V. *et al.* (2005) 'Serum- and Glucocorticoid-Regulated Kinase 1 Regulates Ubiquitin Ligase Neural Precursor Cell-Expressed, Developmentally Down-Regulated Protein 4-2 by Inducing Interaction with 14-3-3', *Molecular Endocrinology*, 19(12), pp. 3073–3084. doi: 10.1210/me.2005-0193.

Biondi, R. M. *et al.* (2001) 'The PIF-binding pocket in PDK1 is essential for activation of S6K and SGK, but not PKB.', *The EMBO journal*. England, 20(16), pp. 4380–4390. doi: 10.1093/emboj/20.16.4380.

Bishé, B., Syed, G. and Siddiqui, A. (2012) 'Phosphoinositides in the hepatitis C virus life cycle', *Viruses*, pp. 2340–2358. doi: 10.3390/v4102340.

Bjørgo, E. *et al.* (2010) 'Cross Talk between Phosphatidylinositol 3-Kinase and Cyclic AMP (cAMP)-Protein Kinase A Signaling Pathways at the Level of a Protein Kinase B/β-Arrestin/cAMP Phosphodiesterase 4 Complex', *Molecular and Cellular Biology*, 30(7), pp. 1660 LP – 1672. doi: 10.1128/MCB.00696-09.

Black, M. H. *et al.* (2019) 'Bacterial pseudokinase catalyzes protein polyglutamylation to inhibit the SidE-family ubiquitin ligases', *Science (New York, N.Y.)*. NLM (Medline), 364(6442), pp. 787–792. doi: 10.1126/science.aaw7446.

Bleeker, F. E. *et al.* (2008) 'AKT1(E17K) in human solid tumours.', *Oncogene*. England, 27(42), pp. 5648–5650. doi: 10.1038/onc.2008.170.

Bogusz, A. M. *et al.* (2006) 'A novel N-terminal hydrophobic motif mediates constitutive degradation of serum- and glucocorticoid-induced kinase-1 by the ubiquitin-proteasome pathway.', *The FEBS journal*. England, 273(13), pp. 2913–2928. doi: 10.1111/j.1742-4658.2006.05304.x.

Boini, K. M. *et al.* (2008) 'Role of serum- and glucocorticoid-inducible kinase SGK1 in glucocorticoid regulation of renal electrolyte excretion and blood pressure.', *Kidney & blood pressure research*. Switzerland, 31(4), pp. 280–289. doi: 10.1159/000151666.

Bondeson, D. P. *et al.* (2015) 'Catalytic in vivo protein knockdown by small-molecule PROTACs', *Nat Chem Biol*. Nature Publishing Group, a division of Macmillan Publishers Limited. All Rights Reserved., 11(8), pp. 611–617. Available at: http://dx.doi.org/10.1038/nchembio.1858.

Bondeson, D. P. *et al.* (2018) 'Lessons in PROTAC Design from Selective Degradation with a Promiscuous Warhead.', *Cell chemical biology*. United States, 25(1), pp. 78-87.e5. doi: 10.1016/j.chembiol.2017.09.010.

Boyd, C. and Naray-Fejes-Toth, A. (2005) 'Gene regulation of ENaC subunits by serum- and glucocorticoid-inducible kinase-1.', *American journal of physiology. Renal physiology*. United States, 288(3), pp. F505-12. doi: 10.1152/ajprenal.00242.2004.

Braccini, L. *et al.* (2015) 'PI3K-C2gamma is a Rab5 effector selectively controlling endosomal Akt2 activation downstream of insulin signalling.', *Nature communications*. England, 6, p. 7400. doi: 10.1038/ncomms8400.

Branon, T. C. *et al.* (2018) 'Efficient proximity labeling in living cells and organisms with TurboID', *Nature Biotechnology*. Nature Publishing Group, a division of Macmillan Publishers Limited. All Rights Reserved., 36, p. 880. Available at: https://doi.org/10.1038/nbt.4201.

Brickley, D. R. *et al.* (2002) 'Ubiquitin modification of serum and glucocorticoid-induced protein kinase-1 (SGK-1).', *The Journal of biological chemistry*. United States, 277(45), pp. 43064–43070. doi: 10.1074/jbc.M207604200.

Brown, E. J. *et al.* (1994) 'A mammalian protein targeted by G1-arresting rapamycin-receptor complex.', *Nature*. England, 369(6483), pp. 756–758. doi: 10.1038/369756a0.

Brownell, J. E. *et al.* (2010) 'Substrate-assisted inhibition of ubiquitin-like protein-activating enzymes: the NEDD8 E1 inhibitor MLN4924 forms a NEDD8-AMP mimetic in situ.', *Molecular cell*. United States, 37(1), pp. 102–111. doi: 10.1016/j.molcel.2009.12.024.

Brugarolas, J. *et al.* (2004) 'Regulation of mTOR function in response to hypoxia by REDD1 and the TSC1/TSC2 tumor suppressor complex', *Genes and Development*, 18(23), pp. 2893–2904. doi: 10.1101/gad.1256804.

Bruhn, M. A. *et al.* (2010) 'Second AKT: the rise of SGK in cancer signalling.', *Growth factors (Chur, Switzerland)*. England, 28(6), pp. 394–408. doi: 10.3109/08977194.2010.518616.

Bruhn, M. A. *et al.* (2013) 'AKT-independent PI3-K signaling in cancer – emerging role for SGK3', *Cancer Management and Research*. Dove Medical Press, 5, pp. 281–292. doi: 10.2147/CMAR.S35178.

Brunet, A. *et al.* (1999) 'Akt promotes cell survival by phosphorylating and inhibiting a Forkhead transcription factor.', *Cell*. United States, 96(6), pp. 857–868.

Brunet, A. *et al.* (2001) 'Protein kinase SGK mediates survival signals by phosphorylating the forkhead transcription factor FKHRL1 (FOXO3a).', *Molecular and cellular biology*. United States, 21(3), pp. 952–965. doi: 10.1128/MCB.21.3.952-965.2001.

Brunetti, L. *et al.* (2018) 'Mutant NPM1 Maintains the Leukemic State through HOX Expression.', *Cancer cell*. United States, 34(3), pp. 499-512.e9. doi: 10.1016/j.ccell.2018.08.005.

Buckley, D. L. *et al.* (2015) 'HaloPROTACS: Use of Small Molecule PROTACs to Induce Degradation of HaloTag Fusion Proteins.', *ACS chemical biology*. United States, 10(8), pp. 1831–1837. doi: 10.1021/acschembio.5b00442.

Burke, B. E. *et al.* (2013) 'BioID : A Screen for Protein-Protein Interactions BioID : A Screen for Protein-Protein Interactions', *Wiley Online Library*, (November 2013). doi: 10.1002/0471140864.ps1923s74.

Burslem, G. M. *et al.* (2019) 'Targeting BCR-ABL1 in Chronic Myeloid Leukemia by PROTAC-mediated Targeted Protein Degradation', *Cancer Research*, p. canres.1236.2019. doi: 10.1158/0008-5472.CAN-19-1236.

Busjahn, A. *et al.* (2002) 'Serum- and glucocorticoid-regulated kinase (SGK1) gene and blood pressure.', *Hypertension (Dallas, Tex. : 1979)*. United States, 40(3), pp. 256–260.

Bylund, L. *et al.* (2004) 'Analysis of the cytogenetic stability of the human embryonal kidney cell line 293 by cytogenetic and STR profiling approaches.', *Cytogenetic and genome research*. Switzerland, 106(1), pp. 28–32. doi: 10.1159/000078556.

Cao, H. *et al.* (2019) 'Functional role of SGK3 in PI3K/Pten driven liver tumor development', *BMC cancer*. BioMed Central, 19(1), p. 343. doi: 10.1186/s12885-019-5551-2.

Carpten, J. D. *et al.* (2007) 'A transforming mutation in the pleckstrin homology domain of AKT1 in cancer.', *Nature*. England, 448(7152), pp. 439–444. doi: 10.1038/nature05933.

Castel, P. *et al.* (2016) 'PDK1-SGK1 Signaling Sustains AKT-Independent mTORC1 Activation and Confers Resistance to PI3Kα Inhibition', *Cancer cell*. Cell Press, 30(2), pp. 229–242. doi: 10.1016/j.ccell.2016.06.004.

Caussinus, E. and Affolter, M. (2016) 'deGradFP: A System to Knockdown GFP-Tagged Proteins.', *Methods in molecular biology (Clifton, N.J.)*. United States, 1478, pp. 177–187. doi: 10.1007/978-1-4939-6371-3_9.

Caussinus, E., Kanca, O. and Affolter, M. (2012) 'Fluorescent fusion protein knockout mediated by anti-GFP nanobody.', *Nature structural & molecular biology*. United States, 19(1), pp. 117–121. doi: 10.1038/nsmb.2180.

CGAN (2012) 'Comprehensive molecular portraits of human breast tumours.', *Nature*. England, 490(7418), pp. 61–70. doi: 10.1038/nature11412.

Chang, M. T. *et al.* (2016) 'Identifying recurrent mutations in cancer reveals widespread lineage diversity and mutational specificity.', *Nature biotechnology*. United States, 34(2), pp. 155–163. doi: 10.1038/nbt.3391.

Chantranupong, L. *et al.* (2014) 'The sestrins interact with gator2 to negatively regulate the amino-acid-sensing pathway upstream of mTORC1', *Cell Reports*. Elsevier, 9(1), pp. 1–8. doi: 10.1016/j.celrep.2014.09.014.

Chantranupong, L. *et al.* (2016) 'The CASTOR Proteins Are Arginine Sensors for the mTORC1 Pathway', *Cell*. Cell Press, 165(1), pp. 153–164. doi: 10.1016/j.cell.2016.02.035.

Chen, C.-Y. *et al.* (2018) 'PTEN: Tumor Suppressor and Metabolic Regulator ', *Frontiers in Endocrinology* , p. 338. Available at: https://www.frontiersin.org/article/10.3389/fendo.2018.00338.

Chen, H.-K. *et al.* (2003) 'Interaction of Akt-phosphorylated ataxin-1 with 14-3-3 mediates neurodegeneration in spinocerebellar ataxia type 1.', *Cell*. United States, 113(4), pp. 457–468. doi: 10.1016/s0092-8674(03)00349-0.

Chen, J.-B. *et al.* (2018) 'Glucocorticoid-Inducible Kinase 2 Promotes Bladder Cancer Cell Proliferation, Migration and Invasion by Enhancing beta-catenin/c-Myc Signaling Pathway.', *Journal of Cancer*. Australia, 9(24), pp. 4774–4782. doi: 10.7150/jca.25811.

Chen, S. Y. *et al.* (1999) 'Epithelial sodium channel regulated by aldosterone-induced protein sgk', *Proceedings of the National Academy of Sciences of the United States of America*. The National Academy of Sciences, 96(5), pp. 2514–2519. doi: 10.1073/pnas.96.5.2514.

Chen, X. *et al.* (2018) 'Cryo-EM structure of human mTOR complex 2', *Cell Research*. Nature Publishing Group, 28(5), pp. 518–528. doi: 10.1038/s41422-018-0029-3.

Cheung, S. M. S. *et al.* (2007) 'Regulation of phosphoinositide 3-kinase signaling by oxidants: hydrogen peroxide selectively enhances immunoreceptor-induced recruitment of phosphatidylinositol (3,4) bisphosphate-binding PH domain proteins.', *Cellular signalling*. England, 19(5), pp. 902–912. doi: 10.1016/j.cellsig.2006.10.013.

Chin, Y. R. *et al.* (2014) 'Targeting Akt3 signaling in triple-negative breast cancer.', *Cancer research*. United States, 74(3), pp. 964–973. doi: 10.1158/0008-5472.CAN-13-2175.

Chu, N. *et al.* (2018) 'Akt Kinase Activation Mechanisms Revealed Using Protein Semisynthesis In Brief Dissecting the molecular interactions leading to Akt activation points to a chain of events distinct from existing models', *Cell*, 174, pp. 897-907.e14. doi: 10.1016/j.cell.2018.07.003.

Cianfanelli, V. *et al.* (2015) 'Ambra1 at a glance', *Journal of Cell Science*. Company of Biologists Ltd, 128(11), pp. 2003–2008. doi: 10.1242/jcs.168153.

Clift, D. *et al.* (2018) 'A Method for the Acute and Rapid Degradation of Endogenous Proteins', *Cell*. Elsevier, 171(7), pp. 1692-1706.e18. doi: 10.1016/j.cell.2017.10.033.

Cohen, P. (2002) 'The origins of protein phosphorylation.', *Nature cell biology*, 4(5), pp. E127-30. doi: 10.1038/ncb0502-e127.

Cohen, P. and Alessi, D. R. (2013) 'Kinase drug discovery--what's next in the field?', *ACS chemical biology*. United States, 8(1), pp. 96–104. doi: 10.1021/cb300610s.

Cohen, Y. *et al.* (2010) 'AKT1 pleckstrin homology domain E17K activating mutation in endometrial carcinoma.', *Gynecologic oncology*. United States, 116(1), pp. 88–91. doi: 10.1016/j.ygyno.2009.09.038.

Collins, B. J. *et al.* (2003) 'In vivo role of the PIF-binding docking site of PDK1 defined by knock-in mutation.', *The EMBO journal*. England, 22(16), pp. 4202–4211. doi: 10.1093/emboj/cdg407.

Croessmann, S. *et al.* (2018) 'PIK3CA C2 Domain Deletions Hyperactivate Phosphoinositide 3-kinase (PI3K), Generate Oncogene Dependence, and Are Exquisitely Sensitive to PI3Kalpha Inhibitors.', *Clinical cancer research : an official journal of the American Association for Cancer Research*. United States, 24(6), pp. 1426–1435. doi: 10.1158/1078-0432.CCR-17-2141.

Cromm, P. M. *et al.* (2018) 'Addressing Kinase-Independent Functions of Fak via PROTAC-Mediated Degradation', *Journal of the American Chemical Society*. American Chemical Society, 140(49), pp. 17019–17026. doi: 10.1021/jacs.8b08008.

Cross, D. A. *et al.* (1995) 'Inhibition of glycogen synthase kinase-3 by insulin mediated by protein kinase B.', *Nature*. England, 378(6559), pp. 785–789. doi: 10.1038/378785a0.

Cui, J. *et al.* (2015) 'A secretory kinase complex regulates extracellular protein phosphorylation', *eLife*. eLife Sciences Publications Ltd, 2015(4). doi: 10.7554/eLife.06120.

Cui, J. *et al.* (2017) 'Structure of Fam20A reveals a pseudokinase featuring a unique disulfide pattern and inverted ATP-binding.', *eLife*, 6. doi: 10.7554/eLife.23990.

Dahlberg, J. *et al.* (2011) 'Genetic variants in serum and glucocortocoid regulated kinase 1, a regulator of the epithelial sodium channel, are associated with ischaemic stroke.', *Journal of hypertension*. England, 29(5), pp. 884–889. doi: 10.1097/HJH.0b013e3283455117.

Datta, S. R. *et al.* (1997) 'Akt phosphorylation of BAD couples survival signals to the cell-intrinsic death machinery.', *Cell*. United States, 91(2), pp. 231–241.

Datta, S. R. *et al.* (2000) '14-3-3 proteins and survival kinases cooperate to inactivate BAD by BH3 domain phosphorylation.', *Molecular cell*. United States, 6(1), pp. 41–51.

Davies, B. R. *et al.* (2012) 'Preclinical pharmacology of AZD5363, an inhibitor of AKT: pharmacodynamics, antitumor activity, and correlation of monotherapy activity with genetic background.', *Molecular cancer therapeutics*. United States, 11(4), pp. 873–887. doi: 10.1158/1535-7163.MCT-11-0824-T.

Davies, M. A. *et al.* (2008) 'A novel AKT3 mutation in melanoma tumours and cell lines.', *British journal of cancer*. England, 99(8), pp. 1265–1268. doi: 10.1038/sj.bjc.6604637.

Debonneville, C. *et al.* (2001) 'Phosphorylation of Nedd4-2 by Sgk1 regulates epithelial Na(+) channel cell surface expression', *The EMBO journal*. Oxford University Press, 20(24), pp. 7052–7059. doi: 10.1093/emboj/20.24.7052.

Denise, C. *et al.* (2015) '5-fluorouracil resistant colon cancer cells are addicted to OXPHOS to survive and enhance stem-like traits', *Oncotarget*. Impact Journals LLC, 6(39), pp. 41706–41721. doi: 10.18632/oncotarget.5991.

Devabhaktuni, A. *et al.* (2019) 'TagGraph reveals vast protein modification landscapes from large tandem mass spectrometry datasets', *Nature Biotechnology*. Nature Publishing Group. doi: 10.1038/s41587-019-0067-5.

Diehl, J. A. *et al.* (1998) 'Glycogen synthase kinase-3beta regulates cyclin D1 proteolysis and subcellular localization.', *Genes & development*. United States, 12(22), pp. 3499–3511. doi: 10.1101/gad.12.22.3499.

Dieter, M. *et al.* (2004) 'Regulation of glucose transporter SGLT1 by ubiquitin ligase Nedd4-2 and kinases

SGK1, SGK3, and PKB.', *Obesity research*. United States, 12(5), pp. 862–870. doi: 10.1038/oby.2004.104.

Dijkers, P. F. *et al.* (2002) 'FKHR-L1 can act as a critical effector of cell death induced by cytokine withdrawal: protein kinase B-enhanced cell survival through maintenance of mitochondrial integrity.', *The Journal of cell biology*. United States, 156(3), pp. 531–542. doi: 10.1083/jcb.200108084.

Do, H. *et al.* (2008) 'Detection of the transforming AKT1 mutation E17K in non-small cell lung cancer by high resolution melting.', *BMC research notes*. England, 1, p. 14. doi: 10.1186/1756-0500-1-14.

Domin, J. *et al.* (2005) 'The class II phosphoinositide 3-kinase PI3K-C2β regulates cell migration by a PtdIns(3)P dependent mechanism', *Journal of Cellular Physiology*, 205(3), pp. 452–462. doi: 10.1002/jcp.20478.

Ebner, M., Sinkovics, B., *et al.* (2017) 'Localization of mTORC2 activity inside cells', *The Journal of Cell Biology*.

Ebner, M., Lučić, I., *et al.* (2017) 'PI(3,4,5)P3 Engagement Restricts Akt Activity to Cellular Membranes', *Molecular Cell*, 65(3), pp. 416-431.e6. doi: https://doi.org/10.1016/j.molcel.2016.12.028.

Edinger, A. L. and Thompson, C. B. (2002) 'Akt maintains cell size and survival by increasing mTOR-dependent nutrient uptake.', *Molecular biology of the cell*. United States, 13(7), pp. 2276–2288. doi: 10.1091/mbc.01-12-0584.

Efeyan, A. *et al.* (2013) 'Regulation of mTORC1 by the Rag GTPases is necessary for neonatal autophagy and survival', *Nature*, 493(7434), pp. 679–683. doi: 10.1038/nature11745.

Egan, D. F. *et al.* (2015) 'Small Molecule Inhibition of the Autophagy Kinase ULK1 and Identification of ULK1 Substrates.', *Molecular cell*. United States, 59(2), pp. 285–297. doi: 10.1016/j.molcel.2015.05.031.

Eguez, L. *et al.* (2005) 'Full intracellular retention of GLUT4 requires AS160 Rab GTPase activating protein.', *Cell metabolism*. United States, 2(4), pp. 263–272. doi: 10.1016/j.cmet.2005.09.005.

Ellis, M. J. and Perou, C. M. (2013) 'The genomic landscape of breast cancer as a therapeutic roadmap', *Cancer Discovery*, 3(1), pp. 27–34. doi: 10.1158/2159-8290.CD-12-0462.

Erb, M. A. *et al.* (2017) 'Transcription control by the ENL YEATS domain in acute leukaemia.', *Nature*. England, 543(7644), pp. 270–274. doi: 10.1038/nature21688.

Escobedo, J. A. *et al.* (1991) 'cDNA cloning of a novel 85 kd protein that has SH2 domains and regulates binding of PI3-kinase to the PDGF beta-receptor.', *Cell*. United States, 65(1), pp. 75–82.

Eylenstein, A. *et al.* (2011) 'Stimulation of Ca2+-channel Orai1/STIM1 by serum- and glucocorticoid-inducible kinase 1 (SGK1)', *The FASEB Journal*. Federation of American Societies for Experimental Biology, 25(6), pp. 2012–2021. doi: 10.1096/fj.10-178210.

Fagerli, U.-M. *et al.* (2011) 'Serum/glucocorticoid-regulated kinase 1 (SGK1) is a prominent target gene of the transcriptional response to cytokines in multiple myeloma and supports the growth of myeloma cells.', *Oncogene*. England, 30(28), pp. 3198–3206. doi: 10.1038/onc.2011.79.

Fan, F. *et al.* (2012) 'On the catalytic mechanism of human ATP citrate lyase.', *Biochemistry*, 51(25), pp. 5198–211. doi: 10.1021/bi300611s.

Faresse, N. *et al.* (2012) 'Inducible kidney-specific Sgk1 knockout mice show a salt-losing phenotype.', *American journal of physiology. Renal physiology*. United States, 302(8), pp. F977-85. doi: 10.1152/ajprenal.00535.2011.

Fejes-Toth, G. *et al.* (2008) 'Epithelial Na+ channel activation and processing in mice lacking SGK1.', *American journal of physiology. Renal physiology*. United States, 294(6), pp. F1298-305. doi: 10.1152/ajprenal.00579.2007.

Ferguson, F. M. and Gray, N. S. (2018) 'Kinase inhibitors: the road ahead', *Nature Reviews Drug Discovery*. Nature Publishing Group, a division of Macmillan Publishers Limited. All Rights Reserved., 17, p. 353. Available at: https://doi.org/10.1038/nrd.2018.21.

Folkes, A. J. *et al.* (2008) 'The identification of 2-(1H-indazol-4-yl)-6-(4-methanesulfonyl-piperazin-1-ylmethyl)-4-morpholin-4-yl-t hieno[3,2-d]pyrimidine (GDC-0941) as a potent, selective, orally bioavailable inhibitor of class I PI3 kinase for the treatment of cancer .', *Journal of medicinal chemistry*. United States, 51(18), pp. 5522–5532. doi: 10.1021/jm800295d.

Forbes, S. A. *et al.* (2011) 'COSMIC: mining complete cancer genomes in the Catalogue of Somatic Mutations in Cancer', *Nucleic acids research*. 2010/10/15. Oxford University Press, 39(Database issue), pp. D945–D950. doi: 10.1093/nar/gkq929.

Franco, I. *et al.* (2014) 'PI3K class II α controls spatially restricted endosomal PtdIns3P and Rab11 activation to promote primary cilium function', *Developmental cell*. Cell Press, 28(6), pp. 647–658. doi: 10.1016/j.devcel.2014.01.022.

Frias, M. A. *et al.* (2006) 'mSin1 is necessary for Akt/PKB phosphorylation, and its isoforms define three distinct mTORC2s.', *Current biology : CB*. England, 16(18), pp. 1865–1870. doi: 10.1016/j.cub.2006.08.001.

Frost, J. *et al.* (2016) 'Potent and selective chemical probe of hypoxic signalling downstream of HIF-α hydroxylation via VHL inhibition', *Nature Communications*. The Author(s), 7, p. 13312. Available at: http://dx.doi.org/10.1038/ncomms13312.

Fuhs, S. R. *et al.* (2015) 'Monoclonal 1- and 3-Phosphohistidine Antibodies: New Tools to Study Histidine Phosphorylation.', *Cell*, 162(1), pp. 198–210. doi: 10.1016/j.cell.2015.05.046.

Fuhs, S. R. and Hunter, T. (2017) 'pHisphorylation: the emergence of histidine phosphorylation as a reversible regulatory modification', *Current Opinion in Cell Biology*. Elsevier Ltd, pp. 8–16. doi: 10.1016/j.ceb.2016.12.010.

Fujio, Y. *et al.* (2000) 'Akt promotes survival of cardiomyocytes in vitro and protects against ischemia-reperfusion injury in mouse heart.', *Circulation*. United States, 101(6), pp. 660–667. doi: 10.1161/01.cir.101.6.660.

Fulcher, L. J. *et al.* (2016) 'An affinity-directed protein missile system for targeted proteolysis.', *Open biology*. England, 6(10). doi: 10.1098/rsob.160255.

Furuya, T. *et al.* (2010) 'Negative regulation of Vps34 by Cdk mediated phosphorylation.', *Molecular cell*. United States, 38(4), pp. 500–511. doi: 10.1016/j.molcel.2010.05.009.

Gadd, M. S. *et al.* (2017) 'Structural basis of PROTAC cooperative recognition for selective protein degradation.', *Nature chemical biology*. United States, 13(5), pp. 514–521. doi: 10.1038/nchembio.2329.

Galdeano, C. *et al.* (2014) 'Structure-Guided Design and Optimization of Small Molecules Targeting the Protein–Protein Interaction between the von Hippel–Lindau (VHL) E3 Ubiquitin Ligase and the Hypoxia Inducible Factor (HIF) Alpha Subunit with in Vitro Nanomolar Affinities', *Journal of Medicinal Chemistry*. American Chemical Society, 57(20), pp. 8657–8663. doi: 10.1021/jm5011258.

Gamba, G. (2005) 'Molecular physiology and pathophysiology of electroneutral cation-chloride cotransporters.', *Physiological reviews*, 85(2), pp. 423–93. doi: 10.1152/physrev.00011.2004.

Gan, X. *et al.* (2011) 'Evidence for direct activation of mTORC2 kinase activity by phosphatidylinositol 3,4,5-trisphosphate.', *The Journal of biological chemistry*. United States, 286(13), pp. 10998–11002. doi: 10.1074/jbc.M110.195016.

García-Bermúdez, J. *et al.* (2015) 'PKA Phosphorylates the ATPase Inhibitory Factor 1 and Inactivates Its Capacity to Bind and Inhibit the Mitochondrial H+-ATP Synthase', *Cell Reports*, 12(12), pp. 2143–2155. doi: https://doi.org/10.1016/j.celrep.2015.08.052.

Garcia-Martinez, J. M. and Alessi, D. R. (2008) 'mTOR complex 2 (mTORC2) controls hydrophobic motif phosphorylation and activation of serum- and glucocorticoid-induced protein kinase 1 (SGK1).', *The Biochemical journal*. England, 416(3), pp. 375–385. doi: 10.1042/BJ20081668.

Ginsberg, M. D. *et al.* (2003) 'PKA-dependent binding of mRNA to the mitochondrial AKAP121 protein.', *Journal of molecular biology*. England, 327(4), pp. 885–897. doi: 10.1016/s0022-2836(03)00173-6.

Gong, G. Q. *et al.* (2018) 'Identification, structure modification, and characterization of potential small-molecule SGK3 inhibitors with novel scaffolds.', *Acta pharmacologica Sinica*. United States. doi: 10.1038/s41401-018-0087-6.

Gonzalez-Angulo, A. M. and Blumenschein, G. R. (2013) 'Defining biomarkers to predict sensitivity to PI3K/Akt/mTOR pathway inhibitors in breast cancer', *Cancer Treatment Reviews*, 39(4), pp. 313–320. doi: 10.1016/j.ctrv.2012.11.002.

Grahammer, F. *et al.* (2006) 'Renal function of gene-targeted mice lacking both SGK1 and SGK3.', *American journal of physiology. Regulatory, integrative and comparative physiology*. United States, 290(4), pp. R945-50. doi: 10.1152/ajpregu.00484.2005.

Guertin, D. A. *et al.* (2006) 'Ablation in mice of the mTORC components raptor, rictor, or mLST8 reveals that mTORC2 is required for signaling to Akt-FOXO and PKCalpha, but not S6K1.', *Developmental cell*. United States, 11(6), pp. 859–871. doi: 10.1016/j.devcel.2006.10.007.

Gulluni, F. *et al.* (2019) 'Class II PI3K Functions in Cell Biology and Disease', *Trends in Cell Biology*. Elsevier, 29(4), pp. 339–359. doi: 10.1016/j.tcb.2019.01.001.

Vander Haar, E. *et al.* (2007) 'Insulin signalling to mTOR mediated by the Akt/PKB substrate PRAS40.', *Nature cell biology*. England, 9(3), pp. 316–323. doi: 10.1038/ncb1547.

Halland, N. *et al.* (2015) 'Discovery of N-[4-(1H-Pyrazolo[3,4-b]pyrazin-6-yl)-phenyl]-sulfonamides as Highly Active and Selective SGK1 Inhibitors.', *ACS medicinal chemistry letters*. United States, 6(1), pp. 73–78. doi: 10.1021/ml5003376.

Han, S. *et al.* (2017) 'Proximity Biotinylation as a Method for Mapping Proteins Associated with mtDNA in Living Cells', *Cell Chemical Biology*. Elsevier Ltd, 24(3), pp. 404–414. doi: 10.1016/j.chembiol.2017.02.002.

Han, X. *et al.* (2019) 'Discovery of ARD-69 as a Highly Potent Proteolysis Targeting Chimera (PROTAC) Degrader of Androgen Receptor (AR) for the Treatment of Prostate Cancer', *Journal of Medicinal Chemistry*. American Chemical Society, 62(2), pp. 941–964. doi: 10.1021/acs.jmedchem.8b01631.

Hanks, S. K. and Hunter, T. (1995) 'Protein kinases 6. The eukaryotic protein kinase superfamily: kinase (catalytic) domain structure and classification.', *The FASEB Journal*. Federation of American Societies for Experimental Biology, 9(8), pp. 576–596. doi: 10.1096/fasebj.9.8.7768349.

Hara, K. *et al.* (2002) 'Raptor, a binding partner of target of rapamycin (TOR), mediates TOR action.', *Cell*. United States, 110(2), pp. 177–189.

Hardman, G. *et al.* (2019) 'Strong anion exchange-mediated phosphoproteomics reveals extensive human non-canonical phosphorylation', *The EMBO Journal*. doi: 10.15252/embj.2018100847.

Hastie, C. J., McLauchlan, H. J. and Cohen, P. (2006) 'Assay of protein kinases using radiolabeled ATP: a protocol.', *Nature protocols*. England, 1(2), pp. 968–971. doi: 10.1038/nprot.2006.149.

Heitman, J., Movva, N. R. and Hall, M. N. (1991) 'Targets for cell cycle arrest by the immunosuppressant rapamycin in yeast.', *Science (New York, N.Y.)*. United States, 253(5022), pp. 905–909.

Herman, P. K., Stack, J. H. and Emr, S. D. (1991) 'A genetic and structural analysis of the yeast Vps15 protein kinase: evidence for a direct role of Vps15p in vacuolar protein delivery.', *The EMBO journal*. England, 10(13), pp. 4049–4060.

Hill, S. M., Wrobel, L. and Rubinsztein, D. C. (2019) 'Post-translational modifications of Beclin 1 provide multiple strategies for autophagy regulation', *Cell Death and Differentiation*. Nature Publishing Group, pp. 617–629. doi: 10.1038/s41418-018-0254-9.

Hindupur, S. K. *et al.* (2018) 'The protein histidine phosphatase LHPP is a tumour suppressor', *Nature*. Nature Publishing Group, 555(7698), pp. 678–682. doi: 10.1038/nature26140.

Hirai, H. *et al.* (2010) 'MK-2206, an allosteric Akt inhibitor, enhances antitumor efficacy by standard chemotherapeutic agents or molecular targeted drugs in vitro and in vivo.', *Molecular cancer therapeutics*. United States, 9(7), pp. 1956–1967. doi: 10.1158/1535-7163.MCT-09-1012.

Hoffmann, R. *et al.* (1998) 'cAMP-specific phosphodiesterase HSPDE4D3 mutants which mimic activation and changes in rolipram inhibition triggered by protein kinase A phosphorylation of Ser-54: generation of a molecular model.', *The Biochemical journal*. England, 333 (Pt 1, pp. 139–149. doi: 10.1042/bj3330139.

Huang, D. Y. *et al.* (2004) 'Impaired regulation of renal K+ elimination in the sgk1-knockout mouse.', *Journal of the American Society of Nephrology : JASN*. United States, 15(4), pp. 885–891.

Huang, D. Y., Boini, K. M., Friedrich, B., *et al.* (2006) 'Blunted hypertensive effect of combined fructose and high-salt diet in gene-targeted mice lacking functional serum- and glucocorticoid-inducible kinase SGK1.', *American journal of physiology. Regulatory, integrative and comparative physiology*. United States, 290(4), pp. R935-44. doi: 10.1152/ajpregu.00382.2005.

Huang, D. Y., Boini, K. M., Osswald, H., *et al.* (2006) 'Resistance of mice lacking the serum- and glucocorticoid-inducible kinase SGK1 against salt-sensitive hypertension induced by a high-fat diet.', *American journal of physiology. Renal physiology*. United States, 291(6), pp. F1264-73. doi: 10.1152/ajprenal.00299.2005.

Huang, H.-T. *et al.* (2018) 'A Chemoproteomic Approach to Query the Degradable Kinome Using a Multi-kinase Degrader.', *Cell chemical biology*. United States, 25(1), pp. 88-99.e6. doi: 10.1016/j.chembiol.2017.10.005.

Huang, W.-C. and Chen, C.-C. (2005) 'Akt Phosphorylation of p300 at Ser-1834 Is Essential for Its Histone Acetyltransferase and Transcriptional Activity', *Molecular and Cellular Biology*. American Society for Microbiology, 25(15), pp. 6592–6602. doi: 10.1128/mcb.25.15.6592-6602.2005.

Huang, X. and Dixit, V. M. (2016) 'Drugging the undruggables: exploring the ubiquitin system for drug development', *Cell Research*. The Author(s), 26, p. 484. Available at: http://dx.doi.org/10.1038/cr.2016.31.

Hughes, S. J. and Ciulli, A. (2017) 'Molecular recognition of ternary complexes: a new dimension in the structure-guided design of chemical degraders', *Essays in biochemistry*. Portland Press Ltd., 61(5), pp. 505–516. doi: 10.1042/EBC20170041.

Humphrey, S. J., Azimifar, S. B. and Mann, M. (2015) 'High-throughput phosphoproteomics reveals in vivo insulin signaling dynamics', *Nature Biotechnology*. Nature Publishing Group, 33(9), pp. 990–995. doi: 10.1038/nbt.3327.

Hunter, T. (2012) 'Why nature chose phosphate to modify proteins.', *Philosophical transactions of the Royal Society of London. Series B, Biological sciences*, 367(1602), pp. 2513–6. doi: 10.1098/rstb.2012.0013.

Ichimura, T. *et al.* (2005) '14-3-3 proteins modulate the expression of epithelial Na+ channels by phosphorylation-dependent interaction with Nedd4-2 ubiquitin ligase.', *The Journal of biological chemistry*. United States, 280(13), pp. 13187–13194. doi: 10.1074/jbc.M412884200.

Ikenoue, T. *et al.* (2005) 'Functional analysis of PIK3CA gene mutations in human colorectal cancer.', *Cancer research*. United States, 65(11), pp. 4562–4567. doi: 10.1158/0008-5472.CAN-04-4114.

Inoki, K. *et al.* (2002) 'TSC2 is phosphorylated and inhibited by Akt and suppresses mTOR signalling.', *Nature cell biology*. England, 4(9), pp. 648–657. doi: 10.1038/ncb839.

Inoki, K. *et al.* (2003) 'Rheb GTPase is a direct target of TSC2 GAP activity and regulates mTOR signaling.', *Genes & development*. United States, 17(15), pp. 1829–1834. doi: 10.1101/gad.1110003.

Itakura, E. *et al.* (2008) 'Beclin 1 forms two distinct phosphatidylinositol 3-kinase complexes with mammalian Atg14 and UVRAG.', *Molecular biology of the cell*. United States, 19(12), pp. 5360–5372. doi: 10.1091/mbc.e08-01-0080.

Jacinto, E. *et al.* (2004) 'Mammalian TOR complex 2 controls the actin cytoskeleton and is rapamycin insensitive.', *Nature cell biology*. England, 6(11), pp. 1122–1128. doi: 10.1038/ncb1183.

Jacinto, E. *et al.* (2006) 'SIN1/MIP1 Maintains rictor-mTOR Complex Integrity and Regulates Akt Phosphorylation and Substrate Specificity', *Cell*, 127(1), pp. 125–137. doi: https://doi.org/10.1016/j.cell.2006.08.033.

James, S. R. *et al.* (1996) 'Specific binding of the Akt-1 protein kinase to phosphatidylinositol 3,4,5-trisphosphate without subsequent activation', *The Biochemical journal*, 315 (Pt 3(Pt 3), pp. 709–713. doi: 10.1042/bj3150709.

Jewell, J. L., Russell, R. C. and Guan, K.-L. (2013) 'Amino acid signalling upstream of mTOR.', *Nature reviews. Molecular cell biology*. England, 14(3), pp. 133–139. doi: 10.1038/nrm3522.

Jia, R. and Bonifacino, J. S. (2019) 'Lysosome Positioning Influences mTORC2 and AKT Signaling', *Molecular Cell*, 75(1), pp. 26-38.e3. doi: https://doi.org/10.1016/j.molcel.2019.05.009.

Jiang, F. and Doudna, J. A. (2017) 'CRISPR–Cas9 Structures and Mechanisms', *Annual Review of Biophysics*. Annual Reviews, 46(1), pp. 505–529. doi: 10.1146/annurev-biophys-062215-010822.

Jiang, W. *et al.* (2018) 'The PIK3CA E542K and E545K mutations promote glycolysis and proliferation via induction of the beta-catenin/SIRT3 signaling pathway in cervical cancer.', *Journal of hematology & oncology*. England, 11(1), p. 139. doi: 10.1186/s13045-018-0674-5.

Jiang, X. *et al.* (2017) 'VPS34 stimulation of p62 phosphorylation for cancer progression.', *Oncogene*. England, 36(50), pp. 6850–6862. doi: 10.1038/onc.2017.295.

Jin, L. *et al.* (2008) 'Mechanism of ubiquitin-chain formation by the human anaphase-promoting complex.', *Cell*. United States, 133(4), pp. 653–665. doi: 10.1016/j.cell.2008.04.012.

Johnson, L. N. *et al.* (1998) 'The structural basis for substrate recognition and control by protein kinases 1', *FEBS Letters*. John Wiley & Sons, Ltd, 430(1–2), pp. 1–11. doi: 10.1016/S0014-5793(98)00606-1.

Kaizuka, T. *et al.* (2010) 'Tti1 and Tel2 are critical factors in mammalian target of rapamycin complex assembly.', *The Journal of biological chemistry*. United States, 285(26), pp. 20109–20116. doi: 10.1074/jbc.M110.121699.

Kalender, A. *et al.* (2010) 'Metformin, independent of AMPK, inhibits mTORC1 in a rag GTPase-dependent manner', *Cell Metabolism*, 11(5), pp. 390–401. doi: 10.1016/j.cmet.2010.03.014.

Kan, Z. *et al.* (2010) 'Diverse somatic mutation patterns and pathway alterations in human cancers.', *Nature*. England, 466(7308), pp. 869–873. doi: 10.1038/nature09208.

Kang, S., Bader, A. G. and Vogt, P. K. (2005) 'Phosphatidylinositol 3-kinase mutations identified in human cancer are oncogenic.', *Proceedings of the National Academy of Sciences of the United States of America*. United States, 102(3), pp. 802–807. doi: 10.1073/pnas.0408864102.

Kazyken, D. *et al.* (2019) 'AMPK directly activates mTORC2 to promote cell survival during acute energetic stress', *Science Signaling*, 12(585), p. eaav3249. doi: 10.1126/scisignal.aav3249.

Kihara, A. *et al.* (2001) 'Two distinct Vps34 phosphatidylinositol 3-kinase complexes function in autophagy and carboxypeptidase Y sorting in Saccharomyces cerevisiae.', *The Journal of cell biology*. United States, 152(3), pp. 519–530. doi: 10.1083/jcb.152.3.519.

Kim, D.-H. *et al.* (2002) 'mTOR interacts with raptor to form a nutrient-sensitive complex that signals to the cell growth machinery.', *Cell*. United States, 110(2), pp. 163–175.

Kim, D.-H. *et al.* (2003) 'GbetaL, a positive regulator of the rapamycin-sensitive pathway required for the nutrient-sensitive interaction between raptor and mTOR.', *Molecular cell*. United States, 11(4), pp. 895–904.

Kim, D. U. *et al.* (2019) 'Inhibition of phosphodiesterase 4D decreases the malignant properties of DLD-1 colorectal cancer cells by repressing the AKT/mTOR/Myc signaling pathway.', *Oncology letters*. Greece, 17(3), pp. 3589–3598. doi: 10.3892/ol.2019.9996.

Kim, E. *et al.* (2008) 'Regulation of TORC1 by Rag GTPases in nutrient response.', *Nature cell biology*. England, 10(8), pp. 935–945. doi: 10.1038/ncb1753.

Kim, J. *et al.* (2013) 'Differential regulation of distinct Vps34 complexes by AMPK in nutrient stress and autophagy.', *Cell*. United States, 152(1–2), pp. 290–303. doi: 10.1016/j.cell.2012.12.016.

Kim, M. S. *et al.* (2008) 'Mutational analysis of oncogenic AKT E17K mutation in common solid cancers and acute leukaemias.', *British journal of cancer*. England, 98(9), pp. 1533–1535. doi: 10.1038/sj.bjc.6604212.

Knaevelsrud, H. *et al.* (2010) 'UVRAG mutations associated with microsatellite unstable colon cancer do not affect autophagy.', *Autophagy*. United States, 6(7), pp. 863–870. doi: 10.4161/auto.6.7.13033.

Kobayashi, T. *et al.* (1999) 'Characterization of the structure and regulation of two novel isoforms of serum- and glucocorticoid-induced protein kinase.', *The Biochemical journal*. England, 344 Pt 1, pp. 189–197.

Kohn, A. D. *et al.* (1996) 'Expression of a constitutively active Akt Ser/Thr kinase in 3T3-L1 adipocytes stimulates glucose uptake and glucose transporter 4 translocation.', *The Journal of biological chemistry*. United States, 271(49), pp. 31372–31378. doi: 10.1074/jbc.271.49.31372.

Komander, D. (2009) 'The emerging complexity of protein ubiquitination.', *Biochemical Society transactions*. England, 37(Pt 5), pp. 937–953. doi: 10.1042/BST0370937.

Kriegsmann, M. *et al.* (2014) 'Mutational profiles in triple-negative breast cancer defined by ultradeep multigene sequencing show high rates of PI3K pathway alterations and clinically relevant entity subgroup specific differences', *Oncotarget*, 5(20), pp. 9952–9965. doi: 10.18632/oncotarget.2481.

Kwon, A. *et al.* (2019) 'Tracing the origin and evolution of pseudokinases across the tree of life', *Science Signaling*. American Association for the Advancement of Science, 12(578). doi: 10.1126/scisignal.aav3810.

Lahiry, P. *et al.* (2010) 'Kinase mutations in human disease: interpreting genotype-phenotype relationships.', *Nature reviews. Genetics*. England, 11(1), pp. 60–74. doi: 10.1038/nrg2707.

Lai, A. C. *et al.* (2016) 'Modular PROTAC Design for the Degradation of Oncogenic BCR-ABL.', *Angewandte Chemie (International ed. in English)*. Germany, 55(2), pp. 807–810. doi: 10.1002/anie.201507634.

Lamothe, S. M. and Zhang, S. (2013) 'The serum- and glucocorticoid-inducible kinases SGK1 and SGK3 regulate hERG channel expression via ubiquitin ligase Nedd4-2 and GTPase Rab11.', *The Journal of biological chemistry*. United States, 288(21), pp. 15075–15084. doi: 10.1074/jbc.M113.453670.

Lang, F. *et al.* (2006) '(Patho)physiological Significance of the Serum- and Glucocorticoid-Inducible Kinase Isoforms', *Physiological Reviews*. American Physiological Society, 86(4), pp. 1151–1178. doi: 10.1152/physrev.00050.2005.

Lang, F., Artunc, F. and Vallon, V. (2009) 'The physiological impact of the serum and glucocorticoid-inducible kinase SGK1.', *Current opinion in nephrology and hypertension*. England, 18(5), pp. 439–448. doi: 10.1097/MNH.0b013e32832f125e.

Lang, F. and Voelkl, J. (2013) 'Therapeutic potential of serum and glucocorticoid inducible kinase inhibition.', *Expert opinion on investigational drugs*. England, 22(6), pp. 701–714. doi: 10.1517/13543784.2013.778971.

Laplante, M. and Sabatini, D. M. (2012) 'mTOR signaling in growth control and disease', *Cell*, 149(2), pp. 274–293. doi: 10.1016/j.cell.2012.03.017.

Lee, D.-F. *et al.* (2007) 'IKK beta suppression of TSC1 links inflammation and tumor angiogenesis via the mTOR pathway.', *Cell*. United States, 130(3), pp. 440–455. doi: 10.1016/j.cell.2007.05.058.

Lee, D. H. and Goldberg, A. L. (1998) 'Proteasome inhibitors: valuable new tools for cell biologists.', *Trends in cell biology*. England, 8(10), pp. 397–403.

Lee, I. *et al.* (2005) 'cAMP-dependent tyrosine phosphorylation of subunit I inhibits cytochrome c oxidase activity.', *The Journal of biological chemistry*. United States, 280(7), pp. 6094–6100. doi: 10.1074/jbc.M411335200.

Li, H., Zuo, J. and Tang, W. (2018) 'Phosphodiesterase-4 Inhibitors for the Treatment of Inflammatory Diseases ', *Frontiers in Pharmacology* , p. 1048. Available at: https://www.frontiersin.org/article/10.3389/fphar.2018.01048.

Li, J. *et al.* (1997) 'PTEN, a putative protein tyrosine phosphatase gene mutated in human brain, breast, and prostate cancer.', *Science (New York, N.Y.)*. United States, 275(5308), pp. 1943–1947.

Li, W. *et al.* (2008) 'Genome-wide and functional annotation of human E3 ubiquitin ligases identifies MULAN, a mitochondrial E3 that regulates the organelle's dynamics and signaling.', *PloS one*. United States, 3(1), p. e1487. doi: 10.1371/journal.pone.0001487.

Liang, C. *et al.* (2008) 'Beclin1-binding UVRAG targets the class C Vps complex to coordinate autophagosome maturation and endocytic trafficking.', *Nature cell biology*. England, 10(7), pp. 776–787. doi: 10.1038/ncb1740.

Liang, J. *et al.* (2002) 'PKB/Akt phosphorylates p27, impairs nuclear import of p27 and opposes p27-mediated G1 arrest.', *Nature medicine*. United States, 8(10), pp. 1153–1160. doi: 10.1038/nm761.

Liang, X. *et al.* (2017) 'Therapeutic inhibition of SGK1 suppresses colorectal cancer.', *Experimental & molecular medicine*. United States, 49(11), p. e399. doi: 10.1038/emm.2017.184.

Liaw, D. *et al.* (1997) 'Germline mutations of the PTEN gene in Cowden disease, an inherited breast and thyroid cancer syndrome.', *Nature genetics*. United States, 16(1), pp. 64–67. doi: 10.1038/ng0597-64.

Lin, D.-C. *et al.* (2013) 'Genomic and functional characterizations of phosphodiesterase subtype 4D in human cancers', *Proceedings of the National Academy of Sciences*, 110(15), pp. 6109 LP – 6114. doi: 10.1073/pnas.1218206110.

Liu, D., Yang, X. and Songyang, Z. (2000) 'Identification of CISK, a new member of the SGK kinase family that promotes IL-3-dependent survival', *Current Biology*, 10(19), pp. 1233–1236. doi: https://doi.org/10.1016/S0960-9822(00)00733-8.

Liu, F. *et al.* (2018) 'Prolonged inhibition of class I PI3K promotes liver cancer stem cell expansion by augmenting SGK3/GSK-3β/β-catenin signalling', *Journal of experimental & clinical cancer research : CR*. BioMed Central, 37(1), p. 122. doi: 10.1186/s13046-018-0801-8.

Liu, J. *et al.* (2017) 'SGK2 promotes hepatocellular carcinoma progression and mediates GSK-3β/β-catenin signaling in HCC cells', *Tumor Biology*. SAGE Publications Ltd STM, 39(6), p. 1010428317700408. doi: 10.1177/1010428317700408.

Liu, P. *et al.* (2014) 'Dual phosphorylation of Sin1 at T86 and T398 negatively regulates mTORC2 complex integrity and activity', *Protein and Cell*. Springer-Verlag GmbH Co. KG, 5(3), pp. 171–177. doi: 10.1007/s13238-014-0021-8.

Liu, P. *et al.* (2015) 'PtdIns(3,4,5)P3-Dependent Activation of the mTORC2 Kinase Complex.', *Cancer discovery*. United States, 5(11), pp. 1194–1209. doi: 10.1158/2159-8290.CD-15-0460.

Liu, Y. *et al.* (2019) 'SGK2 promotes renal cancer progression via enhancing ERK 1/2 and AKT phosphorylation.', *European review for medical and pharmacological sciences*. Italy, 23(7), pp. 2756–2767. doi: 10.26355/eurrev_201904_17549.

Los, G. V *et al.* (2008) 'HaloTag: a novel protein labeling technology for cell imaging and protein analysis.', *ACS chemical biology*. United States, 3(6), pp. 373–382. doi: 10.1021/cb800025k.

Lu, J. *et al.* (2015) 'Hijacking the E3 Ubiquitin Ligase Cereblon to Efficiently Target BRD4.', *Chemistry & biology*. United States, 22(6), pp. 755–763. doi: 10.1016/j.chembiol.2015.05.009.

Lu, L. *et al.* (2019) 'Inhibition of the STAT3 target SGK1 sensitizes diffuse large B cell lymphoma cells to AKT inhibitors', *Blood cancer journal*. Nature Publishing Group UK, 9(4), p. 43. doi: 10.1038/s41408-019-0203-y.

Lu, M. *et al.* (2011) 'mSIN1 protein mediates SGK1 protein interaction with mTORC2 protein complex and is required for selective activation of the epithelial sodium channel.', *The Journal of biological chemistry*. United States, 286(35), pp. 30647–30654. doi: 10.1074/jbc.M111.257592.

Lučic, I. *et al.* (2018) 'Conformational sampling of membranes by Akt controls its activation and inactivation', *Proceedings of the National Academy of Sciences of the United States of America*. National

Academy of Sciences, 115(17), pp. E3940–E3949. doi: 10.1073/pnas.1716109115.

Ma, L. *et al.* (2005) 'Phosphorylation and functional inactivation of TSC2 by Erk implications for tuberous sclerosis and cancer pathogenesis.', *Cell*. United States, 121(2), pp. 179–193. doi: 10.1016/j.cell.2005.02.031.

Ma, M. *et al.* (2017) 'Cryo-EM structure and biochemical analysis reveal the basis of the functional difference between human PI3KC3-C1 and -C2.', *Cell research*. England, 27(8), pp. 989–1001. doi: 10.1038/cr.2017.94.

Ma, X. *et al.* (2017) 'MTORC1-mediated NRBF2 phosphorylation functions as a switch for the class III PtdIns3K and autophagy.', *Autophagy*. United States, 13(3), pp. 592–607. doi: 10.1080/15548627.2016.1269988.

MacDougall, L. K., Domin, J. and Waterfield, M. D. (1995) 'A family of phosphoinositide 3-kinases in Drosophila identifies a new mediator of signal transduction', *Current Biology*, 5(12), pp. 1404–1415. doi: 10.1016/S0960-9822(95)00278-8.

Maehama, T. and Dixon, J. E. (1998) 'The tumor suppressor, PTEN/MMAC1, dephosphorylates the lipid second messenger, phosphatidylinositol 3,4,5-trisphosphate.', *The Journal of biological chemistry*. United States, 273(22), pp. 13375–13378. doi: 10.1074/jbc.273.22.13375.

Maejima, Y. *et al.* (2013) 'Mst1 inhibits autophagy by promoting the interaction between Beclin1 and Bcl-2.', *Nature medicine*. United States, 19(11), pp. 1478–1488. doi: 10.1038/nm.3322.

Maffucci, T. and Falasca, M. (2014) 'New insight into the intracellular roles of class II phosphoinositide 3-kinases', *Biochemical Society Transactions*. Portland Press Ltd, pp. 1378–1382. doi: 10.1042/BST20140140.

Malik, N. *et al.* (2018) 'Mechanism of activation of SGK3 by growth factors via the Class 1 and Class 3 PI3Ks.', *The Biochemical journal*. England, 475(1), pp. 117–135. doi: 10.1042/BCJ20170650.

Malik, N. *et al.* (2019) 'Phosphoproteomics reveals that the hVPS34 regulated SGK3 kinase specifically phosphorylates endosomal proteins including Syntaxin-7, Syntaxin-12, RFIP4 and WDR44', *bioRxiv*. Cold Spring Harbor Laboratory, p. 741652. doi: 10.1101/741652.

Mamane, Y. *et al.* (2004) 'eIF4E--from translation to transformation.', *Oncogene*. England, 23(18), pp. 3172–3179. doi: 10.1038/sj.onc.1207549.

Maniaci, C. *et al.* (2017) 'Homo-PROTACs: bivalent small-molecule dimerizers of the VHL E3 ubiquitin ligase to induce self-degradation.', *Nature communications*. England, 8(1), p. 830. doi: 10.1038/s41467-017-00954-1.

Manning, B. D. *et al.* (2002) 'Identification of the tuberous sclerosis complex-2 tumor suppressor gene product tuberin as a target of the phosphoinositide 3-kinase/akt pathway.', *Molecular cell*. United States, 10(1), pp. 151–162.

Manning, B. D. and Cantley, L. C. (2007) 'AKT/PKB signaling: navigating downstream', *Cell*, 129(7), pp. 1261–1274. doi: 10.1016/j.cell.2007.06.009.

Manning, G. *et al.* (2002) 'The protein kinase complement of the human genome.', *Science (New York, N.Y.)*. United States, 298(5600), pp. 1912–1934. doi: 10.1126/science.1075762.

Marat, A. L. *et al.* (2017) 'mTORC1 activity repression by late endosomal phosphatidylinositol 3,4-bisphosphate.', *Science (New York, N.Y.)*. United States, 356(6341), pp. 968–972. doi: 10.1126/science.aaf8310.

Margaria, J. P. *et al.* (2019) 'Class II PI3Ks at the Intersection between Signal Transduction and Membrane Trafficking', *Biomolecules*. MDPI, 9(3), p. 104. doi: 10.3390/biom9030104.

Martinez, J. *et al.* (2015) 'Molecular characterization of LC3-associated phagocytosis reveals distinct roles for Rubicon, NOX2 and autophagy proteins.', *Nature cell biology*. England, 17(7), pp. 893–906. doi: 10.1038/ncb3192.

Matsunaga, K. *et al.* (2009) 'Two Beclin 1-binding proteins, Atg14L and Rubicon, reciprocally regulate autophagy at different stages.', *Nature cell biology*. England, 11(4), pp. 385–396. doi: 10.1038/ncb1846.

Matsunaga, K. *et al.* (2010) 'Autophagy requires endoplasmic reticulum targeting of the PI3-kinase complex via Atg14L.', *The Journal of cell biology*. United States, 190(4), pp. 511–521. doi: 10.1083/jcb.200911141.

Matsunaga, K., Noda, T. and Yoshimori, T. (2009) 'Binding Rubicon to cross the Rubicon.', *Autophagy*. United States, 5(6), pp. 876–877. doi: 10.4161/auto.9098.

Maurice, D. H. *et al.* (2014) 'Advances in targeting cyclic nucleotide phosphodiesterases', *Nature reviews. Drug discovery*, 13(4), pp. 290–314. doi: 10.1038/nrd4228.

Mayo, L. D. and Donner, D. B. (2001) 'A phosphatidylinositol 3-kinase/Akt pathway promotes translocation of Mdm2 from the cytoplasm to the nucleus.', *Proceedings of the National Academy of Sciences of the United States of America*. United States, 98(20), pp. 11598–11603. doi: 10.1073/pnas.181181198.

McCormick, J. A. *et al.* (2004) 'Targeted disruption of the protein kinase SGK3/CISK impairs postnatal hair follicle development.', *Molecular biology of the cell*. United States, 15(9), pp. 4278–4288. doi: 10.1091/mbc.e04-01-0027.

McKenna, M., McGarrigle, S. and Pidgeon, G. P. (2018) 'The next generation of PI3K-Akt-mTOR pathway inhibitors in breast cancer cohorts', *Biochimica et Biophysica Acta (BBA) - Reviews on Cancer*, 1870(2), pp. 185–197. doi: https://doi.org/10.1016/j.bbcan.2018.08.001.

Medema, R. H. *et al.* (2000) 'AFX-like Forkhead transcription factors mediate cell-cycle regulation by Ras and PKB through p27kip1.', *Nature*. England, 404(6779), pp. 782–787. doi: 10.1038/35008115.

Mika, D. and Conti, M. (2016) 'PDE4D phosphorylation: A coincidence detector integrating multiple signaling pathways', *Cellular Signalling*, 28(7), pp. 719–724. doi: https://doi.org/10.1016/j.cellsig.2015.11.001.

Mikolcevic, P. *et al.* (2012) 'Cyclin-dependent kinase 16/PCTAIRE kinase 1 is activated by cyclin Y and is essential for spermatogenesis.', *Molecular and cellular biology*, 32(4), pp. 868–79. doi: 10.1128/MCB.06261-11.

Mikosz, C. A. *et al.* (2001) 'Glucocorticoid receptor-mediated protection from apoptosis is associated with induction of the serine/threonine survival kinase gene, sgk-1.', *The Journal of biological chemistry*. United States, 276(20), pp. 16649–16654. doi: 10.1074/jbc.M010842200.

Miller, L. A. (2011) 'The national practitioner data bank: A primer for clinicians', *Journal of Perinatal and Neonatal Nursing*, 25(3), pp. 224–225. doi: 10.1097/JPN.0b013e3182257331.

Miller, T. W. *et al.* (2011) 'Mutations in the phosphatidylinositol 3-kinase pathway: role in tumor progression and therapeutic implications in breast cancer.', *Breast cancer research : BCR*. England, 13(6), p. 224. doi: 10.1186/bcr3039.

Mishra, R. R. *et al.* (2018) 'Reactivation of cAMP Pathway by PDE4D Inhibition Represents a Novel Druggable Axis for Overcoming Tamoxifen Resistance in ER-positive Breast Cancer.', *Clinical cancer research : an official journal of the American Association for Cancer Research*. United States, 24(8), pp. 1987–2001. doi: 10.1158/1078-0432.CCR-17-2776.

Mora, A. *et al.* (2004) 'PDK1 , the master regulator of AGC kinase signal transduction', *Seminars in Cell & Developmental Biology*, 15, pp. 161–170. doi: 10.1016/j.semcdb.2003.12.022.

Munson, M. J. *et al.* (2015) 'mTOR activates the VPS34-UVRAG complex to regulate autolysosomal tubulation and cell survival.', *The EMBO journal*. England, 34(17), pp. 2272–2290. doi: 10.15252/embj.201590992.

Murphy, E. and Steenbergen, C. (2008) 'Mechanisms underlying acute protection from cardiac ischemia-reperfusion injury', *Physiological reviews*, 88(2), pp. 581–609. doi: 10.1152/physrev.00024.2007.

Murray, J. T. *et al.* (2004) 'Exploitation of KESTREL to identify NDRG family members as physiological

substrates for SGK1 and GSK3.', *The Biochemical journal*. England, 384(Pt 3), pp. 477–488. doi: 10.1042/BJ20041057.

Murray, J. T. *et al.* (2005) 'Identification of different specificity requirements between SGK1 and PKBalpha.', *FEBS letters*, 579(5), pp. 991–4. doi: 10.1016/j.febslet.2004.12.069.

Myers, M. P. *et al.* (1998) 'The lipid phosphatase activity of PTEN is critical for its tumor supressor function.', *Proceedings of the National Academy of Sciences of the United States of America*. United States, 95(23), pp. 13513–13518. doi: 10.1073/pnas.95.23.13513.

Nabet, B. *et al.* (2018) 'The dTAG system for immediate and target-specific protein degradation', *Nature Chemical Biology*, 14(5), pp. 431–441. doi: 10.1038/s41589-018-0021-8.

Naray-Fejes-Toth, A. *et al.* (1999) 'sgk is an aldosterone-induced kinase in the renal collecting duct. Effects on epithelial na+ channels.', *The Journal of biological chemistry*. United States, 274(24), pp. 16973–16978. doi: 10.1074/jbc.274.24.16973.

Nasir, O. *et al.* (2009) 'Relative resistance of SGK1 knockout mice against chemical carcinogenesis', *IUBMB Life*. John Wiley & Sons, Ltd, 61(7), pp. 768–776. doi: 10.1002/iub.209.

Natsume, T. *et al.* (2016) 'Rapid Protein Depletion in Human Cells by Auxin-Inducible Degron Tagging with Short Homology Donors.', *Cell reports*. United States, 15(1), pp. 210–218. doi: 10.1016/j.celrep.2016.03.001.

Nemazanyy, I. *et al.* (2013) 'Defects of Vps15 in skeletal muscles lead to autophagic vacuolar myopathy and lysosomal disease.', *EMBO molecular medicine*. England, 5(6), pp. 870–890. doi: 10.1002/emmm.201202057.

Nero, T. L. *et al.* (2014) 'Oncogenic protein interfaces: small molecules, big challenges.', *Nature reviews. Cancer*. England, 14(4), pp. 248–262. doi: 10.1038/nrc3690.

Newton, K. *et al.* (2008) 'Ubiquitin chain editing revealed by polyubiquitin linkage-specific antibodies.', *Cell*. United States, 134(4), pp. 668–678. doi: 10.1016/j.cell.2008.07.039.

Nishimura, K. *et al.* (2009) 'An auxin-based degron system for the rapid depletion of proteins in nonplant cells.', *Nature methods*. United States, 6(12), pp. 917–922. doi: 10.1038/nmeth.1401.

Nora, E. P. *et al.* (2017) 'Targeted Degradation of CTCF Decouples Local Insulation of Chromosome Domains from Genomic Compartmentalization.', *Cell*. United States, 169(5), pp. 930-944.e22. doi: 10.1016/j.cell.2017.05.004.

Nunes, J. *et al.* (2019) 'Targeting IRAK4 for Degradation with PROTACs.', *ACS medicinal chemistry letters*. United States, 10(7), pp. 1081–1085. doi: 10.1021/acsmedchemlett.9b00219.

Ohashi, Y. *et al.* (2016) 'Characterization of Atg38 and NRBF2, a fifth subunit of the autophagic Vps34/PIK3C3 complex.', *Autophagy*. United States, 12(11), pp. 2129–2144. doi: 10.1080/15548627.2016.1226736.

Ohkuma, S. *et al.* (1993) 'Inhibition of cell growth by bafilomycin A1, a selective inhibitor of vacuolar H(+)-ATPase.', *In vitro cellular & developmental biology. Animal*. Germany, 29A(11), pp. 862–866.

Olson, C. M. *et al.* (2018) 'Pharmacological perturbation of CDK9 using selective CDK9 inhibition or degradation.', *Nature chemical biology*. United States, 14(2), pp. 163–170. doi: 10.1038/nchembio.2538.

Ou, C.-Y. *et al.* (2010) 'Two cyclin-dependent kinase pathways are essential for polarized trafficking of presynaptic components.', *Cell*. United States, 141(5), pp. 846–858. doi: 10.1016/j.cell.2010.04.011.

Papa, S. (2002) 'The NDUFS4 nuclear gene of complex I of mitochondria and the cAMP cascade', *Biochimica et Biophysica Acta (BBA) - Bioenergetics*, 1555(1), pp. 147–153. doi: https://doi.org/10.1016/S0005-2728(02)00270-0.

Parikh, C. *et al.* (2012) 'Disruption of PH-kinase domain interactions leads to oncogenic activation of AKT in human cancers.', *Proceedings of the National Academy of Sciences of the United States of America*.

United States, 109(47), pp. 19368–19373. doi: 10.1073/pnas.1204384109.

Park, J.-M. *et al.* (2016) 'The ULK1 complex mediates MTORC1 signaling to the autophagy initiation machinery via binding and phosphorylating ATG14.', *Autophagy*. United States, 12(3), pp. 547–564. doi: 10.1080/15548627.2016.1140293.

Parmigiani, A. *et al.* (2014) 'Sestrins Inhibit mTORC1 Kinase Activation through the GATOR Complex', *Cell Reports*. Elsevier, 9(4), pp. 1281–1291. doi: 10.1016/j.celrep.2014.10.019.

Pasham, V. *et al.* (2011) 'Regulation of gastric acid secretion by the serum and glucocorticoid inducible kinase isoform SGK3.', *Journal of gastroenterology*. Japan, 46(3), pp. 305–317. doi: 10.1007/s00535-010-0348-8.

Pearce, L. R. *et al.* (2007) 'Identification of Protor as a novel Rictor-binding component of mTOR complex-2.', *The Biochemical journal*. England, 405(3), pp. 513–522. doi: 10.1042/BJ20070540.

Pearson, R. B. and Kemp, B. E. (1991) 'Protein kinase phosphorylation site sequences and consensus specificity motifs: tabulations.', *Methods in enzymology*, 200, pp. 62–81. doi: 10.1016/0076-6879(91)00127-i.

Perez, E. E. *et al.* (2008) 'Establishment of HIV-1 resistance in CD4+ T cells by genome editing using zinc-finger nucleases.', *Nature biotechnology*. United States, 26(7), pp. 808–816. doi: 10.1038/nbt1410.

del Peso, L. *et al.* (1997) 'Interleukin-3-induced phosphorylation of BAD through the protein kinase Akt.', *Science (New York, N.Y.)*. United States, 278(5338), pp. 687–689.

Peterson, T. R. *et al.* (2009) 'DEPTOR is an mTOR inhibitor frequently overexpressed in multiple myeloma cells and required for their survival.', *Cell*. United States, 137(5), pp. 873–886. doi: 10.1016/j.cell.2009.03.046.

Petrocca, F. *et al.* (2013) 'A Genome-wide siRNA Screen Identifies Proteasome Addiction as a Vulnerability of Basal-like Triple-Negative Breast Cancer Cells', *Cancer Cell*. Elsevier, 24(2), pp. 182–196. doi: 10.1016/j.ccr.2013.07.008.

Pettersson, M. and Crews, C. M. (2019) 'PROteolysis TArgeting Chimeras (PROTACs) — Past, present and future', *Drug Discovery Today: Technologies*. doi: https://doi.org/10.1016/j.ddtec.2019.01.002.

Phung, T. L. *et al.* (2006) 'Pathological angiogenesis is induced by sustained Akt signaling and inhibited by rapamycin.', *Cancer cell*. United States, 10(2), pp. 159–170. doi: 10.1016/j.ccr.2006.07.003.

Popow, J. *et al.* (2019) 'Highly Selective PTK2 Proteolysis Targeting Chimeras to Probe Focal Adhesion Kinase Scaffolding Functions', *Journal of Medicinal Chemistry*. American Chemical Society, 62(5), pp. 2508–2520. doi: 10.1021/acs.jmedchem.8b01826.

Posor, Y. *et al.* (2013) 'Spatiotemporal control of endocytosis by phosphatidylinositol-3,4-bisphosphate.', *Nature*. England, 499(7457), pp. 233–237. doi: 10.1038/nature12360.

Prabu, S. K. *et al.* (2006) 'Protein kinase A-mediated phosphorylation modulates cytochrome c oxidase function and augments hypoxia and myocardial ischemia-related injury.', *The Journal of biological chemistry*. United States, 281(4), pp. 2061–2070. doi: 10.1074/jbc.M507741200.

Qin, J. *et al.* (2004) 'IRAK4 kinase activity is redundant for interleukin-1 (IL-1) receptor-associated kinase phosphorylation and IL-1 responsiveness.', *The Journal of biological chemistry*. United States, 279(25), pp. 26748–26753. doi: 10.1074/jbc.M400785200.

Rajakulendran, T. and Sicheri, F. (2010) 'Allosteric protein kinase regulation by pseudokinases: insights from STRAD.', *Science signaling*, 3(111), p. pe8. doi: 10.1126/scisignal.3111pe8.

Ran, F. A., Hsu, P. D., Lin, C.-Y., *et al.* (2013) 'Double nicking by RNA-guided CRISPR Cas9 for enhanced genome editing specificity.', *Cell*. United States, 154(6), pp. 1380–1389. doi: 10.1016/j.cell.2013.08.021.

Ran, F. A., Hsu, P. D., Wright, J., *et al.* (2013) 'Genome engineering using the CRISPR-Cas9 system', *Nature protocols*. 2013/10/24, 8(11), pp. 2281–2308. doi: 10.1038/nprot.2013.143.

Rana, S. *et al.* (2019) 'Selective degradation of CDK6 by a palbociclib based PROTAC.', *Bioorganic & medicinal chemistry letters*. England, 29(11), pp. 1375–1379. doi: 10.1016/j.bmcl.2019.03.035.

Rao, A. D. *et al.* (2013) 'Polymorphisms in the serum- and glucocorticoid-inducible kinase 1 gene are associated with blood pressure and renin response to dietary salt intake.', *Journal of human hypertension*. England, 27(3), pp. 176–180. doi: 10.1038/jhh.2012.22.

De Rasmo, D. *et al.* (2008) 'cAMP-dependent protein kinase regulates the mitochondrial import of the nuclear encoded NDUFS4 subunit of complex I.', *Cellular signalling*. England, 20(5), pp. 989–997. doi: 10.1016/j.cellsig.2008.01.017.

De Rasmo, D. *et al.* (2015) 'Intramitochondrial adenylyl cyclase controls the turnover of nuclear-encoded subunits and activity of mammalian complex I of the respiratory chain', *Biochimica et Biophysica Acta (BBA) - Molecular Cell Research*, 1853(1), pp. 183–191. doi: https://doi.org/10.1016/j.bbamcr.2014.10.016.

De Rasmo, D. *et al.* (2016) 'cAMP regulates the functional activity, coupling efficiency and structural organization of mammalian FOF1 ATP synthase', *Biochimica et Biophysica Acta (BBA) - Bioenergetics*, 1857(4), pp. 350–358. doi: https://doi.org/10.1016/j.bbabio.2016.01.006.

Richardson, C. and Alessi, D. R. (2008) 'The regulation of salt transport and blood pressure by the WNK-SPAK/OSR1 signalling pathway', *Journal of Cell Science*, 121(20), pp. 3293–3304. doi: 10.1242/jcs.029223.

Richter, W. and Conti, M. (2002) 'Dimerization of the type 4 cAMP-specific phosphodiesterases is mediated by the upstream conserved regions (UCRs).', *The Journal of biological chemistry*. United States, 277(43), pp. 40212–40221. doi: 10.1074/jbc.M203585200.

Richter, W. and Conti, M. (2004) 'The oligomerization state determines regulatory properties and inhibitor sensitivity of type 4 cAMP-specific phosphodiesterases.', *The Journal of biological chemistry*. United States, 279(29), pp. 30338–30348. doi: 10.1074/jbc.M312687200.

Ring, A. M. *et al.* (2007) 'An SGK1 site in WNK4 regulates Na+ channel and K+ channel activity and has implications for aldosterone signaling and K+ homeostasis.', *Proceedings of the National Academy of Sciences of the United States of America*. United States, 104(10), pp. 4025–4029. doi: 10.1073/pnas.0611728104.

Rodriguez-Viciana, P. *et al.* (1994) 'Phosphatidylinositol-3-OH kinase as a direct target of Ras.', *Nature*. England, 370(6490), pp. 527–532. doi: 10.1038/370527a0.

Rostislavleva, K. *et al.* (2015) 'Structure and flexibility of the endosomal Vps34 complex reveals the basis of its function on membranes.', *Science (New York, N.Y.)*. United States, 350(6257), p. aac7365. doi: 10.1126/science.aac7365.

Roy, M. J. *et al.* (2019) 'SPR-Measured Dissociation Kinetics of PROTAC Ternary Complexes Influence Target Degradation Rate', *ACS Chemical Biology*. American Chemical Society, 14(3), pp. 361–368. doi: 10.1021/acschembio.9b00092.

Rozansky, D. J. *et al.* (2009) 'Aldosterone mediates activation of the thiazide-sensitive Na-Cl cotransporter through an SGK1 and WNK4 signaling pathway.', *The Journal of clinical investigation*. United States, 119(9), pp. 2601–2612. doi: 10.1172/JCI38323.

Rudolph, M. *et al.* (2016) 'AKT1 (E17K) mutation profiling in breast cancer: prevalence, concurrent oncogenic alterations, and blood-based detection.', *BMC cancer*. England, 16, p. 622. doi: 10.1186/s12885-016-2626-1.

Russell, R. C. *et al.* (2013) 'ULK1 induces autophagy by phosphorylating Beclin-1 and activating VPS34 lipid kinase.', *Nature cell biology*. England, 15(7), pp. 741–750. doi: 10.1038/ncb2757.

Sabatini, D. M. *et al.* (1994) 'RAFT1: a mammalian protein that binds to FKBP12 in a rapamycin-dependent fashion and is homologous to yeast TORs.', *Cell*. United States, 78(1), pp. 35–43.

Sabers, C. J. *et al.* (1995) 'Isolation of a protein target of the FKBP12-rapamycin complex in mammalian

cells.', *The Journal of biological chemistry*. United States, 270(2), pp. 815–822. doi: 10.1074/jbc.270.2.815.

Saleh-Gohari, N. and Helleday, T. (2004) 'Conservative homologous recombination preferentially repairs DNA double-strand breaks in the S phase of the cell cycle in human cells.', *Nucleic acids research*. England, 32(12), pp. 3683–3688. doi: 10.1093/nar/gkh703.

Samuels, Y. *et al.* (2004) 'High Frequency of Mutations of the PIK3CA Gene in Human Cancers', *Science*, 304(5670), p. 554. doi: 10.1126/science.1096502.

Sancak, Y. *et al.* (2007) 'PRAS40 is an insulin-regulated inhibitor of the mTORC1 protein kinase.', *Molecular cell*. United States, 25(6), pp. 903–915. doi: 10.1016/j.molcel.2007.03.003.

Sancak, Y. *et al.* (2008) 'The Rag GTPases bind raptor and mediate amino acid signaling to mTORC1.', *Science (New York, N.Y.)*. United States, 320(5882), pp. 1496–1501. doi: 10.1126/science.1157535.

Sancak, Y. *et al.* (2010) 'Ragulator-Rag complex targets mTORC1 to the lysosomal surface and is necessary for its activation by amino acids.', *Cell*. United States, 141(2), pp. 290–303. doi: 10.1016/j.cell.2010.02.024.

Sandu, C. *et al.* (2005) 'Decreased intestinal glucose transport in the sgk3-knockout mouse.', *Pflugers Archiv : European journal of physiology*. Germany, 451(3), pp. 437–444. doi: 10.1007/s00424-005-1474-7.

Sano, H. *et al.* (2003) 'Insulin-stimulated phosphorylation of a Rab GTPase-activating protein regulates GLUT4 translocation.', *The Journal of biological chemistry*. United States, 278(17), pp. 14599–14602. doi: 10.1074/jbc.C300063200.

Sarbassov, D. D. *et al.* (2004) 'Rictor, a novel binding partner of mTOR, defines a rapamycin-insensitive and raptor-independent pathway that regulates the cytoskeleton.', *Current biology : CB*. England, 14(14), pp. 1296–1302. doi: 10.1016/j.cub.2004.06.054.

Sarbassov, D. D. *et al.* (2005) 'Phosphorylation and Regulation of Akt/PKB by the Rictor-mTOR Complex', *Science*, 307(5712), pp. 1098–1101. doi: 10.1126/science.1106148.

Sarbassov, D. D. *et al.* (2006) 'Prolonged rapamycin treatment inhibits mTORC2 assembly and Akt/PKB.', *Molecular cell*. United States, 22(2), pp. 159–168. doi: 10.1016/j.molcel.2006.03.029.

Saxton, R. A., Chantranupong, L., *et al.* (2016) 'Mechanism of arginine sensing by CASTOR1 upstream of mTORC1', *Nature*. Nature Publishing Group, 536(7615), pp. 229–233. doi: 10.1038/nature19079.

Saxton, R. A., Knockenhauer, K. E., *et al.* (2016) 'Structural basis for leucine sensing by the Sestrin2-mTORC1 pathway', *Science*. American Association for the Advancement of Science, 351(6268), pp. 53–58. doi: 10.1126/science.aad2087.

Saxton, R. A. and Sabatini, D. M. (2017) 'mTOR Signaling in Growth, Metabolism, and Disease', *Cell*. Cell Press, pp. 960–976. doi: 10.1016/j.cell.2017.02.004.

Schmidt, E.-M., Gu, S., *et al.* (2012) 'Serum- and glucocorticoid-dependent kinase-1-induced cell migration is dependent on vinculin and regulated by the membrane androgen receptor.', *The FEBS journal*. England, 279(7), pp. 1231–1242. doi: 10.1111/j.1742-4658.2012.08515.x.

Schmidt, E.-M., Kraemer, B. F., *et al.* (2012) 'SGK1 sensitivity of platelet migration.', *Cellular physiology and biochemistry : international journal of experimental cellular physiology, biochemistry, and pharmacology*. Germany, 30(1), pp. 259–268. doi: 10.1159/000339062.

Schroder, W. A. *et al.* (2007) 'Human Sin1 contains Ras-binding and pleckstrin homology domains and suppresses Ras signalling', *Cellular Signalling*, 19(6), pp. 1279–1289. doi: 10.1016/j.cellsig.2007.01.013.

Schulman, B. A. and Harper, J. W. (2009) 'Ubiquitin-like protein activation by E1 enzymes: the apex for downstream signalling pathways.', *Nature reviews. Molecular cell biology*. England, 10(5), pp. 319–331. doi: 10.1038/nrm2673.

Schwab, M. *et al.* (2008) 'Association of SGK1 gene polymorphisms with type 2 diabetes.', *Cellular physiology and biochemistry : international journal of experimental cellular physiology, biochemistry, and pharmacology*. Germany, 21(1–3), pp. 151–160. doi: 10.1159/000113757.

Sekimoto, T., Fukumoto, M. and Yoneda, Y. (2004) '14-3-3 suppresses the nuclear localization of threonine 157-phosphorylated p27(Kip1).', *The EMBO journal*. England, 23(9), pp. 1934–1942. doi: 10.1038/sj.emboj.7600198.

Sette, C. and Conti, M. (1996) 'Phosphorylation and activation of a cAMP-specific phosphodiesterase by the cAMP-dependent protein kinase. Involvement of serine 54 in the enzyme activation.', *The Journal of biological chemistry*. United States, 271(28), pp. 16526–16534. doi: 10.1074/jbc.271.28.16526.

Shaw, A. S. *et al.* (2014) 'Kinases and Pseudokinases: Lessons from RAF', *Molecular and Cellular Biology*. American Society for Microbiology, 34(9), pp. 1538–1546. doi: 10.1128/mcb.00057-14.

Shehata, S. N. *et al.* (2012) 'Analysis of substrate specificity and cyclin Y binding of PCTAIRE-1 kinase.', *Cellular signalling*. England, 24(11), pp. 2085–2094. doi: 10.1016/j.cellsig.2012.06.018.

Shehata, S. N. *et al.* (2015) 'Cyclin Y phosphorylation- and 14-3-3-binding-dependent activation of PCTAIRE-1/CDK16', *Biochemical Journal*. Portland Press Ltd, 469(3), pp. 409–420. doi: 10.1042/BJ20150486.

Shi, C.-S. and Kehrl, J. H. (2010) 'TRAF6 and A20 regulate lysine 63-linked ubiquitination of Beclin-1 to control TLR4-induced autophagy.', *Science signaling*. United States, 3(123), p. ra42. doi: 10.1126/scisignal.2000751.

Shibata, N. *et al.* (2018) 'Pharmacological difference between degrader and inhibitor against oncogenic BCR-ABL kinase', *Scientific Reports*, 8(1), p. 13549. doi: 10.1038/s41598-018-31913-5.

Shin, I. *et al.* (2002) 'PKB/Akt mediates cell-cycle progression by phosphorylation of p27(Kip1) at threonine 157 and modulation of its cellular localization.', *Nature medicine*. United States, 8(10), pp. 1145–1152. doi: 10.1038/nm759.

Shinzawa-Itoh, K. *et al.* (2007) 'Structures and physiological roles of 13 integral lipids of bovine heart cytochrome c oxidase.', *The EMBO journal*. England, 26(6), pp. 1713–1725. doi: 10.1038/sj.emboj.7601618.

Shull, A. Y. *et al.* (2012) 'Novel somatic mutations to PI3K pathway genes in metastatic melanoma.', *PloS one*. United States, 7(8), p. e43369. doi: 10.1371/journal.pone.0043369.

Skolnik, E. Y. *et al.* (1991) 'Cloning of PI3 kinase-associated p85 utilizing a novel method for expression/cloning of target proteins for receptor tyrosine kinases.', *Cell*. United States, 65(1), pp. 83–90.

Slagsvold, T. *et al.* (2006) 'CISK attenuates degradation of the chemokine receptor CXCR4 via the ubiquitin ligase AIP4', *The EMBO journal*. 2006/08/03, 25(16), pp. 3738–3749. doi: 10.1038/sj.emboj.7601267.

Smith, B. E. *et al.* (2019) 'Differential PROTAC substrate specificity dictated by orientation of recruited E3 ligase', *Nature Communications*, 10(1), p. 131. doi: 10.1038/s41467-018-08027-7.

Snyder, P. M., Olson, D. R. and Thomas, B. C. (2002) 'Serum and glucocorticoid-regulated kinase modulates Nedd4-2-mediated inhibition of the epithelial Na+ channel.', *The Journal of biological chemistry*. United States, 277(1), pp. 5–8. doi: 10.1074/jbc.C100623200.

Solaini, G., Sgarbi, G. and Baracca, A. (2011) 'Oxidative phosphorylation in cancer cells', *Biochimica et Biophysica Acta (BBA) - Bioenergetics*, 1807(6), pp. 534–542. doi: https://doi.org/10.1016/j.bbabio.2010.09.003.

Sommer, E. M. *et al.* (2013) 'Elevated SGK1 predicts resistance of breast cancer cells to Akt inhibitors.', *The Biochemical journal*. England, 452(3), pp. 499–508. doi: 10.1042/BJ20130342.

Sondka, Z. *et al.* (2018) 'The COSMIC Cancer Gene Census: describing genetic dysfunction across all human cancers', *Nature Reviews Cancer*, 18(11), pp. 696–705. doi: 10.1038/s41568-018-0060-1.

Sreelatha, A. *et al.* (2018) 'Protein AMPylation by an Evolutionarily Conserved Pseudokinase.', *Cell*, 175(3), pp. 809-821.e19. doi: 10.1016/j.cell.2018.08.046.

Srivastava, S. *et al.* (2016) 'Histidine phosphorylation relieves copper inhibition in the mammalian

potassium channel KCa3.1.', *eLife*, 5. doi: 10.7554/eLife.16093.

Stambolic, V. *et al.* (1998) 'Negative regulation of PKB/Akt-dependent cell survival by the tumor suppressor PTEN.', *Cell*. United States, 95(1), pp. 29–39.

Stephens, L. *et al.* (1994) 'A novel phosphoinositide 3 kinase activity in myeloid-derived cells is activated by G protein beta gamma subunits.', *Cell*. United States, 77(1), pp. 83–93.

Stephens, L. R. and Downes, C. P. (1990) 'Product-precursor relationship amongst inositol polyphosphates: Incorporation of [32P]P(i) into myo-inositol 1,3,4,6-tetrakisphosphate, myo-inositol 1,3,4,5-tetrakisphosphate, myo-inositol 3,4,5,6-tetrakisphosphate and myo-inositol 1,3,4,5,6-pentakisphosphate in intact avian erythrocytes', *Biochemical Journal*, 265(2), pp. 435–452. doi: 10.1042/bj2650435.

Stephens, P. J. *et al.* (2012) 'The landscape of cancer genes and mutational processes in breast cancer.', *Nature*. England, 486(7403), pp. 400–404. doi: 10.1038/nature11017.

Stern, H. M. *et al.* (2015) 'PTEN loss is associated with worse outcome in HER2-Amplified breast cancer patients but is not associated with trastuzumab resistance', *Clinical Cancer Research*, 21(9), pp. 2065–2074. doi: 10.1158/1078-0432.CCR-14-2993.

Stjepanovic, G. *et al.* (2017) 'Vps34 Kinase Domain Dynamics Regulate the Autophagic PI 3-Kinase Complex.', *Molecular cell*. United States, 67(3), pp. 528-534.e3. doi: 10.1016/j.molcel.2017.07.003.

Su, H. *et al.* (2017) 'VPS34 Acetylation Controls Its Lipid Kinase Activity and the Initiation of Canonical and Non-canonical Autophagy', *Molecular Cell*. Cell Press, 67(6), pp. 907-921.e7. doi: 10.1016/j.molcel.2017.07.024.

Swaffer, M. P. *et al.* (2016) 'CDK Substrate Phosphorylation and Ordering the Cell Cycle In Brief Article CDK Substrate Phosphorylation and Ordering the Cell Cycle', *Cell*, 167, pp. 1750-1750.e16. doi: 10.1016/j.cell.2016.11.034.

Taha, C. *et al.* (1999) 'Opposite translational control of GLUT1 and GLUT4 glucose transporter mRNAs in response to insulin. Role of mammalian target of rapamycin, protein kinase b, and phosphatidylinositol 3-kinase in GLUT1 mRNA translation.', *The Journal of biological chemistry*. United States, 274(46), pp. 33085–33091. doi: 10.1074/jbc.274.46.33085.

Takats, S. *et al.* (2014) 'Interaction of the HOPS complex with Syntaxin 17 mediates autophagosome clearance in Drosophila.', *Molecular biology of the cell*. United States, 25(8), pp. 1338–1354. doi: 10.1091/mbc.E13-08-0449.

Tatebe, H. *et al.* (2017) 'Substrate specificity of TOR complex 2 is determined by a ubiquitin-fold domain of the Sin1 subunit', *eLife*, 6. doi: 10.7554/eLife.19594.

Tee, A. R. *et al.* (2003) 'Tuberous sclerosis complex gene products, Tuberin and Hamartin, control mTOR signaling by acting as a GTPase-activating protein complex toward Rheb.', *Current biology : CB*. England, 13(15), pp. 1259–1268.

Testa, A. *et al.* (2018) '3-Fluoro-4-hydroxyprolines: Synthesis, Conformational Analysis, and Stereoselective Recognition by the VHL E3 Ubiquitin Ligase for Targeted Protein Degradation', *Journal of the American Chemical Society*. American Chemical Society, 140(29), pp. 9299–9313. doi: 10.1021/jacs.8b05807.

Thedieck, K. *et al.* (2007) 'PRAS40 and PRR5-like protein are new mTOR interactors that regulate apoptosis.', *PloS one*. United States, 2(11), p. e1217. doi: 10.1371/journal.pone.0001217.

Thoresen, S. B. *et al.* (2010) 'A phosphatidylinositol 3-kinase class III sub-complex containing VPS15, VPS34, Beclin 1, UVRAG and BIF-1 regulates cytokinesis and degradative endocytic traffic.', *Experimental cell research*. United States, 316(20), pp. 3368–3378. doi: 10.1016/j.yexcr.2010.07.008.

Tomoshige, S., Hashimoto, Y. and Ishikawa, M. (2016) 'Efficient protein knockdown of HaloTag-fused proteins using hybrid molecules consisting of IAP antagonist and HaloTag ligand.', *Bioorganic & medicinal chemistry*. England, 24(14), pp. 3144–3148. doi: 10.1016/j.bmc.2016.05.035.

Tran, H. *et al.* (2003) 'The many forks in FOXO's road.', *Science's STKE : signal transduction knowledge environment*. United States, 2003(172), p. RE5. doi: 10.1126/stke.2003.172.re5.

Tyanova, S. *et al.* (2016) 'The Perseus computational platform for comprehensive analysis of (prote)omics data.', *Nature methods*. United States, 13(9), pp. 731–740. doi: 10.1038/nmeth.3901.

Tyanova, S., Temu, T. and Cox, J. (2016) 'The MaxQuant computational platform for mass spectrometry-based shotgun proteomics.', *Nature protocols*. England, 11(12), pp. 2301–2319. doi: 10.1038/nprot.2016.136.

Vallon, V. *et al.* (2009) 'Expression and phosphorylation of the Na+-Cl- cotransporter NCC in vivo is regulated by dietary salt, potassium, and SGK1.', *American journal of physiology. Renal physiology*. United States, 297(3), pp. F704-12. doi: 10.1152/ajprenal.00030.2009.

Vanhaesebroeck, B. *et al.* (2010) 'The emerging mechanisms of isoform-specific PI3K signalling', *Nature Reviews Molecular Cell Biology*. Nature Publishing Group, 11, p. 329. Available at: https://doi.org/10.1038/nrm2882.

Vanhaesebroeck, B., Stephens, L. and Hawkins, P. (2012) 'PI3K signalling: the path to discovery and understanding.', *Nature reviews. Molecular cell biology*. England, pp. 195–203. doi: 10.1038/nrm3290.

Vasudevan, K. M. *et al.* (2009) 'AKT-independent signaling downstream of oncogenic PIK3CA mutations in human cancer', *Cancer cell*, 16(1), pp. 21–32. doi: 10.1016/j.ccr.2009.04.012.

Vellinga, T. T. *et al.* (2015) 'SIRT1/PGC1alpha-Dependent Increase in Oxidative Phosphorylation Supports Chemotherapy Resistance of Colon Cancer.', *Clinical cancer research : an official journal of the American Association for Cancer Research*. United States, 21(12), pp. 2870–2879. doi: 10.1158/1078-0432.CCR-14-2290.

Viglietto, G. *et al.* (2002) 'Cytoplasmic relocalization and inhibition of the cyclin-dependent kinase inhibitor p27(Kip1) by PKB/Akt-mediated phosphorylation in breast cancer.', *Nature medicine*. United States, 8(10), pp. 1136–1144. doi: 10.1038/nm762.

Villunger, A. *et al.* (2003) 'p53- and drug-induced apoptotic responses mediated by BH3-only proteins puma and noxa.', *Science (New York, N.Y.)*. United States, 302(5647), pp. 1036–1038. doi: 10.1126/science.1090072.

Virbasius, J. V *et al.* (2001) 'Activation of the Akt-related cytokine-independent survival kinase requires interaction of its phox domain with endosomal phosphatidylinositol 3-phosphate', *Proceedings of the National Academy of Sciences of the United States of America*. 2001/10/23. The National Academy of Sciences, 98(23), pp. 12908–12913. doi: 10.1073/pnas.221352898.

Vitari, A. C. *et al.* (2005) 'The WNK1 and WNK4 protein kinases that are mutated in Gordon's hypertension syndrome phosphorylate and activate SPAK and OSR1 protein kinases.', *The Biochemical journal*, 391(Pt 1), pp. 17–24. doi: 10.1042/BJ20051180.

Vogt, P. K. *et al.* (2007) 'Cancer-specific mutations in phosphatidylinositol 3-kinase.', *Trends in biochemical sciences*. England, 32(7), pp. 342–349. doi: 10.1016/j.tibs.2007.05.005.

Walczak, H., Iwai, K. and Dikic, I. (2012) 'Generation and physiological roles of linear ubiquitin chains.', *BMC biology*. England, 10, p. 23. doi: 10.1186/1741-7007-10-23.

Wang, H. *et al.* (2016) 'Serum- and glucocorticoid-inducible kinase SGK2 regulates human organic anion transporters 4 via ubiquitin ligase Nedd4-2.', *Biochemical pharmacology*. England, 102, pp. 120–129. doi: 10.1016/j.bcp.2015.11.024.

Wang, H., Zhang, J. and You, G. (2019) 'The mechanistic links between insulin and human organic anion transporter 4.', *International journal of pharmaceutics*. Netherlands, 555, pp. 165–174. doi: 10.1016/j.ijpharm.2018.11.040.

Wang, K. *et al.* (2010) 'SGK1-dependent Intestinal Tumor Growth in APC-deficient Mice', *Cellular Physiology and Biochemistry*, 25(2–3), pp. 271–278. doi: 10.1159/000276561.

Wang, L. *et al.* (2007) 'PRAS40 regulates mTORC1 kinase activity by functioning as a direct inhibitor of substrate binding.', *The Journal of biological chemistry*. United States, 282(27), pp. 20036–20044. doi: 10.1074/jbc.M702376200.

Wang, M. *et al.* (2019) 'Inhibition of SGK1 confers vulnerability to redox dysregulation in cervical cancer', *Redox biology*. 2019/05/20. Elsevier, 24, p. 101225. doi: 10.1016/j.redox.2019.101225.

Wang, Y. *et al.* (2011) 'SGK3 is an estrogen-inducible kinase promoting estrogen-mediated survival of breast cancer cells', *Mol Endocrinol*, pp. 72–82. doi: 10.1210/me.2010-0294.

Wang, Y. *et al.* (2014) 'Coordinated regulation of serum- and glucocorticoid-inducible kinase 3 by a C-terminal hydrophobic motif and Hsp90-Cdc37 chaperone complex.', *The Journal of biological chemistry*. United States, 289(8), pp. 4815–4826. doi: 10.1074/jbc.M113.518480.

Webster, M. K. *et al.* (1993) 'Characterization of sgk, a novel member of the serine/threonine protein kinase gene family which is transcriptionally induced by glucocorticoids and serum.', *Molecular and cellular biology*. United States, 13(4), pp. 2031–2040. doi: 10.1128/mcb.13.4.2031.

Webster, M. K., Goya, L. and Firestone, G. L. (1993) 'Immediate-early transcriptional regulation and rapid mRNA turnover of a putative serine/threonine protein kinase.', *The Journal of biological chemistry*. United States, 268(16), pp. 11482–11485.

Wei, W. *et al.* (2005) 'The v-Jun point mutation allows c-Jun to escape GSK3-dependent recognition and destruction by the Fbw7 ubiquitin ligase.', *Cancer cell*. United States, 8(1), pp. 25–33. doi: 10.1016/j.ccr.2005.06.005.

Weintraub, A. S. *et al.* (2017) 'YY1 Is a Structural Regulator of Enhancer-Promoter Loops.', *Cell*. United States, 171(7), pp. 1573-1588.e28. doi: 10.1016/j.cell.2017.11.008.

Welcker, M. *et al.* (2003) 'Multisite phosphorylation by Cdk2 and GSK3 controls cyclin E degradation.', *Molecular cell*. United States, 12(2), pp. 381–392.

Whitman, M. *et al.* (1988) 'Type I phosphatidylinositol kinase makes a novel inositol phospholipid, phosphatidylinositol-3-phosphate.', *Nature*. England, 332(6165), pp. 644–646. doi: 10.1038/332644a0.

Wickliffe, K. E. *et al.* (2011) 'K11-linked ubiquitin chains as novel regulators of cell division.', *Trends in cell biology*. England, 21(11), pp. 656–663. doi: 10.1016/j.tcb.2011.08.008.

Wieland, T. and Attwood, P. V (2015) 'Alterations in reversible protein histidine phosphorylation as intracellular signals in cardiovascular disease.', *Frontiers in pharmacology*, 6, p. 173. doi: 10.3389/fphar.2015.00173.

Winter, G. E. *et al.* (2015) 'DRUG DEVELOPMENT. Phthalimide conjugation as a strategy for in vivo target protein degradation.', *Science (New York, N.Y.)*. United States, 348(6241), pp. 1376–1381. doi: 10.1126/science.aab1433.

Wolfson, R. L. *et al.* (2016) 'Sestrin2 is a leucine sensor for the mTORC1 pathway', *Science*. American Association for the Advancement of Science, 351(6268), pp. 43–48. doi: 10.1126/science.aab2674.

Wolfson, R. L. *et al.* (2017) 'KICSTOR recruits GATOR1 to the lysosome and is necessary for nutrients to regulate mTORC1', *Nature*. Nature Publishing Group, 543(7645), pp. 438–442. doi: 10.1038/nature21423.

Woo, S.-Y. *et al.* (2007) 'PRR5, a Novel Component of mTOR Complex 2, Regulates Platelet-derived Growth Factor Receptor β Expression and Signaling', *Journal of Biological Chemistry* , 282(35), pp. 25604–25612. doi: 10.1074/jbc.M704343200.

Wu, W. *et al.* (2004) 'Microarray analysis reveals glucocorticoid-regulated survival genes that are associated with inhibition of apoptosis in breast epithelial cells.', *Cancer research*. United States, 64(5), pp. 1757–1764.

Wulff, P. *et al.* (2002) 'Impaired renal Na(+) retention in the sgk1-knockout mouse.', *The Journal of clinical investigation*. United States, 110(9), pp. 1263–1268. doi: 10.1172/JCI15696.

Xu, D. *et al.* (2016) 'Serum- and glucocorticoid-inducible kinase sgk2 stimulates the transport activity of human organic anion transporters 1 by enhancing the stability of the transporter.', *International journal of biochemistry and molecular biology*. United States, 7(1), pp. 19–26.

Xu, J. *et al.* (2012) 'SGK3 is associated with estrogen receptor expression in breast cancer', *Breast cancer research and treatment*. 2012/05/11, 134(2), pp. 531–541. doi: 10.1007/s10549-012-2081-x.

Yang, C. *et al.* (2016) 'Acquired CDK6 amplification promotes breast cancer resistance to CDK4/6 inhibitors and loss of ER signaling and dependence', *Oncogene*. The Author(s), 36, p. 2255. Available at: https://doi.org/10.1038/onc.2016.379.

Yang, G. *et al.* (2015) 'A Positive Feedback Loop between Akt and mTORC2 via SIN1 Phosphorylation', *Cell Reports*. Elsevier B.V., 12(6), pp. 937–943. doi: 10.1016/j.celrep.2015.07.016.

Yang, J. *et al.* (2019) 'Targeting PI3K in cancer: mechanisms and advances in clinical trials', *Molecular Cancer*, 18(1), p. 26. doi: 10.1186/s12943-019-0954-x.

Yao, C. A. *et al.* (2017) 'Association of mSin1 with mTORC2 Ras and Akt reveals a crucial domain on mSin1 involved in Akt phosphorylation', *Oncotarget*. Impact Journals LLC, 8(38), pp. 63392–63404. doi: 10.18632/oncotarget.18818.

Yao, L.-J. *et al.* (2011) 'Novel role for SGK3 in glucose homeostasis revealed in SGK3/Akt2 double-null mice', *Molecular endocrinology (Baltimore, Md.)*. 2011/10/06. Endocrine Society, 25(12), pp. 2106–2118. doi: 10.1210/me.2010-0329.

Yeh, E. *et al.* (2004) 'A signalling pathway controlling c-Myc degradation that impacts oncogenic transformation of human cells.', *Nature cell biology*. England, 6(4), pp. 308–318. doi: 10.1038/ncb1110.

Yi, K. H. *et al.* (2012) 'Functional analysis of non-hotspot AKT1 mutants found in human breast cancers identifies novel driver mutations: implications for personalized medicine', *Oncotarget*. Impact Journals LLC, 4(1), pp. 29–34. doi: 10.18632/oncotarget.755.

Yi, K. H. and Lauring, J. (2015) 'Recurrent AKT mutations in human cancers: functional consequences and effects on drug sensitivity', *Oncotarget*. Impact Journals LLC, 7(4), pp. 4241–4251. doi: 10.18632/oncotarget.6648.

Yoshioka, K. *et al.* (2012) 'Endothelial PI3K-C2alpha, a class II PI3K, has an essential role in angiogenesis and vascular barrier function.', *Nature medicine*. United States, 18(10), pp. 1560–1569. doi: 10.1038/nm.2928.

Young, L. N. *et al.* (2016) 'Dynamics and architecture of the NRBF2-containing phosphatidylinositol 3-kinase complex I of autophagy.', *Proceedings of the National Academy of Sciences of the United States of America*. United States, 113(29), pp. 8224–8229. doi: 10.1073/pnas.1603650113.

Zalckvar, E. *et al.* (2009) 'Phosphorylation of Beclin 1 by DAP-kinase promotes autophagy by weakening its interactions with Bcl-2 and Bcl-XL.', *Autophagy*. United States, 5(5), pp. 720–722. doi: 10.4161/auto.5.5.8625.

Zardavas, D., Fumagalli, D. and Loi, S. (2012) 'Phosphatidylinositol 3-kinase/AKT/mammalian target of rapamycin pathway inhibition: A breakthrough in the management of luminal (ER +HER2-) breast cancers?', *Current Opinion in Oncology*, 24(6), pp. 623–634. doi: 10.1097/CCO.0b013e328358a2b5.

Zelzer, E. *et al.* (1998) 'Insulin induces transcription of target genes through the hypoxia-inducible factor HIF-1alpha/ARNT.', *The EMBO journal*. England, 17(17), pp. 5085–5094. doi: 10.1093/emboj/17.17.5085.

Zemtsova, I. M. *et al.* (2010) 'Blunted IgE-mediated activation of mast cells in mice lacking the serum- and glucocorticoid-inducible kinase SGK3', *American journal of physiology. Cell physiology*. 2010/08/04. American Physiological Society, 299(5), pp. C1007–C1014. doi: 10.1152/ajpcell.00539.2009.

Zeng, J. *et al.* (1999) 'Protein-protein recognition: an experimental and computational study of the R89K mutation in Raf and its effect on Ras binding.', *Protein science : a publication of the Protein Society*, 8(1), pp. 50–64. doi: 10.1110/ps.8.1.50.

Zengerle, M., Chan, K.-H. and Ciulli, A. (2015) 'Selective Small Molecule Induced Degradation of the BET Bromodomain Protein BRD4.', *ACS chemical biology*. United States, 10(8), pp. 1770–1777. doi: 10.1021/acschembio.5b00216.

Zhang, W. *et al.* (2007) 'Aldosterone-induced Sgk1 relieves Dot1a-Af9-mediated transcriptional repression of epithelial Na+ channel alpha.', *The Journal of clinical investigation*. United States, 117(3), pp. 773–783. doi: 10.1172/JCI29850.

Zhao, L. and Vogt, P. K. (2008) 'Helical domain and kinase domain mutations in p110alpha of phosphatidylinositol 3-kinase induce gain of function by different mechanisms.', *Proceedings of the National Academy of Sciences of the United States of America*. United States, 105(7), pp. 2652–2657. doi: 10.1073/pnas.0712169105.

Zheng, X. *et al.* (2014) 'Ischemic preconditioning inhibits mitochondrial permeability transition pore opening through the PTEN/PDE4 signaling pathway', *Cardiology*. 2014/10/04, 129(3), pp. 163–173. doi: 10.1159/000363646.

Zhong, Y. *et al.* (2009) 'Distinct regulation of autophagic activity by Atg14L and Rubicon associated with Beclin 1-phosphatidylinositol-3-kinase complex.', *Nature cell biology*. England, pp. 468–476. doi: 10.1038/ncb1854.

Zhou, B. *et al.* (2019) 'Mitochondrial Permeability Uncouples Elevated Autophagy and Lifespan Extension', *Cell*, 177(2), pp. 299-314.e16. doi: https://doi.org/10.1016/j.cell.2019.02.013.

Zhou, B. P., Liao, Y., Xia, W., Spohn, B., *et al.* (2001) 'Cytoplasmic localization of p21Cip1/WAF1 by Akt-induced phosphorylation in HER-2/neu-overexpressing cells.', *Nature cell biology*. England, 3(3), pp. 245–252. doi: 10.1038/35060032.

Zhou, B. P., Liao, Y., Xia, W., Zou, Y., *et al.* (2001) 'HER-2/neu induces p53 ubiquitination via Akt-mediated MDM2 phosphorylation.', *Nature cell biology*. England, 3(11), pp. 973–982. doi: 10.1038/ncb1101-973.

Zhou, R. and Snyder, P. M. (2005) 'Nedd4-2 phosphorylation induces serum and glucocorticoid-regulated kinase (SGK) ubiquitination and degradation.', *The Journal of biological chemistry*. United States, 280(6), pp. 4518–4523. doi: 10.1074/jbc.M411053200.

Zhu, H. *et al.* (2010) 'Evolutionarily Conserved Role of Calcineurin in Phosphodegron-Dependent Degradation of Phosphodiesterase 4D', *Molecular and Cellular Biology*, 30(18), pp. 4379 LP – 4390. doi: 10.1128/MCB.01193-09.

Zinzalla, V. *et al.* (2011) 'Activation of mTORC2 by association with the ribosome.', *Cell*. United States, 144(5), pp. 757–768. doi: 10.1016/j.cell.2011.02.014.

Zoncu, R. *et al.* (2011) 'mTORC1 senses lysosomal amino acids through an inside-out mechanism that requires the vacuolar H(+)-ATPase.', *Science (New York, N.Y.)*. United States, 334(6056), pp. 678–683. doi: 10.1126/science.1207056.